CERN 67-26
Vol. II
August 1967

ORGANISATION EUROPÉENNE POUR LA RECHERCHE NUCLÉAIRE
CERN EUROPEAN ORGANIZATION FOR NUCLEAR RESEARCH

INTERNATIONAL COLLOQUIUM ON BUBBLE CHAMBERS

held at Heidelberg

April 13-14, 1967

Proceedings
edited by
H. Leutz

GENEVA
1967

CONTENTS

VOLUME I

4.1 VIBRATION OF BUBBLE CHAMBER LIQUID DURING EXPANSION

M.S. Dykes and G. Bachy
CERN

(Presented by M.S. Dykes)

Introduction

Because the velocity of sound in the liquid of a bubble chamber is finite, the pressure throughout a bubble chamber during the expansion - recompression cycle will not in general be uniform at a particular instant. Pressure differences throughout the sensitive regions of present day chambers are small, but will not necessarily be so in large chambers.

It is also clear that the power consumption of larger chamber expansion systems will be considerable if the systems are designed as scaled-up versions of present types. This latter consideration makes the use of a freely-oscillating system attractive, since the energy exchanges during expansion are within the system (potential energy of fluid $\rightarrow$ kinetic energy of fluid and piston $\rightarrow$ potential energy of fluid) and the expansion system need only replace the energy losses during the cycle, which may be expected to be small. Several chambers under design propose to use such a freely oscillating system.

This paper discusses the determination of pressure variation and pressure time curves for a very simple system operating in a state of free oscillation.

2.1 The problem which has been considered in most detail is the behaviour of the simple system shown in Fig. 1. We consider a chamber whose cross section (of area S) is constant in the direction of piston motion. We measure position in the chamber as distance x from the closed end; the chamber depth is L. The gas cushion is sufficiently large for variations in its pressure p_g caused by piston movement to be negligible.

M is the mass of the piston.

With the piston free (not constrained by the expansion mechanism) and at rest, the chamber pressure p is given by:

$$p = p_o = pg - \frac{Mg}{S} - \rho_o gx \qquad (1)$$

ρ_o being the density of the chamber fluid and g the acceleration due to gravity.

In what follows the term $\rho_o gx$ (the static head), which in liquid hydrogen amounts to about 25 gms.f./sq.cm. per metre of depth, will be neglected.

We take the pressure p_o under quiescent conditions in equation 1 as a reference pressure, and define excess pressure P as the departure from this value:

$$P = p - p_o \qquad (2)$$

With P = 0 everywhere each particle of fluid is in its reference position, and the particle displacement ξ is everywhere zero. ξ is positive in the direction of positive x.

The expansion mechanism now forces the piston into the chamber to raise the excess pressure to a value Po, constant throughout the chamber. At time t = 0, the mechanism releases the piston, which performs a free oscillation about its reference position.

In order to determine the pressure distribution and fluid movements at later times, we must solve a one-dimensional wave equation throughout the fluid for ζ :

$$\frac{1}{c^2}\frac{\delta^2\zeta}{\delta t^2} = \frac{\delta^2\zeta}{\delta x^2} \qquad (3a)$$

or for P:

$$\frac{1}{c^2}\frac{\delta^2 P}{\delta t^2} = \frac{\delta^2 P}{\delta x^2} \qquad (3b)$$

where c = velocity of sound in the liquid.

P and ζ are approximately related by

$$P = - c^2 \rho_o \frac{\delta\zeta}{\delta x} \qquad (4)$$

The above equations are derived in references 1 and 2.

We choose to consider equation (3b) which may be shown by the technique of separation of variables to have a general solution of the form

$$P = \left(A \cos\frac{\alpha x}{L} + B \sin\frac{\alpha x}{L}\right)\left(D \cos\frac{\alpha ct}{L} + E \sin\frac{\alpha ct}{L}\right) \qquad (5)$$

where A, B, D, E and α are determined by boundary conditions in space (x) and time (t).

Now at x = 0, the end of the chamber, we must have an antinode of pressure so that $\frac{\delta P}{\delta x} = 0$ at x = 0 for all t; hence B = 0.

Also at t = 0 the chamber fluid is at rest so that $\frac{\delta P}{\delta t} = 0$ for all x; hence E = 0.

We are left, for our special case, with

$$P = A \cos \frac{\alpha x}{L} \cos \frac{\alpha c t}{L} \qquad (6)$$

as a general solution, where D has been set equal to unity without loss of generality.

To find α we write down the condition that the piston acceleration is produced by the excess pressure at x = L:

$$M \left(\frac{\delta^2 \xi}{\delta t^2}\right)_{x=L} = SA \cos\alpha \cos \frac{\alpha c t}{L} \qquad (7)$$

By equations 2 and 4:

$$\frac{\delta^2 \xi}{\delta t^2} = c^2 \frac{\delta^2 \xi}{\delta x^2} = c^2 \frac{\delta}{\delta x} \left(\frac{\delta \xi}{\delta x}\right) = c^2 \frac{\delta}{\delta x} \left(- \frac{P}{c^2 \rho_o}\right)$$

So that

$$\left(\frac{\delta^2 \xi}{\delta t^2}\right)_{x=L} = - \frac{1}{\rho_o} \left(\frac{\delta P}{\delta x}\right)_{x=L}$$

Thus, substituting in equation 7 yields

$$\frac{\alpha MA}{\rho_o L} \sin\alpha \cos\frac{\alpha ct}{L} = SA \cos\alpha \cos\frac{\alpha ct}{L}$$

Or $$C\alpha = Cot\alpha \qquad (8)$$

where $$C = \frac{M}{\rho_o SL} = \frac{\text{PISTON MASS}}{\text{FLUID MASS}}$$

Equation 8 is the pulsatence equation for the system; values of α satisfying 8 give the frequencies and pressure distributions of the various modes of vibration of which the system is capable. There are of course an infinity of values of α, and for each one there exists an independent solution of equation 3bof the form of equation 6.

Thus a complete solution of equation 3btakes the form:

$$P = \sum_{n=1}^{\infty} A_n \cos\frac{\alpha_n x}{L} \cos\frac{\alpha_n ct}{L} \qquad (9)$$

To determine the values of an appropriate to our case, we must find the unique combination of modal amplitudes giving constant pressure Po throughout the chamber at t = 0, i.e.

$$P_o = \sum_{n=1}^{\infty} A_n \cos\frac{\alpha_n x}{L} \qquad (10)$$

In reference 2 is a discussion of the orthogonality of the proper functions $\cos\frac{\alpha_n x}{L}$ of systems similar to ours, and it may be shown that (with $m \neq n$):

$$\int_0^L \cos\frac{\alpha_n x}{L} \cos\frac{\alpha_m x}{L} \, dx = 0 \qquad (11)$$

(This is easily verified, carrying out the integration and using

from equation 8 the fact that $\frac{\cot\alpha_m}{\alpha_m} = \frac{\cot\alpha_n}{\alpha_n}$).

We may carry out a process akin to Fourier analysis determining the coefficient A_n, for example, by multiplying both sides of equation 10 by $\cos \frac{\alpha_n x}{L}$ and integrating:

$$\int_0^L P_o \cos\frac{\alpha_n x}{L}\,dx = A1 \int_0^L \cos\frac{\alpha_1 x}{L}\cos\frac{\alpha_n x}{L}\,dx + \ldots + A_n \int_0^L \cos^2\frac{\alpha_n x}{L}\,dx + \ldots$$

All terms on the right-hand side except the n^{th} vanish, by equation 11, leaving

$$A_n = \frac{P_o \int_0^L \cos\frac{\alpha_n x}{L}\,dx}{\int_0^L \cos^2\frac{\alpha_n x}{L}\,dx}$$

i.e. $$A_n = Po \cdot \frac{4\alpha_n}{(2\alpha_n + \sin 2\alpha_n)} \qquad (12)$$

Equation 12 may be used to determine the coefficients A_n once the values of α_n from equation 8 are known.

Pressure at any time and place in the chamber can then be determined from the series given by equation 9. It is found that these series conve ge quite well, the larger the value of C the better being the convergence. Good accuracy (say better than 1%) may always be obtained by taking twenty terms, but the first 220 values of α_n and A_n have been computed for the following values of C:

0, 0.01, 0.1, 0.2, 0.5, 1.0, 2.0, 5.0, and 10.0.

Appendix 1 shows the first 20 values of α_n.

To determine piston and fluid movements, we note that from equation 4

$$\xi = -\frac{1}{c\rho_o}\left[\int_o^x P\,dx\right] \qquad (13)$$

since $\xi = 0$ at $x = 0$ always

so that a general expression for ξ is

$$\xi = -\frac{1}{c^2\rho_o}\left[\sum_{n=1}^{\infty}\frac{LA_n}{\alpha_n}\sin\frac{\alpha_n x}{L}\cos\frac{\alpha_n ct}{L}\right] \qquad (14)$$

Results calculated from equations 9 and 4 will be discussed later.

2.2 The above argument can readily be extended to cover certain more complex systems.

2.2.1 If the expansion system contains a spring which exerts on the piston a force $-K\,(\xi)_{x=L}$, we may rewrite equation 7 as

$$M\left(\frac{\delta^2}{\delta t^2}\right)_{x=L} = SA\cos\alpha\cos\frac{\alpha ct}{L} - K\,(\xi)_{x=L} \qquad (15)$$

Substitution in this equation, using equations 6 and 13 yields

$$\mathrm{Cot}\alpha = C\alpha - \frac{KL}{Sc^2\rho_o\alpha} \qquad (16)$$

which is a new pulsatence equation giving the frequencies and pressure distributions in the various system modes.

2.2.2 If the chamber has no longer a constant section S with x, then it is shown in references 1 and 2 that the wave equation 2 may be replaced by

$$\frac{1}{c^2}\frac{\delta^2\xi}{\delta t^2} = \frac{\delta}{\delta x}\left[\frac{1}{S(x)}\frac{\delta}{\delta x}\left(S(x)\cdot\xi\right)\right] \qquad (17)$$

or, neglecting second order differentials

$$\frac{1}{c^2}\frac{\delta^2\xi}{\delta t^2} = \frac{1}{S(x)}\frac{\delta}{\delta x}\left[S(x)\frac{\delta\xi}{\delta x}\right] \qquad (18)$$

Separating variables and writing

$$\xi = X(x) \cdot T(t)$$

$$\frac{\delta^2 T}{\delta t^2} + \frac{\alpha^2 c^2}{L^2} T = 0 \qquad (19)$$

and

$$\frac{\delta^2 X}{\delta x^2} + \frac{1}{S}\frac{\delta s}{\delta x}\frac{\delta X}{\delta x} + \frac{\alpha^2}{L^2} X = 0 \qquad (20)$$

where again α has to be determined from the conditions at the piston. Equation 20 can be integrated (numerically if necessary) to find the pressure distribution along the chamber in each mode; equation 19 shows that the time-variation of pressure at any place in one mode is still sinusoidal as in the simple "organ-pipe" model discussed in paragraph 2.1. A procedure analogous to the analysis of paragraph 2.1 can be used to determine pressure distributions and pressure-time curves for one-shot operation.

2.2.3 In the more general case where it is not supposed that the chamber section varies slowly with x but has still cylindrical symmetry, we may attempt a solution by writing the wave equation in cylindrical co-ordinates:

$$\frac{1}{c^2}\frac{\delta^2\xi}{\delta t^2} = \Delta\xi$$

Writing $(x, r, t) = X(x,r) \cdot T(t)$

leads to

$$\frac{\delta^2 T}{\delta t^2} + \frac{\alpha^2 c^2}{L^2} T = 0$$

and

$$\frac{\delta^2 X}{\delta r^2} + \frac{1}{r}\frac{\delta X}{\delta r} + \frac{\delta^2 X}{\delta x^2} + \frac{\alpha^2}{L^2} X = 0$$

Limit conditions must express the fact that piston acceleration is a function of mean pressure at the piston, and that fluid motion at the walls is entirely parallel to the walls.

An attempt will be made to describe motion and pressure distribution in the CERN 3.5 Metre Chamber and its model using the methods outlined in para. 2.2; results will be given in a later paper.

3. We return to a discussion of the results calculated for the simple system shown in Fig. 1.

3.1 Piston movement

Fig. 2 shows how the piston moves during the first cycle of the free oscillation for different piston masses; for zero-mass piston the movement is triangular in time, and becomes nearly sinusoidal with even very small piston masses. The time scale is non-dimensional: T_0 is the natural period of the fundamental mode of the system, and is equal to

$$\frac{2\pi L}{\alpha_1 c}$$

Table 1 below shows how To varies with the parameter C (the ratio of piston mass to fluid mass) for a chamber 4 m deep and for a chamber 7 m deep, filled with liquid hydrogen at 25°K, for which c = 960 m/sec. approximately.

Also shown is the piston mass corresponding to the value of C, assuming that the chamber has a diameter of 10 metres.

C	Chamber Depth 4 m		Chamber Depth 7 m	
	To (mS.)	Piston Mass (tonnes)	To (mS.)	Piston Mass (tonnes)
0	16.7	0	29	0
0.01	16.8	.2	29.4	.35
0.1	18.4	2	32	3.5
0.2	19.9	4	34.8	7
0.5	24.3	10	42.5	17.5
1.0	30.5	20	53.5	35.
2.0	40.1	40	70.1	70.
5.0	60.5	100	106	175
10.0	84.1	200	147.2	350

Table 1

3.2 Zero Mass Piston

Figs. 3 to 6 show pressure-time curves at various points in the chamber, and also show pressure distributions throughout the chamber at various times, all for various values of the parameter C.

The behaviour of the pure liquid column (C = 0, piston mass zero) is striking and can incidentally be easily deduced from a simple consideration of a pressure wave traversing the chamber four times during the natural periodic time To. The wave starts as a decompression step wave generated as the pressure at the surface drops from ρo to ρg at time zero. This wave is reflected without change of form at time To/4 at the closed end, which is a pressure antinode. The decompression step now travels back through the chamber to the liquid surface, arriving at t = To/2, where it is reflected with a

reversal of sign, since the liquid surface is a node of pressure. At this time the whole chamber is at uniform pressure - Po. The cycle is completed as this compression wave traverses the chamber twice again, reaching the liquid surface at time To leaving the whole chamber at pressure Po. Pressure-time curves deduced from this model agree with the calculated results shown in Figs. 2 and 3.

Thissystem with a zero mass piston then gives ideal behaviour in two respects: twice in the cycle (at To/2 and To) the chamber fluid has uniform pressure and zero velocity throughout, giving uniform sensitivity for bubble growth at $\frac{To}{2}$ and leaving no wave energy in the fluid at time To when the piston can be stopped or "caught" by a ratchet-like expansion mechanism. The pressure-time curve could in principle be "stretched" to increase the sensitive time, by "catching" the piston at time To/2 and holding it for a few milliseconds.

3.3 Piston with Finite Mass

The curves for non-zero C show how the behaviour of the liquid column is modified by the presence of a piston having finite mass. For a very light piston (C = 0.1) the pressure uniformity at time To/2 is very good through some 80°/o of the chamber but a wave leaving the piston gives large pressure changes in this region. At the end of the first cycle (t = To) the wave is again evident; its energy has been roughly estimated as about .015 joule per litre of chamber liquid assuming a total pressure drop of 4 atmospheres (i.e. Po = 2 atmospheres).

If the piston weight is increased to half that of the fluid (C = 0.5) the system is clearly not usable since pressure distribution at half-cycle would give very variable sensitivity throughout the chamber. It is necessary to increase the piston weight to

twice that of the fluid (C = 2.0) before the pressure distributions are again acceptable.

Also included in Fig. 6 are the curves showing pressure distributions which would exist in a system oscillating continuously in its fundamental mode: for values of C greater than 2 there is little to choose from the point of view of pressure uniformity between continuous and "one-shot" operation. Pressure-time curves shown in Figs 4 and 5 show that for large values of C the variation is almost sinusoidal, while for small values the curves change with position in the chamber and tend to have a flat portion around t = To/2, which is a useful feature. Also pressure drops near the piston are of short duration; this could help with spurious boiling. In examining these curves it should be remembered that the time-scale is non-dimensional and that the time To is some four times as long for C = 5 as for C = 0. (See Table 1).

3.4 Summary

The results above show that in a large bubble chamber of simple shape, acceptable pressure distribution and pressure-time curves can be obtained with a relatively simple expansion system consisting of a piston and a "latch" mechanism, and of course some sort of energy make-up device to replace the slight energy losses during the oscillation. The "spring force" associated with the oscillation comes entirely from the liquid itself.

Heavy pistons can operate "one-shot" or in continuous oscillation, but with a relatively long pressure-time curves with possible difficulties due to spurious boiling. If it were possible to construct a very light piston (say C = 0.2), it would then be possible with "one-shot" operation to have relatively fast pressure-time

curves with good pressure uniformity in the region away from the piston; the pressure under the piston, however, because of the low piston inertia, hardly departs from the gas-cushion pressure, which can be very near to (perhaps even above) the vapour pressure of the fluid. One might hope that these conditions would minimise spurious boiling, and hence the dynamic heat-load.

APPENDIX 1

Solutions of $\alpha = C \cot \alpha$

n \ C =	0	0.01	0.1	0.2	0.5	1.0	2.0	5.0	10.0
1	1.5707	1.555	1.429	1.314	1.077	0.860	0.653	0.433	0.311
2	4.7123	4.665	4.306	4.033	3.643	3.426	3.292	3.204	3.173
3	7.8588	7.776	7.228	6.909	6.578	6.437	6.361	6.315	6.299
4	10.9954	10.887	10.200	9.893	9.629	9.529	9.477	9.446	9.435
5	14.1371	13.998	13.214	12.935	12.722	12.645	12.606	12.582	12.574
6	17.2786	17.109	16.259	16.010	15.833	15.771	15.740	15.721	15.714
7	20.4202	20.221	19.327	19.105	18.954	18.902	18.876	18.860	18.855
8	23.5618	23.333	22.411	22.212	22.081	22.036	22.014	22.000	21.996
9	26.703	26.445	25.506	25.327	25.212	25.172	25.152	25.141	25.137
10	29.845	29.558	28.610	28.448	28.345	28.309	28.292	28.281	28.278
11	32.987	32.671	31.721	31.573	31.479	31.447	31.432	31.422	31.419
12	36.128	35.785	34.837	34.700	34.615	34.586	34.572	34.563	34.560
13	39.270	38.899	37.957	37.830	37.752	37.725	37.712	37.704	37.702
14	42.411	42.014	41.079	40.962	40.889	40.865	40.853	40.845	40.843
15	45.553	45.129	44.205	44.095	44.028	44.005	43.993	43.986	43.984
16	48.694	48.245	47.332	47.229	47.166	47.145	47.134	47.128	47.126
17	51.836	51.362	50.461	50.364	50.305	50.285	50.275	50.269	50.267
18	54.978	54.479	53.591	53.500	53.444	53.426	53.416	53.411	53.409
19	58.119	57.596	56.723	56.636	56.584	56.566	56.557	56.552	56.550
20	61.609	60.715	59.856	59.774	59.724	59.707	59.699	59.694	59.692

References

1) Waves, C.A.Coulson, Oliver and Boyd 1955

2) An Introduction to the Theory of Vibrating Systems, W.G.Bickley and A.Talbot, Oxford, Clarendon Press, 1961

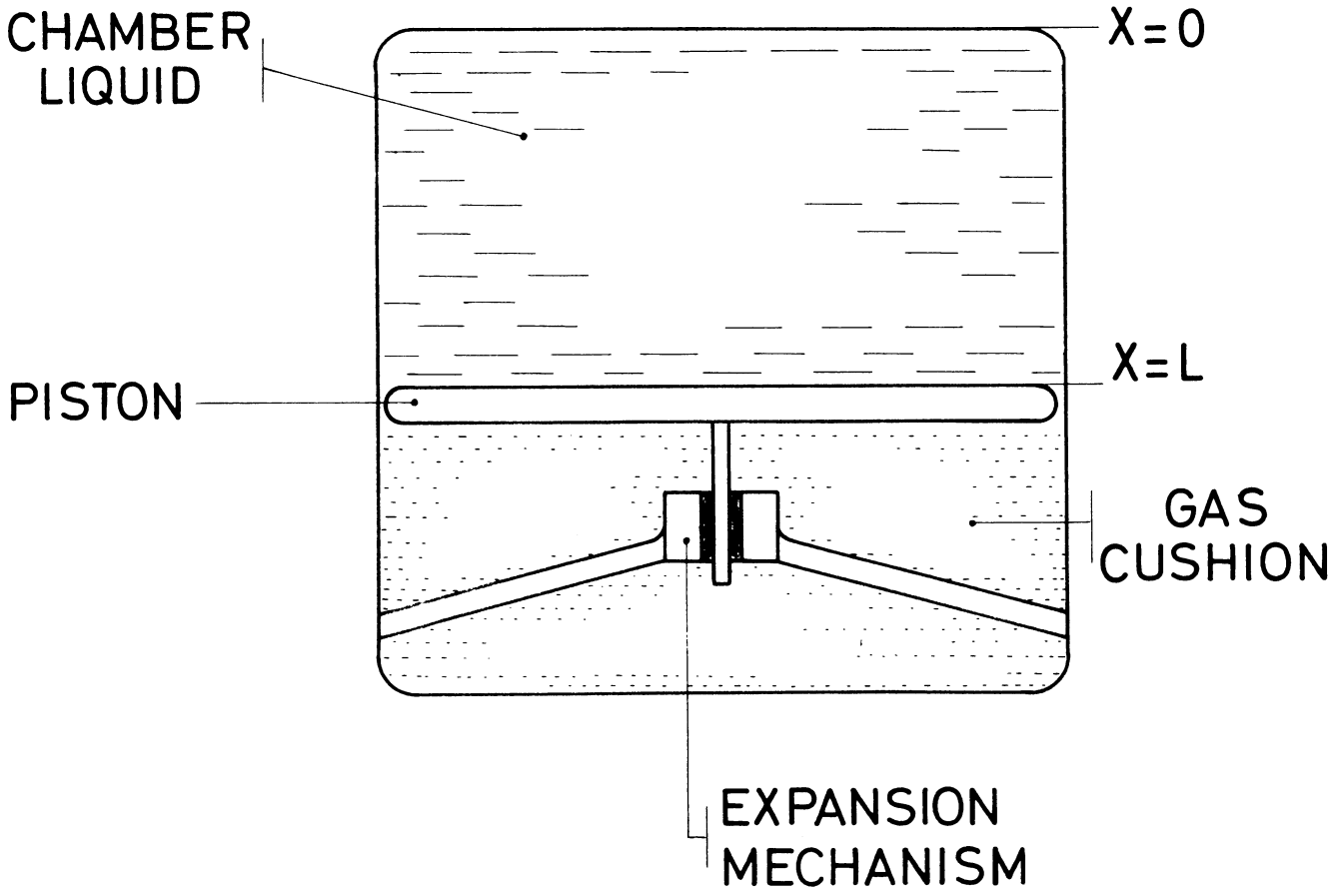
CHAMBER
LIQUID
X=0
PISTON
X=L
GAS
CUSHION
EXPANSION
MECHANISM

FIG:1

PISTON MOVEMENT

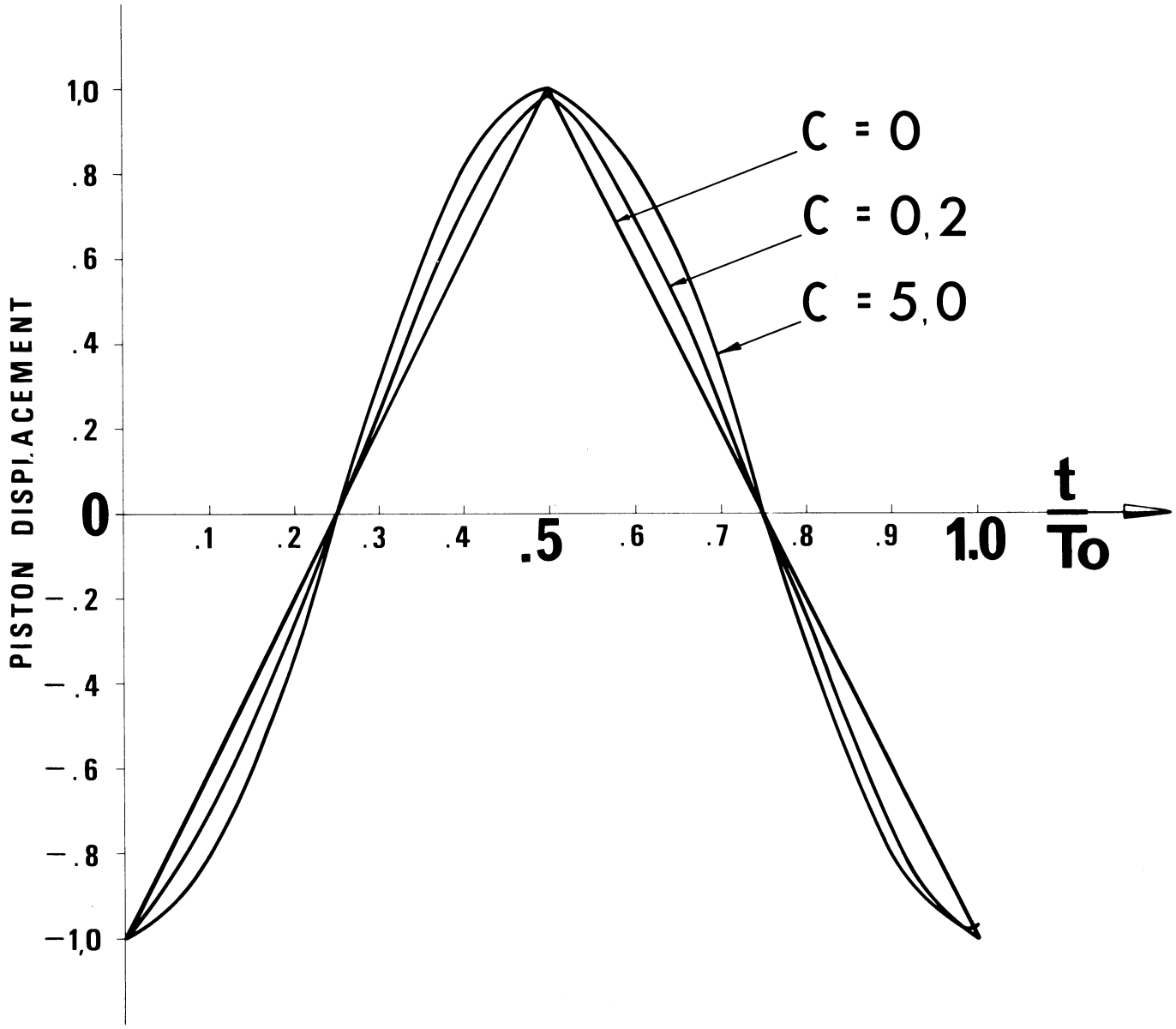

FIG:2

PRESSURE-TIME CURVES

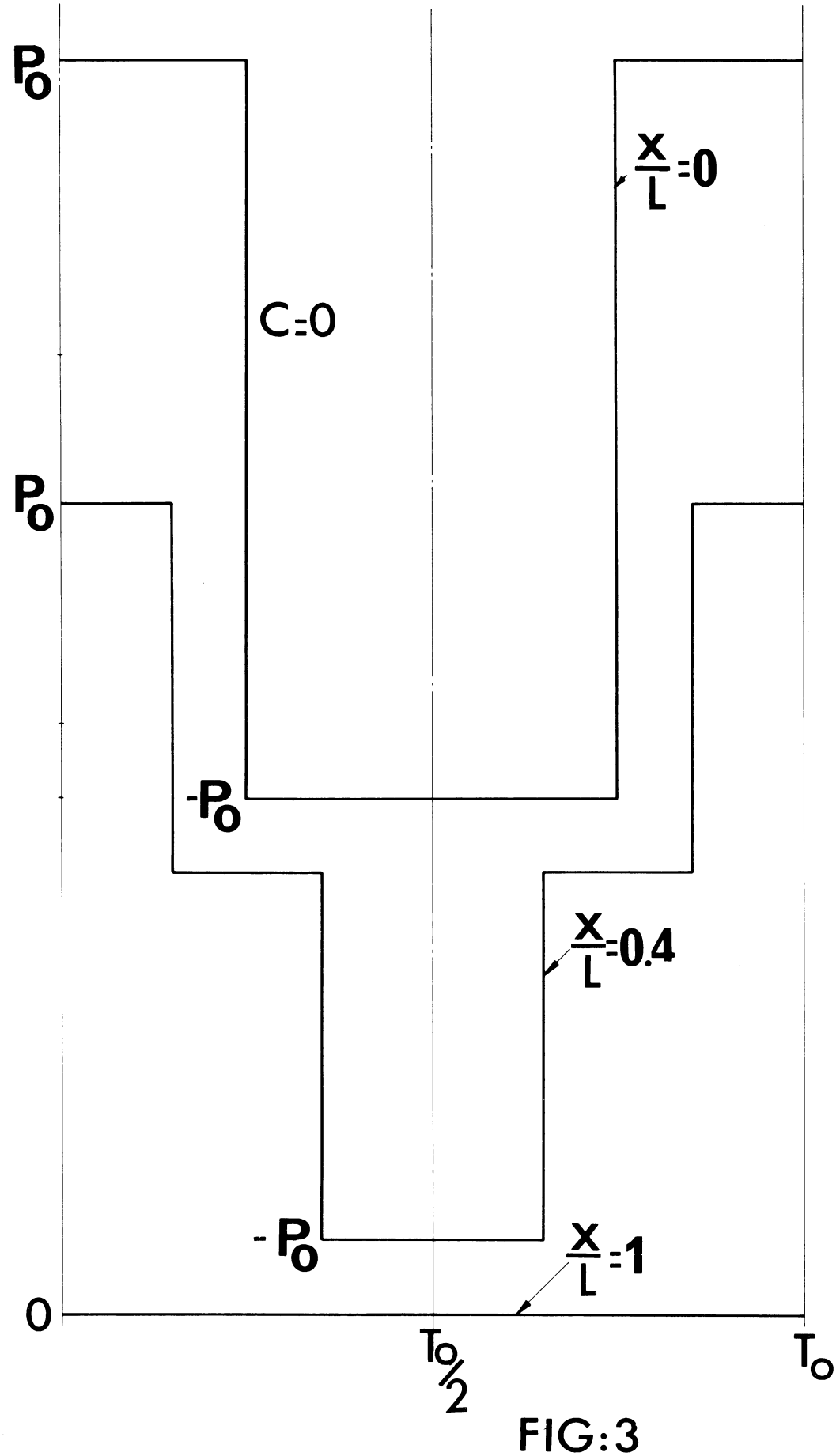

FIG:3

PRESSURE-TIME CURVES

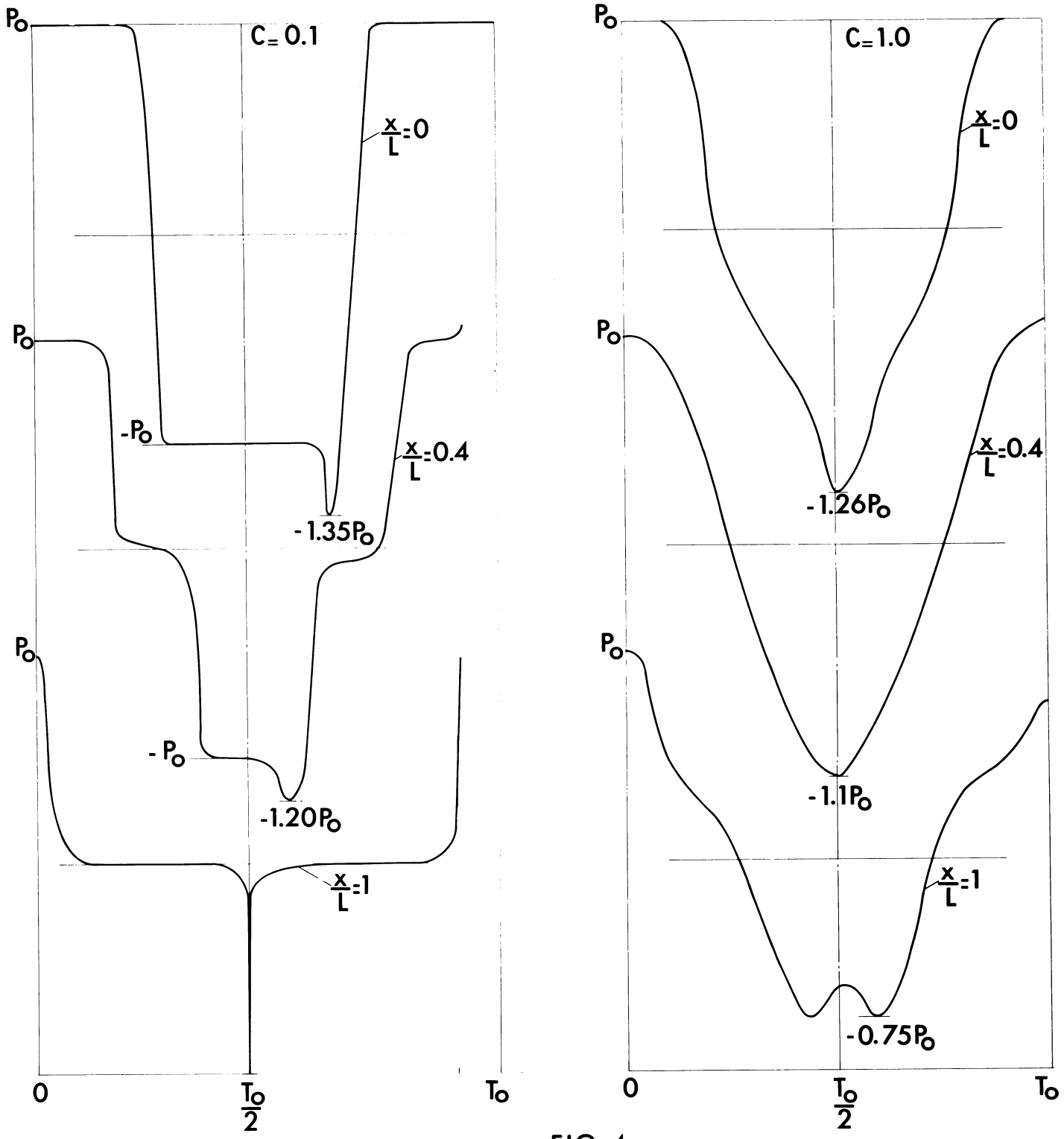

FIG:4

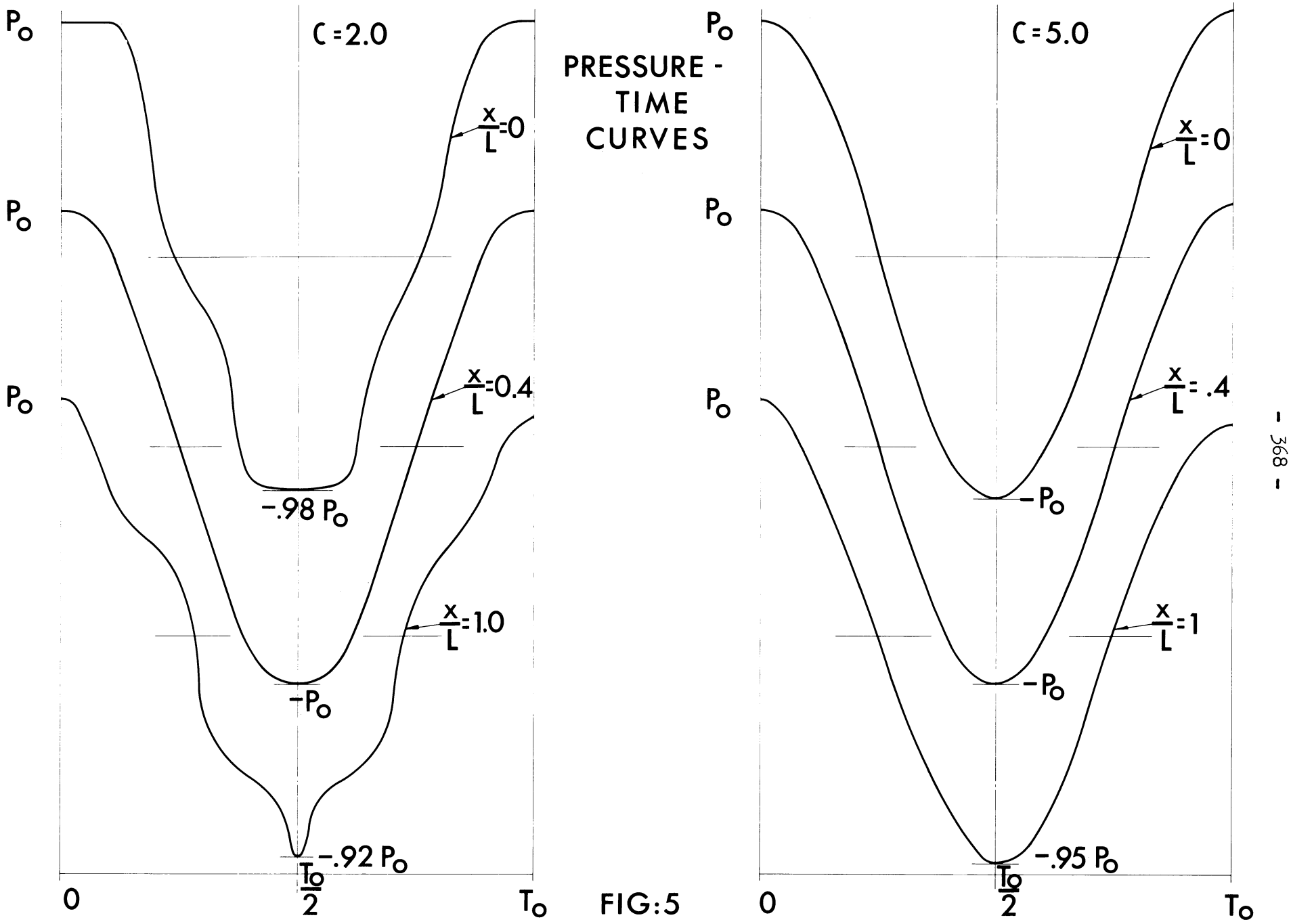
C = 2.0
C = 5.0
PRESSURE - TIME CURVES
P_o
$\frac{x}{L}=0$
$\frac{x}{L}=0.4$
$\frac{x}{L}=1.0$
$\frac{x}{L}=.4$
$\frac{x}{L}=1$
$-.98\ P_o$
$-P_o$
$-.92\ P_o$
$-.95\ P_o$
0
$\frac{T_o}{2}$
T_o

FIG:5

PRESSURE DISTRIBUTION IN THE CHAMBER

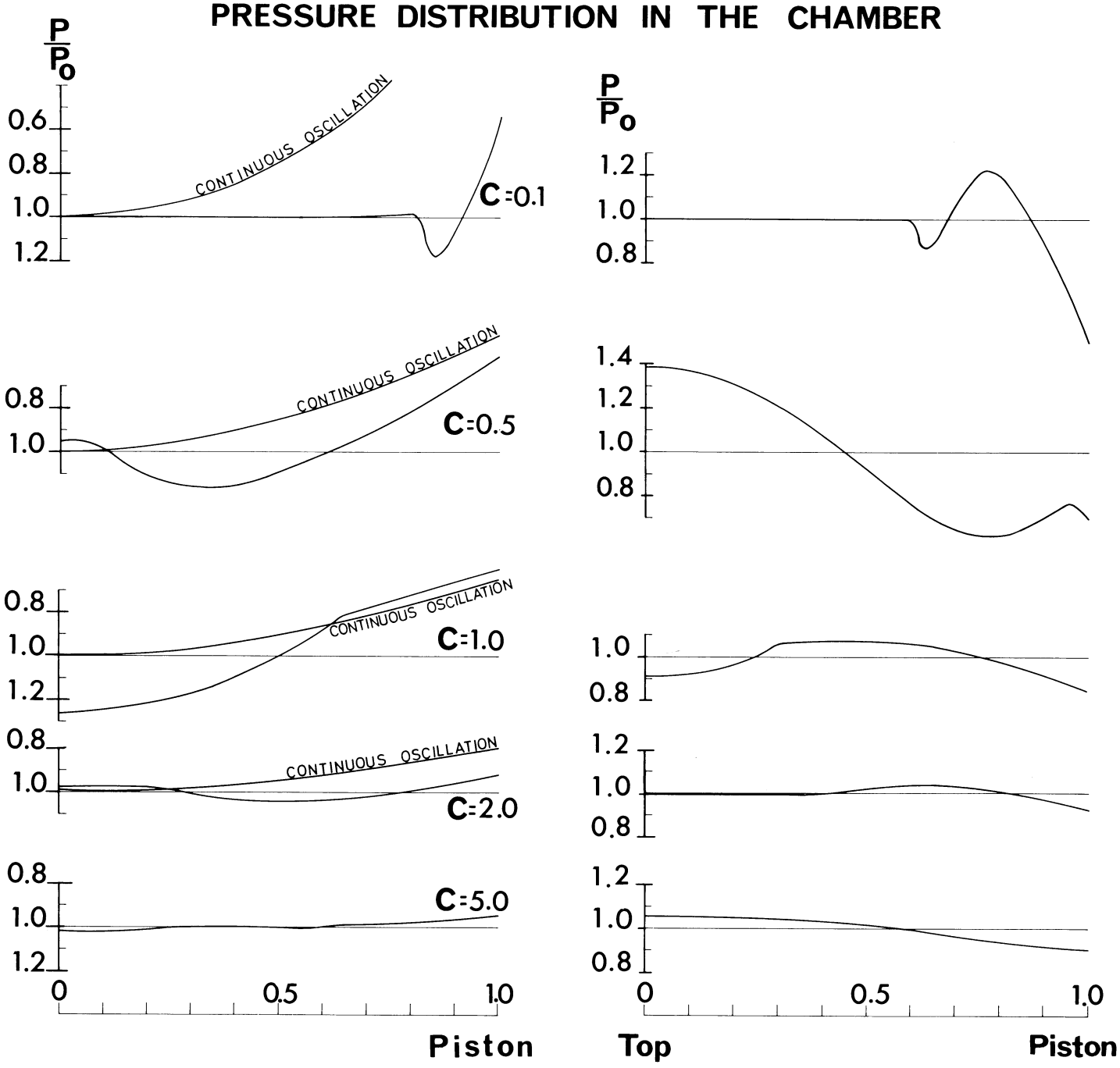

AT TIME $\frac{T_o}{2}$ FIG:6 AT TIME T_o

4.2 POSSIBILITY OF A FAST CYCLING HYDROGEN BUBBLE CHAMBER

J. Badier

Ecole Polytechnique, Paris.

For many bubble chamber projects, a possible improvement is to increase the repetition rate. But the possibility of this operation is not well known. To study this point, an experiment was performed with a 15 cm hydrogen bubble chamber, in collaboration with the "Département Saturne" of Saclay and with the "Ecole Polytechnique - Collège de France" group. Some hypotheses were formulated and will be described here ; they are not yet definitive ; they have to be verified.

It is possible to expand the chamber again as soon as the hydrogen is in the same state as before the preceding expansion. Two effects increase the minimum time between two expansions :

- the remaining inhomogeneities like bubbles and curls ;
- the variations of the pressure and of the mean temperature.

This last effect could be eliminated by a strong refrigeration or by operation with 5 to 15 fast cycled expansions separated by a waiting time of 2 or 3 seconds.

The real problem consists in the remaining bubbles ; they are of three types :

- Useful bubbles (along the tracks) ;
- Spurious bubbles (along gaskets) ;
- Emulsion created by a very strong ebullition (near the piston).

For the useful bubbles, a law was established.

Calling t_o the time of the expansion, p_s the saturation pressure, τ the bubble condensation time, ΔP the overpressure, one has :

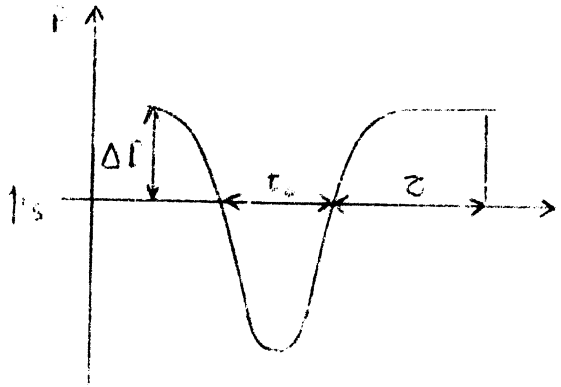

Fig. 1

$$\frac{\tau}{\sqrt{t_o}} = f\ (T\ ,\ \Delta P)$$

τ is little if t_o is little.

The figure 2 is a representation of this law. To minimize τ , it is necessary to operate with an overpressure of 2 atmospheres (4 atm. are preferable ; it is not useful to go higher). It is good to increase the temperature, but, at high temperature, bubbles grow very slowly and optics forbid too little bubbles.

The figure 3 shows the expected bubble radius after 1 msec. A reasonable temperature is 27° K, giving a radius of 100 μ.

Thus a possible set of parameters to operate a fast cycling chamber is :

t_o = 5 msec

ΔP = 4 Atm, T = 27° K) Pressure = 9 Atm.

R_o = 100 μ

N = 40 cycles/s.

The influence of temperature on the extinction of bubbles

was verified (Fig. 4).

For the parasitic bubbles, some observations were made.

The peaks do not create bubbles, but the holes and cracks do. If the depth of the hole is small, bubbles are created at rest.

If the depth is greater, they are created with an initial velocity.

But if the depth is very great, no bubble appear : one may think that they are trapped at the bottom.

The figure 5 shows bubbles appearing near an indium seal and their tracks.

For the creation of an emulsion under the piston, it is striking that greater is the overpressure, greater is the emulsion. It is probably because higher is the temperature above the piston, higher is the temperature under it, the piston being badly isolated.

Now some important modifications are bring to the e xperimental chamber to verify if one obtain a high repetition rate with the given conditions. The exactitude of the precedent laws of evolution of bubbles will be also tested.

If these assumptions were confirmed, a possible apparatus would be a chamber operated at 40 cycles by second. A good choice of size would be 80 cm because it allow a total width of edge less than 0.25 radiation lengths. The adjonction of a system of spark-chambers would then be possible.

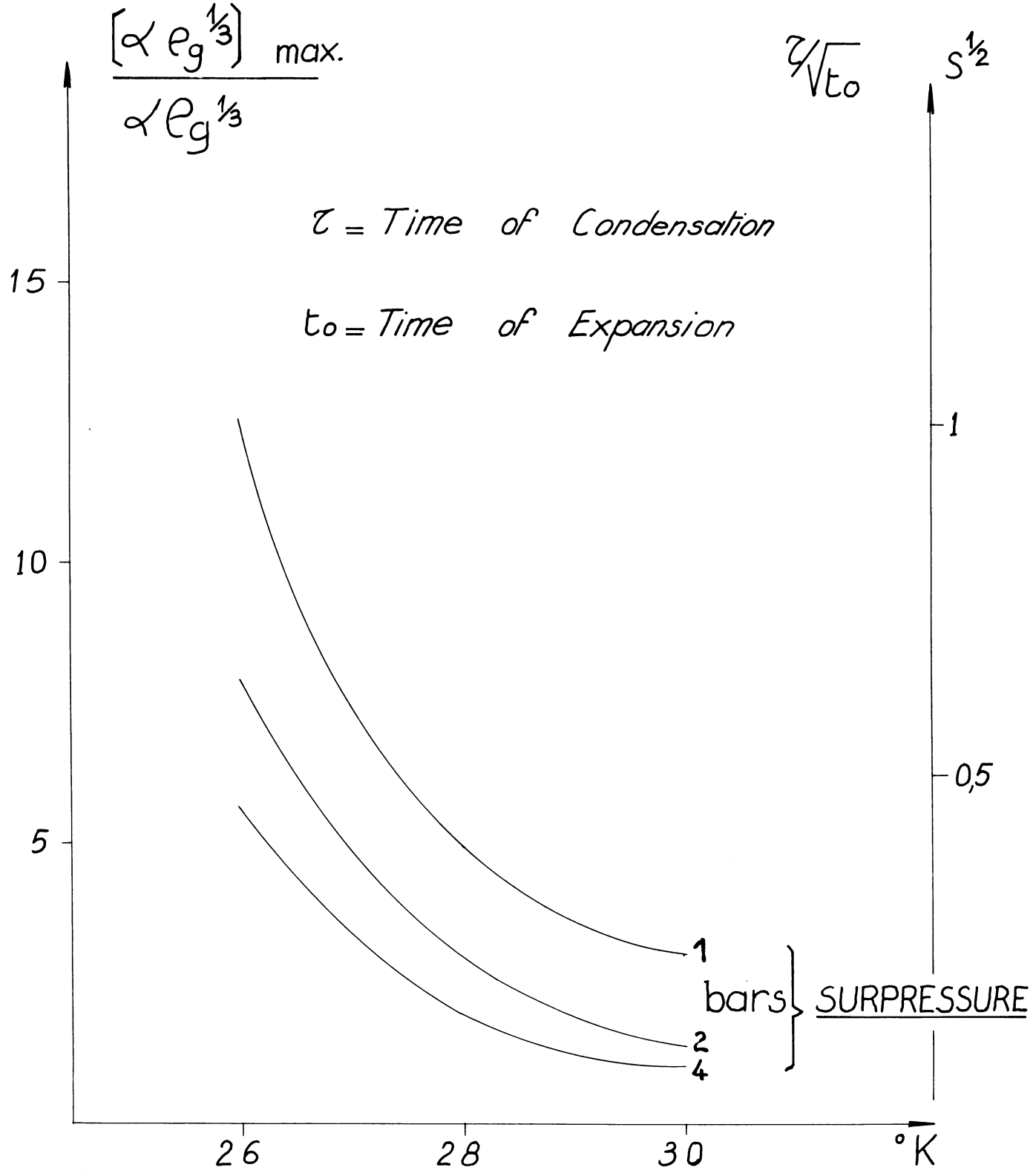
$\frac{[\alpha \rho_g^{1/3}]_{max.}}{\alpha \rho_g^{1/3}}$
$\tau/\sqrt{t_o}$
$s^{1/2}$
τ = Time of Condensation
t_o = Time of Expansion
15
10
5
1
0,5
1
2
4
bars
SURPRESSURE
26
28
30
°K

Fig. 2

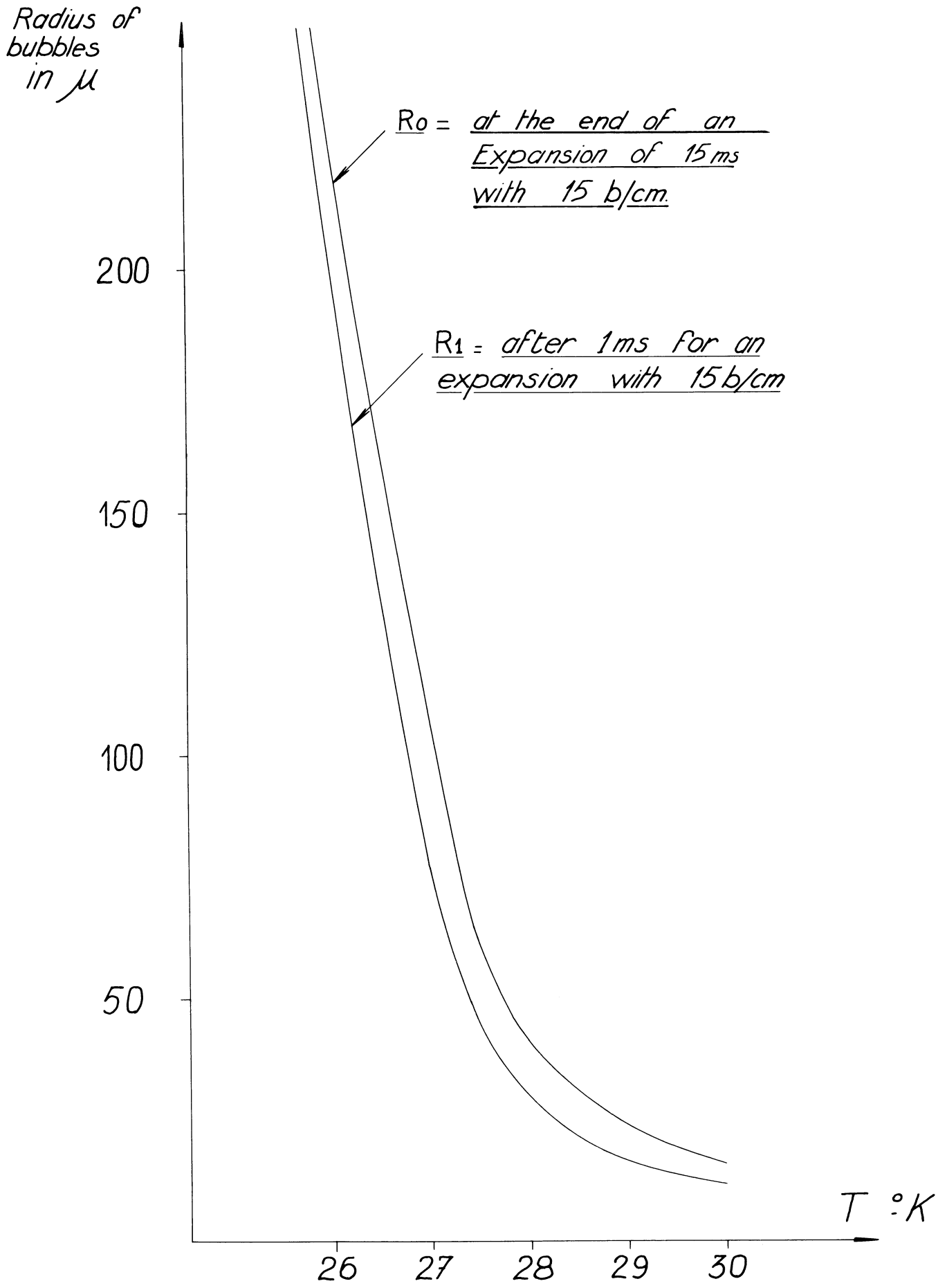
Radius of bubbles in μ
200
150
100
50
R0 = at the end of an Expansion of 15 ms with 15 b/cm.
R1 = after 1 ms for an expansion with 15 b/cm
T °K
26
27
28
29
30

Fig. 3

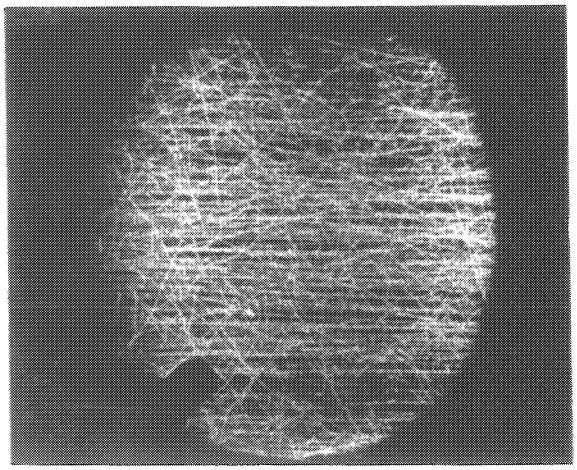

t = 0 msec

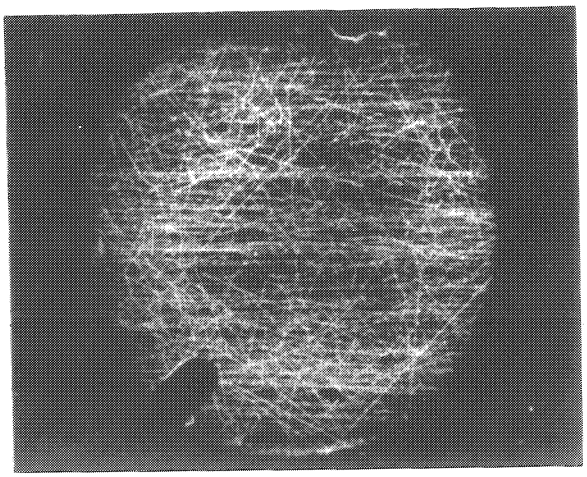

t = 4 msec

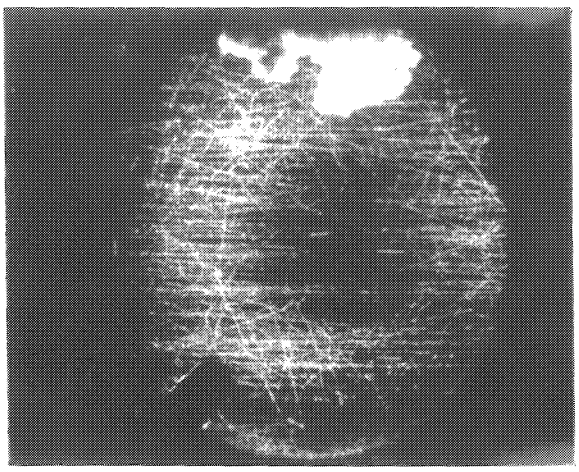

t = 8 msec

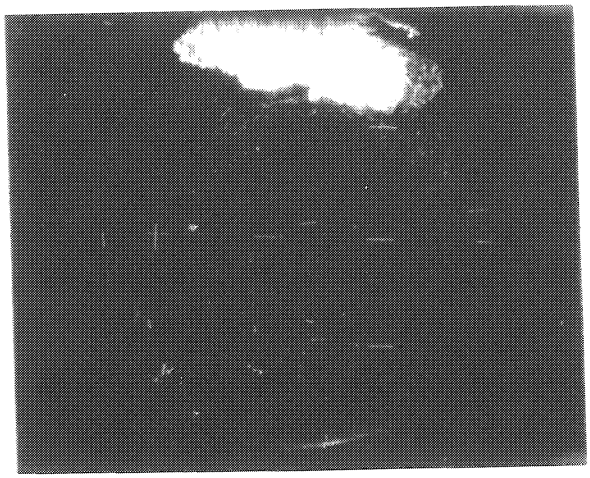

t = 16 msec

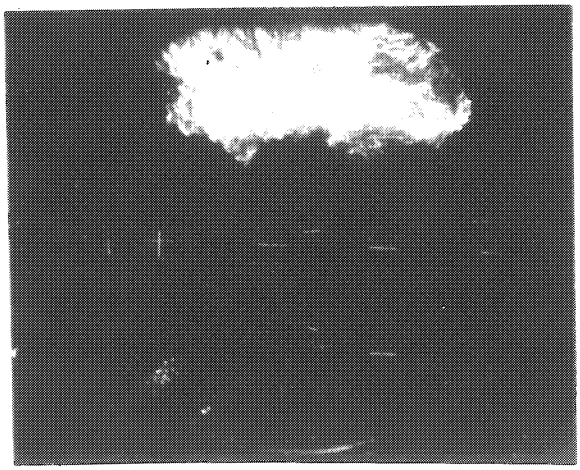

t = 32 msec

Fig. .4

Disparition des bulles - température : 29,2 ° K
(surpression - 5 kg).

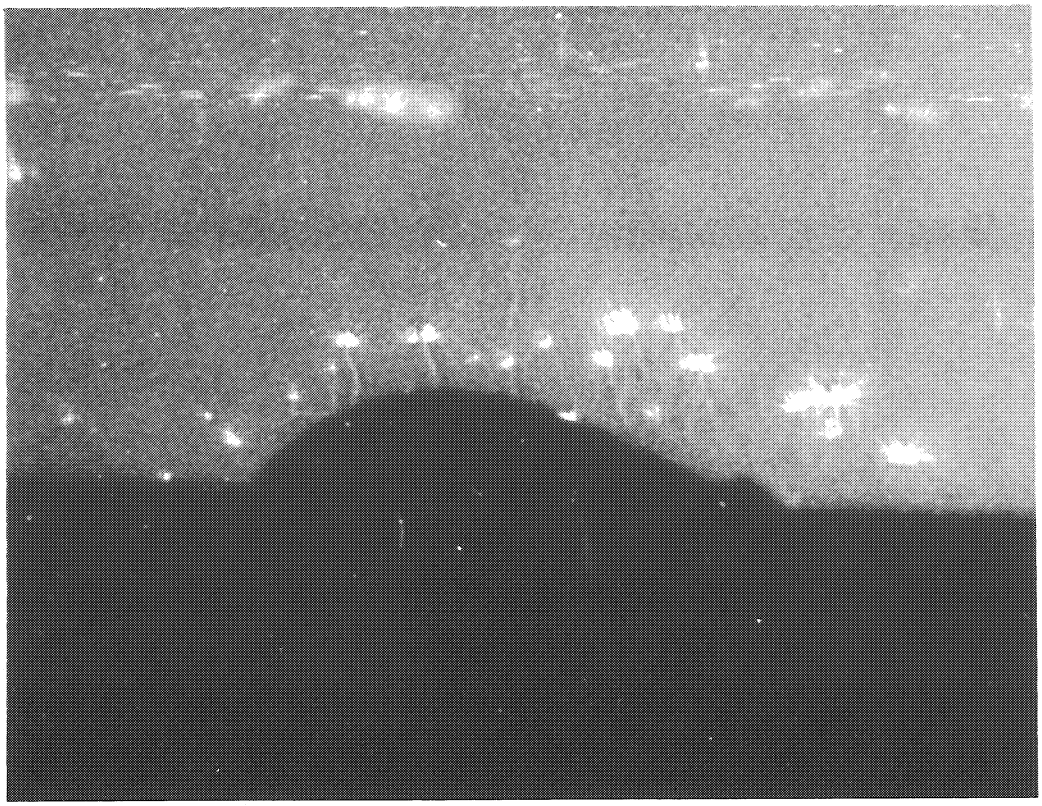

Fig. 5

4.3 SPECIAL DEVICES FOR A FAST CYCLING HYDROGEN BUBBLE CHAMBER

Ch. Gregory

Ecole Polytechnique, Paris.

The apparatus with the 15 cm (6 liters) utilized by Dr. Badier has been modified with a view to allow a verification of his calculations. In order to answer the conditions required by these calculations, it was necessary to modify the thermal regulation, the optic and the cameras, and the expansion system.

The expansion system has been fitted to the new sixty liters chamber. The motor cylinder serves now as an energy regenerator. On the top part, a pneumatic locking device has been added, and a self-exhausting cylinder which supplies the energy lost during each to-and-fro movement.

The operation is the following (see fig. 1) :

At the initial time, the locking pressure P_ℓ is on top of the locking piston, under the locking piston, there is no pressure since the outlet is open by the mean of the distributor-spool shaped shaft. The locking force is : $P_\ell \times S_\ell$.

The inlet of the self exhausting cylinder is open by the mean of another distributor-spool shape on the shaft. If one opens the admitting valve, the pressure increases and creates an increasing force $P_e S_e$.

In the motor cylinder, the spring force $(P_1 - P_2) S$ is constant.

As soon as

$$(P_1 - P_2) S + P_e S_e - P_\ell S_\ell$$

becomes negative, the shaft moves with a small acceleration, but the tightness provided by the initial position of the locking piston disappeares, at the same time the outlet closes. $P_\ell S_\ell$ disappears completly within a very short time. The total initial acceleration will be :

$$\frac{(P_1 - P_2) S + P_e S_e}{m} \sim 3 \cdot 10^3 \text{ ms}^{-2}$$

At half the travel of the shaft, the exhausting piston comes out of the cylinder, which allows the quick release of pressure P_e. At this moment, the speed is maximum.

The spring force in the motor cylinder absorbing and restoring the kinetic energy allows the shaft to come back to the initial position with a low speed.

As soon as the seal is obtained by the locking piston on the gasket, the outlet, open again, allows the quick release of pressure P_ℓ under the locking piston. The locking force is then P_ℓ S_ℓ again.

If one maintains the admitting valve open, another expansion will be trigged again by the increasing pressure in the self exhausting cylinder. This allows to operate at a frequency which depends only on the flow, the number of expansions depending on the flow and on the admission time.

We made a model which operates up to frequency of 45 per second, the time of the total expansion movement was about 12 millisecond, whith a stroke length of 20 millimeters.

The unic valve used calibrates the admission time.

The measurements made with a pressure gadge may be seen on figure 1.

To be able to photograph bubbles of a 100 microns radius, we choosed to begin with the usual dark field illuminating system, with two vertical and parallel windows (Fig. 2).

However, another chamber with one horizontal window at the bottom has been studed (Fig. 3).

Things have been done to make easy the setting of either one

or the other.

To photograph bubbles, we will use two types of cameras. The first one, normal, will allow one photograph at each pulse of the synchrotron Saturne. The second one, has been studed to be capable of about thirty double stereo photographs up to a frequency of 50 per second.

Each translation is trigged b a pneumatic valve.

Besides, in order to be able to form a better notion of the evolution of bubbles, we studed a camera which can take ten photographs to a frequency of five hundred to one thousand per second.

A pneumatic valve trigges the translation of 10 little mirrors. The film does not move. The resolution power is about 8 microns. The depth of focus is little. A white field illuminating system will be used.

Because of the operating temperature of 27° K and of the pressure of 4 atmosphers above the piston, the chamber has been constructed so, that it can operate at a pressure of 10 atmosphere (Fig. 4).

To operate with an overpressure of 4 atmosphers without ebullition under the piston, the illuminated volume, the space under the piston and the space above the piston, are as thermaly insulated as possible.

Because of spurious bubbles, we took care to avoid holes and slits, particularly at the window gaskets. The tightness is obtained by an indium gasket between the chamber and the glass. An inflatable ring is outside (Fig. 5).

The setting of the different parts is already begun on the experimental area of Saturne at Saclay. We still hope to put hydrogen in the chamber during the beginning of July.

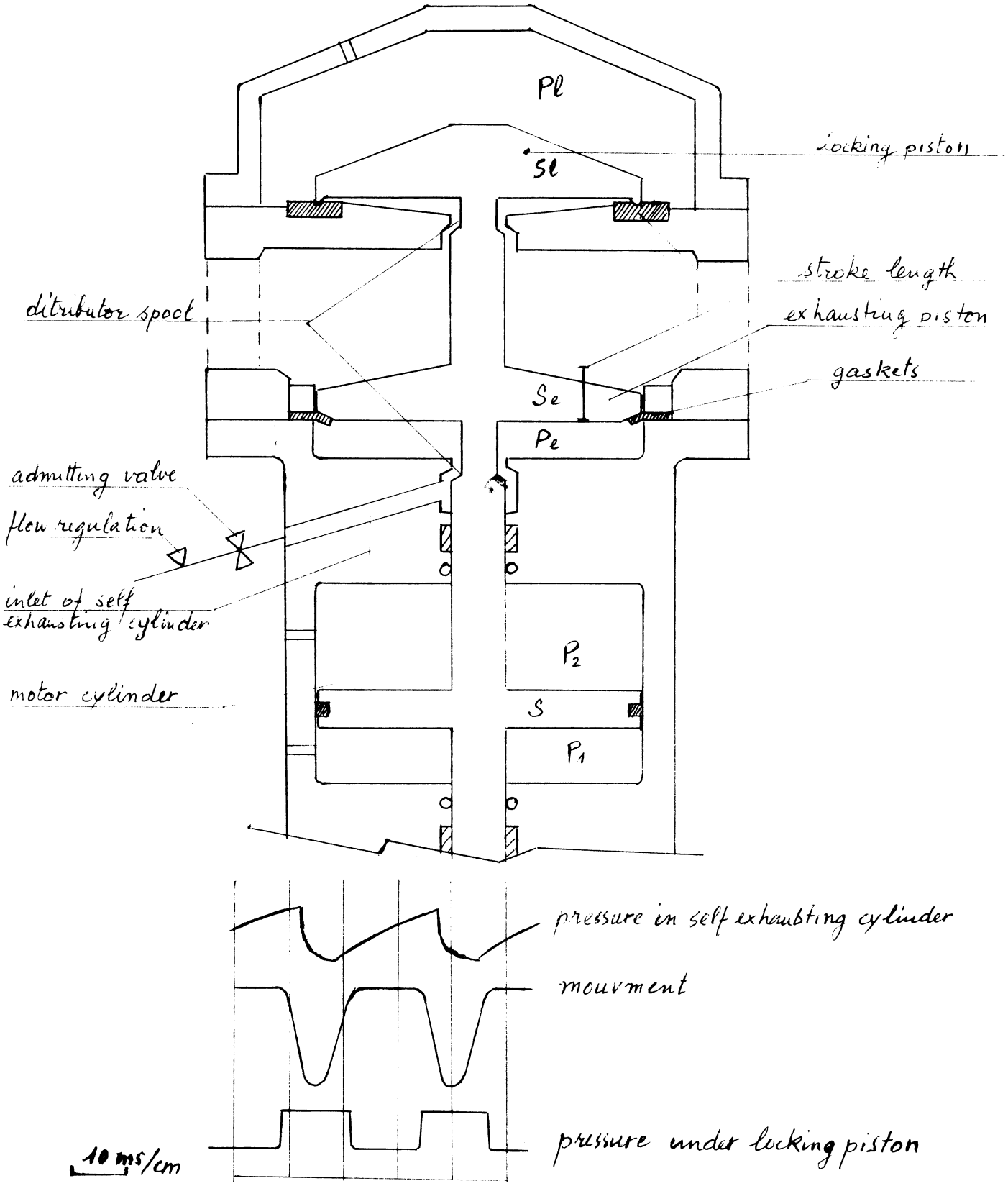
Pl
locking piston
Sl
stroke length
exhausting piston
distributor spool
gaskets
Se
Pe
admitting valve
flow regulation
inlet of self exhausting cylinder
motor cylinder
P2
S
P1
pressure in self exhausting cylinder
mouvment
pressure under locking piston
10 ms/cm

Fig. 1

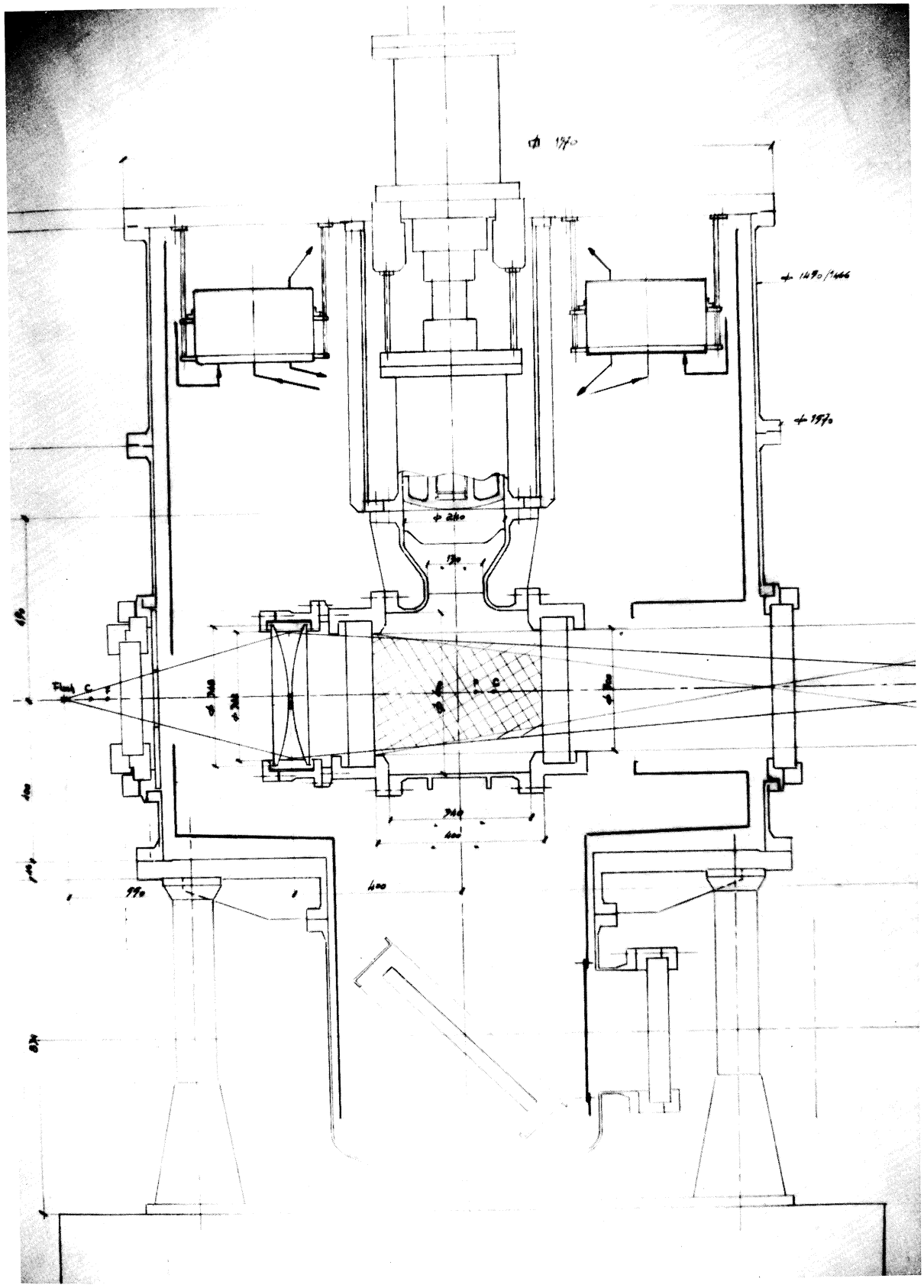

Fig. 2

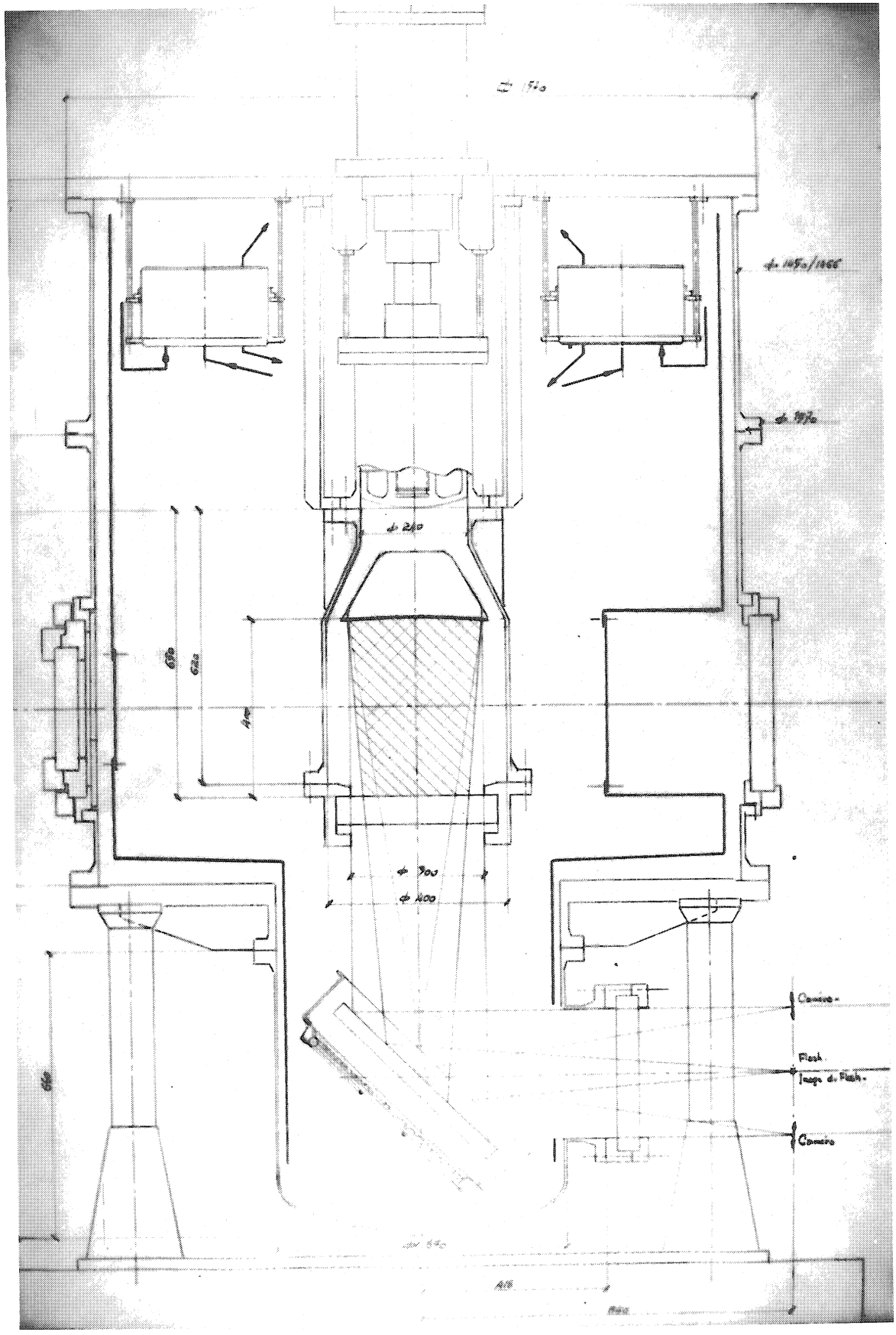

Fig. 3

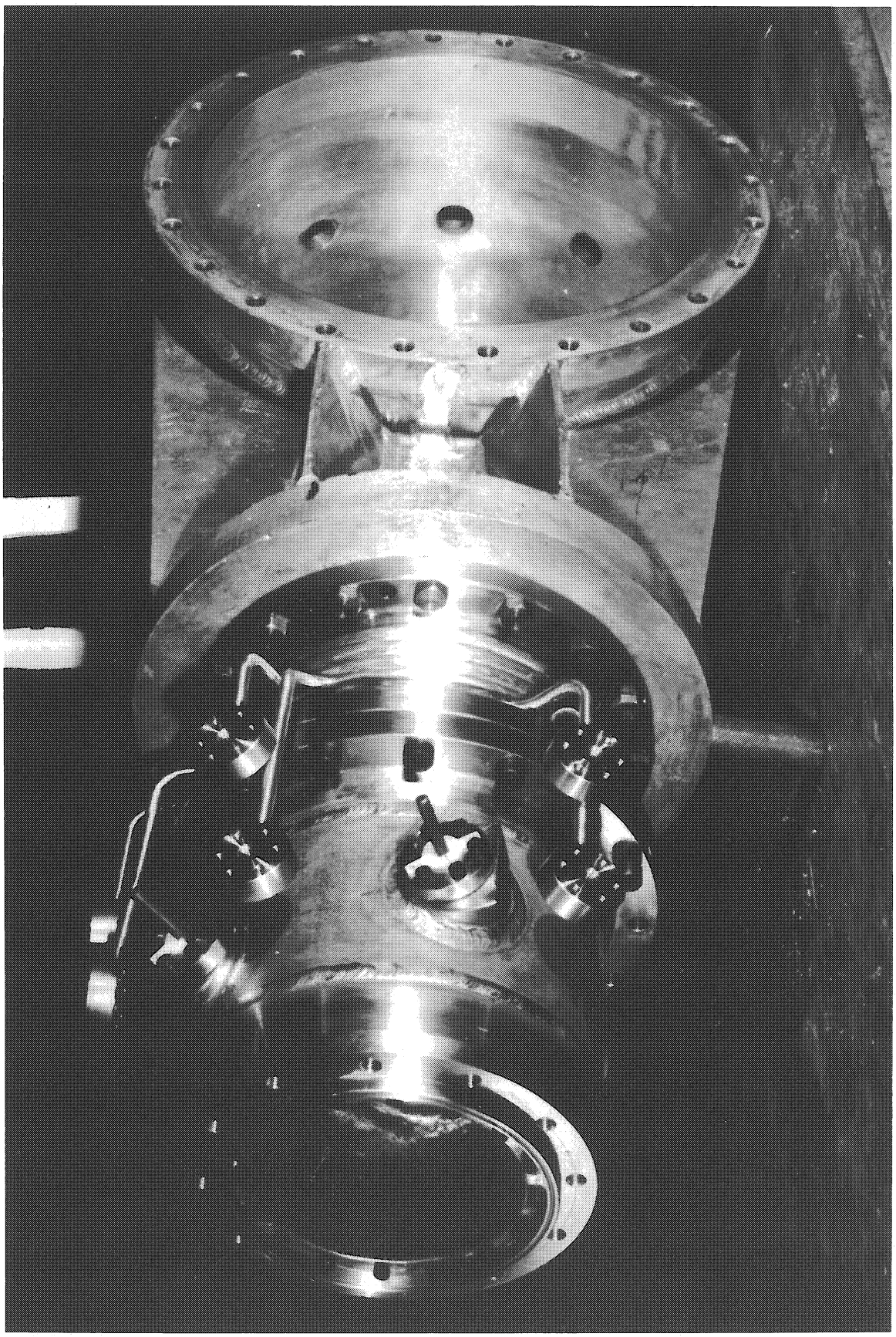

Fig. 4

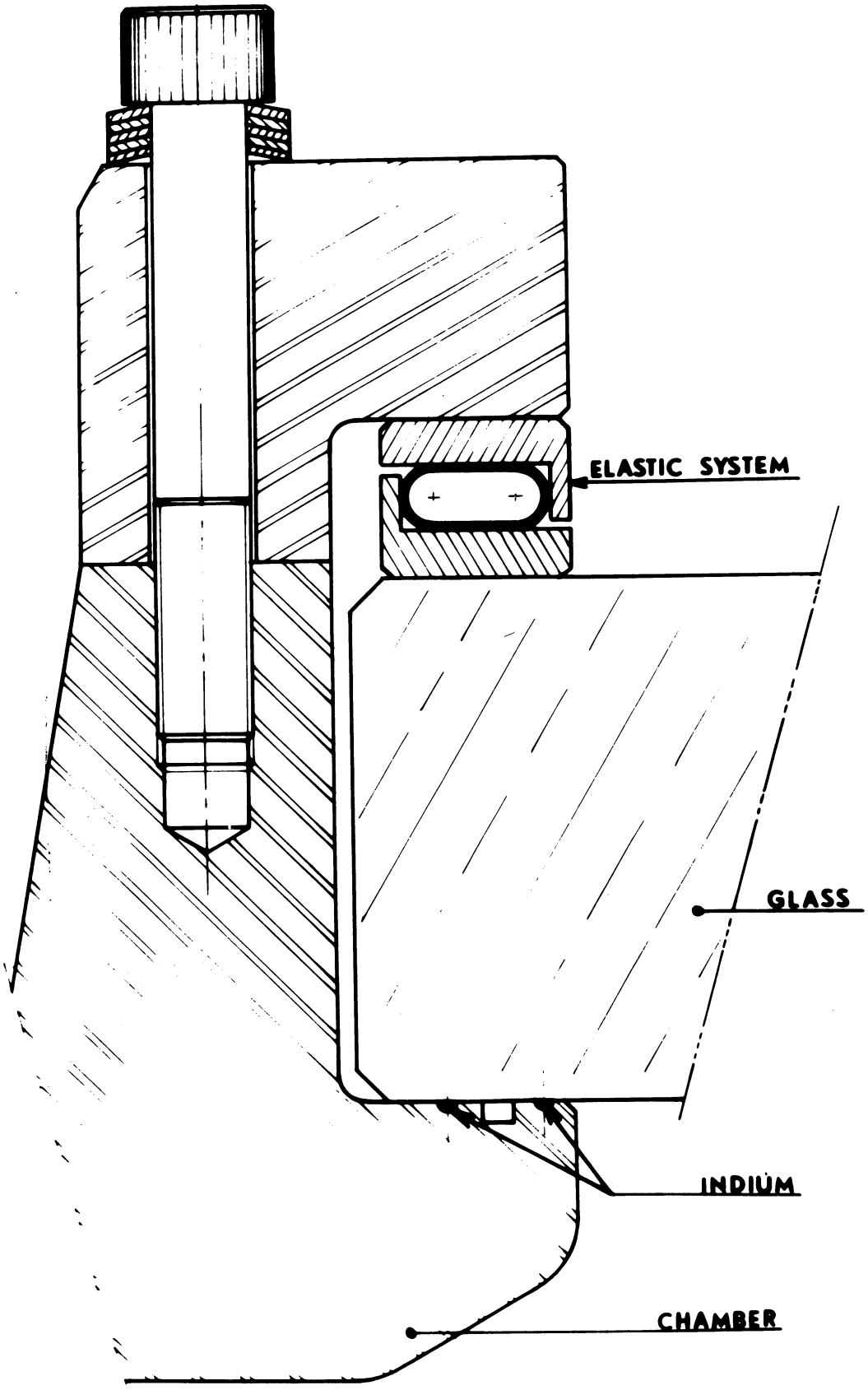

Fig. 5

4.4 ON THE FORMATION OF BUBBLES IN LIQUID HYDROGEN

G. Harigel*, G. Horlitz and S. Wolff

Deutsches Elektronen-Synchroton,
DESY, Hamburg.

Abstract

Photographs of the tracks of electrons having energies around 2 GeV have been taken in the DESY 85-cm Bubble-chamber with a scale-one optical system in bright field illumination. Growth and recompression of bubbles as well as bubble densities have been observed between 24.5 and 28.0 ^{o}K. Bubble sizes as a function of time have been measured at different temperatures, with expanded pressure and overpressure as varying parameters.

A summary is given of the experimental results, as well as a comparison between different theories on the behaviour of bubble growth and recompression; a more detailed account can be found in reference 1.

Theory of Bubble Growth

The problem of bubble growth has been treated theoretically by several authors [2, 3, 4].

For the speed of bubble growth as function of time t at constant pressure, Plesset and Zwick [3] have given the following expression:

$$(1) \quad \frac{dR}{dt} = \sqrt{\frac{3}{\pi}} \frac{\sqrt{k \cdot c_p \cdot \rho_l}}{L \cdot \rho_v} \cdot (T_l - T_v) \frac{1}{\sqrt{t}}$$

$$= \frac{1}{2} \cdot A \cdot \frac{1}{\sqrt{t}}$$

with k = thermal conductivity

c_p = specific heat of the liquid at constant pressure

---

* Now in the Study Group for a Big European Bubble Chamber (CERN)

ρ_l = density of the liquid
ρ_v = density of the vapor in the bubble
L = latent heat of vaporization
T_l = temperature in the liquid at large distance from the bubble
T_v = temperature of the vapor inside the bubble
R = bubble radius

The temperature T_v in the bubble is the equilibrium vapor-pressure temperature which corresponds to the instantaneous pressure p_d (dynamical pressure) in the liquid.

If p_d does not depend on time, one can integrate this equation under the assumption that thermodynamical equilibrium in the bubble is always established within time intervals which are short compared to the time in which the bubble radius is noticeably changed. One obtains for the bubble radius

(2) $R = A \cdot \sqrt{t}$

Since under normal operation conditions the pressure p_d varies with time, Equation (2) cannot be compared with the experimental results directly. Taking into account this pressure variation, A becomes a function of time ($A \longrightarrow A(t)$) and one must write instead of (1),

(1a) $\frac{dR}{dt} = \cdot \frac{1}{2} \cdot A(t) \cdot \frac{1}{\sqrt{t}}$

Another deviation from ideal conditions is caused by the bubbles moving upwards under the force of gravity towards regions at the initial temperature of the liquid T_l. This effect leads to corrections which have been calculated by Aleksandrov et al.[5].

For a comparison between theory and experiment one has to measure the following parameters:

$R(t)$

$p_d(t)$

T_l

Experimental Arrangement

Our experimental arrangement is shown in Fig.1. The DESY bubble chamber - with the dimensions 85 x 40 x 40 cm^3 - is normally equipped with three cameras each having a photographic lens stopped down to F = 32. One of these cameras was removed to a distance of about 3 m from the center of the bubble chamber and gave bubble photos of scale 1:1 with a telephoto lens of 800 mm focal length. The two normal cameras were illuminated by two linear flashes of 120 Joules and about 100 μs half-widths. They were focussed at a space beside the cameras by a condensor lens for dark field illumination. For the 1:1 camera we reduced the flash to 10 Joules and about 10 μs half-width. The image of this flash was focussed into the camera lens because the relation between the diameter of the bubble and that of the image is better defined in bright field illumination.

The fourth camera was a television camera having a zoom lens [6]. This camera very rapidly gave information about the conditions in the chamber. Fig.2 shows a typical television picture.

The instanteneous pressure $p_d(t)$ in the chamber was measured using a piezoelectric quartz gauge located at the bottom of the chamber. The amplified signal was displayed and photographed on the screen of an oscilloscope.

Fig.3 shows a typical pressure curve. The expansion cycle starts from a static pressure p_s which is higher than the equilibrium vapor pressure p_v, passes through a minimum p_{min} at the time $t(p_{min})$, and comes back to its initial value. For investigating the bubble growth and recompression, the particles were injected at $t(p_{min})$. For the bubble density investigations, the electrons were injected at different times before that moment.

Fig.4 shows some photographs of bubbles taken at different times after beam injection. It should be mentioned that we did not photograph one individual bubble at different times. Assuming that, under equal thermodynamical conditions, the behaviour of the bubbles

is exactly reproducible, we took a number of photographs at each fixed flash delay (time interval between injection and flash triggering). For each set of parameters we measured the diameters of about 20 bubbles.

Temperature was determined by means of hydrogen vapor pressure thermometers.

Experimental Results

Fig.5 shows bubble radii as a function of time for $t < 4$ ms at temperatures between 24.5 and 28.0 ^{o}K. A comparison with theory is given in Fig.6 for one of our measured curves. Curve (a) represents the experimental points empirically fitted by

(3) $R = (A' + B \cdot t) \cdot \sqrt{t}$

A' corresponds to A in Formula (1), B is an empirical parameter which approximates the time dependance of the parameters due to the variation of pressure. One expects $B \lesseqgtr 0$ for $\frac{dp}{dt} \gtreqless 0$.

Curve (c) is calculated from (1a) using the measured pressure in the chamber.

Curve (d) is calculated taking into account the ascent of bubbles.

A comparison of all our measurements with theory is given in Fig.7. This picture shows the relative differences between measured and calculated bubble growth parameters A(0), i.e. the initial bubble growth parameters derived from our measurements. The agreement is reasonable within our experimental errors; no significant systematic deviations could be found. The numbers assigned to the measured points correspond to the numbers of the curves in Fig.5.

Fig.8 shows the factor A(0) as a function of temperature, with the bubble density being the parameter. The rate of bubble growth at constant bubble density increases with decreasing temperature, which is important for practical applications.

Fig. 9 represents the total life of a bubble from its origin to complete recompression. For making rough estimates we have approximated the time dependence of bubble radius during the period of recompression by a straight line which allows the determination of recompression time with a maximum error of about 50 per cent. Within our parameter variations this time of recompression is mainly influenced by the amount of overpressure ($p_{over} = p_s - p_v$).

Several approaches have been made to calculate the time of recompression from the parameters in a bubble chamber [5, 7]. A modest agreement of our measurements could be found with calculations of Aleksandrov et al.[5], which were made supposing that the heat transport limits the speed of recompression and which took into account the bubble movement due to gravity. Other solutions of the problem neglected ascent or were based on inertial forces; they yielded collapse times which differed by an order of magnitude from our experimental results.

Fig. 10 shows bubble densities in a p-T diagram. We measured bubble densities between 0 and about 35 bubbles per cm. The curve of sensitivity is found to lie about 2 kp/cm^2 below the equilibrium vapor pressure curve. Since the expansion system of our chamber did not allow expansion ratios of more than about 1 per cent, no serious attempt could be made to reach the foam limit.

Conclusions

Our measurements show that heat transfer plays the predominant part in the process of bubble growth, in accordance with the theory of Plesset and Zwick. If we take into account the time dependence of parameters we find reasonable agreement between calculations and measurements for small growth-times. For constant bubble densities the velocity of bubble growth increases rapidly with decreasing operating temperatures of the chamber. Heat transfer is also predominant in bubble recompression, whereas inertial forces seem to be negligible. The ascent of bubbles has been shown to be of great importance in the case of recompression; a rough agreement with the theoretical predictions by Aleksandrov et al. has been found.

References

1. G.Harigel, G.Horlitz, S.Wolff, DESY Report 67/14.
2. M.Volmer, Kinetik der Phasenbildung. Dresden 1939.
3. M.S.Plesset, S.A.Zwick, J.Appl.Phys. 25, 493 (1954)
4. H.K.Foster, N.Zuber, J.Appl.Phys. 25, 474 (1954)
5. Yu.A.Aleksandrov, G.S.Voronov, N.B.Delone, Pribory i Tekhnika Eksperimenta, No.2, 41 (1963)
6. Erfahrungen bei der Verwendung einer Fernsehkamera zur Beobachtung von Blasenkammer-Spuren. DESY-B1-. 1966. Internal Report, unpublished.
7. L.W.Florschütz, B.T.Chao, Journal of Heat Transfer, 209 (1965)

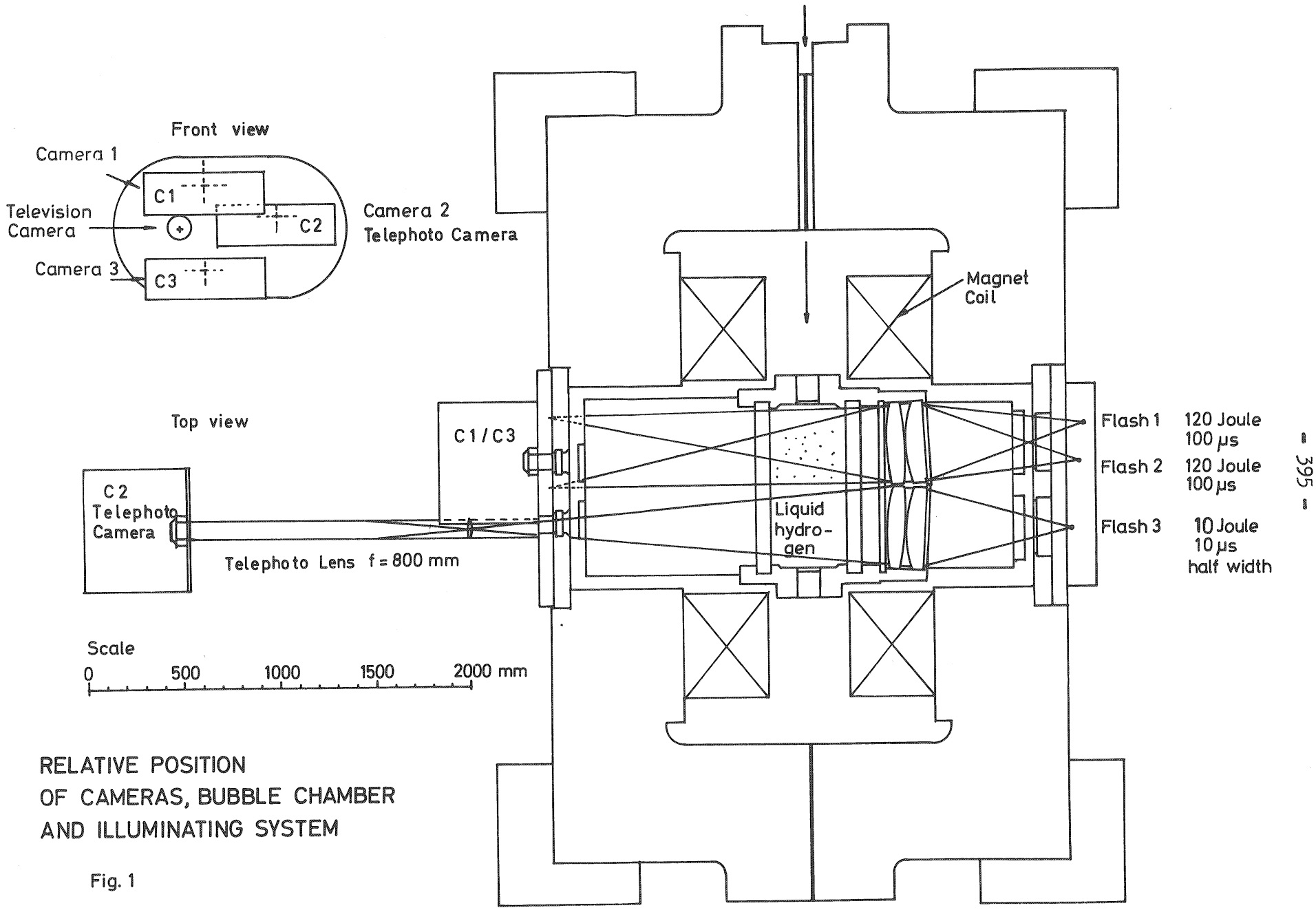

RELATIVE POSITION
OF CAMERAS, BUBBLE CHAMBER
AND ILLUMINATING SYSTEM

Fig. 1

Bubble Track Photographs Taken from the Television Screen

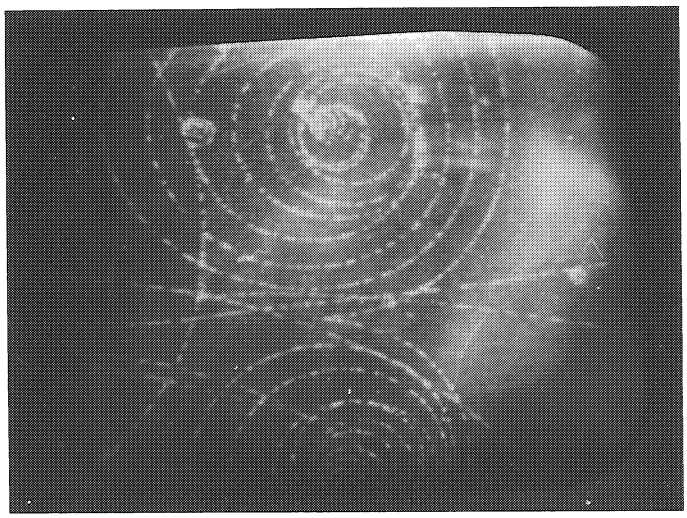

f = 240 mm

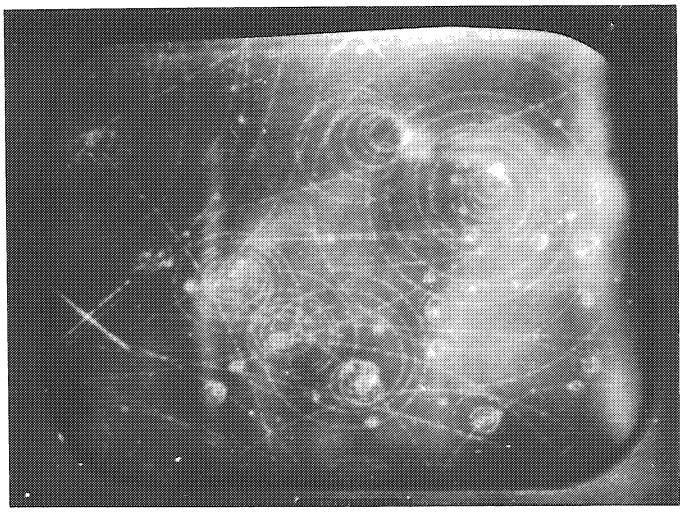

f = 150 mm

Fig. 2

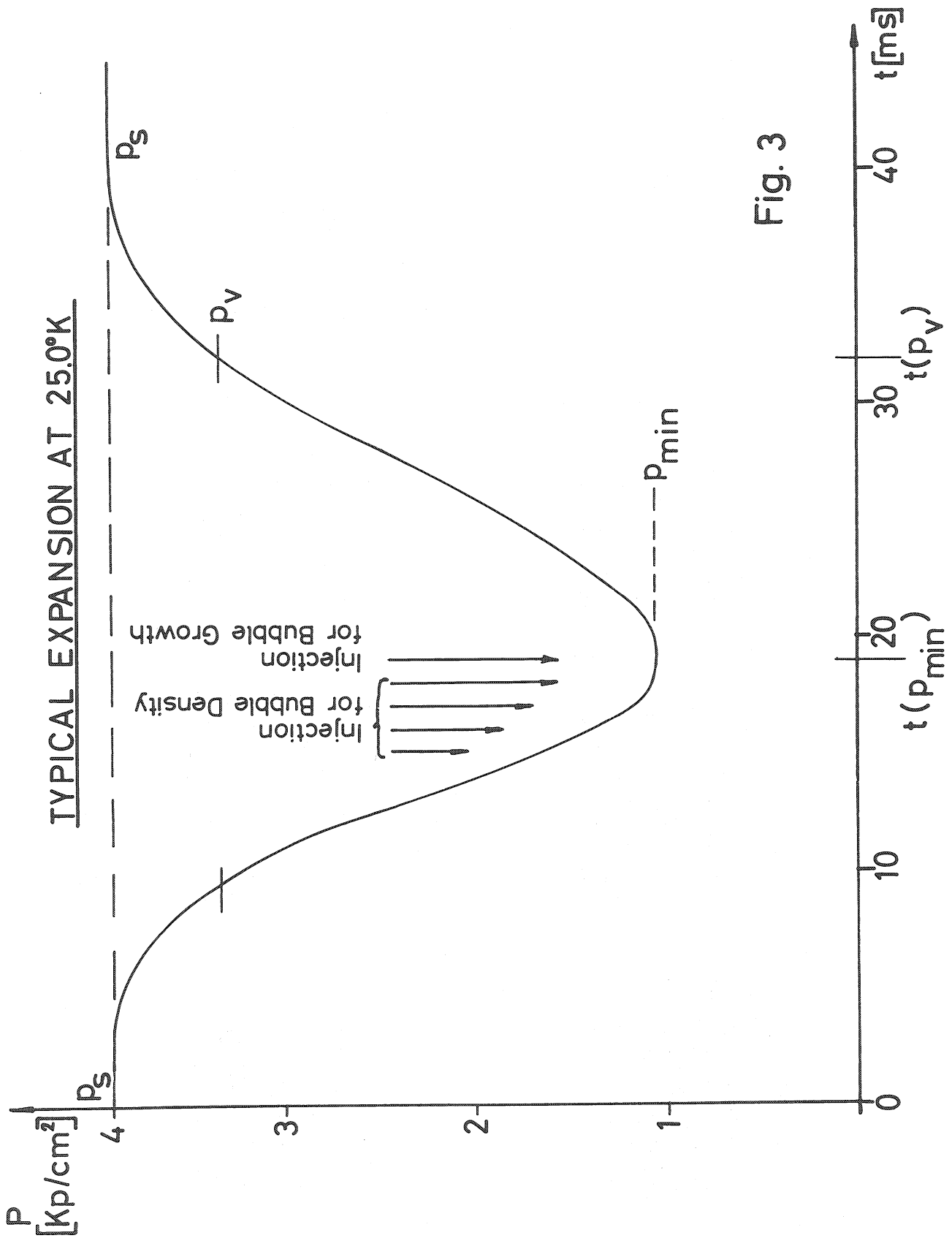
TYPICAL EXPANSION AT 25.0°K
P [kp/cm²]
p_s
p_v
p_{min}
Injection for Bubble Density
Injection for Bubble Growth
t [ms]
t (p_{min})
t (p_v)
0
10
20
30
40
1
2
3
4

Fig. 3

Typical Photographs of Bubble Growth at Different Flash Delays

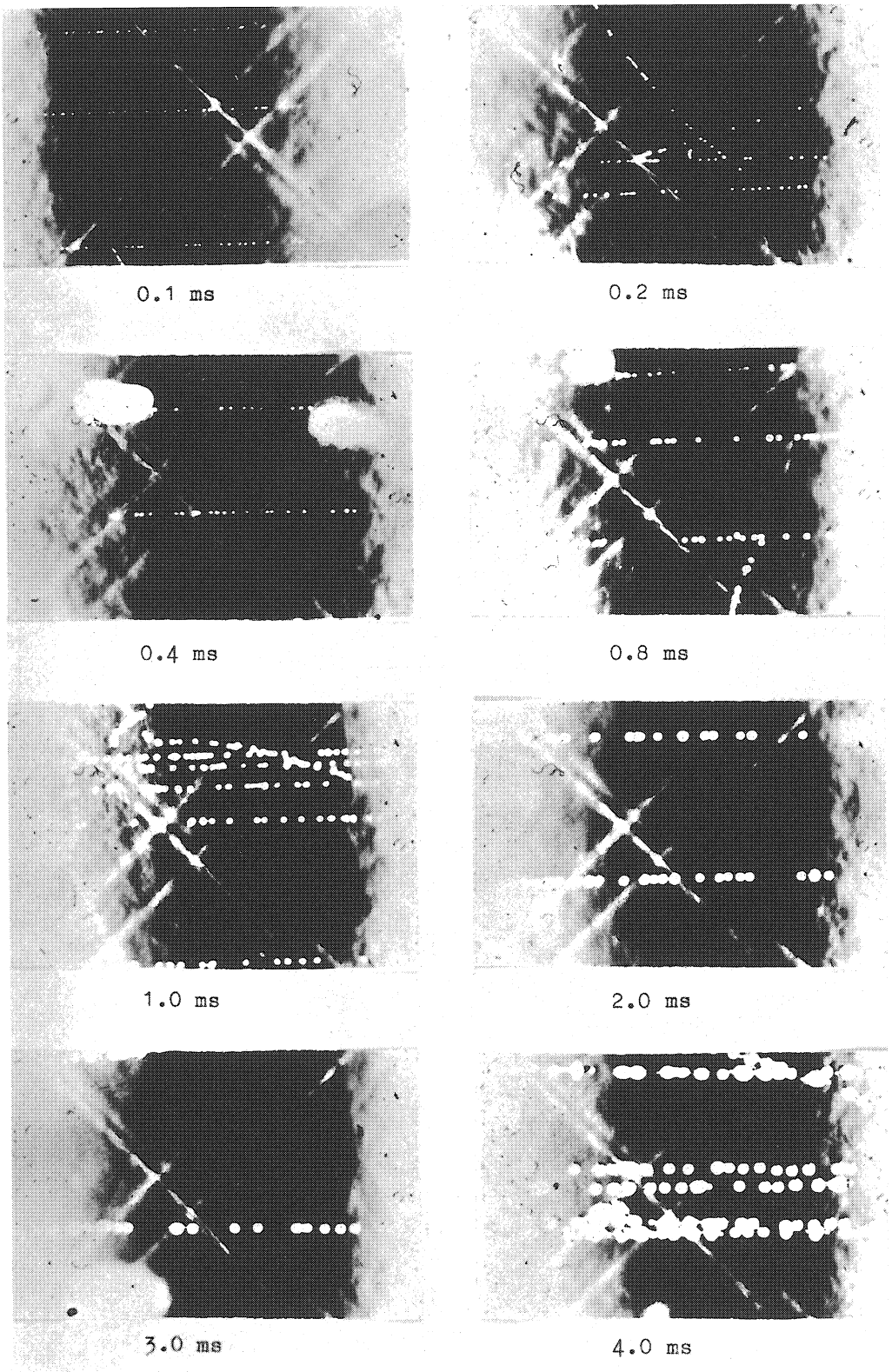

Fig.4

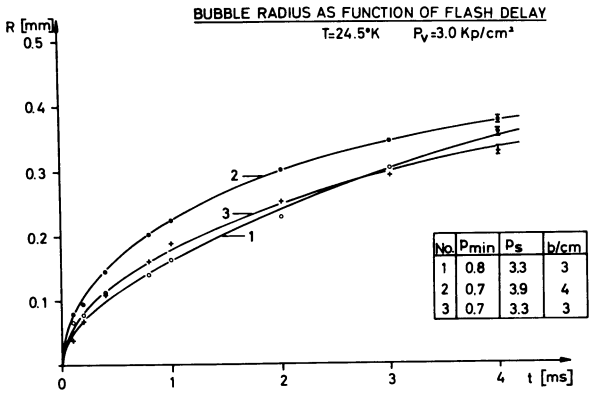
BUBBLE RADIUS AS FUNCTION OF FLASH DELAY
T=24.5°K Pv=3.0 Kp/cm²
R [mm]
t [ms]
1
2
3
No. Pmin Ps b/cm
1 0.8 3.3 3
2 0.7 3.9 4
3 0.7 3.3 3

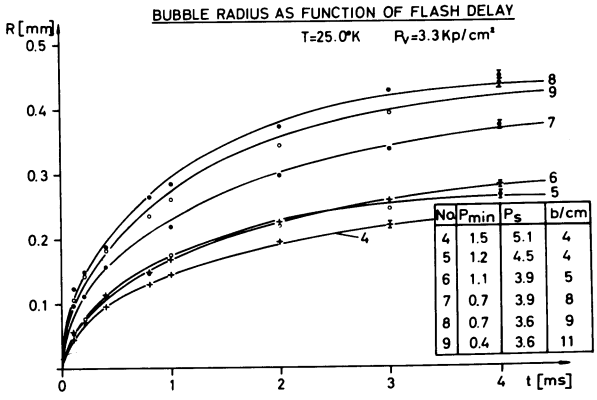
BUBBLE RADIUS AS FUNCTION OF FLASH DELAY
T=25.0°K Pv=3.3 Kp/cm²
R [mm]
t [ms]
4
5
6
7
8
9
No. Pmin Ps b/cm
4 1.5 5.1 4
5 1.2 4.5 4
6 1.1 3.9 5
7 0.7 3.9 8
8 0.7 3.6 9
9 0.4 3.6 11

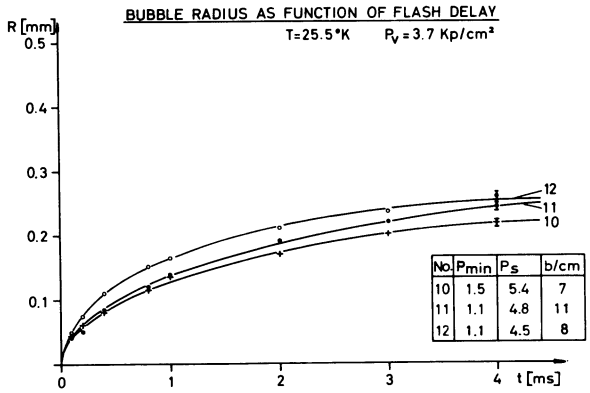
BUBBLE RADIUS AS FUNCTION OF FLASH DELAY
T=25.5°K Pv=3.7 Kp/cm²
R [mm]
t [ms]
10
11
12
No. Pmin Ps b/cm
10 1.5 5.4 7
11 1.1 4.8 11
12 1.1 4.5 8

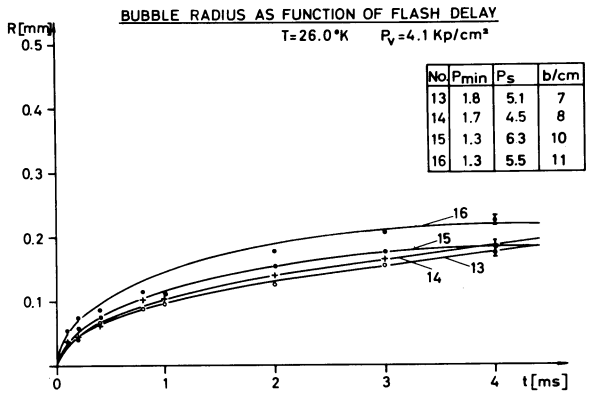
BUBBLE RADIUS AS FUNCTION OF FLASH DELAY
T=26.0°K Pv=4.1 Kp/cm²
R [mm]
t [ms]
13
14
15
16
No. Pmin Ps b/cm
13 1.8 5.1 7
14 1.7 4.5 8
15 1.3 6.3 10
16 1.3 5.5 11

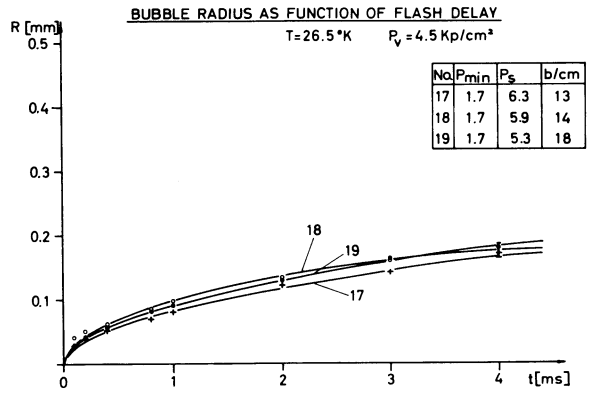
BUBBLE RADIUS AS FUNCTION OF FLASH DELAY
T=26.5°K Pv=4.5 Kp/cm²
R [mm]
t [ms]
17
18
19
No. Pmin Ps b/cm
17 1.7 6.3 13
18 1.7 5.9 14
19 1.7 5.3 18

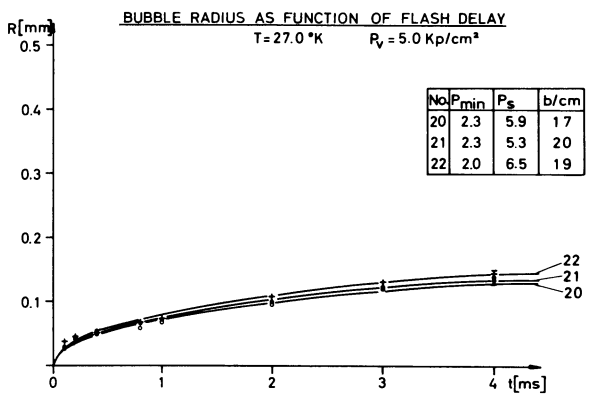
BUBBLE RADIUS AS FUNCTION OF FLASH DELAY
T=27.0°K Pv=5.0 Kp/cm²
R [mm]
t [ms]
20
21
22
No. Pmin Ps b/cm
20 2.3 5.9 17
21 2.3 5.3 20
22 2.0 6.5 19

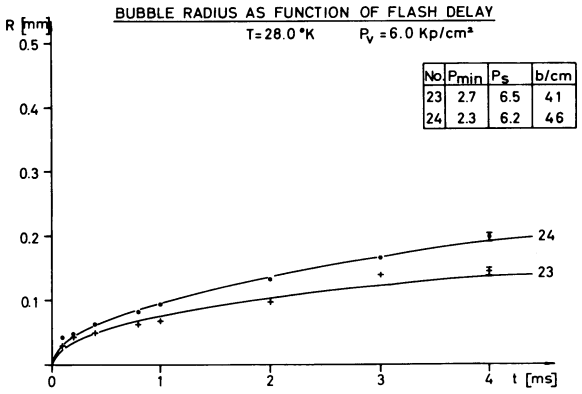
BUBBLE RADIUS AS FUNCTION OF FLASH DELAY
T=28.0°K Pv=6.0 Kp/cm²
R [mm]
t [ms]
23
24
No. Pmin Ps b/cm
23 2.7 6.5 41
24 2.3 6.2 46

Fig. 5

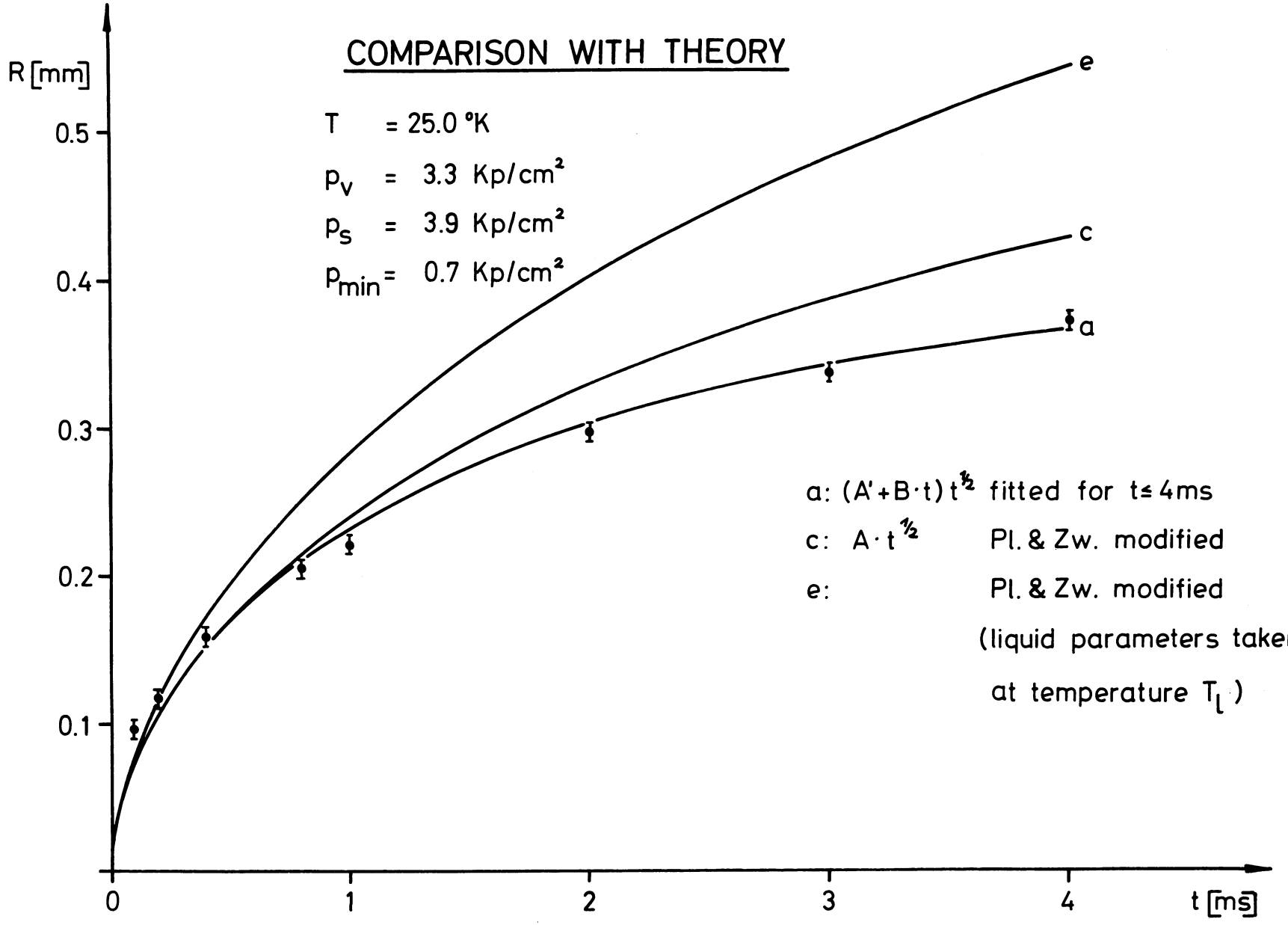
COMPARISON WITH THEORY
T = 25.0 °K
p_v = 3.3 Kp/cm²
p_s = 3.9 Kp/cm²
p_{min} = 0.7 Kp/cm²
R [mm]
0.5
0.4
0.3
0.2
0.1
0
1
2
3
4
t [ms]
e
c
a
a: $(A'+B\cdot t)\,t^{1/2}$ fitted for t ≤ 4ms
c: $A\cdot t^{1/2}$ Pl. & Zw. modified
e: Pl. & Zw. modified
(liquid parameters taken
at temperature T_l)

Fig.6

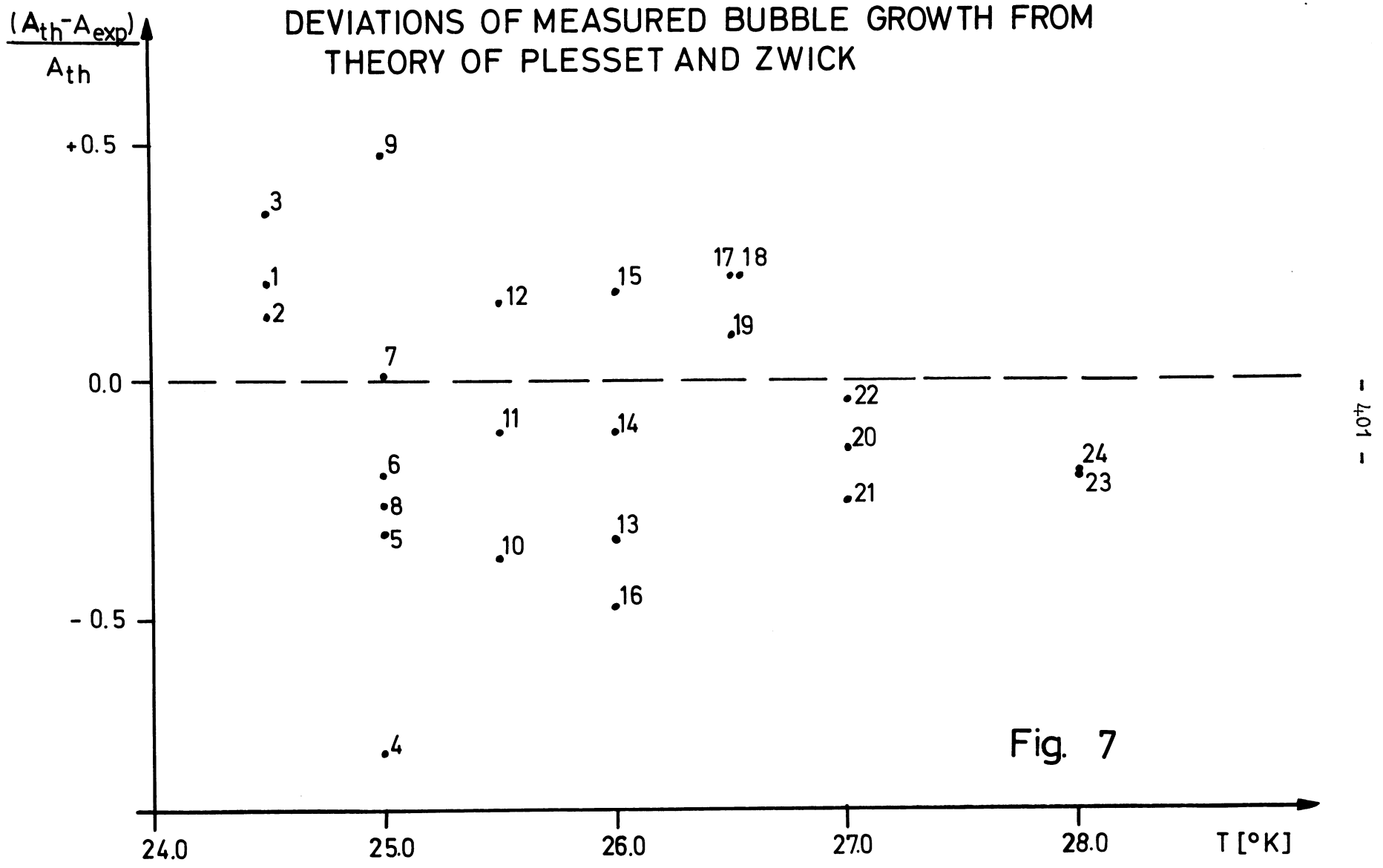
DEVIATIONS OF MEASURED BUBBLE GROWTH FROM THEORY OF PLESSET AND ZWICK
$\frac{(A_{th}-A_{exp})}{A_{th}}$
+0.5
0.0
- 0.5
24.0
25.0
26.0
27.0
28.0
T [°K]
1
2
3
4
5
6
7
8
9
10
11
12
13
14
15
16
17
18
19
20
21
22
23
24

Fig. 7

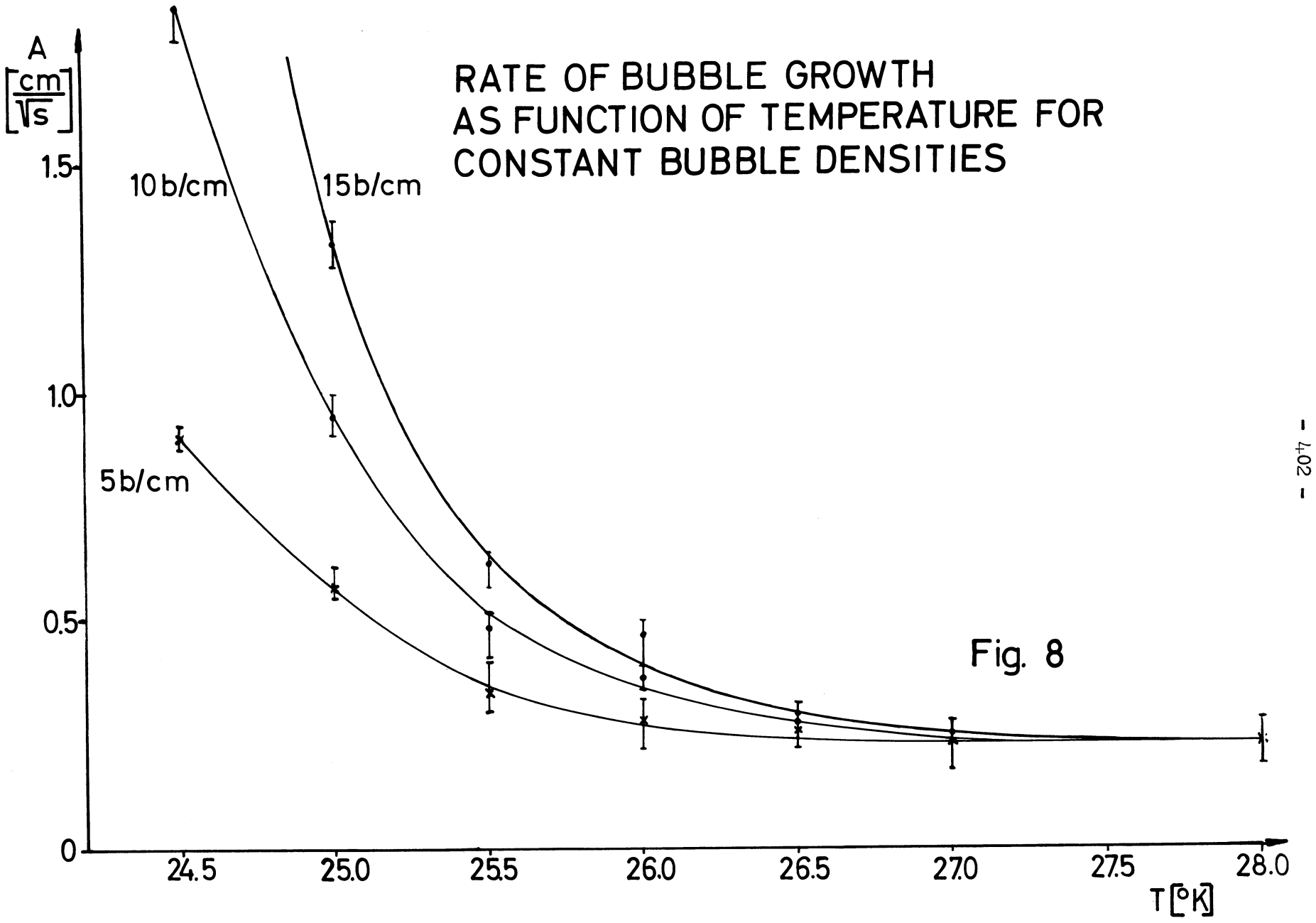
RATE OF BUBBLE GROWTH
AS FUNCTION OF TEMPERATURE FOR
CONSTANT BUBBLE DENSITIES
A
[cm/√s]
1.5
1.0
0.5
0
10 b/cm
15 b/cm
5 b/cm
24.5
25.0
25.5
26.0
26.5
27.0
27.5
28.0
T [°K]

Fig. 8

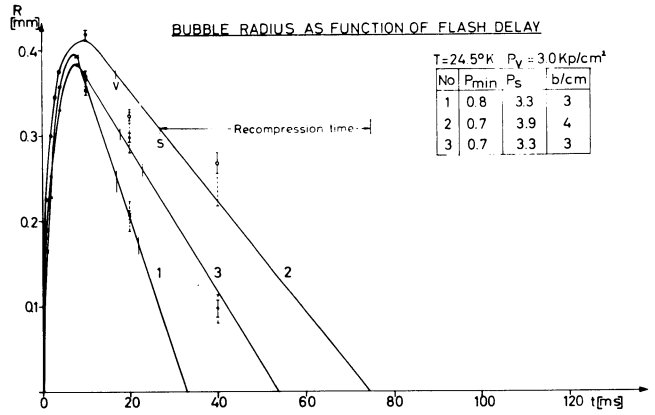

No	P_{min}	P_s	b/cm
1	0.8	3.3	3
2	0.7	3.9	4
3	0.7	3.3	3

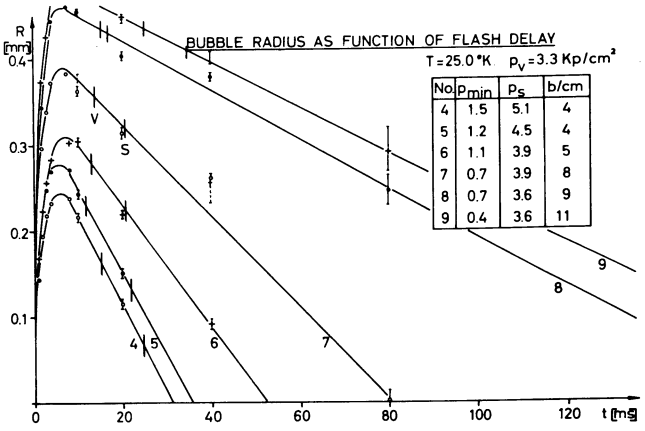

No	P_{min}	P_s	b/cm
4	1.5	5.1	4
5	1.2	4.5	4
6	1.1	3.9	5
7	0.7	3.9	8
8	0.7	3.6	9
9	0.4	3.6	11

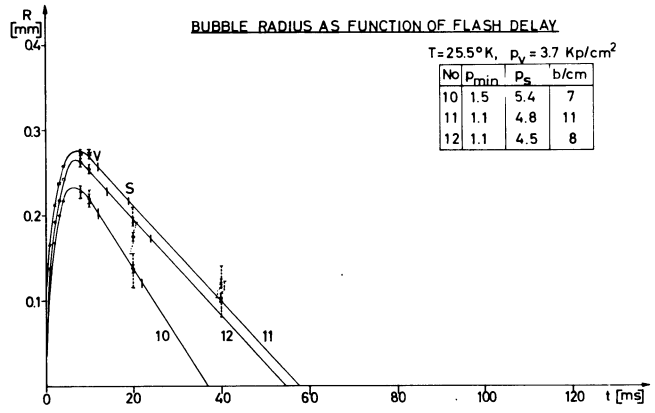

No	P_{min}	P_s	b/cm
10	1.5	5.4	7
11	1.1	4.8	11
12	1.1	4.5	8

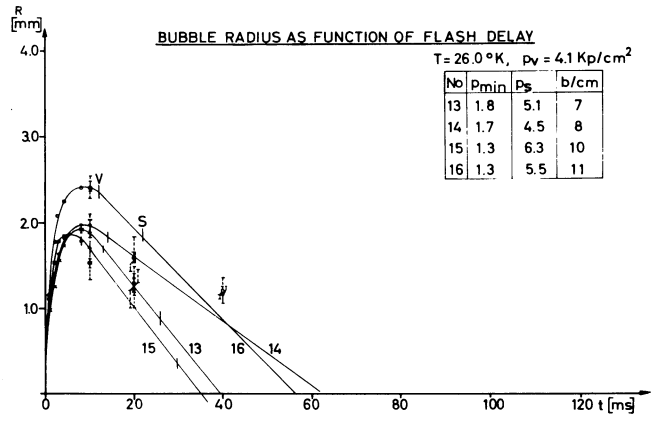

No	P_{min}	P_s	b/cm
13	1.8	5.1	7
14	1.7	4.5	8
15	1.3	6.3	10
16	1.3	5.5	11

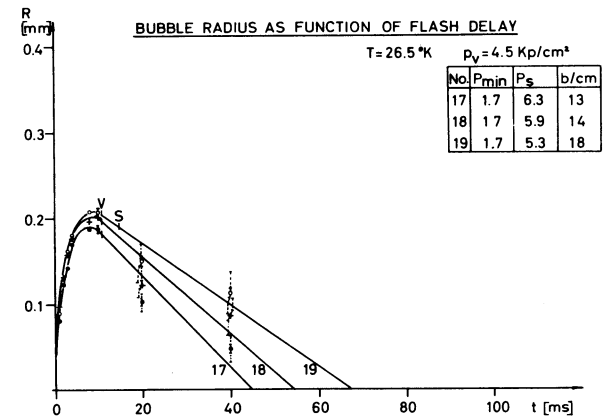

No.	P_{min}	P_s	b/cm
17	1.7	6.3	13
18	1.7	5.9	14
19	1.7	5.3	18

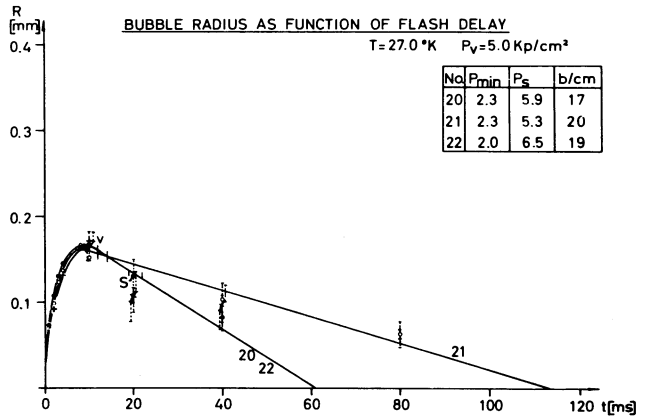

No	P_{min}	P_s	b/cm
20	2.3	5.9	17
21	2.3	5.3	20
22	2.0	6.5	19

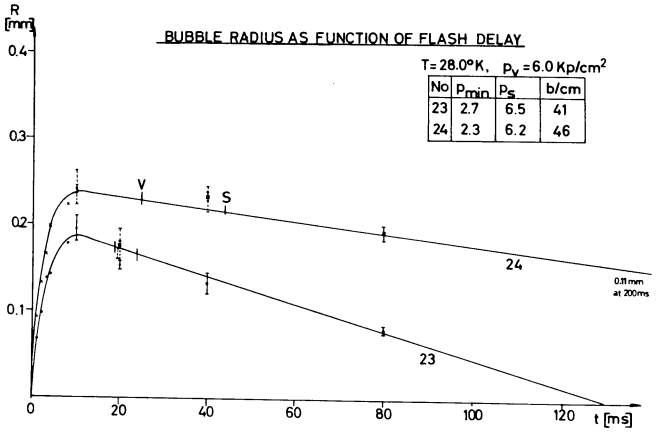

No	P_{min}	P_s	b/cm
23	2.7	6.5	41
24	2.3	6.2	46

Fig. 9

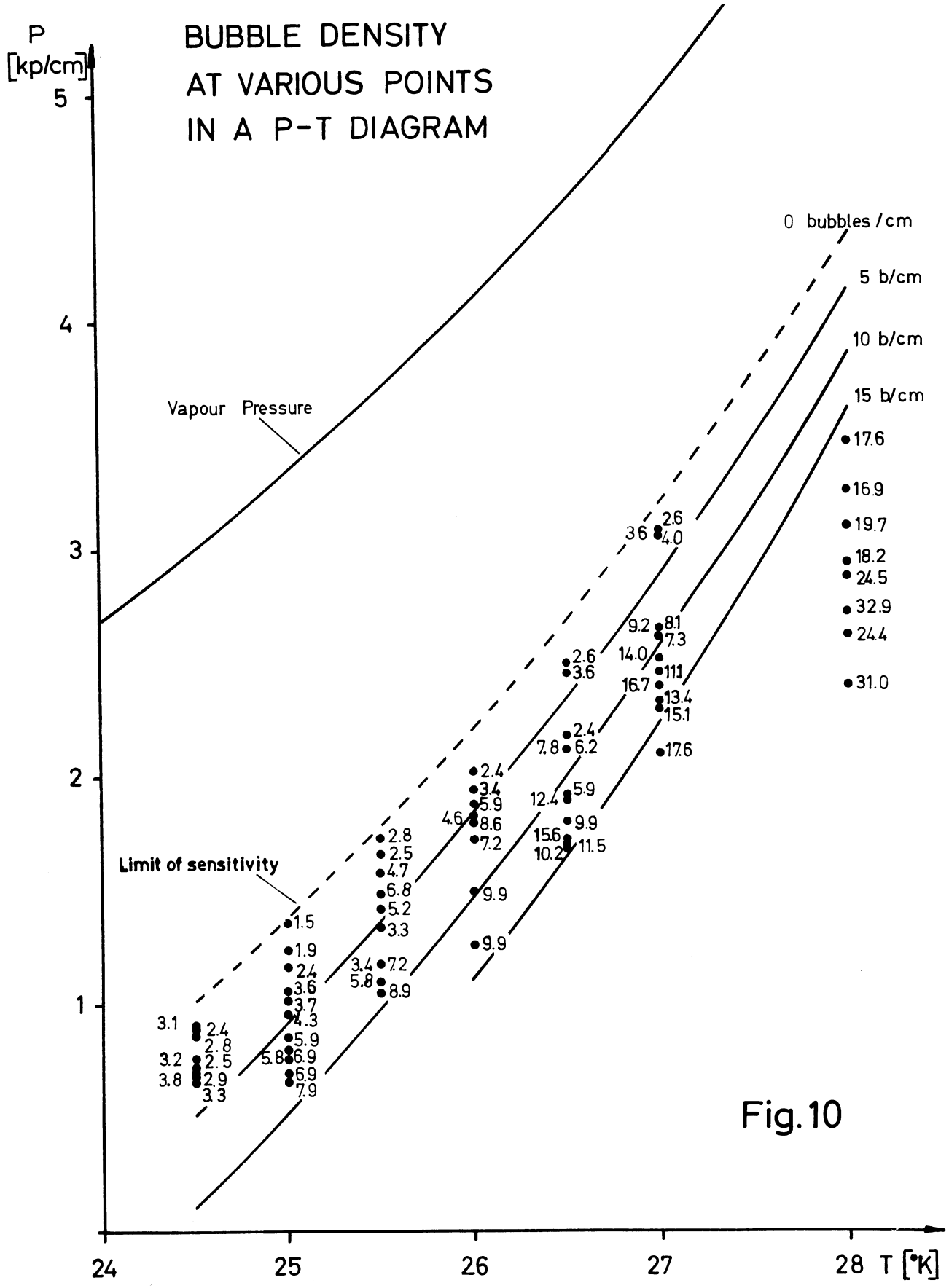
BUBBLE DENSITY
AT VARIOUS POINTS
IN A P-T DIAGRAM
P
[kp/cm]
5
4
3
2
1
Vapour Pressure
Limit of sensitivity
0 bubbles / cm
5 b/cm
10 b/cm
15 b/cm
24
25
26
27
28 T [°K]

Fig. 10

4.5 BUBBLE DENSITY AND GROWTH OF BUBBLES IN PROPANE

P. Kunkel, G. Christenn and M. Scheer

Physikalisches Institut der Universität, Würzburg.

Using 20 MeV electrons from a betatron and a small 350 ccm pressure stabilized bubble chamber the primary bubble density and the rate of bubble growth in propane were investigated. We have studied the dependence of the two quantities on the working parameters of the chamber, i. e. the temperature T and the pressure drop Δp.

Experimental Concept

For a given particle with a certain ionization density along the track the primary bubble density N_o is only a function of temperature and pressure drop in the chamber liquid:

$$N_o = N_o(T, \Delta p) \qquad (1)$$

The actual bubble density N at the time of the photographical registration is always smaller than N_o, because with increasing diameter of the bubbles some of the bubbles will grow together. Therefore the actual bubble density is a function of temperature, pressure drop and the time delay τ between the passage of the particle and the flash light:

$$N = N(T, \Delta p, \tau) \qquad (2)$$

The decrease of the actual bubble density with time of growth is demonstrated in fig. 1, which shows the same 5 mm part of an electron track for two different values of τ.

We made use of a very simple argument for the relation between the actual and the primary bubble density. The primary bubbles are distributed statistically along the track. For a given diameter ϕ of

the bubbles due to the chosen parameters temperature, pressure drop and delay time for flash, two primary bubbles must be generated with a distance at least equal to this diameter to be counted separately. In analogy to the loss of counts in a counter set of given resolution time the loss of bubbles can be described by the simple formula:

$$N = \frac{N_o}{1 + N_o \phi} \tag{3}$$

As a good approximation for the diameter of the bubbles we use the relation:

$$\phi(\tau) = 2r = 2c\sqrt{\tau} \tag{4}$$

c defines the rate of bubble growth, which is a function of T and Δp:

$$c = c(T, \Delta p) \tag{5}$$

With (4) the relation between the actual bubble density and the diameter of the bubbles can be written as:

$$N = \frac{N_o}{1 + N_o \cdot 2c \cdot \sqrt{\tau}} \tag{6}$$

or

$$\frac{1}{N} = \frac{1}{N_o} + 2c\sqrt{\tau} \tag{7}$$

1/N plotted versus $\sqrt{\tau}$ should be a straight line with the slope 2 c. Thus it is possible to determine the rate of bubble growth from the actual bubble density without explicite knowledge of the bubble diameter $\phi(\tau)$.

Experimental Results

We have measured the bubble density as a function of flash delay for several combinations of temperature and pressure drop. As an example the results for a fixed temperature of 65.55 °C are given in fig. 2. By extrapolation $\tau \to 0$ we get directly the primary bubble density. Similar measurements were carried out for six temperatures.

In fig. 3 the values of the primary bubble density are plotted as a function of the pressure drop with the temperature as parameter. For the two higher values of temperature we achieved the maximum bubble density with 120 bubbles/cm; a further increase of the pressure drop caused foaming in the entire chamber. The onset of each curve is given by the minimum pressure drop for which the chamber liquid is just sensitive.

Fig. 4 shows 1/N plotted versus $\sqrt{\tau}$ again for the temperature 65.55°C. The assumed relation between the actual bubble density and the time of growth seems to be confirmed by the results of these measurements. In this way we obtained the rates of bubble growth for all chosen combinations of temperature and pressure drop.

In fig. 5 the results of our measurements are collected. The two quantities of interest are plotted in a p,T-diagram as curves of constant bubble density and curves of constant rate of bubble growth. The curves of constant bubble density lie between the limit of sensitivity and the limit of foam; all these curves can be extrapolated easily to cross in the critical point of propane (T_c = 96,8° C, p_c = 42,0 atm). The curves of constant rate of bubble growth have a considerably different slope. From the diagram it can be seen how for fixed chamber sensitivity (given by the primary bubble density) the rate of growth decreases with increasing temperature.

The results for the primary bubble density will appear in "Angewandte Physik" 22, 410 (1967).

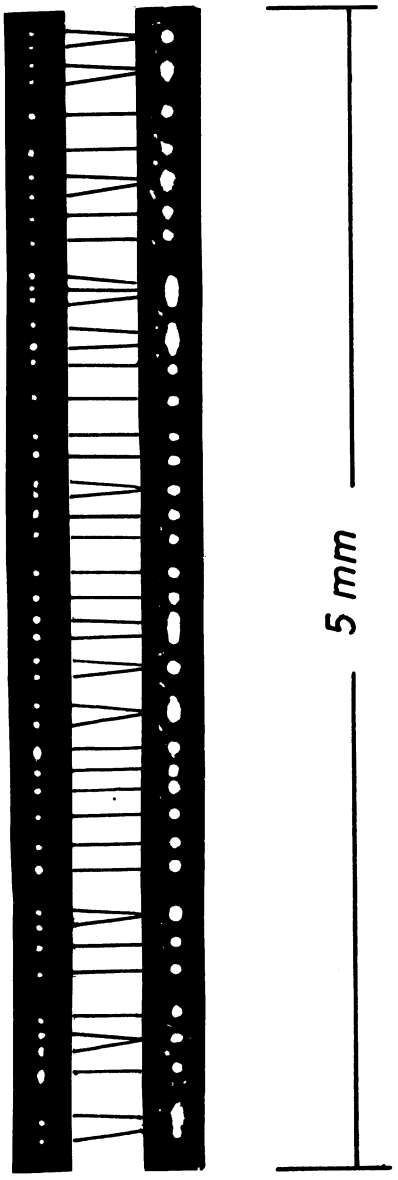

Fig. 1

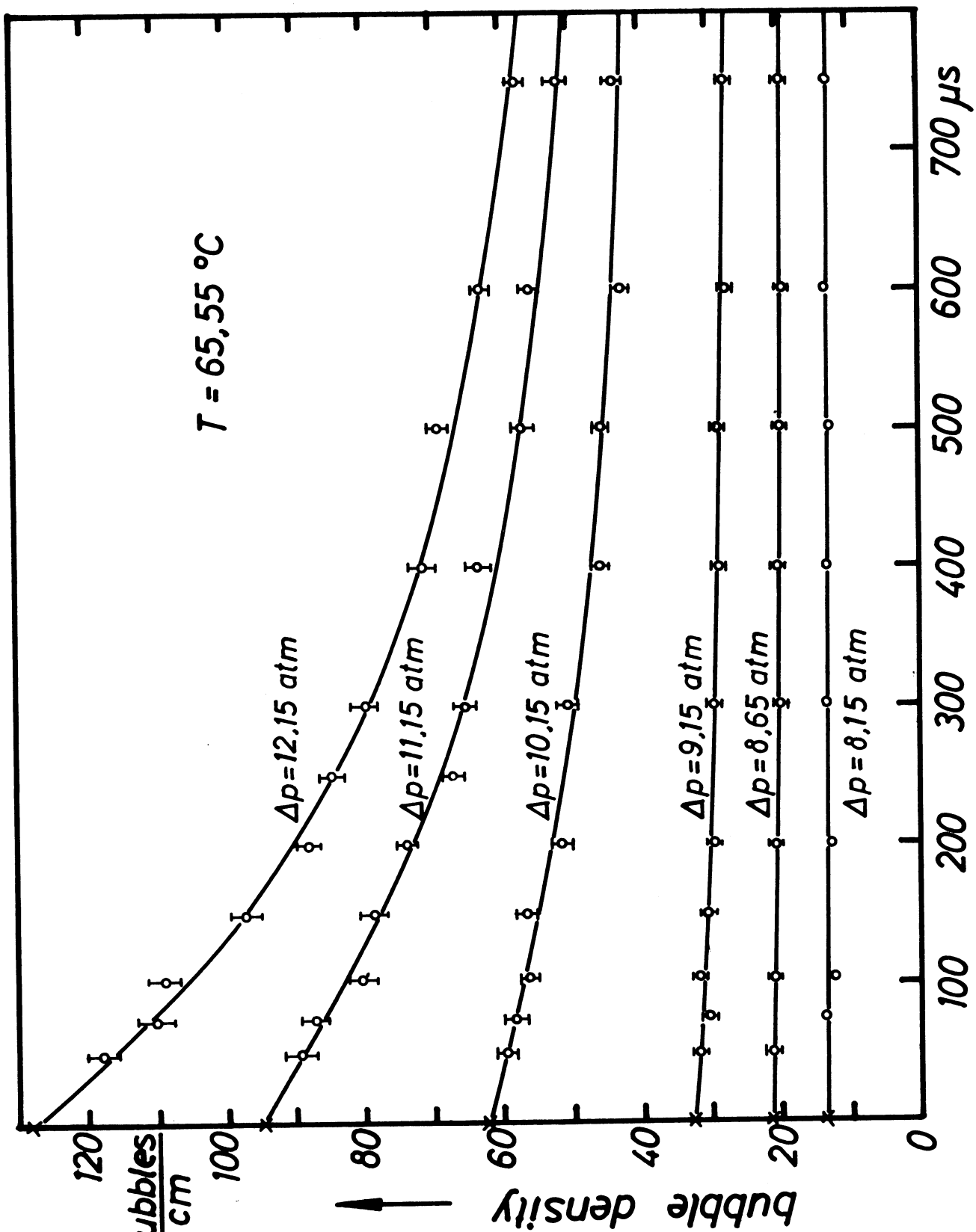
T = 65,55 °C
Δp=12,15 atm
Δp=11,15 atm
Δp=10,15 atm
Δp=9,15 atm
Δp=8,65 atm
Δp=8,15 atm
bubble density
bubbles / cm
120
100
80
60
40
20
0
100
200
300
400
500
600
700 µs
τ

Fig. 2

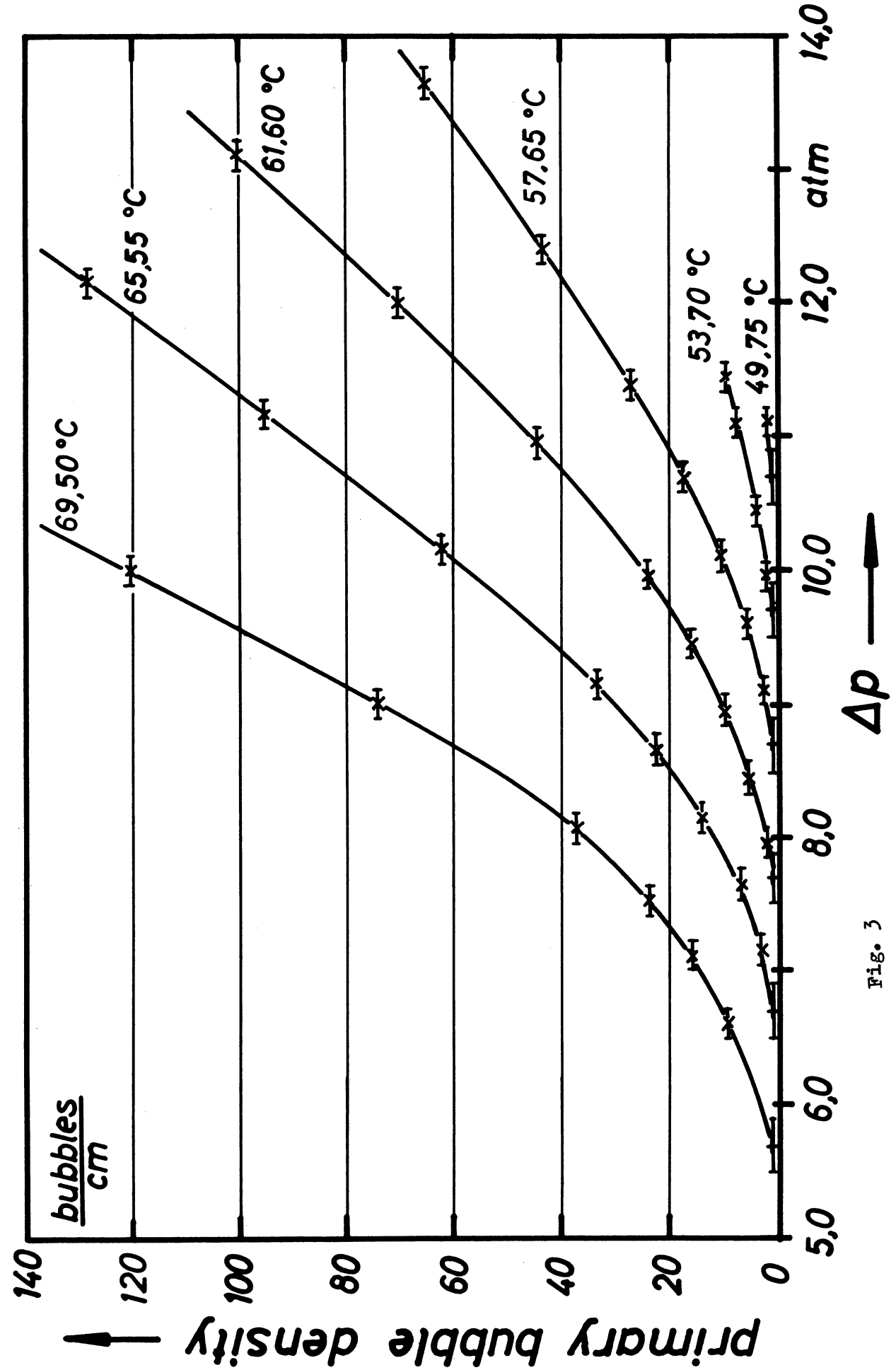
primary bubble density
bubbles / cm
140
120
100
80
60
40
20
0
5,0
6,0
8,0
10,0
12,0
14,0
atm
Δp
69,50 °C
65,55 °C
61,60 °C
57,65 °C
53,70 °C
49,75 °C

Fig. 3

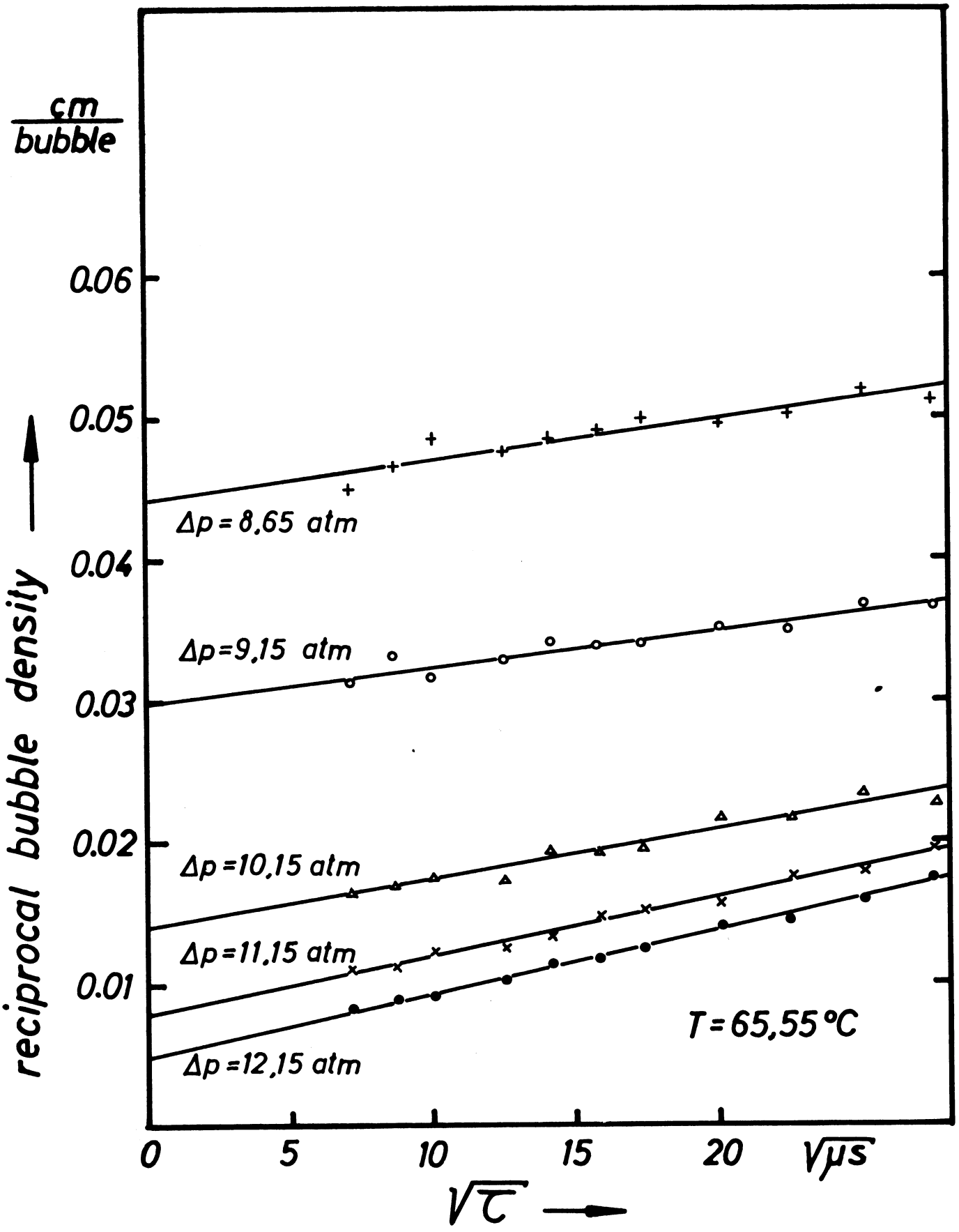
cm
bubble
reciprocal bubble density
0.06
0.05
0.04
0.03
0.02
0.01
Δp = 8,65 atm
Δp=9,15 atm
Δp =10,15 atm
Δp =11,15 atm
Δp =12,15 atm
T = 65,55 °C
0
5
10
15
20
√μs
√τ

Fig. 4

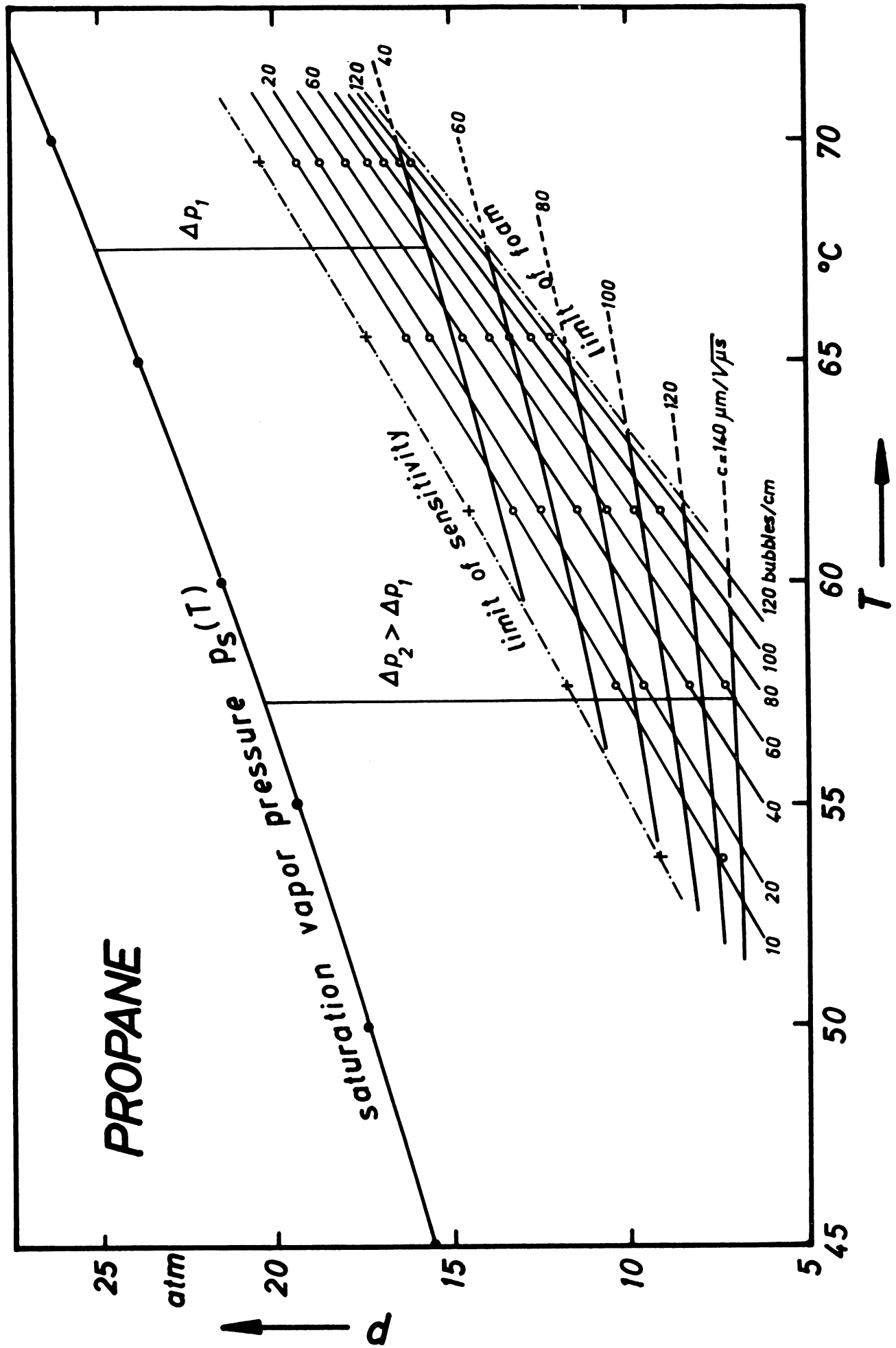
PROPANE
saturation vapor pressure $p_s(T)$
Δp_1
$\Delta p_2 > \Delta p_1$
limit of sensitivity
limit of foam
c = 140 μm/√μs
120 bubbles/cm
20
60
120
40
60
80
100
120
10
20
40
60
80
100
p
atm
25
20
15
10
5
45
50
55
60
65
°C
70
T

Fig. 5

4.6 TEMPERATURE MEASUREMENTS IN THE CERN 1 m³ HEAVY LIQUID BUBBLE CHAMBER

K.H. Eberle

CERN.

Temperature measurements were carried out in the CERN HLBC to obtain a better understanding of its thermal behaviour and to determine the parameters needed for an improvement of its temperature regulation.

Introduction

The CERN HLBC is essentially a cylindrical steel vessel with its centre axis placed horizontally (internal diameter 1.20 m, length 1.05 m). The chamber is closed at one end by a glass window 0.27 m thick, which is protected by a pressurized safety tank; on the other end, a Vulkolan plastic membrane separates the working liquid from the pneumatic system.

The stainless steel wall is 40 mm thick and surrounded by eight longitudinal closed sections through which water is circulated in closed loops; each two opposite sections are connected in parallel.

Temperature control of the chamber is achieved by detecting temperatures in the chamber wall, 1 mm away from the inner surface, in the middle of each water section, and a feedback system acting on the circulating water through heat exchangers (Fig. 1).

Therefore, only the temperatures in the chamber wall, near the inner surface, are controlled by feedback systems, allowing no conclusions on the temperatures in the working liquid. Besides, the temperature of each wall section can be set independently from the others, leaving a great

variety of possible settings; by experience, however, optimum conditions are obtained with the reference temperatures of the wall linearly increasing (or decreasing) with chamber height, giving two characteristic values for operation: the temperature ϑ_o of the bottom circuit and the temperature difference $\Delta\vartheta$ between the top and the bottom circuit, referred to as temperature gradient. Only those operating conditions were used for the measurements (Fig. 2).

Equipment and Measurements

In order to measure temperatures in the liquid, 56 platinum temperature sensors (platinum wire on cylindrical glass support from Degussa, model P 6, 100 Ω at 0°C) were introduced into the chamber and fixed in four vertical planes made up of bare wire. By assuming the temperature distribution to be symmetrical to the vertical symmetry plane of the chamber, the most efficient utilization was made of the given number of temperature sensors (array shown schematically in Fig. 3). All sensors were calibrated carefully.

A test point selector connected one sensor after the other to one arm of a Wheatstone bridge. Temperatures were read by a digital voltmeter to an accuracy of 0.1° and stored on paper tape, allowing to do a measurement cycle within 2 seconds; so there are no measurement errors due to time lags. The starting pulse for a measurement cycle is given by an independent time base (set to 1 min for the distribution measurements).

The temperature measurements were made with the HLBC filled with Freon 13 B 1 (CF_3Br), cycling under normal pressure conditions at a rate of 2.3 s. No beam was used, as the disturbances caused by a few tracks are small compared to the influence of the other parameters.

The bottom circuit reference temperature was set to 30°C and remained fixed throughout the measurements. Temperature distributions were

measured with temperature gradients of -4^{o}, -2^{o}, -1^{o}, 0^{o}, $+1^{o}$, $+2^{o}$, without flashes and with flash energies of 250 J and 400 J.

In order to learn more about the dynamic behaviour of the chamber, transfer functions have also been measured: starting from a state of thermal equilibrium, the chamber was submitted to forced heating or cooling, and the measuring sequence was 15 s. The transfer functions seen by the temperature sensors in the chamber wall, normally used for the thermal control system, were also recorded.

Results

The results of the distribution measurements are found as average values of consecutive measurements made after thermal equilibrium had been reached. Small calibration errors could be eliminated to a great extent by a statistical evaluation. Therefore, the accuracy of the given values is $+ 0.2^{o}$, $- 0.1^{o}$. A typical example of a temperature distribution is given in Fig. 4.

Considering only the vertical planes, the most important results are as follows:

a) No matter what gradient is set externally, the liquid temperature is highest in and around the centre of the chamber.

b) The liquid temperature is lowest in the lower half of the chamber, but not quite at the bottom.

c) The lowest temperature difference found between any two test points in one single plane was 0.8^{o}, the highest was 1.8^{o}.

d) The lowest temperature difference found between any two test points in the chamber was 1.5^{o}, the highest was 2.3^{o}.

e) The temperature of the liquid rises uniformly with increasing flash energy: by 0.3^{o} for a rise from 0 to 250 J, by another 0.4^{o} for a rise from 250 J to 400 J.

f) The most uniform distribution, comparing different gradient settings, was obtained with gradients of -2^{o} and -4^{o}. The results of those two do not differ very much from each other and confirm experimental findings of the best conditions with regard to picture quality in the HLBC. At temperature gradients between -1^{o} and $+1^{o}$, an instability seems to develop in the liquid which disappears slowly when the gradient is raised to $+2^{o}$.

For the axial direction, the following results were obtained:

a) A steady temperature drop is observed between the window and the membrane. Its average value is 0.8^{o}.

b) The lowest drop observed was 0.6^{o}, the highest 1.2^{o}.

Conclusions

The results of the temperature distribution measurements can be described best by superposing two kinds of temperature distributions: one in the different vertical planes and one in the horizontal direction.

The temperature drop along the chamber axis seems to be due to heat transport through membrane-induced motion of the liquid: the temperature is highest where the liquid is at rest on the window side.

The temperature distributions in the vertical planes show that convection of the liquid plays a surprisingly unsignificant role in heat transfer. From the physics of fluids it is known that such temperature configurations can well exist without convection arising. Althouth the three-dimensional distribution of the heat put into the Freon by the pressure cycle is not very well known, one may conclude from the measurements that the bulk of the liquid behaves nearly like a solid: the temperature is highest in the centre and drops to the outside, where the properly working temperature regulation systems take constantly heat out of the chamber. (This can be very well observed around $30^{o}C$, as heat losses due to radiation from the chamber outside are negligible). The temperature conduction

coefficient calculated for Freon as if it were a solid is $\frac{1}{100}$ times that of the stainless steel wall.

The ultimate cause, however, for the temperature configurations and for the negligible convection as found above is the poor heat transfer from the liquid to the chamber wall. The coefficient of heat transfer, as measured elsewhere, is in the order of 0.3 $kW/m^2.grd$ (compared to a heat input into the chamber of $\approx$ 1.5 kW under the conditions stated above, without flashes). The effect of the poor heat transfer can be seen from the following results, which confirm at the same time the statements made above:

a) An increase of flash power increases the temperature of the liquid uniformly by the same value, although the wall temperatures are held constant.

b) Transfer function measurements show even better the difficulties. The transfer function as defined in Fig.5 is characterised by 3 values: ϑ_{max}, which is the temperature difference of the energy source necessary for forced heating or cooling to the equilibrium temperature of the chamber, the delay time T_t and the "time constant" T_G. In the transfer function measurements with forced cooling, ϑ_{max} was -16^o. While for the temperature sensors in the chamber wall T_t is unmeasurably short and T_G = 125 min, one finds for all test points in the liquid T_t = 6 min, T_G = 215 min.

There are serious problems arising in the temperature control of a big bubble chamber. From the preceding measurements it can be seen that a regulation of only the wall temperature is not adequate. It is essential to improve the heat transfer between liquid and chamber wall and also inside the liquid by stirring, a conclusion which has been reached by other considerations by the MURA Group[1].

I gratefully acknowledge the help of W. Birr who prepared the bubble chamber for this experiment and P. Actis who made up the electronics.

(1) cf.Report of Prof.Wilson Powell in this Colloquium.

Thermal control of chamber wall.

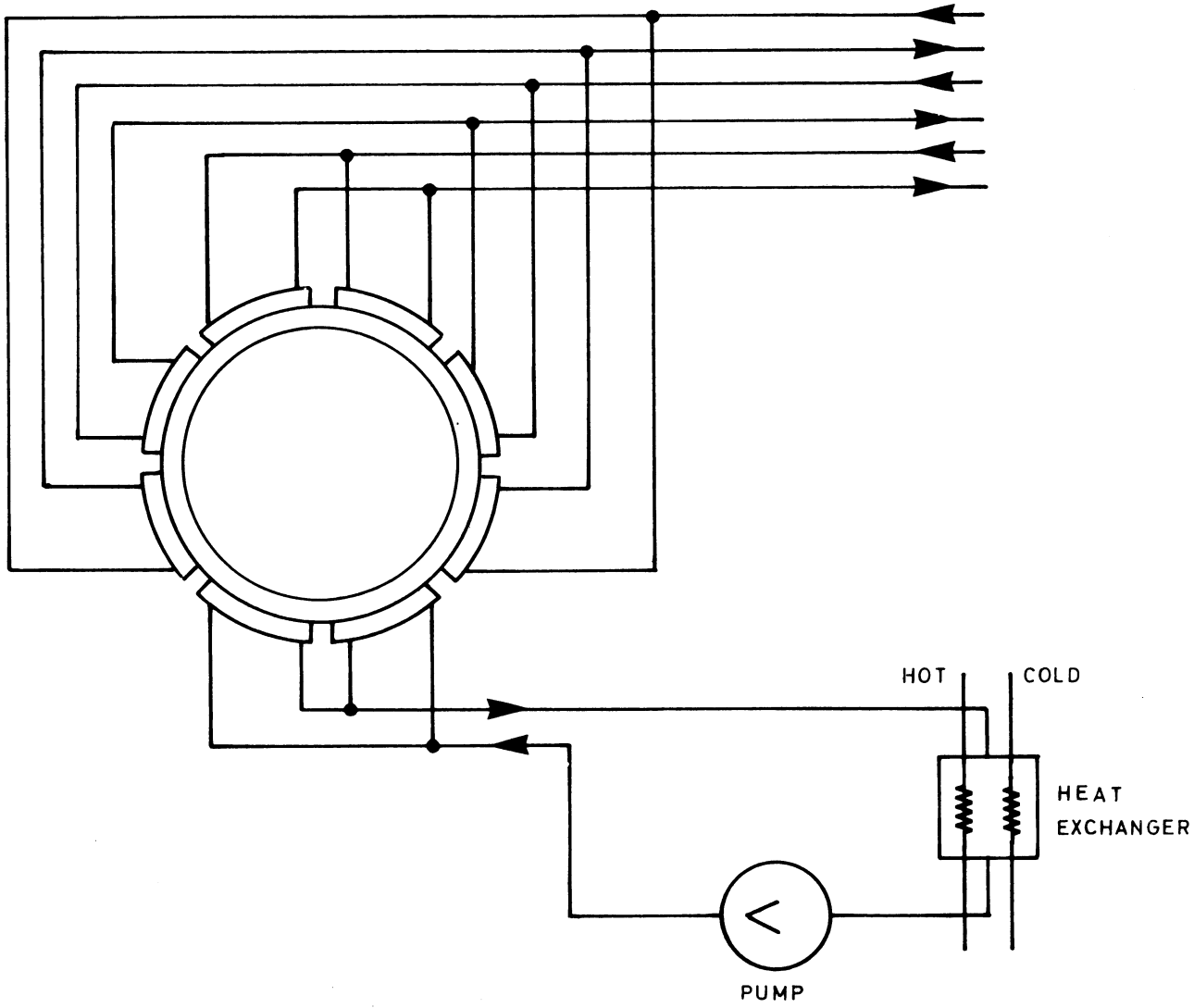

Fig. 2

Definition of temperature gradient

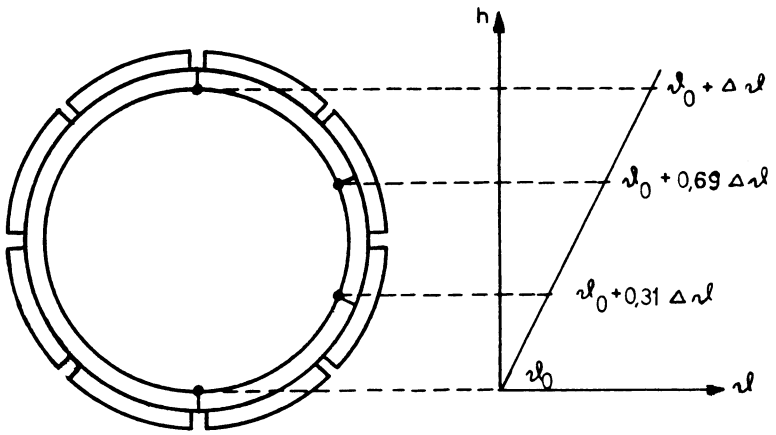

Fig. 3

Temperature sensors in one plane (scale 1:10)

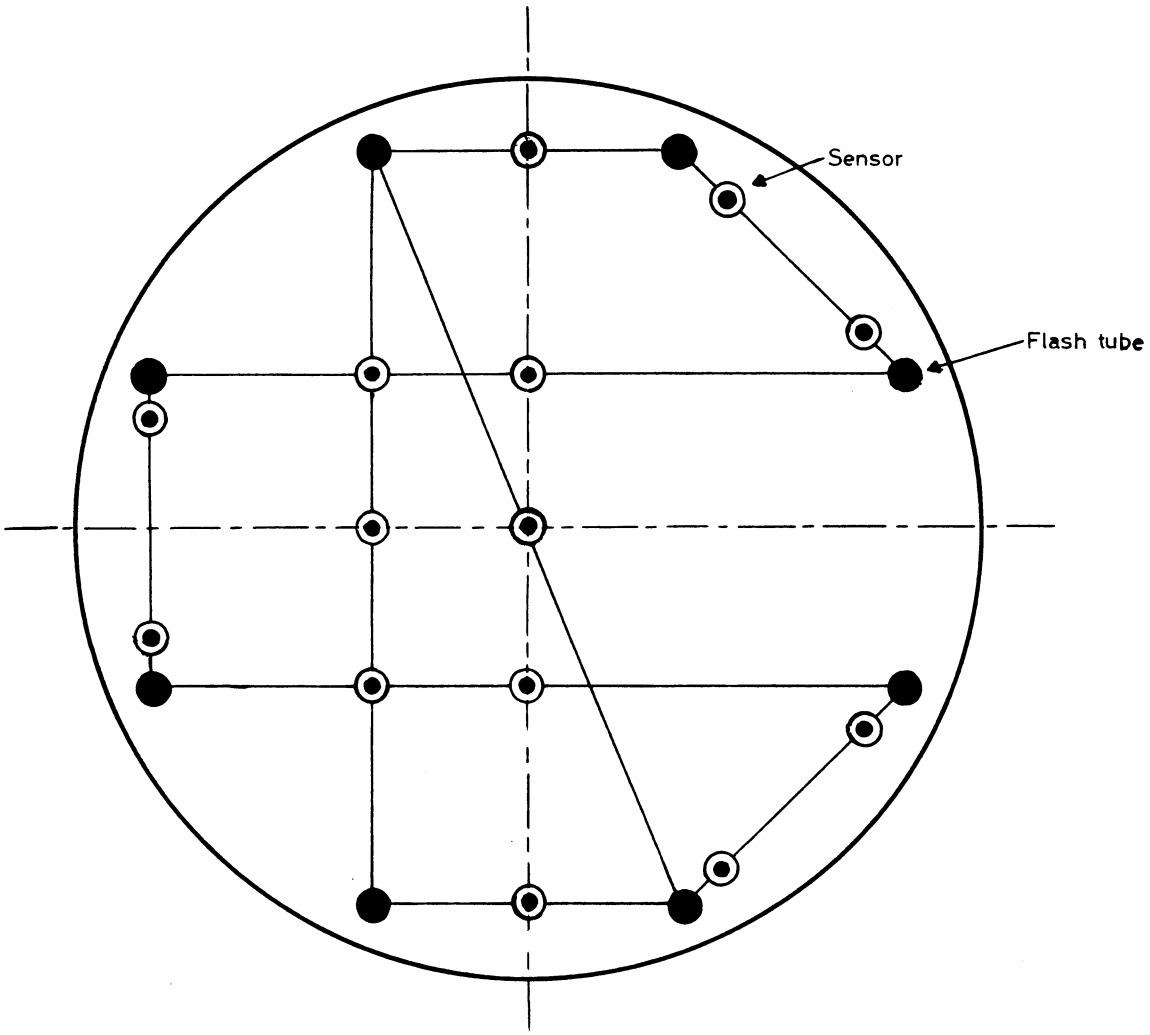

Fig. 4:

Typical temperature distribution

(Gradient -2°, flash energy 400 J)

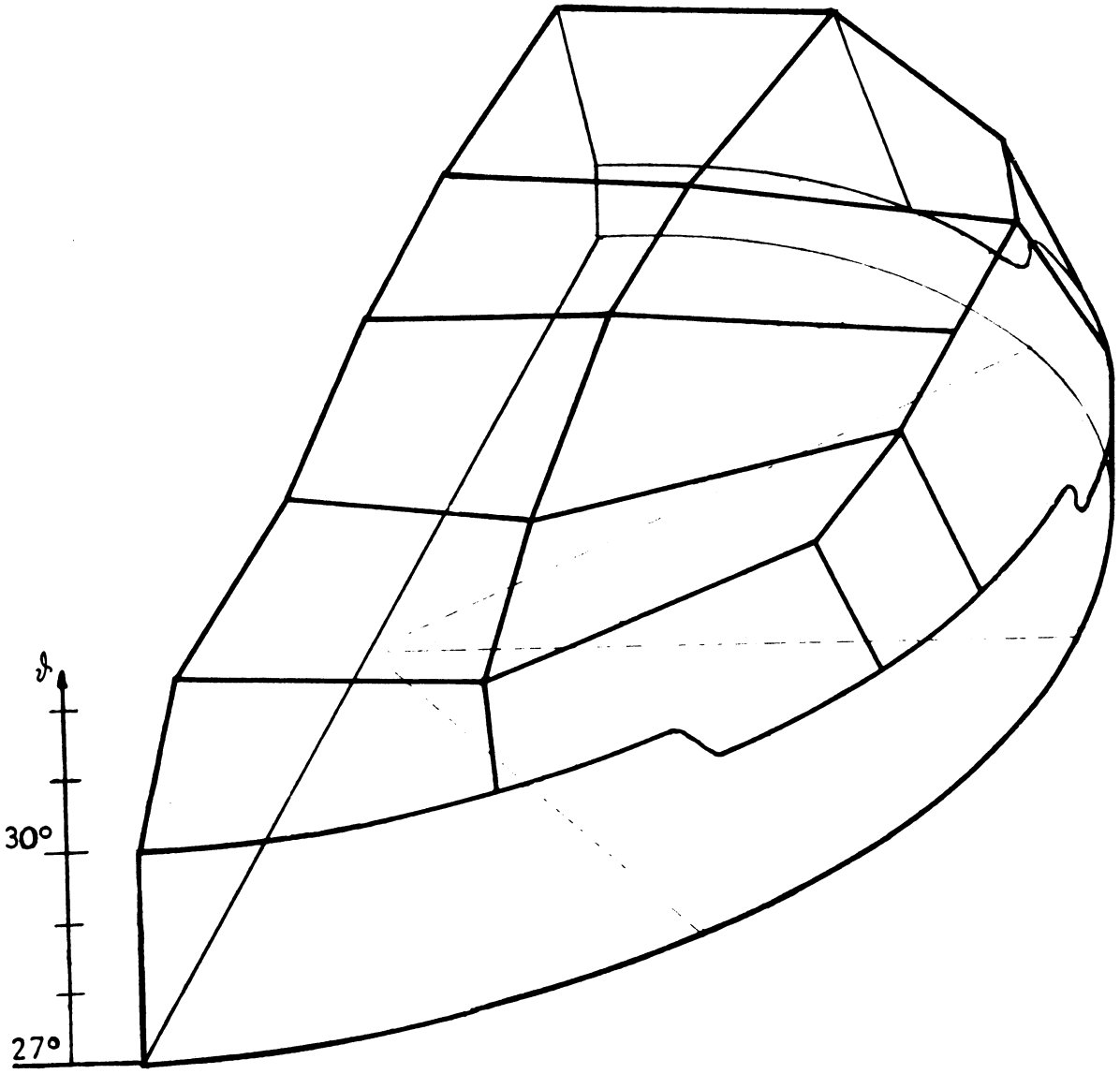

Plane 1 (window side)

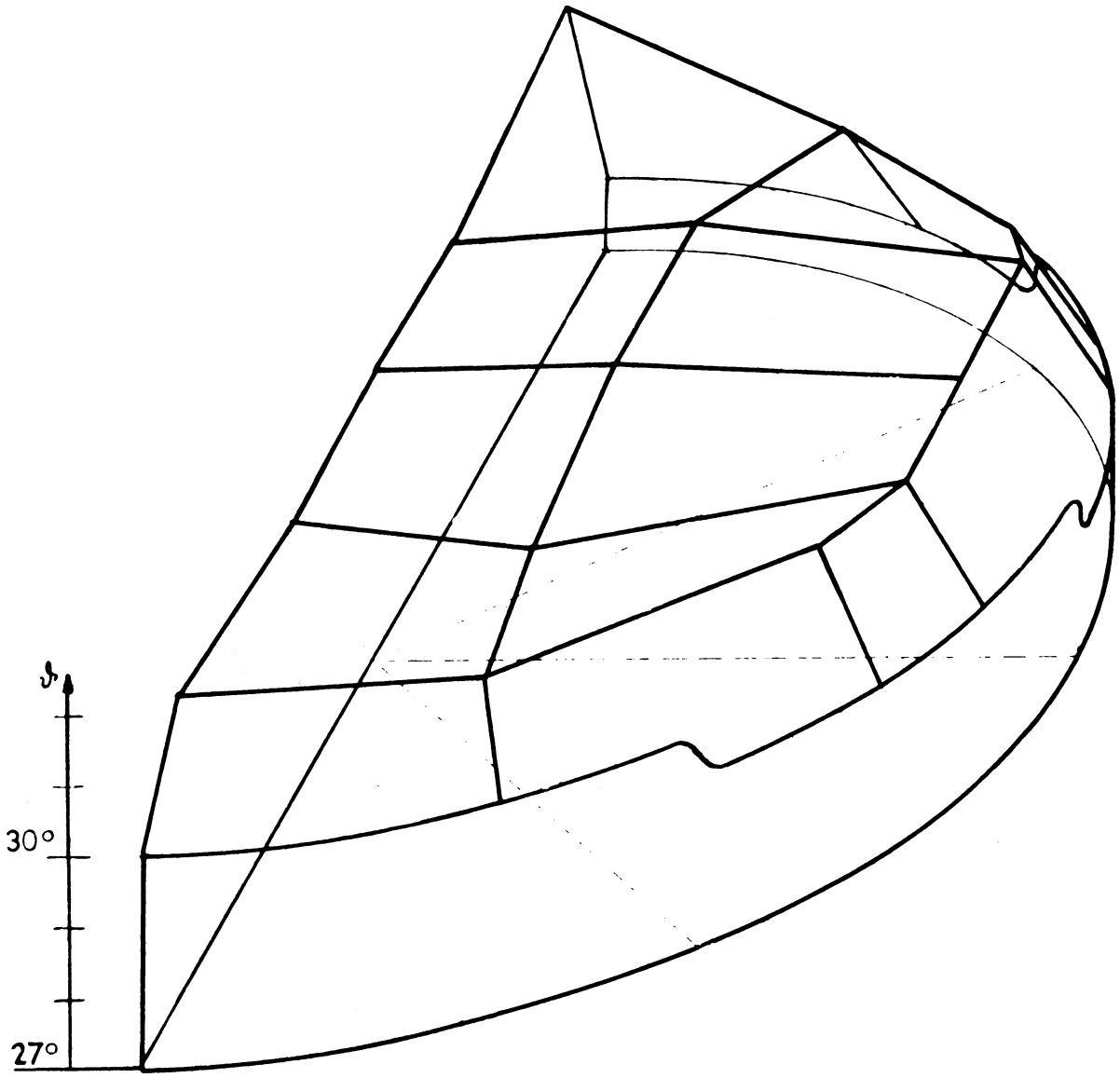

Plane 2

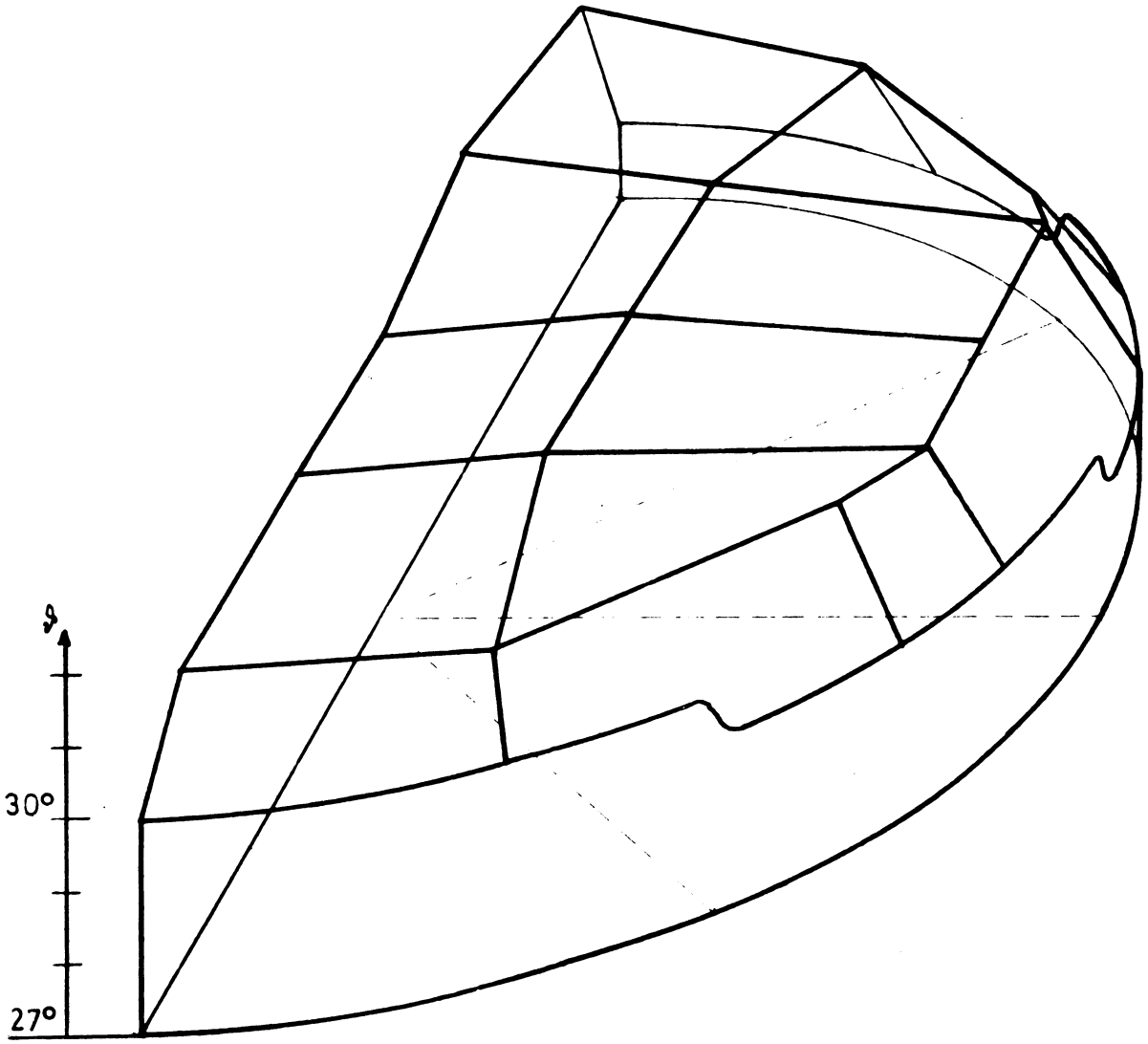

Plane 3

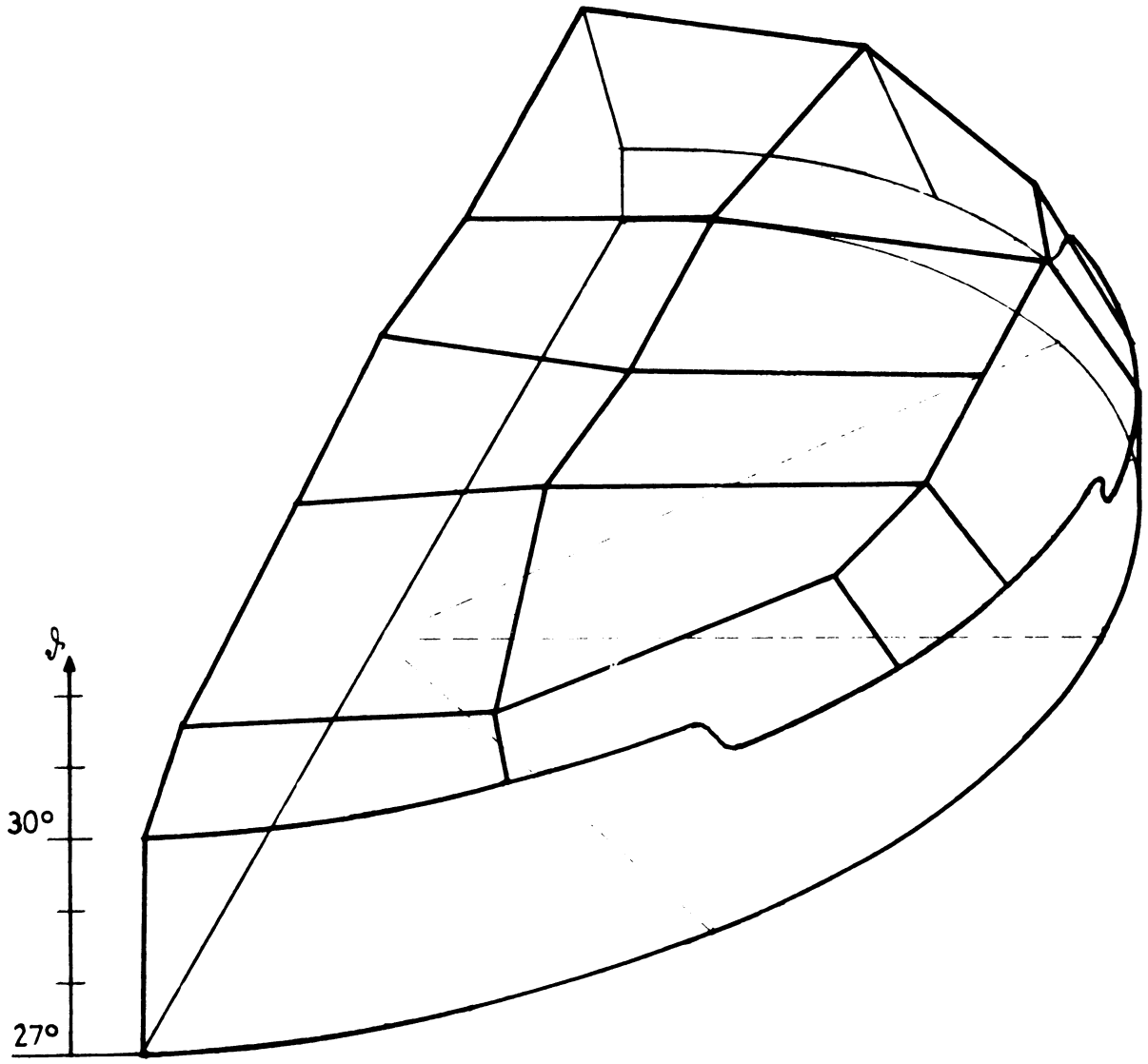

Plane 4 (membrane side)

Fig. 5

Definition of transfer function

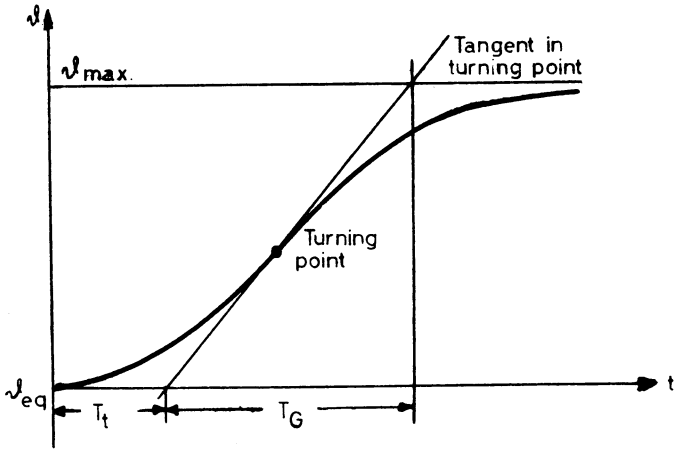

5.1 THE SUPERCONDUCTING MAGNET ASSOCIATED WITH THE ANL 12-FT HYDROGEN BUBBLE CHAMBER *

E.G. Pewitt

Argonne National Laboratory.

When this project was begun two years ago, it was not possible to make a firm decision to use a superconducting coil in the 12-ft chamber system. Although we had constructed a superconducting magnet for the 25-cm ANL-CIT helium chamber, there remained numerous engineering problems. In order to consider using a superconducting coil and still meet the four-year construction schedule, parallel designs of superconducting and conventional coils were undertaken which would be compatible with the hydrogen chamber and with the magnet iron. In addition to dimensional constraints, this fixed the operating field strength at 20 kG and fixed the requirement that the superconducting magnet have its own vacuum container.

In June 1966 the design of the superconducting coil had progressed to a point that a decision was made to construct the magnet with superconducting coils. The design clearly demonstrated that the problems were mechanical and cryogenic in nature and not those of "superconductivity." Detailed cost estimates showed that the capital costs of conventional versus superconducting coils were essentially equal. The decision was based mainly on an expected large saving in operating cost by eliminating the required 10 MW of power which would be required for operating the conventional coils.

Figure 1 is a perspective of the chamber assembly. The magnet container is of all-welded construction with a stainless steel inner vessel and an aluminum vacuum container. The all-welded construction of the inner vessel was chosen instead of demountable cold seals because of space limitations, reliability, and cost. The schedule permits at least one disassembly of the cryostat; however, it is expected that by proper modeling of the problems, this will not be necessary.

The coil support structure (which in reality is the helium vessel) is suspended by eight tension support tubes from the magnet iron. The windings are clamped to 10-cm thick stainless steel girder rings which provide radial stiffness. Radial stability is provided by eight rods attached from the girder ring to the magnet iron, as shown in Fig. 1.

---

* Work performed under the auspices of the U. S. Atomic Energy Commission.

Because of the holes in the top of the iron, the net force on the coil assembly centered between the pole faces is expected to be approximately 20,000 Kg downward. The weight of the cryostat will impose an additional load of 100,000 Kg. Vertical adjustment of 1.25 cm in either direction from center is provided to account for mechanical error in coil position, variation in iron permeabilities, and other effects which tend to perturb the downward force. The force on the coil assembly in the vertical direction changes approximately 100,000 Kg per cm of displacement. The eight vertical supports are designed to support 500,000 Kg in tension. The radial instability forces are calculated to be approximately 20,000 Kg per cm of radial displacement from magnetic center. This force will be transmitted to the iron by the radial support members (see Fig. 1) located at 90 degree intervals. The system is designed to support a transverse load of 250,000 Kg.

The schematic for the cooldown of the coils is shown in Fig. 2. Cold helium gas enters a manifold at the top of each coil compartment. This cold gas mixes with warmer gas within the container, setting up large convective flow which cools the coils uniformly. This method of gas circulation in conjunction with vertical aluminum shunting bars connected to the aluminum coil spacers results in very small thermal gradients and, hence, low stresses during cooldown. A 50-cm internal diameter model with the depth of winding of the full size coil and with the full height of one compartment is being constructed to confirm the cooldown calculations and evaluate clamping techniques. Cooldown time is determined by compressor capacity of the 400 W helium refrigerator and is approximately three days.

The details of the coil construction can be seen in Fig. 3. The coils are held in position by an aluminum tie-rod assembly, which clamps the coils to the 10-cm thick girder rings. Aluminum is used for the clamping bolts to maintain clamping force on the coils as the system is cooled down. The coefficients of thermal expansions are such that the clamping force increases somewhat at $4^{\circ}K$. The details of the coil construction are also shown. Aluminum spacers between coils (not shown in the figure) are located every 6 degrees, and they are faced with a thin electrical insulating material. The coefficient of thermal expansion of aluminum matches the coefficient of the copper-teflon composite of the coil, resulting in very low shear forces on the coil-spacer interface. As mentioned above, the ends of the aluminum spacer blocks are thermally shunted in a vertical direction with large aluminum tie bars to minimize vertical temperature differences within the coil stack during cooldown.

The 2000 amp conductor of the coil is a fully stabilized strip, 5×0.254 cm^2 in cross section. To evade the problem of a reinforced conductor, the coils were designed so that the copper stabilizing material will

support the total hoop stress on the windings. The resulting low current density permits edge cooling and allows the rigid "wafer" construction. A partial list of the magnet parameters is given in Table I.

Table I

MAGNET PARAMETERS

Design Field	18 kG
Design Current	2000 amps
Stable Current (Calculated)	4200 amps
Resistance Ratio of Copper	170-200
Conductor Dimensions	5-cm x 0.254-cm
Total Conductor Weight	45,000 Kg
Weight of Superconductor (NbTi)	2000 Kg
Hoop Stress on Conductor	420 kG/cm^2

The electrical circuit is shown in Fig. 4. With 10-V power supply, the charging rate of the magnet is 0.25 amp/sec, resulting in a total charge time of two and one-half hours. During normal operations, switch S2 will be closed to provide stabilization of the magnet. With S1 and S2 open, the energy dump resistor will adsorb the energy stored in the magnetic field whenever it is desirable to quickly reduce the field. In the unlikely event of an open circuit (conductor breakage), the aluminum vacuum vessel walls will limit the field decay with an 8-sec time constant, preventing energy deposition in the chamber vessel.

The construction has proceeded according to schedule so far, and the completion of the magnet is expected in 1969.

LIST OF FIGURES

1. Perspective of the ANL 12-ft hydrogen bubble chamber
2. Schematic of cooldown plumbing.
3. Cross section of the helium container, depicting roughly one-fourth of the winding. On the right is shown a detailed coil wafer.
4. Electrical circuit of the superconducting coil.

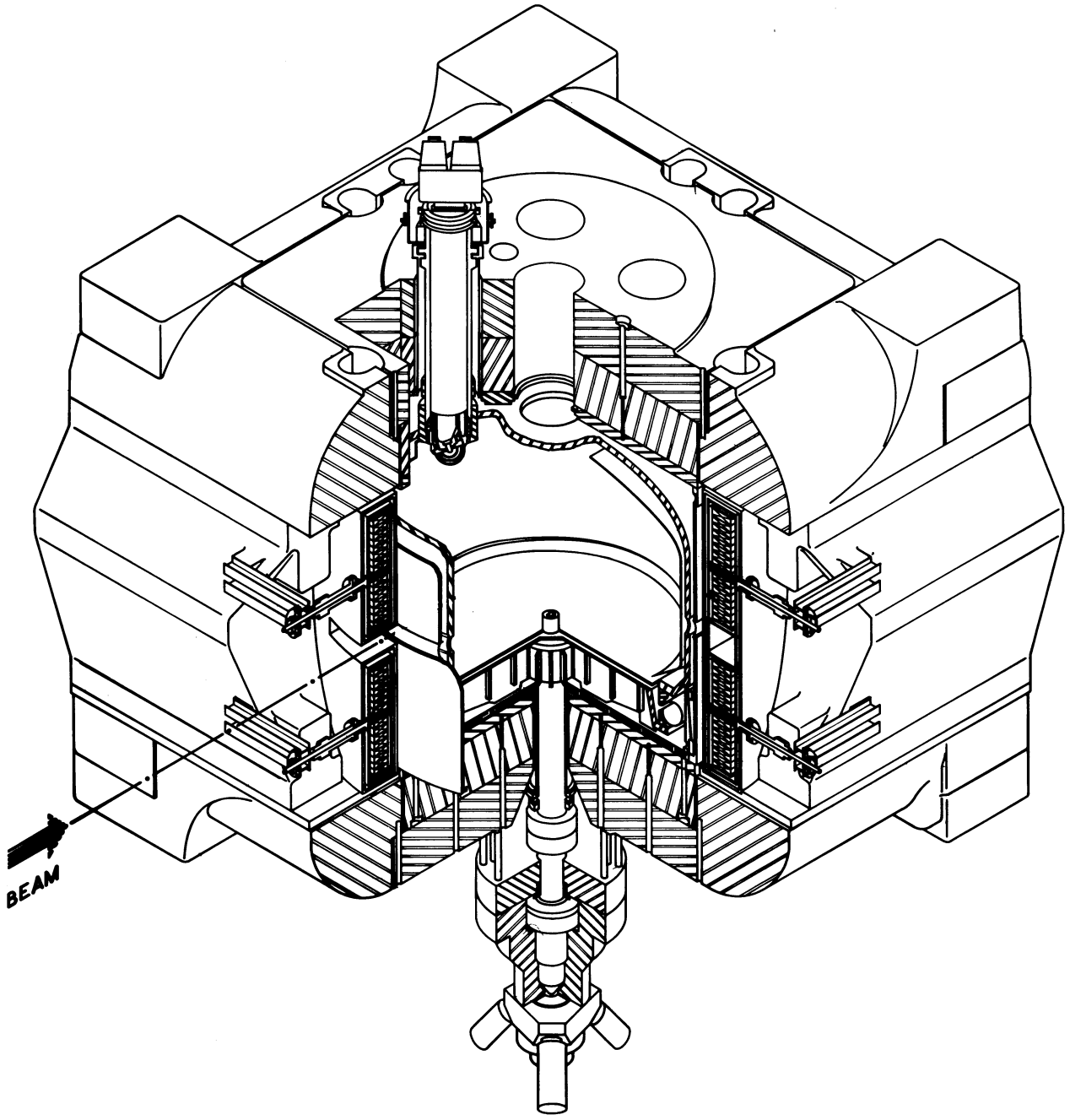

Fig. 1

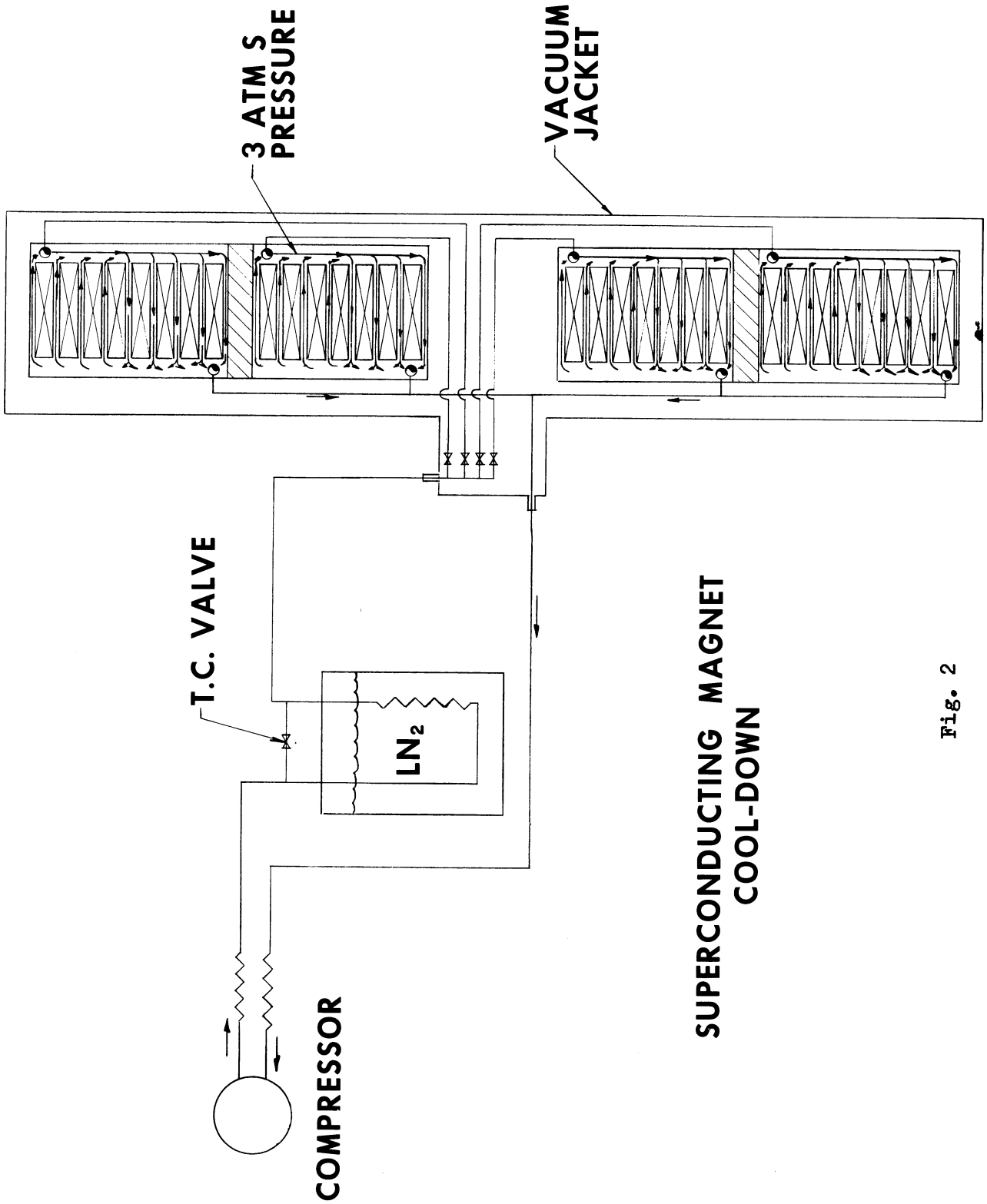
3 ATM S PRESSURE
VACUUM JACKET
T.C. VALVE
LN_2
COMPRESSOR
SUPERCONDUCTING MAGNET COOL-DOWN

Fig. 2

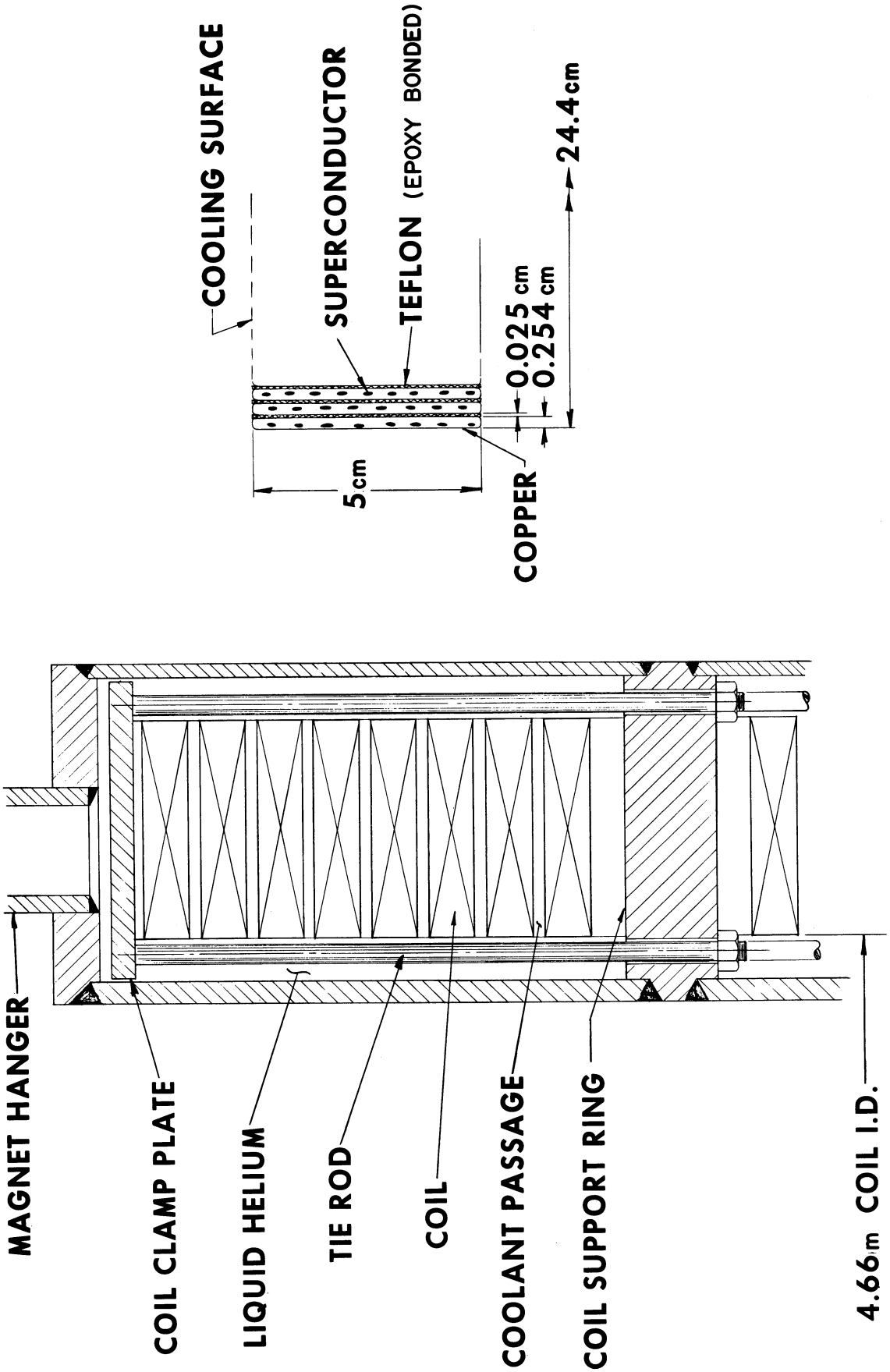
COOLING SURFACE
SUPERCONDUCTOR
TEFLON (EPOXY BONDED)
0.025 cm
0.254 cm
24.4cm
5cm
COPPER
MAGNET HANGER
COIL CLAMP PLATE
LIQUID HELIUM
TIE ROD
COIL
COOLANT PASSAGE
COIL SUPPORT RING
4.66m COIL I.D.

Fig. 3

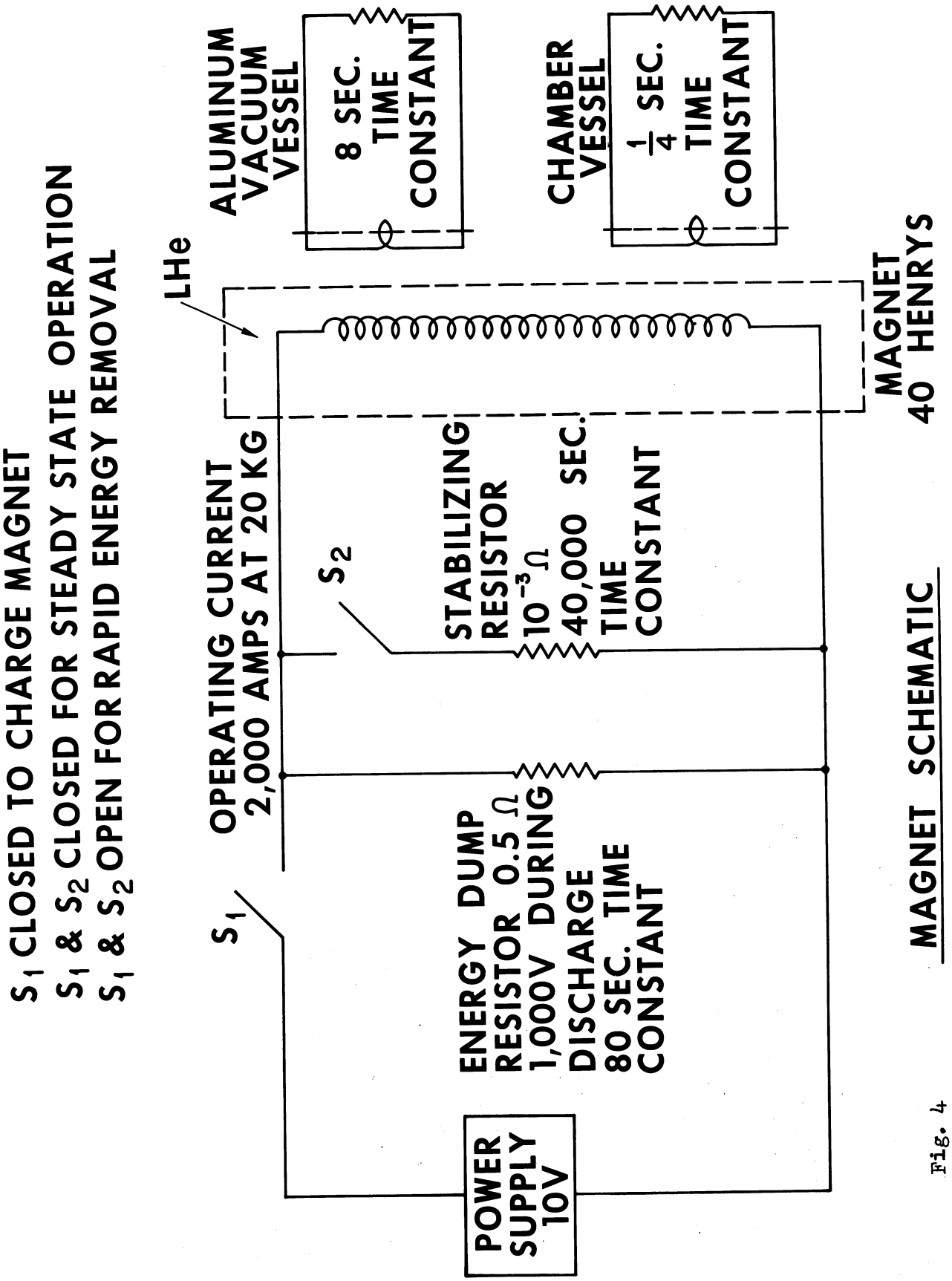
S_1 CLOSED TO CHARGE MAGNET
S_1 & S_2 CLOSED FOR STEADY STATE OPERATION
S_1 & S_2 OPEN FOR RAPID ENERGY REMOVAL
ALUMINUM VACUUM VESSEL
8 SEC. TIME CONSTANT
CHAMBER VESSEL
$\frac{1}{4}$ SEC. TIME CONSTANT
LHe
OPERATING CURRENT 2,000 AMPS AT 20 KG
S_2
STABILIZING RESISTOR $10^{-3}\Omega$ 40,000 SEC. TIME CONSTANT
MAGNET 40 HENRYS
S_1
ENERGY DUMP RESISTOR 0.5 Ω 1,000V DURING DISCHARGE 80 SEC. TIME CONSTANT
POWER SUPPLY 10V
MAGNET SCHEMATIC

Fig. 4

5.2 14-FT BUBBLE CHAMBER RESEARCH AND DEVELOPMENT PROGRAM MECHANICAL DESIGN DETAILS OF MAGNET COIL*)

D.A. Kassner
Brookhaven National Laboratory.

Introduction

Early in the conceptual design phase of the proposed Brookhaven 14' bubble chamber, it was realized that additional research and development was required before the design of some components could be finalized. Rather than setting up a number of individual tests, it was decided to combine, where practical, all tests into one facility. In this manner, not only could the necessary research and development for each component be accomplished, but also the interaction of components could be determined. The scale of this test facility should be large enough so that the extrapolation of the results to the 14' bubble chamber will be reasonable. For these reasons, the design and fabrication of an essentially one-half scale model of the 14' bubble chamber, namely the 7' test facility, was undertaken at Brookhaven. One of the premises used in the design of the 7' test facility was that it should be built with a minimum cost consistent with providing the required information. Also, it was not conceived of as primarily a nuclear research tool, but rather as an engineering test facility - although the possibility does exist at some later date of converting the 7' test facility into an operating bubble chamber.

---

*) Research performed at Brookhaven National Laboratory under the auspices of the U.S. Atomic Energy Commission.

One of the components requiring additional research and development is the superconducting coil. To date, only relatively small coils using the principle of superconductivity have been fabricated and tested. Also, these coils have been wound either using cable type construction, or strip conductors employing edge cooling only. Because of the irregular cross-sectional geometry of cables, they would be difficult, if not impossible, to support against the magnetic forces occurring in very large coils. For economic reasons it is desirable that the 14' coils not only be edge cooled, but also have a percentage of the conductor face area cooled, thereby substantially reducing the quantity of expensive material required -- namely by a factor of 5 or more.

Since none of the superconducting coils to date is of a size or design similar to that required by the 14' bubble chamber, there is a scarcity of needed design, fabrication and operating information. Therefore, in order to acquire the necessary knowledge, it was decided to incorporate into the 7' test facility a superconducting coil.

Except for field strength, every effort was made to use design concepts that could later be applied by scaling to the 14' magnet coil. Wherever calculations were required, they were done in parallel for both 7' and 14' coils. Decisions were based not necessarily on the optimum design for the 7' coil, but rather were based on techniques that eventually could be applied to the 14' coil. In regard to field strength, it was the opinion that the difference between the 20 KG of the 7' and the ultimate 30 KG of the 14' would not substantially alter the validity of the extrapolation. Certainly, a field as high as 20 KG would allow the verification of all calculations and design concepts but at the same time the lower field afforded considerable economics in construction.

Figure No. 1 is a listing of the basic design parameters used in the 7' test facility coil.

Figure No. 2 shows a vertical cross-section through the 7' test facility, detailing the coils and the coil dewar.

It will be noticed from the drawing that the coil dewar is not in an independent vacuum chamber, but rather is contained within the same vacuum chamber that surrounds the hydrogen chamber. Although this concept may represent some loss in flexibility in the utilization of the machine, as well as resulting in additional constraints during the initial construction and tests, the substantial cost reduction represented by a single vacuum chamber appeared to more than offset these disadvantages.

Also, it will be noted that the coils are contained within a single dewar rather than two separate dewars, one for the upper coil and one for the lower coil. The largest force that the coils must be supported against is the attractive force exerted between the coil halves. In the case of the 7' test facility, the total attractive force is 770 tons -- in the 14' bubble chamber the total attractive force is 9,300 tons. If the upper and lower coils are contained within separate dewars, these forces must be restrained by members that connect between the dewar at helium temperature and supports at ambient room temperature. Because of the magnitude of these forces, the cross-sectional area of these support members must of necessity be large, representing a considerable heat leak to the cold dewar. By using a single dewar these support members can be kept internal to the dewar. This means that the only expense in refrigeration resulting from these supports is during the initial cooldown.

The dewar with the coil inside is supported on three legs which in turn are supported by the three main legs of the test facility. These dewar legs are fixed at the bottom and pinned at

the top, allowing them to deflect, compensating for the contraction of the dewar when it is cooled. These three legs represent a minimal heat leak since they must only support the weight of the dewar and coil.

The dewar consists of a 3/8" thick outer wall, a 5/8" thick inner wall, a 3/8" thick semi-circular top and a 1" thick bottom plate all fabricated from type 316 L stainless steel. The semi-circular dewar top is welded to the outer wall, and this assembled unit is then joined to the dewar inner wall and bottom plate by two sealed and bolted flanges. Consideration was given to the possibility of welding the dewar closed, but there is insufficient experience as to the reliability of this type of coil to chance semi-permanently sealing the dewar. Certainly a test facility should be designed so that components can be inspected and if necessary modified with minimum effort.

A complete coil assembly consists of 8 double pancakes below and 8 double pancakes above the beam centerline separated by a bridge structure. The lower coil unit rests on a one-inch thick stainless steel washer and is attached to the bridge by 1/2" diameter tie rods. In a similar fashion, the upper coil is also attached to the bridge. The bridge structure is designed so that it can be separated, allowing the upper and lower coil assemblies to be handled as units.

This modular construction allows the coils to be pre-assembled, including inter-pancake electrical connections, clamps, and etc. external to the dewar. By dividing the coils into two units, the weight of each unit is comparable to the weight of other major components, for example the vacuum chamber and the hydrogen chamber, resulting in optimum crane capacity.

Figure No. 3 shows the various components used in the coil winding itself. The stabilized superconductor strip consists of a

number of parallel paths of Nb-Ti wires metallurgically bonded into O.F.H.C. copper. The strip measures 2 inches wide by .080 inches thick and has a current carrying capacity of about 4000 amperes under the conditions existing in this particular coil.

Turn to turn electrical insulation in the coil windings is provided by a .005 inch thick Mylar strip backed with adhesives which is wound in adjacent to the conductor strip.

To aid in supporting the stresses in the magnet windings, a reinforcing strip made of stainless steel .006 inch thick is wound in with the conductor. The stress in the copper could be limited by greatly increasing the amount of copper in the conductor beyond that required for stabilization. A less expensive technique is to use a separate support strip whose physical properties are superior to copper -- for example, stainless steel.

In a detailed analysis of the stresses produced in the conductor, consideration was given to (a) stresses produced by bending the conductor in the winding process, (b) the hoop stresses caused by the electromagnetic forces, (c) the local compression stresses produced by bearing of the spacer strip on the conductor, (d) the stresses produced by the conductor bending between points of contact on the spacer strip, (e) thermal stresses resulting from the use of stainless steel and copper.

Adjacent to the support strip is the spacer strip which provides cooling channels for the liquid helium refrigerant to make contact with one face of the conductor. One of the design problems that defied solution for a long time was this spacer strip. Contradictory requirements of maximum open area for helium flow, combined with the need for sufficient support of the conductors, complicated the solution.

Support requirements of the spacer strip result from a detailed analysis of the force transfer from one conductor to another. Figure No. 4 shows two typical adjacent conductors with the spacer strip between them, and also a force profile across the coil width. As a result of the magnetic field distribution, the innermost turn of the coil is subjected to a maximum force outward. This force reduces to zero near the outer turn and finally results in a small force inward

on the outermost turns. Because of this force distribution, the spacer strip is required to transfer forces from one turn to the next so that the result will be an essentially uniform force across the width of the coil. It would be practically impossible to guarantee that the support areas of adjacent spacer strips would be located directly in line. Probably at some locations in the coil the support area of one spacer would be located between the support area of an adjacent spacer strip. Essentially this configuration results in the conductor acting as a continuous beam with a central load between supports. The maximum bending moment derived from this configuration is $M = \frac{f\ell}{8} (\ell - \frac{d}{2})$ where f is the unit load on a conductor, d is the circumferential width of support area, ℓ is the circumferential distance between centerlines of the support area.

If d is made equal to $\ell/2$, resulting in 50% support circumferentially, the maximum bending moment and thus the maximum bending stress varies as the square of the distance between centerlines of the support areas. For a value of ℓ = 1/4 inch, this bending stress in the 7' coil conductor is about 1500 psi. To minimize the contribution to the total stress in the conductor from this consideration, it is imperative to limit the distance between support areas. Also, the support areas should be rigid in the radial direction since any deflections would result in non-uniform force distribution across the coil. The result of the support and cooling requirements is that the spacer strip should consist of small solid support areas located on a fine grid. Additionally, the strip should be: (1) inexpensive to fabricate, since 40,000 feet are required in the 7' coil and 120,000 feet for the 14' coil; (2) it should be produced using standard machines and techniques so that the expense and time involved in developing special machinery can be avoided; (3) it should have the same coefficient of thermal expansion as the conductor.

Figure No. 5 shows the details of a spacer strip that satisfies

all the above-mentioned requirements. This strip is fabricated by a two step process using standard machine tools and techniques. In the first step, 8 equally spaced grooves .037 inch deep and 1/8 inch wide are either milled or rolled longitudinally in a .057 inch thick by 2 inches wide strip of copper. The cost of this process is about $.11 per foot. In the second step, sections of copper 1/8 inch wide and 1/4 inch apart are punched out of the strip transverse to the grooves at a cost of $.05 per foot. These two steps leave an array of rectangular "bumps" .057 inch high and 1/8 inch on a side whose centers are 1/4 inch apart. These bumps are carried by three continuous strips .020 inch thick by 1/8 inch wide, that remain after the punching process. The helium coolant may then flow through the longitudinal and transverse grooves between the bumps, resulting in about 75% of the conductor face area exposed to the helium. Including material and processing, the total cost of this spacer strip is about $.50 per foot.

The stabilized superconductor, spacer strip, insulation and stainless steel support strip are spirally wound to form double layered pancakes.

The layers of each pancake are supported and insulated from each other by 1/8 inch thick plastic cooling spacers which are slotted to provide for radial and axial flow of the liquid helium coolant. See Figure No. 6. In a similar fashion, neighboring pancakes are supported and insulated by spacers 5/8 inch thick. These spacers are fabricated from a fiberglass based phenolic that has the same coefficient of expansion as copper, and are located in position by slots that are guided on the tie rods connecting the coil face plates to the bridge structure.

Also shown on Figure No. 6 are the details of the radial clamps. The main function of these clamps is to secure the pancakes when they are removed from the winding fixture prior to installation in the coil units. Lifting of the pancakes will be accomplished by a fixture bolted to these clamps. These clamps are fabricated from

phosphor bronze, having a top and bottom plate with slots for axial flow of helium, an inside plate contoured to match the inside coil radius and a front plate. The front plate contains four set screws that act against two pressure plates, providing a radial clamping force.

Figure No. 7 shows the details of an end clamp for constraining the conductor terminating ends of individual pancakes. The ends are essentially "hooked" around a phenolic clamping block and secured to it by a bolted pressure plate. This results in the ends acting against each other, "locking" up the forces within the pancake. Because the centerline of the end forces are displaced vertically, there results a torque on the clamping block. This torque is balanced by attaching the clamping block to two modified radial clamps that bear on the upper and lower horizontal edges of the coil.

Figure No. 8 shows the proposed configuration of an inter-pancake electrical connector. It consists of a phosphor bronze unit shaped on one side to match the outer coil radius, and on the other side it has an entrance ramp, a flat clamping area and an exit ramp. Ears containing tapped holes protrude top and bottom. Prior to completing the outermost turn, this unit is located in position. The outer turn is then displaced radially 3/4" from the adjacent turn by winding it around the outside face of the connector, allowing sufficient space above and below the conductor for bolts. To provide additional contact area, two parallel superconducting strips are clamped to the outer turn by a 3/4 inch thick pressure plate and six 1/2 inch diameter bolts.

Figure No. 9 shows the complete array of inter-pancake electrical connections. The pattern of electrical connections results in longer lengths of interconnecting strips, providing flexibility should there be any relative motion between pancakes during cooldown or operation. Current enters pancake No. 1 on the upper layer at point (A). It proceeds through the upper spiral, crosses to the

lower layer at the interal cross-over, proceeds through the lower spiral, and exits at point (B) on the lower layer of pancake No. 1. The lower layer of pancake No. 1 is connected to the upper layer of pancake No. 2 at point (C) by the external connector. This stepping procedure is continued until the lower layer of pancake No. 8 is reached (point D). A jumper is provided around the bridge and connected to the upper layer of pancake No. 9 (point E). In a procedure similar to the lower coil half, the current is routed from pancake to pancake in the upper coil, ultimately exiting at the lower layer of the top pancake (point F). Current is returned from this point by a superconducting strip to the bottom of the coil where it exists through the dewar bottom plate completing the electrical circuit.

Figure No. 10 shows the details of the internal crossover. In order to transpose the conductor from the lower layer to the upper layer at the inside diameter of a pancake, it must be edge bent through a distance 2-1/8 inches. This is accomplished over a relatively long length, namely 90^{o} of arc length, to minimize the stress in the conductor. A 1/2 inch thick "cross-over plate" milled on the coil side, providing clearance for the protruding cooling spacer fingers, is located against the inner coil radius. The conductor is guided to the inner face of this plate by an entrance ramp where it is edge bent, bringing it to the level of the upper layer, and then guided back to the inner coil radius by an exit ramp. The conductor is secured to this plate by bolted support clips. Three modified radial type clamps secure the cross-over plate in position against the inner coil radius. To avoid edge bending of the thin stainless steel support strip, it is terminated and joined by hard soldering at each end of the cross-over plate.

Due to manufacturing limitations, the longest length of superconducting strip obtainable is just sufficient to wind a single

pancake layer, necessitating a splice joint on the inner radius. Since there is insufficient confidence in the capability of soft soldered joints to transfer the required force, and hard soldered joints degrade the current carrying capacity of the conductor, a combination of the two soldering techniques is used, eliminating the disadvantages of each method. The ends of the conductors are first hard soldered together. A superconducting strip is then soft soldered on both sides of the splice joint, bypassing the section degraded by the hard soldering. A radial clamp as previously described is located at each of the soft soldered joints, providing a mechanical clamping force on the joint.

A completed pancake is composed of the following components:

1) Coil winding components including superconductor, insulation, support strip and spacer strip.
2) Cooling spacers, 1/8" and 5/8" thick.
3) Radial clamps.
4) End clamp assembly.
5) Electrical connectors.
6) Internal cross-over assembly.
7) Internal splice joint.

Figure No. 11 shows a plane view of a completed pancake assembly, locating the above components.

Acknowledgements

The author wishes to acknowledge the very substantial contributions of the Bubble Chamber Magnet group, in particular G.T. Mulholland, A.G. Prodell and R.P. Shutt to the design of the magnet coils.

DAK:pm

FIGURE CAPTIONS

FIGURE	1	7' Test Facility Coil Parameters
	2	7' Test Facility Vertical Cross Section
	3	7' Test Facility Magnet Coil Components
	4	7' Test Facility Force Distribution
	5	7' Test Facility Spacer Strip
	6	7' Test Facility Details of Cooling Spacers and Radial Clamp
	7	7' Test Facility End Clamp Assembly
	8	7' Test Facility Inter-Pancake Electrical Connector
	9	7' Test Facility Inter-Pancake Electrical Ass'y
	10	7' Test Facility Internal Cross-over
	11	7' Test Facility Plan View Completed Pancake

7' TEST FACILITY
COIL PARAMETERS

NUMBER OF DOUBLE PANCAKES	16
TOTAL NUMBER OF LAYERS	32
TURNS PER LAYER	45
TOTAL NUMBER OF TURNS	1440
COIL CURRENT (AMPERES)	4000
AMPERE TURNS	5.76×10^6
CENTRAL FIELD (KILOGAUSS)	20
MAXIMUM FIELD (KILOGAUSS)	27
DISTANCE BETWEEN SPLIT PAIRS (INCHES)	13.25
COIL INSIDE DIAMETER (INCHES)	94.75
COIL OUTSIDE DIAMETER (INCHES)	108.75
CONDUCTOR LENGTH PER LAYER (FEET)	1250
TOTAL CONDUCTOR LENGTH (FEET)	40,000
WEIGHT PER PANCAKE (POUNDS)	2,000
TOTAL COIL WEIGHT (POUNDS)	32,000

FIGURE 1

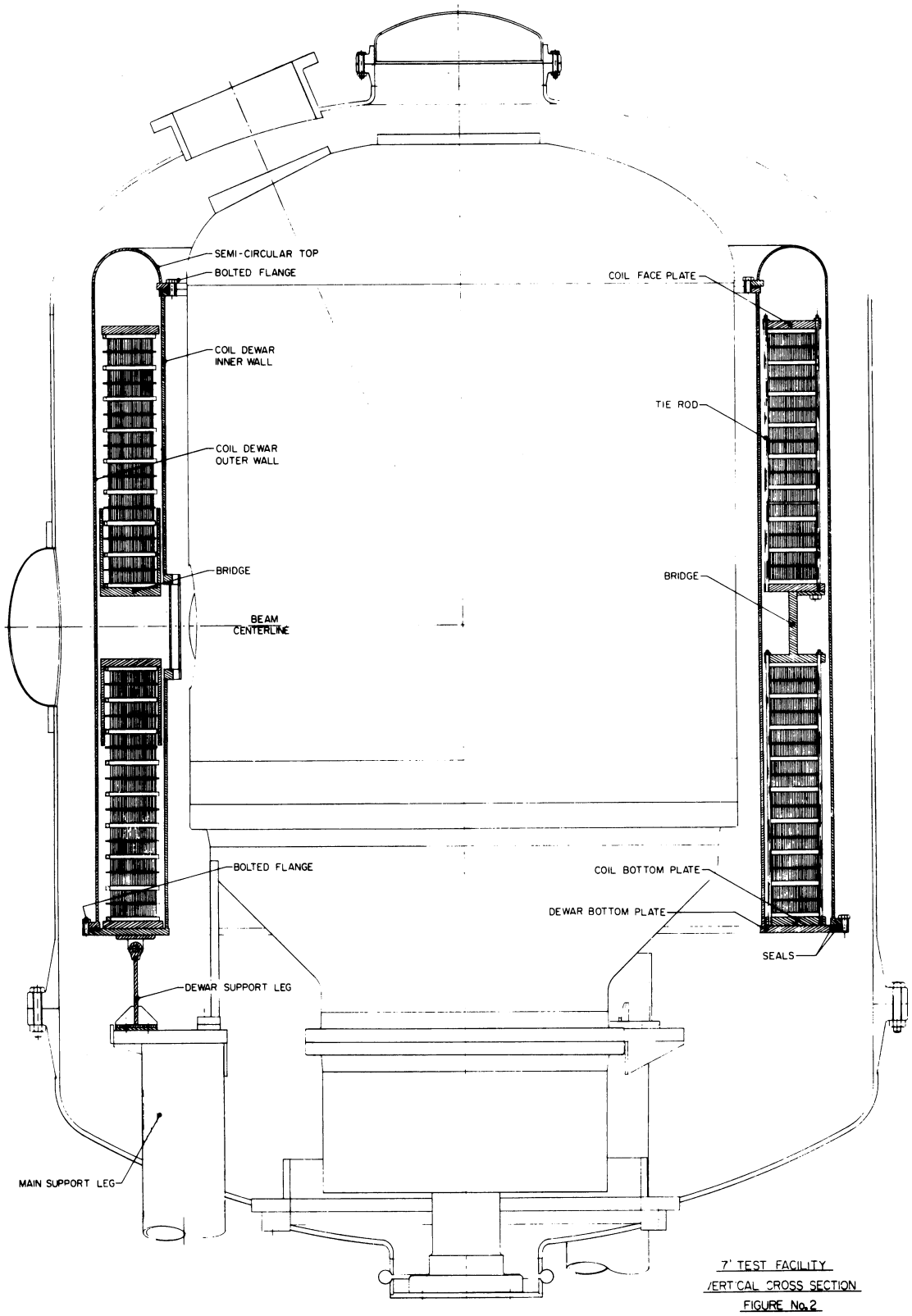

7' TEST FACILITY
VERTICAL CROSS SECTION
FIGURE No. 2

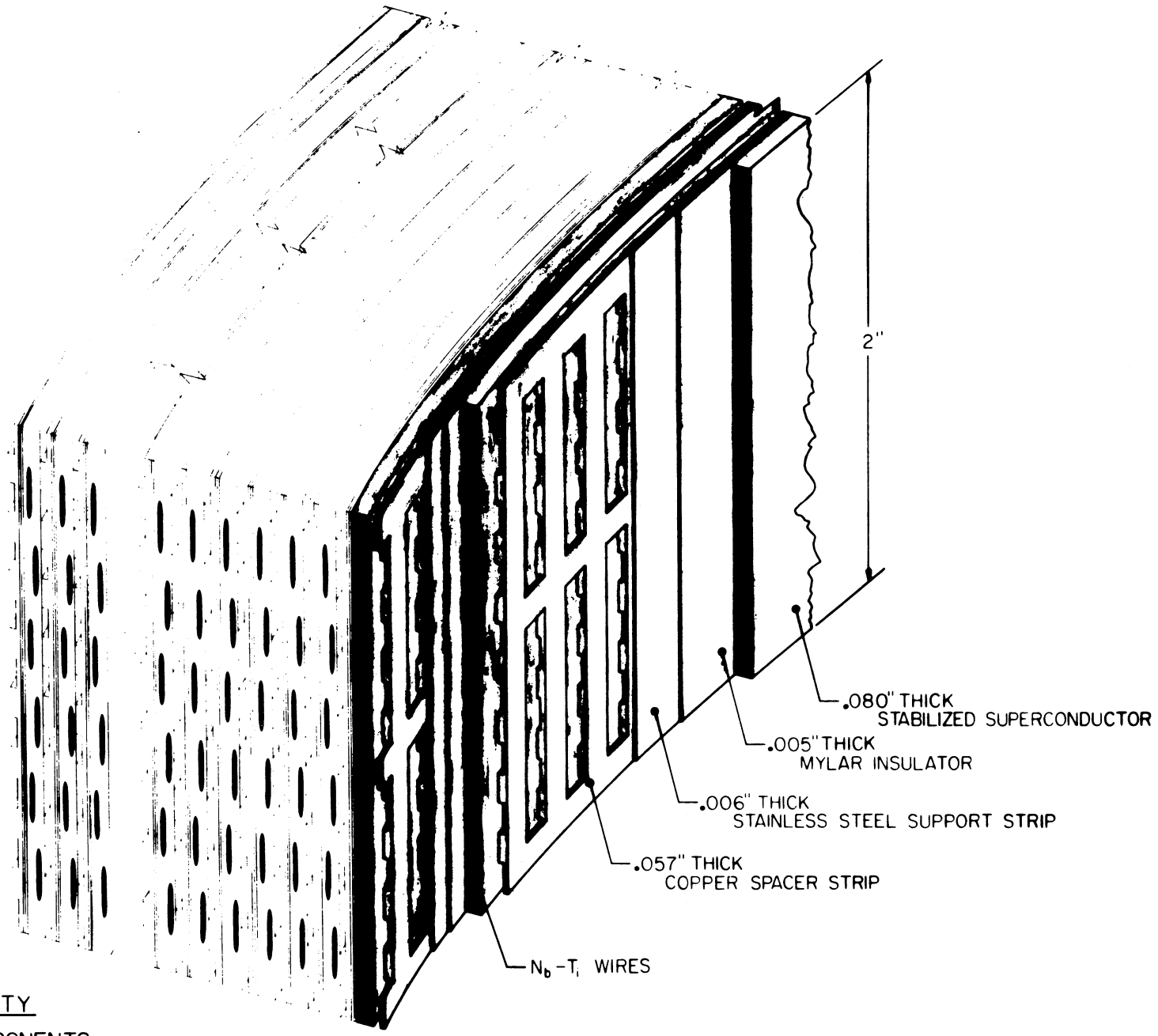

7' TEST FACILITY
MAGNET COIL COMPONENTS
FIGURE No. 3

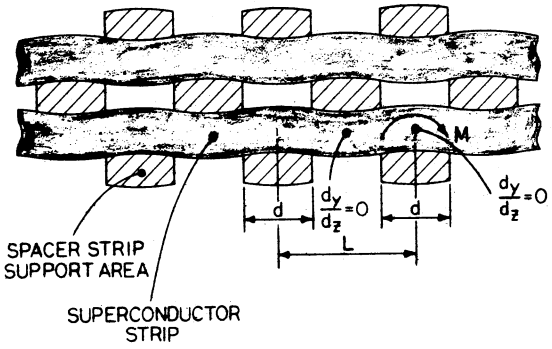

$$M_{max} = \frac{fL}{8}(L-d)$$

Where

M_{max} = MAXIMUM BENDING MOMENT
f = UNIT LOAD ON CONDUCTOR
d = SPACER SUPPORT WIDTH
L = CENTERLINE DISTANCE BETWEEN SUPPORTS

If $d = \frac{L}{2}$

Then

$$M_{max} = \frac{fL^2}{16}$$

FORCE TRANSFER THROUGH SPACER STRIP

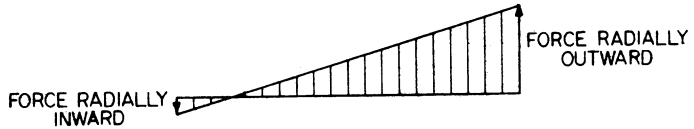

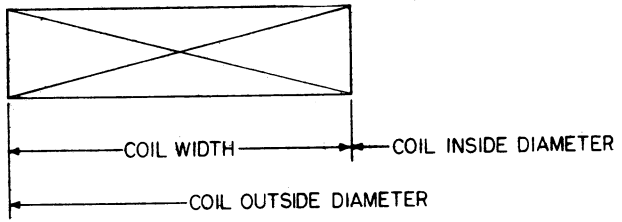

VARIATION OF RADIAL FORCE ACROSS COIL WIDTH

FIGURE 4
7' TEST FACILITY
FORCE DISTRIBUTION

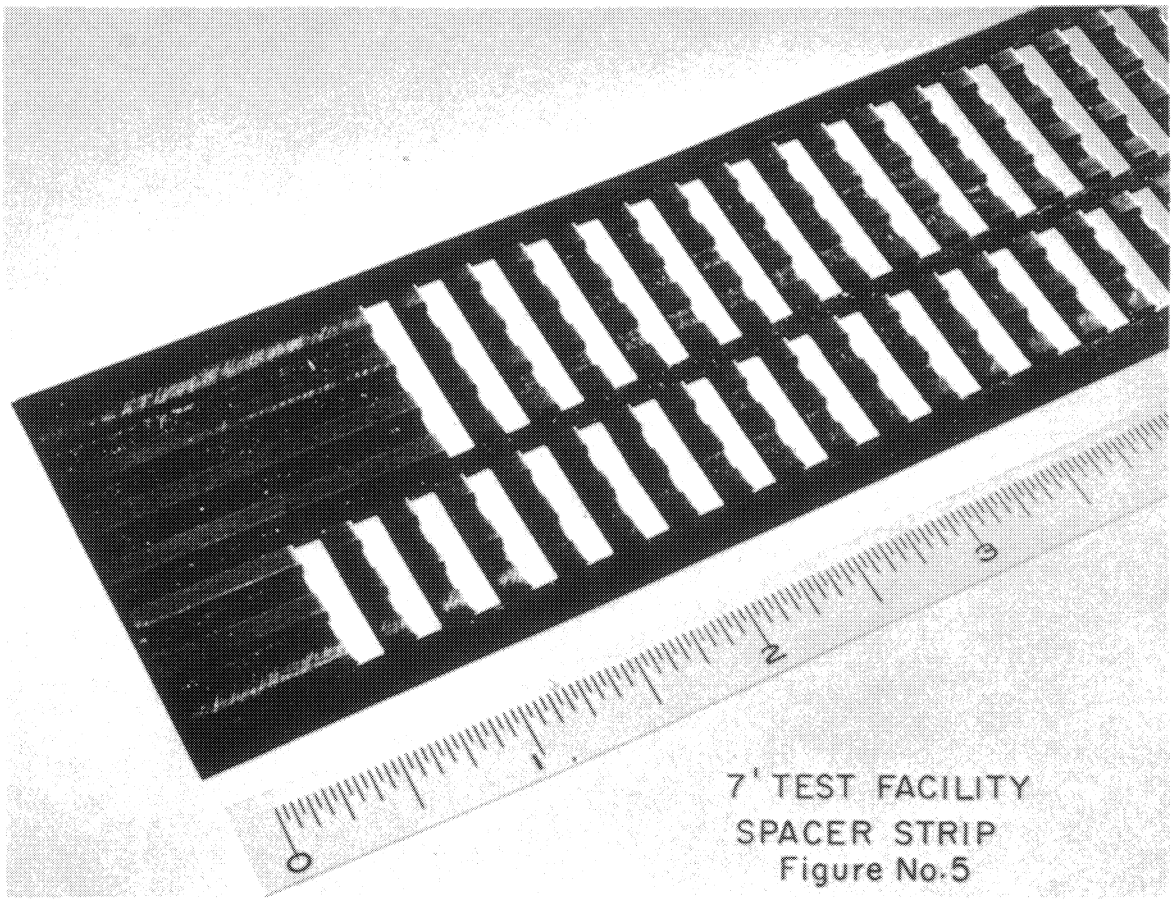

7' TEST FACILITY
SPACER STRIP
Figure No.5

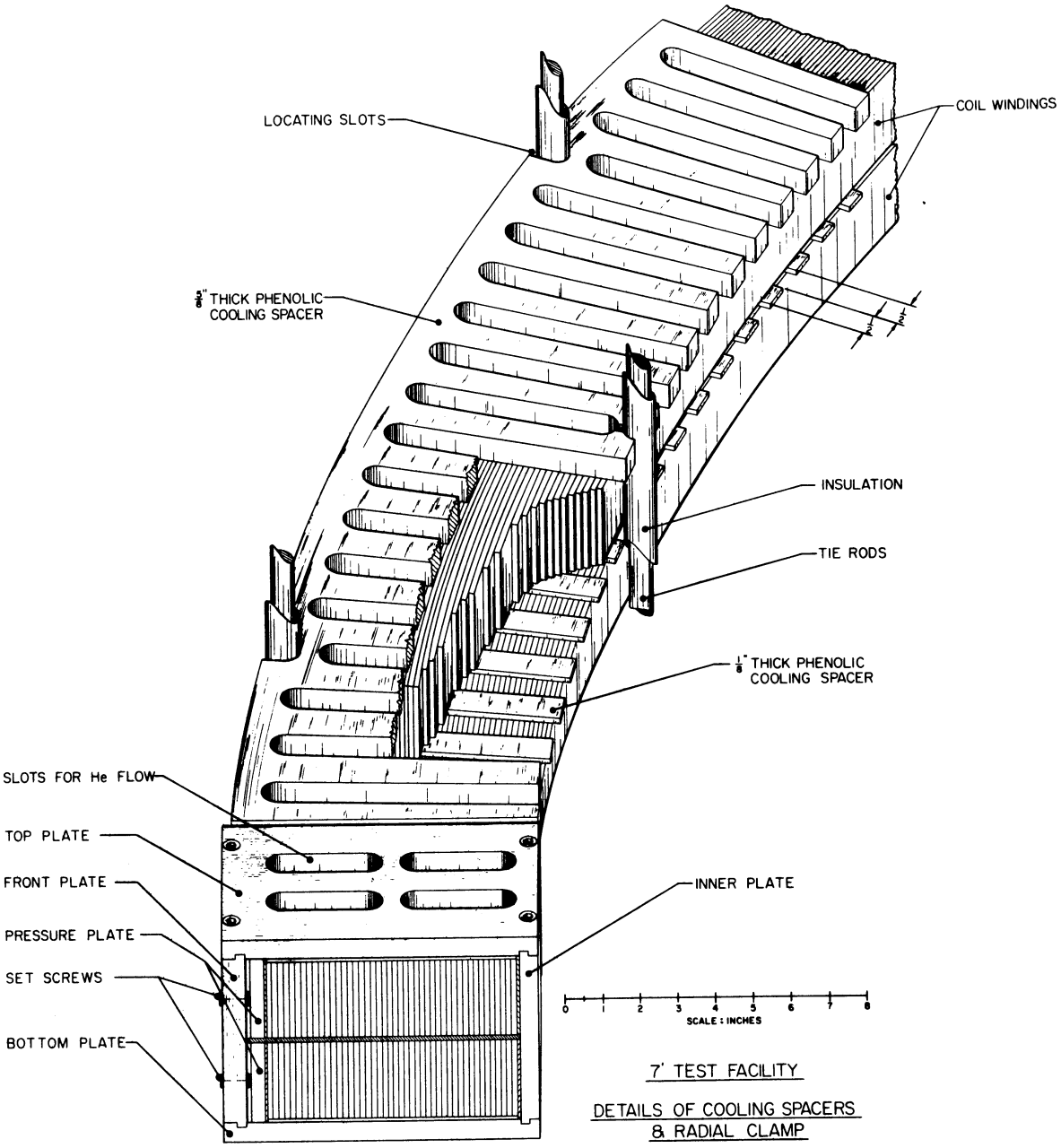

7' TEST FACILITY

DETAILS OF COOLING SPACERS & RADIAL CLAMP

FIGURE No. 6

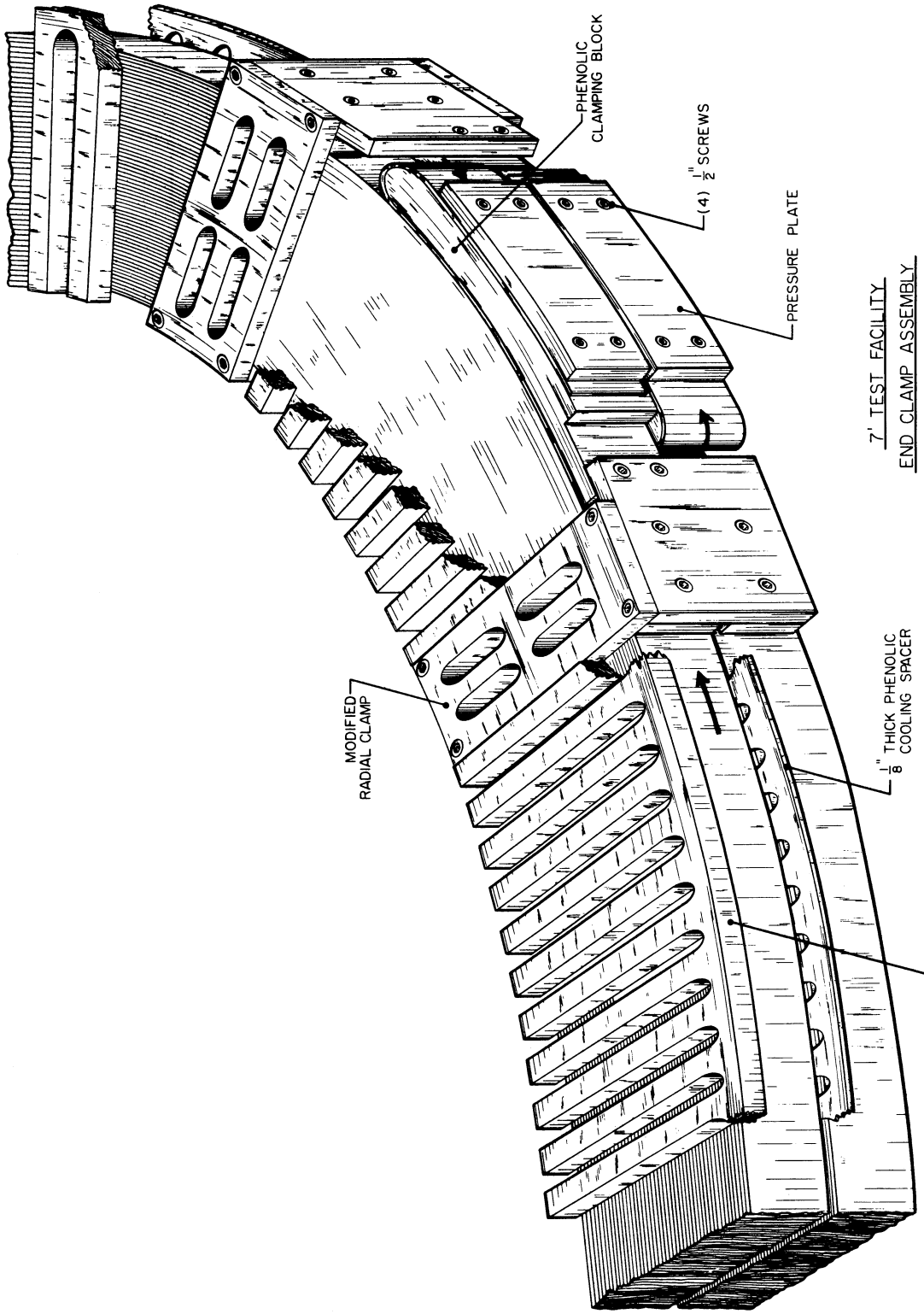

7' TEST FACILITY
END CLAMP ASSEMBLY
FIGURE No. 7

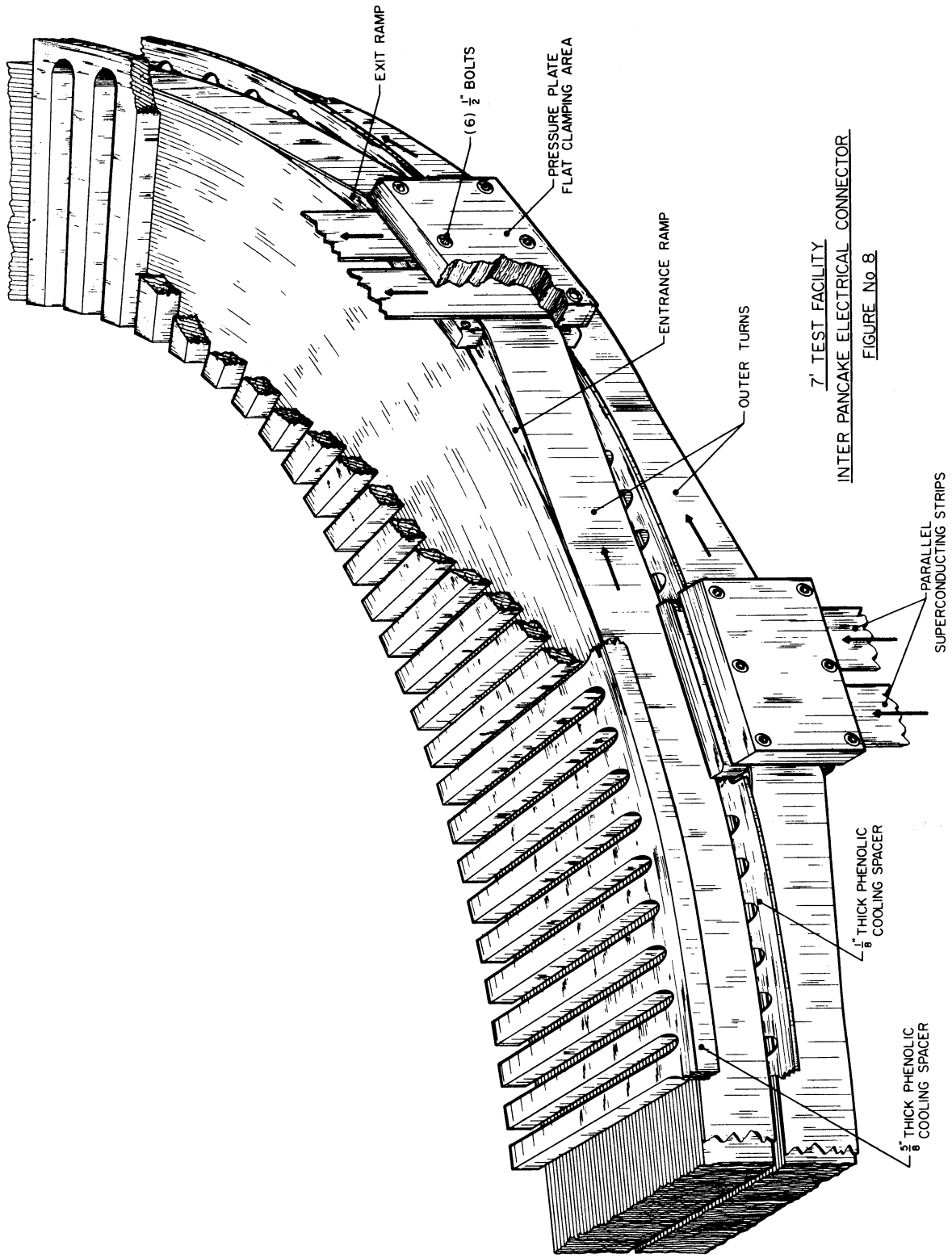

7' TEST FACILITY
INTER PANCAKE ELECTRICAL CONNECTOR
FIGURE No 8

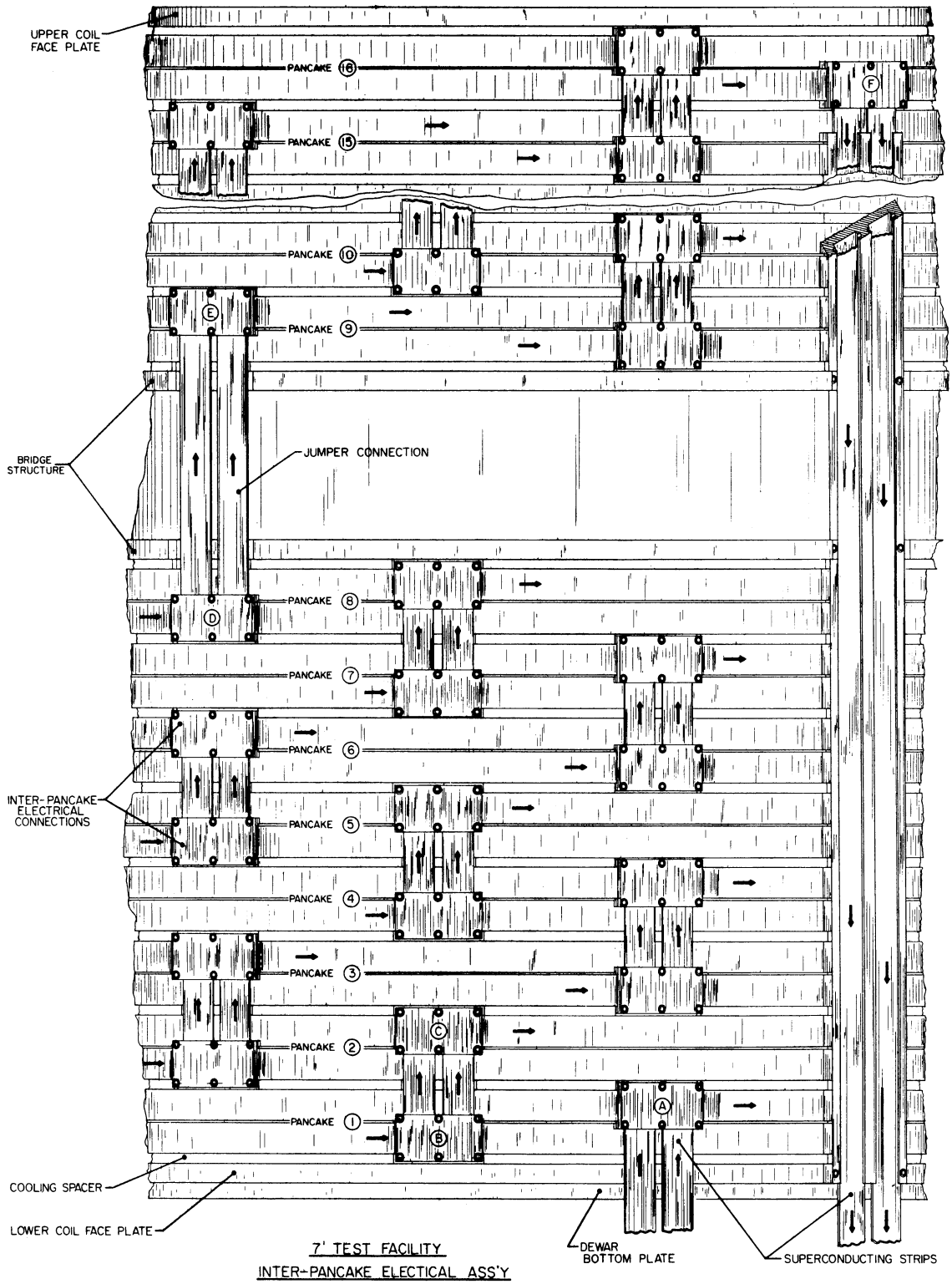

7' TEST FACILITY
INTER-PANCAKE ELECTICAL ASS'Y
FIGURE No. 9

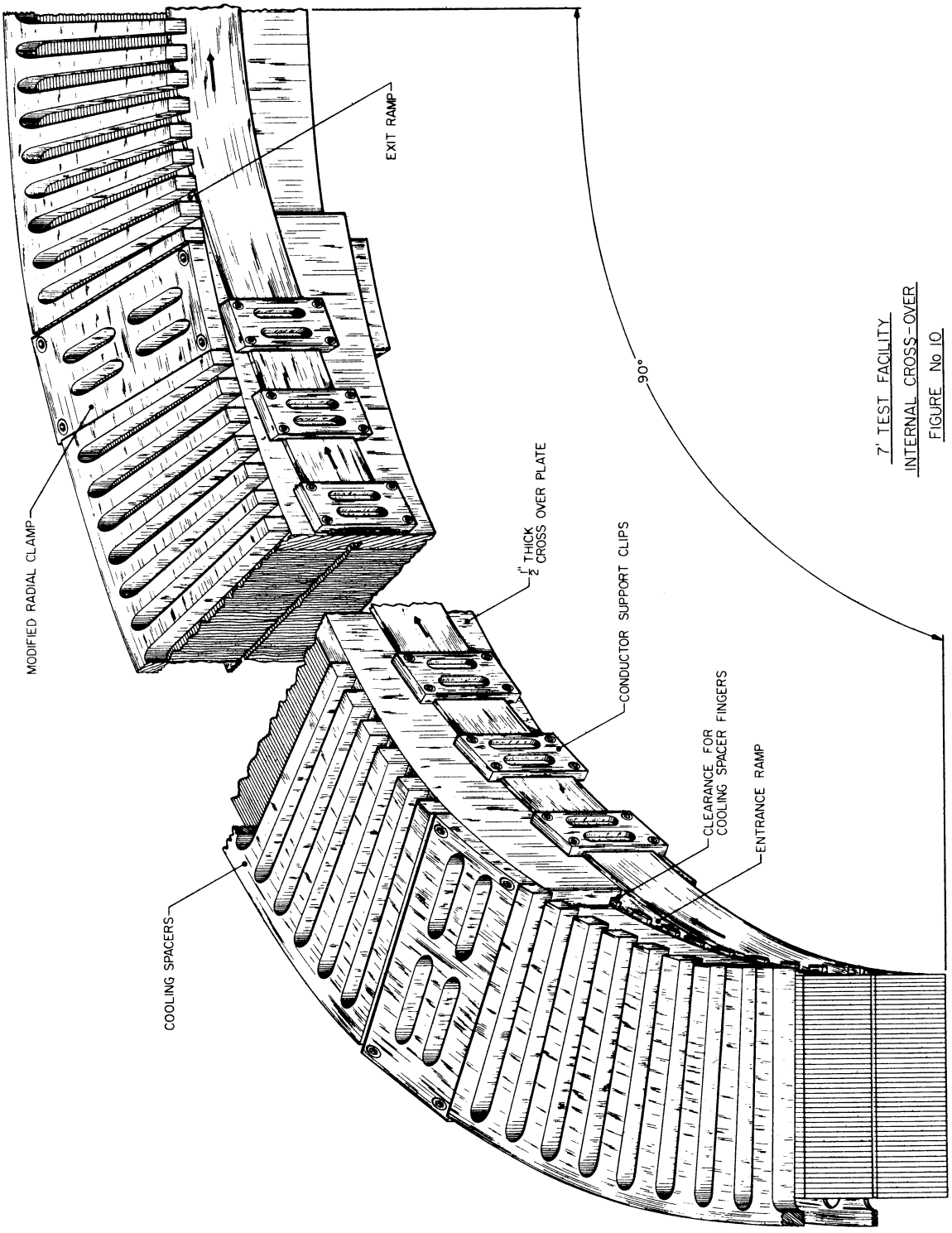

7' TEST FACILITY
INTERNAL CROSS-OVER
FIGURE No 10

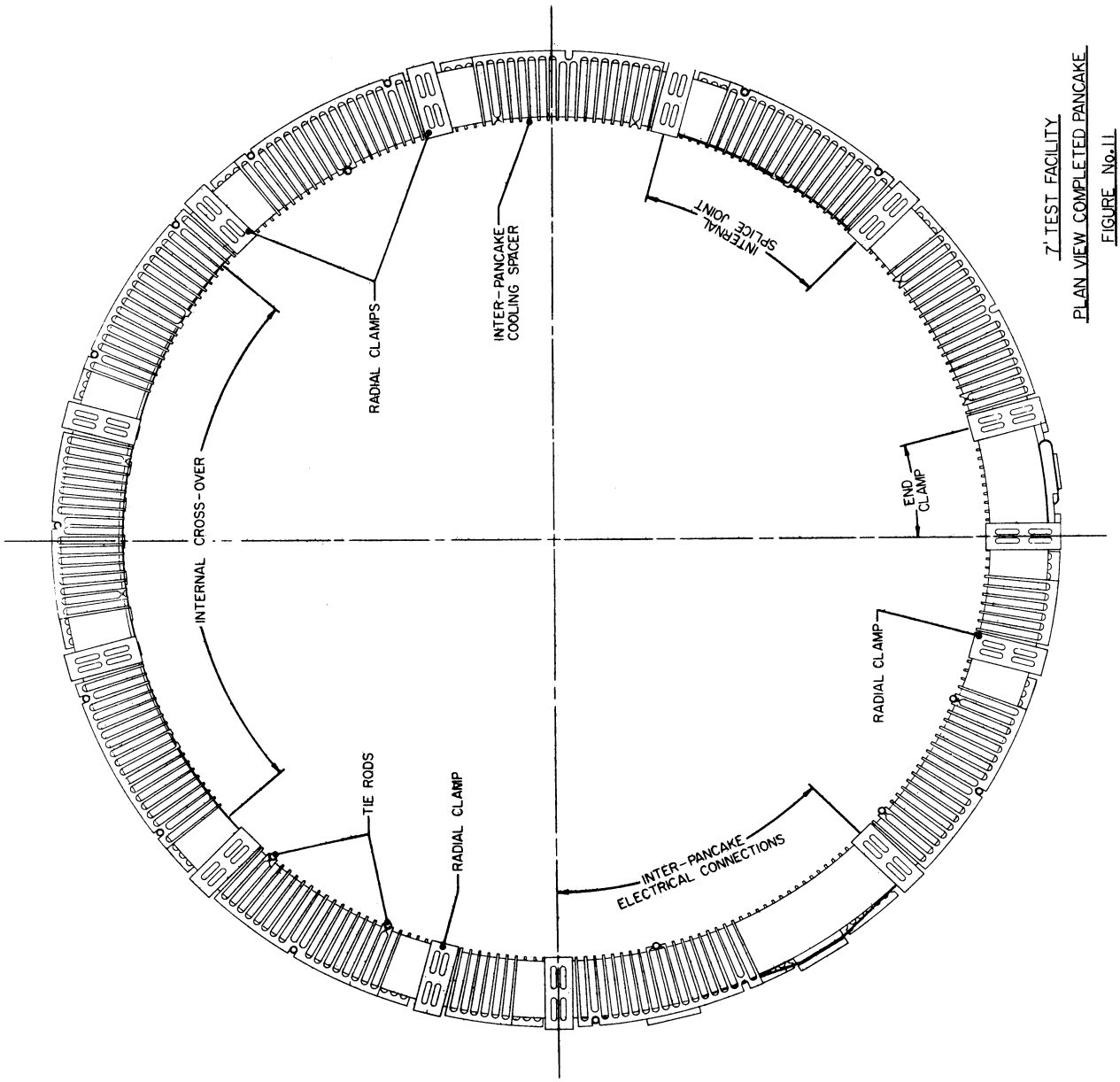

7' TEST FACILITY
PLAN VIEW COMPLETED PANCAKE
FIGURE No.11

5.3 MAGNET DEVELOPMENT PROGRAM FOR THE LARGE EUROPEAN HYDROGEN BUBBLE CHAMBER

Study Group for a Large European Bubble Chamber
CERN
(Presented by F. Wittgenstein)

In order to prepare the technical specification of the coils arrangement for the 3.5 m - chamber, a magnet development programme has been foreseen.

We recalled that the final coils should have the following general features:

Inner diameter:	~ 4700 mm
Pole height:	~ 1600 mm
Intermediate gap:	~ 1000 mm
Central field:	3.5 Teslas
Total stored energy:	~ 750 M joules

The main problem to be investigated experimentally concerns the following points:

- Structure of a possible shielding box.
- Observation of the behaviour of superconductors under magnetic and mechanical stresses.

- Current supply leads up to 12 000 A.
- Discharging energy systems.
- Behaviour of the selected conductor arrangement in case of quenching.
- Control systems.
- Winding techniques.

This talk concerns specially the preparation of the magnet system devoted to the tests of superconductors under mechanical and magnetic stresses.

However chronologically we should mention first the arrangement prepared for the preparation of the test place and some studies on a possible shielding box. The general lay-out of this model, approximative scale 1/20 relative to the chamber magnet, is given in fig. 1. The coil itself has been put at our disposal by the "Commissariat à l'Energie Atomique" in Saclay. As we think that the volume around the chamber should be closed in order to minimise the volume with forced ventilation and to limit the danger of magnetic objects attracted in the stray-field, one solution could be to build this closing wall as a shielding box. Different lay-outs of this box should be investigated. Considering the effect of the stray-field on neighbouring magnetic assemblies one could mention attractive forces of the following orders of magnitude at a distance of 7 m from the chamber centre:

- Air-core of 10^6 At, 1 m Ø $\sim$ 4 tons
- Neutrino shielding $\sim$ 15 tons.

The final decision concerning the shielding should take into account the above mentioned features and the percentage reduction of the stray-field around the chamber versus the financial charges, the risks of inhomogeneous attractive forces and the supplementary ground loads.

To test the conductors as mentioned before we are preparing a test system according to fig. 2.

The magnet should develop a central field of 6 T with a free aperture of 390 mm. This construction corresponds to a stored magnetic energy of about 1.8 M Joules.

Different conductors geometries have been envisaged for the manufacturing of these coils. Two of the most interesting proposals are shown by fig. 3.

The S-conductor uses copper as substrate and the C-conductor is a combination of pure aluminium and stainless steel. The advantages of aluminium appears from the weights comparison. For the S-conductor the weight per meter for 6.6 T is about 140, 7 g and 115,1 g for 4.2 T. For the C-conductor and for both same fields we have 52 g.

Both conductors are graded so that each coil is composed of two parts. The conductor of the inner part should accept a maximum field of 6.6 T and the outer part a maximum field of 4.2 T.

The purpose of the Braracourcix system is to test superconducting short samples under mechanical and magnetic stresses.

Therefore a test device as shown in fig. 4 should be inserted inside of the coils. An elastic bellows deformed by helium under pressure should allow to test the sample under stresses of 12 - 14 kg/mm^2. The tested length should be of the order of 200 mm.

As the nominal current for the coils of the chamber is not yet defined but could be as high as 10.000 A, the current bushings of the test system shall be dimensioned for 12 000 A.

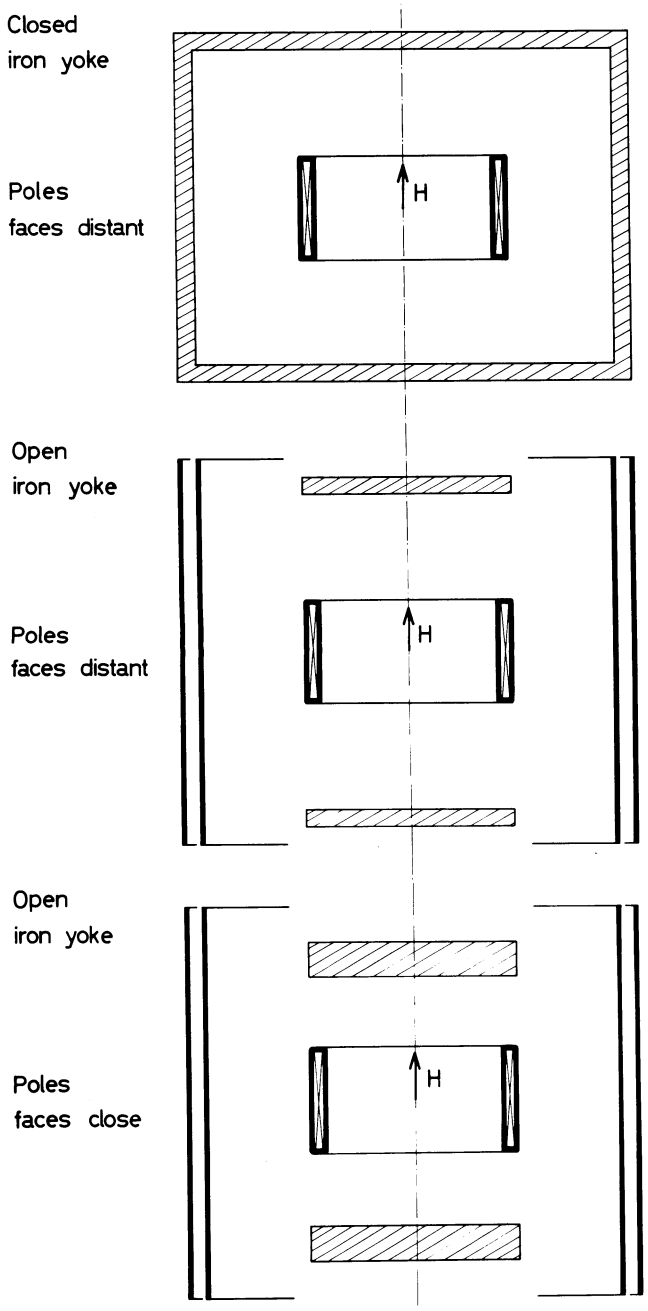

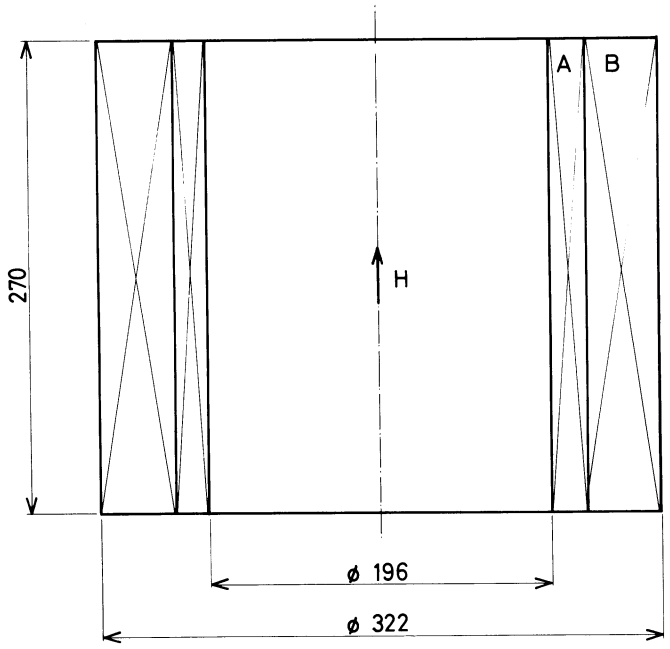

GENERAL CHARACTERISTICS

Rated current : 230 A.

Central field : 3,6 T.

Maximum field : 5,1 T.

Average current density J_A : 5 400 A. cm^2
J_B : 8 680 A. cm^2

Total stored magnetic energy : 68 k. joules

Total length of conductor A : 790 m.
B : 2670 m.

Conductor type
- A : cable Nb. 48% Ti. 3x ø 0,5 mm.
  + Cu. 4x ø 0,6 mm.
- B : cable Nb. 48% Ti. 3x 0,38 mm.
  + Cu. 4x ø 0,45 mm.

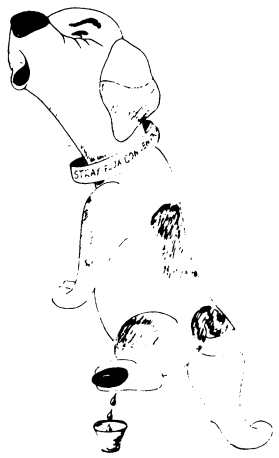

General layout of the AZOR system Fig. : 1

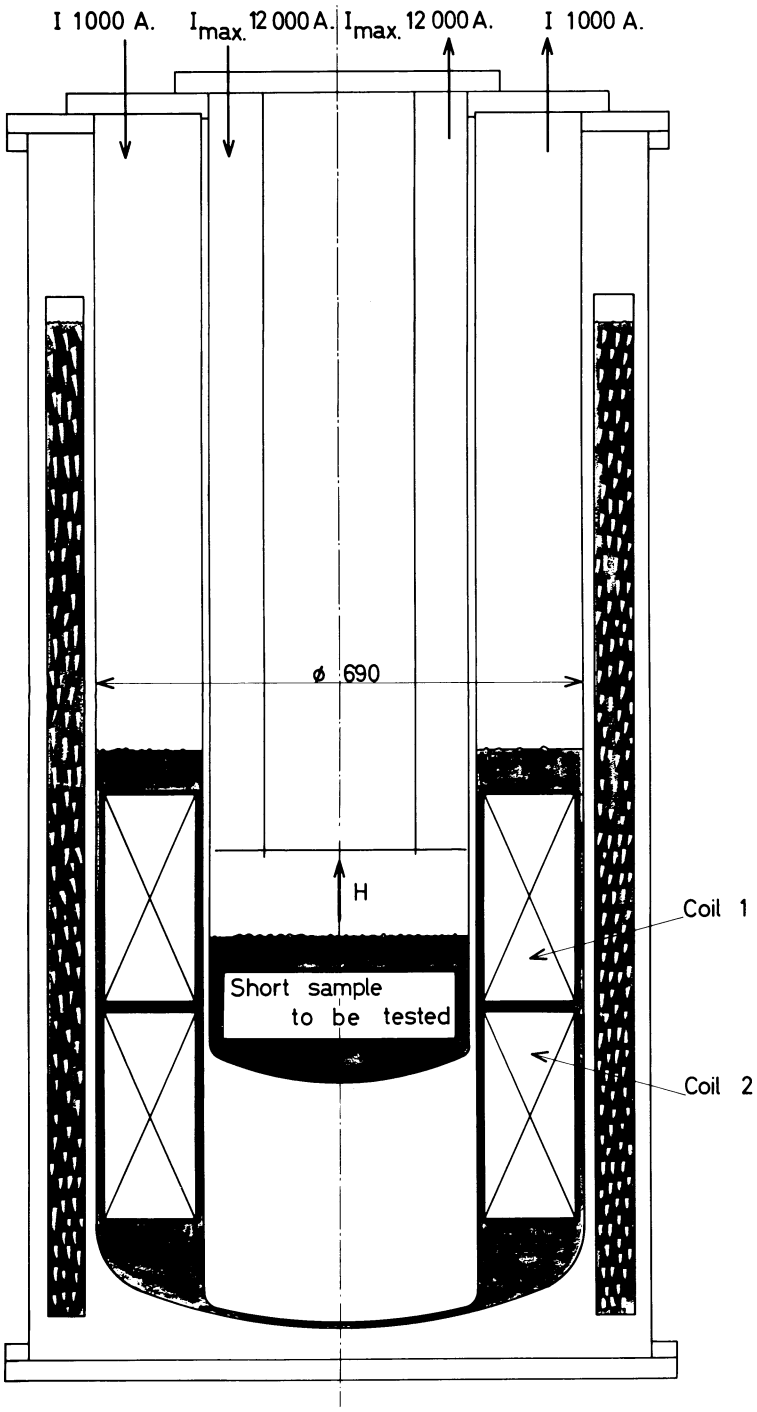

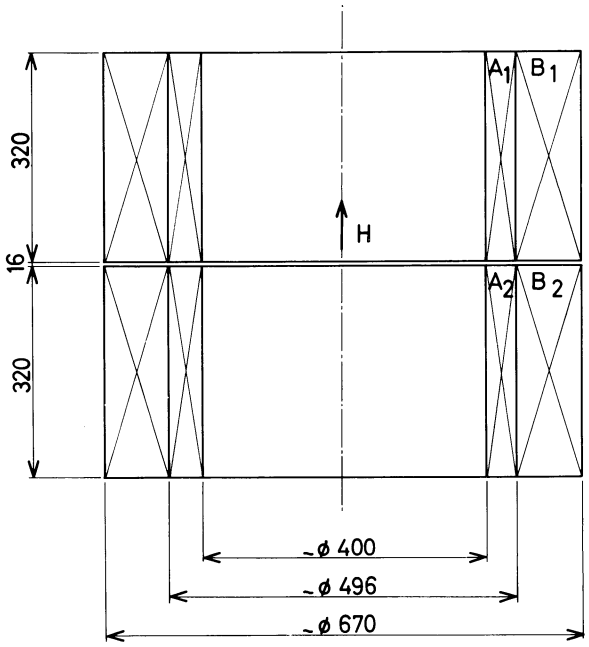

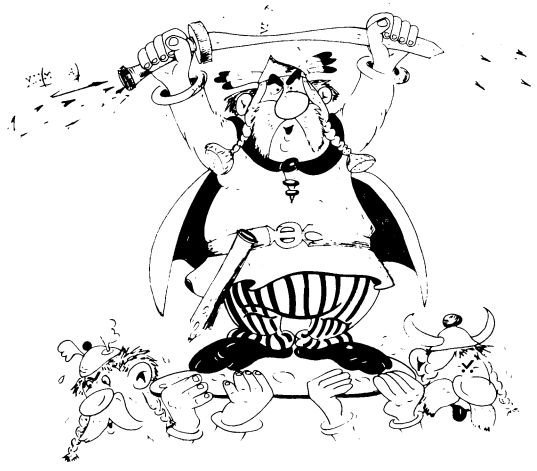

GENERAL CHARACTERISTICS

Rated current	: 1000 A.
Central field	: 6 T.
Maximum field	: 6,6 T.
Average current density Part A_2	: 4 500 A./cm^2
Average current density Parts A_1, B_1, B_2	: 5 000 A./cm^2
Total stored magnetic energy	: ~1,8 M.joules
Total weight $A_1 + B_1$	: ~180 Kg.
Total weight $A_2 + B_2$	: ~405 Kg.
Max. magnetic radial force	: ~33 Kg./cm^2
Total length of conductor	: ~6 800 m.

General layout of the BRARACOURCIX system Fig. : 2

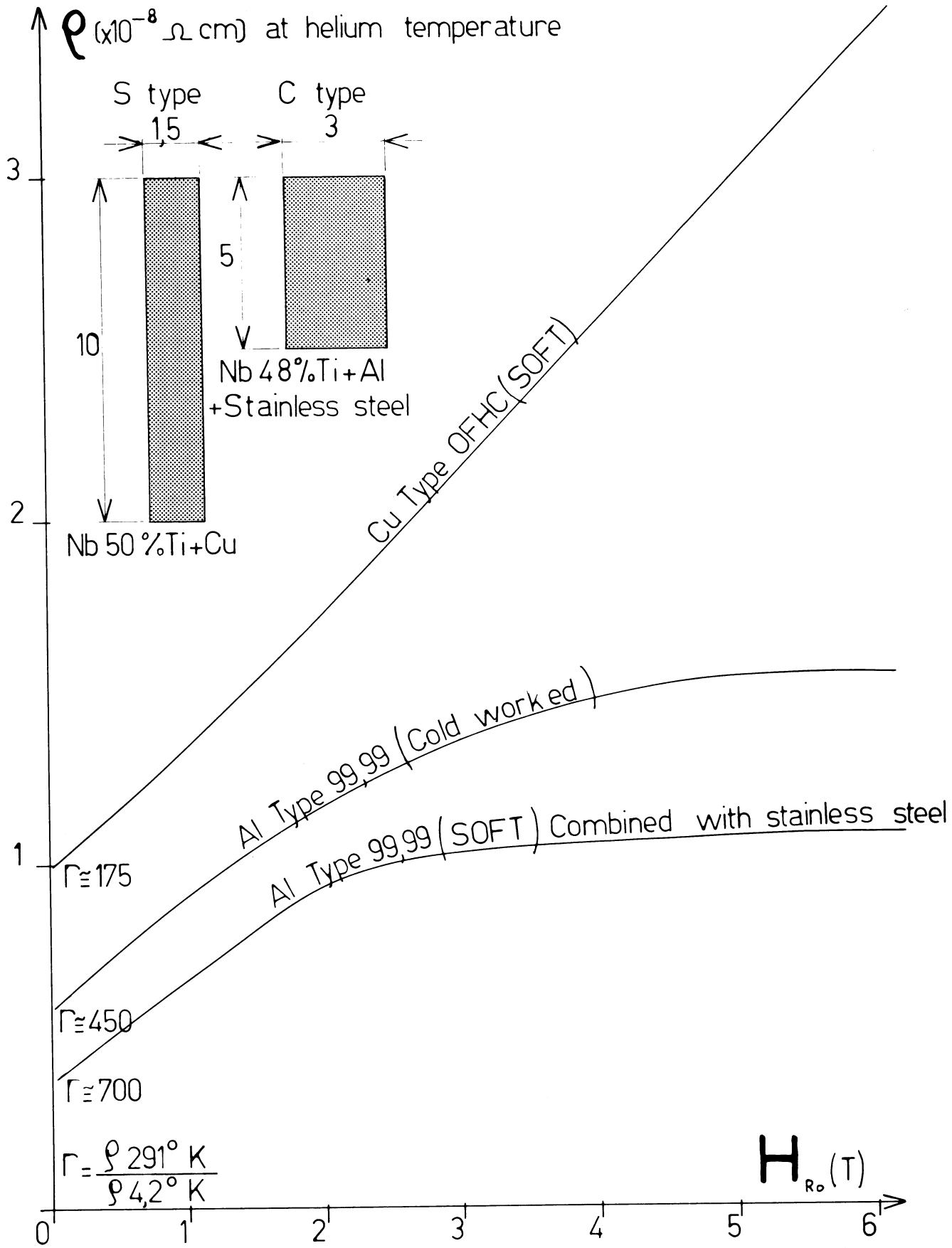

Resistivity measurements of different substrates for superconductors
Geometry of two types of conductors 6,6 T. / 1000 A.

Fig.: 3

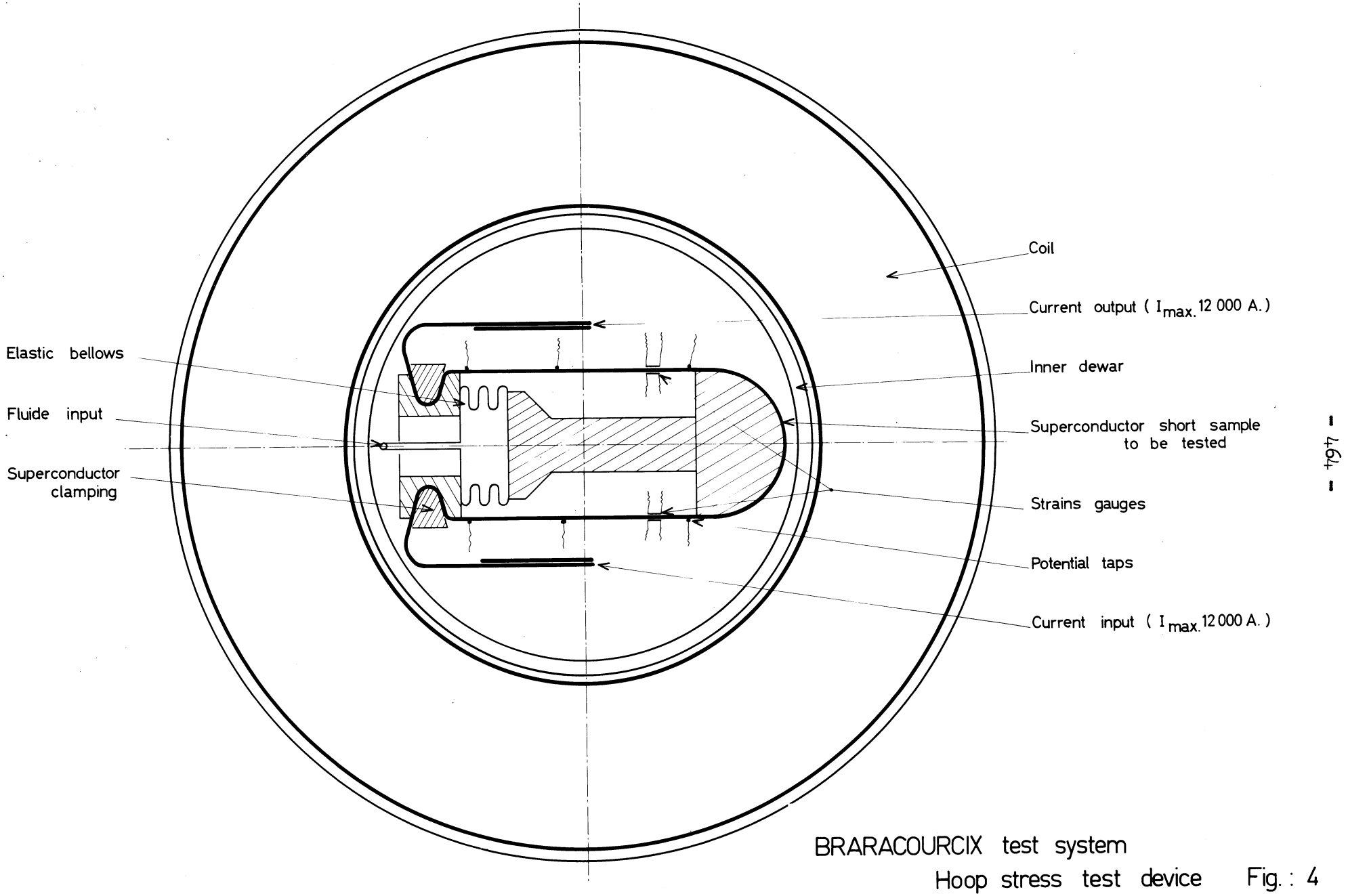

BRARACOURCIX test system
Hoop stress test device Fig. : 4

6.1 CONTROL OF THE EXPANSION IN A HEAVY LIQUID BUBBLE CHAMBER BY ELASTICALLY SUSPENDED PLATES

C.A. Ramm and Ch. Scherer
CERN

It is well known from the influence of the free volume on the boiling on the membrane in a HLBC that the behaviour of the membrane during expansion is of great importance. During tests with the new 1.1 m^3 chamber body of the CERN HLBC it became evident that the increased membrane velocities were such that an adequate control of membrane boiling could not be achieved. In addition to the distribution of membrane velocity many other parameters control the degree of boiling: the material of the membrane, its porosity, surface finish, temperature and initial degree of stretching.

It was concluded that, instead of continuing an unfruitful study of means of controlling these parameters, a better solution would be to change the nature of the velocity distribution in the liquid from that established by a membrane expansion to that established by a piston.

It seemed evident, that a freely suspended rigid plate in front of the membrane would have the effect to force a piston like type of expansion due to the restricted circulation of liquid behind the plate during a rapid expansion cycle. The plate would create two-dimensional rigidity in the flow pattern of the liquid.

Apart from taking away difficulties associated with the membrane, the freely suspended plate has changed markedly the operation of the chamber, giving more sensitivity for the same apparent pressure drop in the gas actuating the membrane, attainable with reduced boiling.

The plate also introduced the advantage of providing a surface separated from the membrane which could be treated as desired, independently of any elastic requirements of the membrane. It has for example been operated to provide an excellent dark background

illumination, it has been covered with scotchlite to give excellent visibility of tracks and has also provided a support for a mirror to view the surface of a beam pipe remote from the cameras.

Preliminary trials were carried out by means of a simple disc (Fig. 2) made from 8 mm Anticorodal Al Mg Si sheet and suitably cut to provide its own supports. The results were an improved cycle i.e. faster expansion under similar conditions (pressures, timings) and the absence of any parasitic boiling on the plate, with the exception of some parts of the slots for which no attempt had been made to achieve a hydrodynamically clean shape.

Following these encouraging tests a more elaborate plain disc version with 4 separate guiding arms and torsion bars, located between membrane and plate was designed and successfully operated in freon C_2ClF_5, freon CF_3Br and propane. With a black paint-coated surface (polyurethane or acrylic paint in freon) this plate is, with the exception of the arm regions at the edge, free of parasitic boiling and gives an excellent black background. The lifetime is superior to 8.10^5 pulses with Anticorodal torsion bars and an even better performance is expected from Titanium alloy (Ti Al V) bars on which, however, only limited experience is available.

In order to keep the useful volume to a maximum, the membrane comes into contact with the disc 2 cm before the fully compressed state. It is essential to keep the plate and hence the membrane positions (free volume) within narrow limits to avoid overstressing of the torsion bars. A simple mechanical position indicator permitting visual checks with an accuracy of $\pm$ 5 mm has been successfully tested and used.

A linear plate displacement of 3.5 cm has been measured in freon, corresponding to a volume of 24.5 litres or 2.05 % a figure which is in good agreement with previous sound velocity measurements.

In order to compensate for gravity effects, it is necessary to adjust the torsion bar attachments and for the given plate size and type of suspension a radial gap of 4 mm between plate edge and chamber body proved to be adequate.

Figure Captions

Fig. 1 Typical membrane boiling in the CERN 1.1 m^3 HLBC (Freon CF_3Br).

Fig. 2 Operation with a simple, 8 mm disc in Freon CF_3Br.

Fig. 3 Operation with the plain disc in propane.

Fig. 4 Scotchlite test picture in Freon CF_3Br.

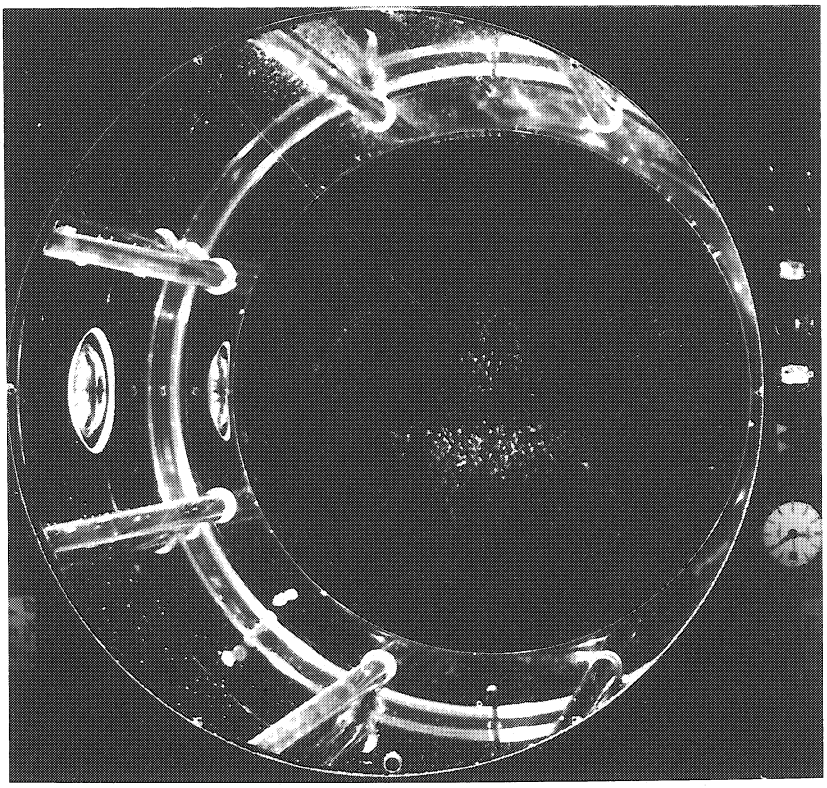

Fig. 1

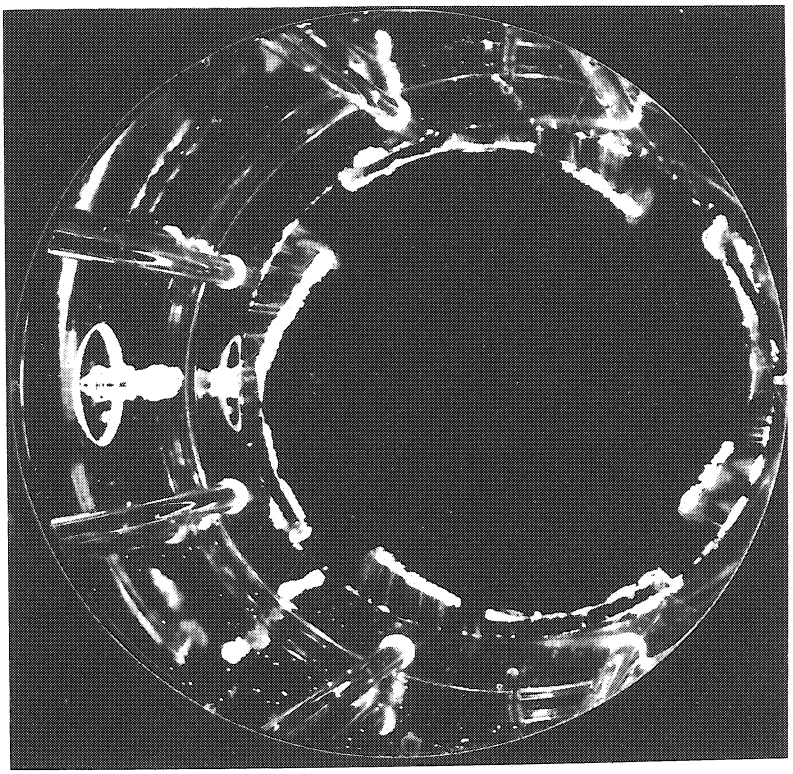

Fig. 2

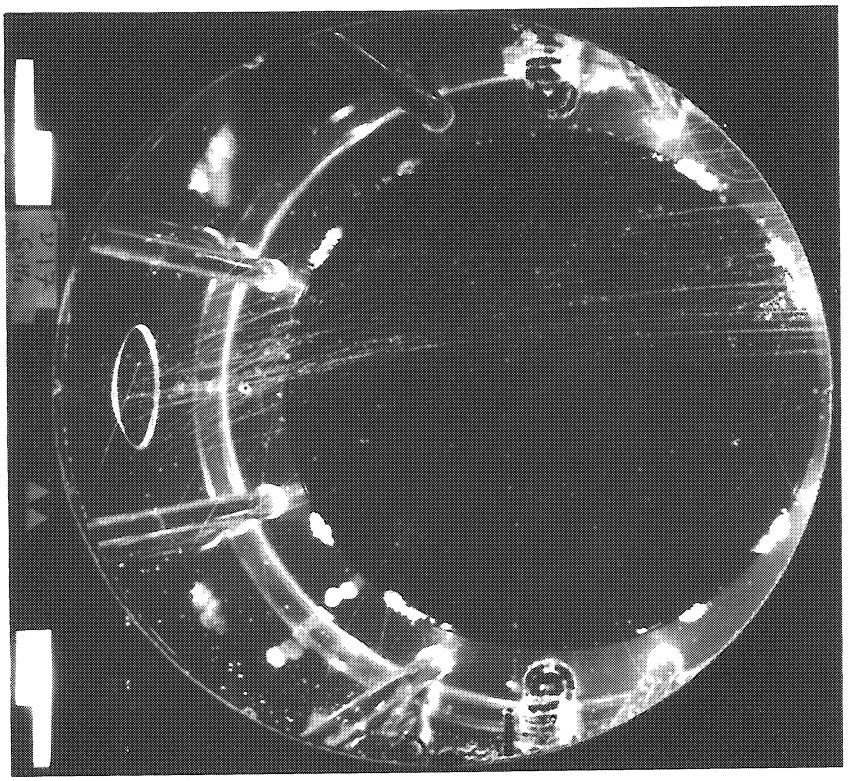

Fig. 3

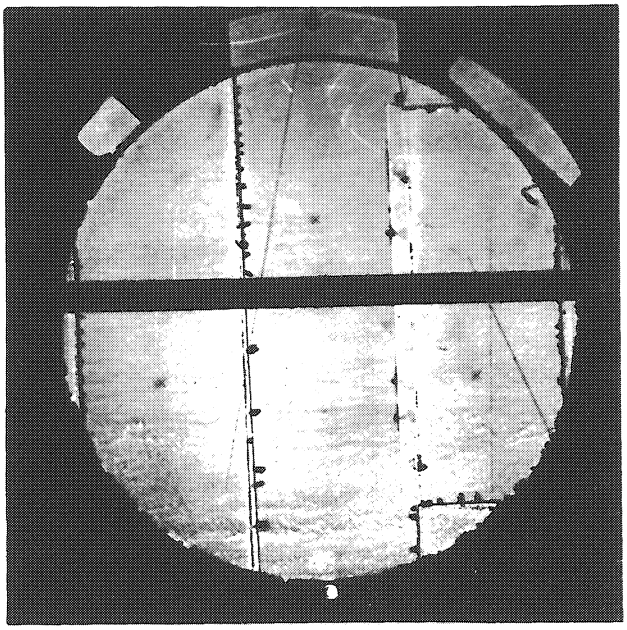

Fig. 4

6.2 EXPANSION SYSTEM FOR THE LARGE EUROPEAN HYDROGEN BUBBLE CHAMBER *)

Study Group for a Large European
Bubble Chamber

CERN

(Presented by G. Linser)

There are two important points, which should be considered by the design of the driving mechanism for the expander of a large hydrogen bubble chamber.

1) The piston stroke must have a very low amplitude and time jitter, since any variation in amplitude means a pressure error in the expanded liquid and therefore a change in bubble density and bubble size. In principle a system with the inheren flexibility and accuracy of electronic components, combined with that of hydraulic power amplifiers in a closed loop servo-system, would be the most suitable mechanism to meet this functional requirement. But power consumption, stability problems with high gain hydraulic power amplifiers and the dimensions of the main components seem to prohibit such a system for large chambers. Properly designed "resonant"* systems are well adapted to give small amplitude jitter, since the amplitude of the piston stroke is given by the spring laws of two gas accumulators, where the two important parameters, gas pressure and gas temperature, can be controlled. In a "resonant" system also a time or flow jitter of the "locking" valve can influence the amplitude. An arrangement where the movement of the poppet or spool of this valve is controlled by the movement of the expansion piston, will also avoid this jitter.

---

*) The "resonant" system is analogous to a mass spring system which is operated at its resonant frequency.

2) It seems to be important for large hydrogen chambers with bright field illumination, where big bubbles are needed (in the order of 0.7 to 1 mm diameter) that the chamber can be expanded to relatively low pressures (in the order of 1 kg/cm^2 absolute or even less) to get the necessary bubble diameters in a short time and to get a convenient bubble density at low temperatures (25 to 25.5°K). This means that the chamber pressure must drop rapidly during expansion, in order not to create too important a volume of spurious bubbles[1]. The springforce of the expansion motor must therefore be made sufficiently large to obtain a short enough natural period for the expansion cycle. This higher energy demand can be dealt by an integrated design, where the accumulators and the locking valve are built into the system. With this design the additional inertial effects of the moving oil and also the losses due to oil pressure drop, are kept to a minimum.

The expansion system now enquired for the 3.5 m chamber is an improved version of the one proposed in the CERN Study Report (BEBC 66-73). It is a resonant type system, combined with a hydraulic locking device. It is designed with the above mentioned points in mind. Figure 1 shows the schematic construction of this system.

In principle, the system consists of two gas accumulators E and R, the expansion piston PE, a high speed locking valve VPR and a servo trigger valve. The annular piston VPR of the recompression accumulator R serves as separation piston between the gas accumulator R and the "locking oil" and at the same time as a high speed, large flow valve. This annular piston acts like a valve poppet and seals in its normal position against an elastic seal S separating the oil volume L from the oil volume RR.

---

1) Some aspects for the layout of the Expansion System of BEBC by G.Harigel.

Before the expansion cycle is started, the whole energy necessary to accelerate the mobile masses of the entire expansion system is stored in the gas accumulator E as potential energy. The force created by the gas pressure p_E acting on the expansion piston area A_E is compensated by the oil pressure p_L acting on the area A_L. The piston VPR is kept tight on its seal S by the oil pressure p_L acting on the area A_{RL}. The trigger valve is closed. The oil pressure p_{RR} is kept at a pressure less than the gas pressure p_R. By opening the trigger valve, the oil pressure p_{RR} is raised to the same value as the oil pressure p_L and since the pressure of the recompression accumulator is lower than the expansion accumulator pressure p_E and the piston area A_R is the same as the expansion piston area A_E, the system starts to move. The oil volume displaced by the expansion piston flows through the gap which is opened by the movement of the piston VPR into the volume displaced by this piston. During this motion, the pressure p_E and the chamber pressure are reduced and the pressure p_R rises. The change of the pressure conditions in the accumulators and chamber leads to a reversed motion of the two pistons, thus recompressing the chamber. The spring laws of the gas accumulators E and R respectively, the pressures p_E and p_R are set to values, which will give together with the spring constant of the liquid hydrogen, the desired expansion stroke. The pulse width of this system is given by the mobile mass and the chosen dimensions of the expansion piston and the accumulators, and is only slightly changed if the piston stroke is changed by setting the accumulator pressure to different values. The damping losses of the system are compensated by an energy supply assisting the upward movement of the piston PD during the recompression cycle (controlled by a second servo valve).

If the mass of the piston VPR equals the total mass of the expansion piston assembly (cold piston, piston rod, expansion piston and piston PD) and if the piston area A_R is the same as the area A_L, the inertia forces, created by the moving masses are cancelled in the system itself.

A development program for a scale model of the above described expansion motor is foreseen in connection with the 1 m test chamber.

The 1 m test chamber has a hydrogen volume of about 1 m^3. The diameter of the "cold" piston is 600 mm and the necessary piston stroke for a volumetric expansion of 1 % is 35 mm. With this chamber will be studied the phenomena of bubble growth and dynamic heat load as a function of the pulse width of the expansion cycle. Since the pulse width must be changed in a wide range the expansion mechanism for this test chamber will therefore be an electro-hydraulic servo controlled system (Fig.2 shows the schematic construction of this system). A small three-stage electro-hydraulic servo valve acts on a four-way spool distributor, which controls the oil flow from the pressure accumulators to the hydraulic expansion piston. With this system the pulse width of the expansion cycle can be changed from 20 msec up to infinite. It is proposed to make two expansions per second, with a minimum time of 100 ms from pulse to pulse. The power consumption of this system is about 120 kW for two full-stroke expansions per second and a total mobile mass of about 60 kg.

'RESONANT' EXPANSION SYSTEM

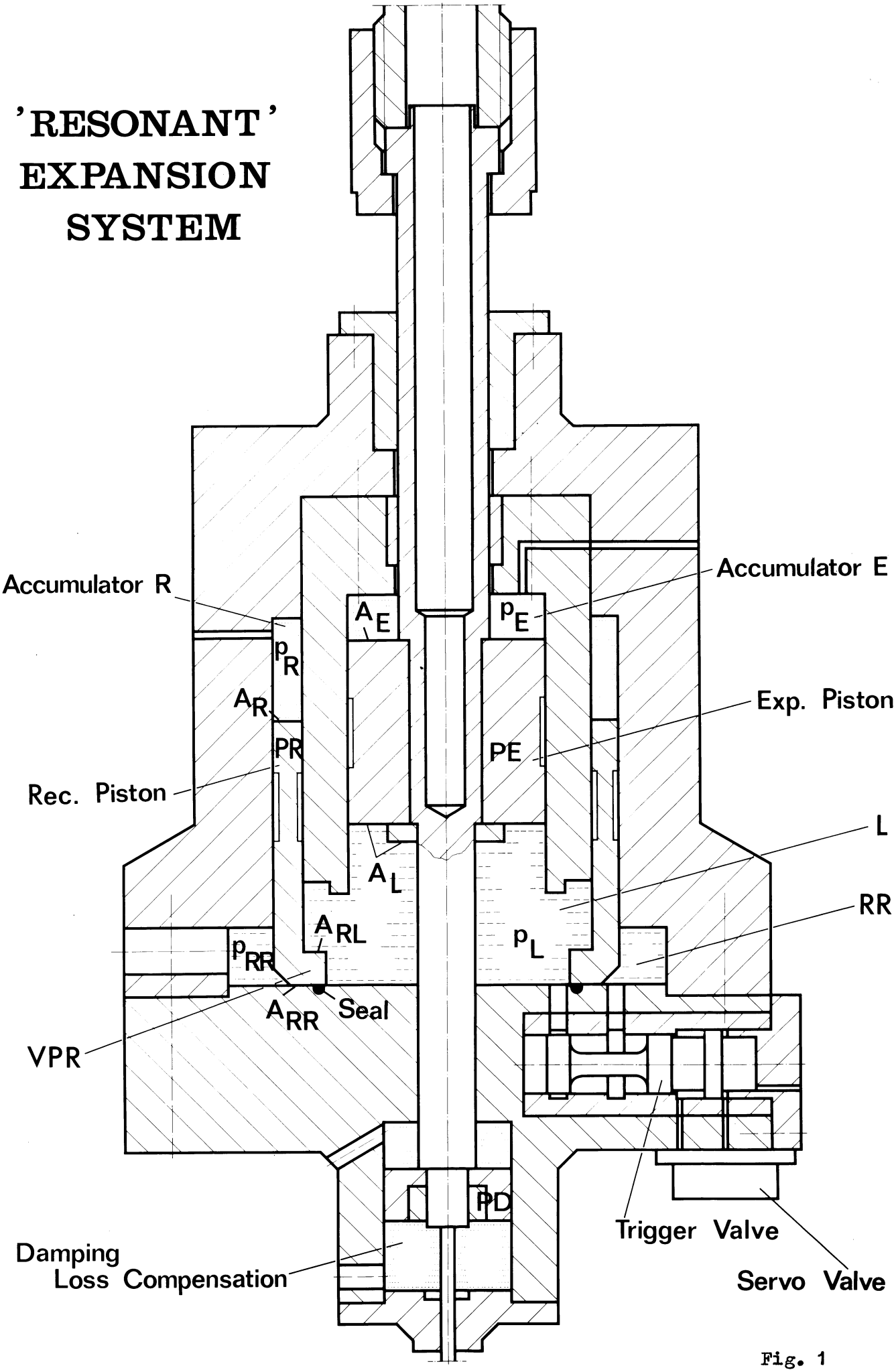

Fig. 1

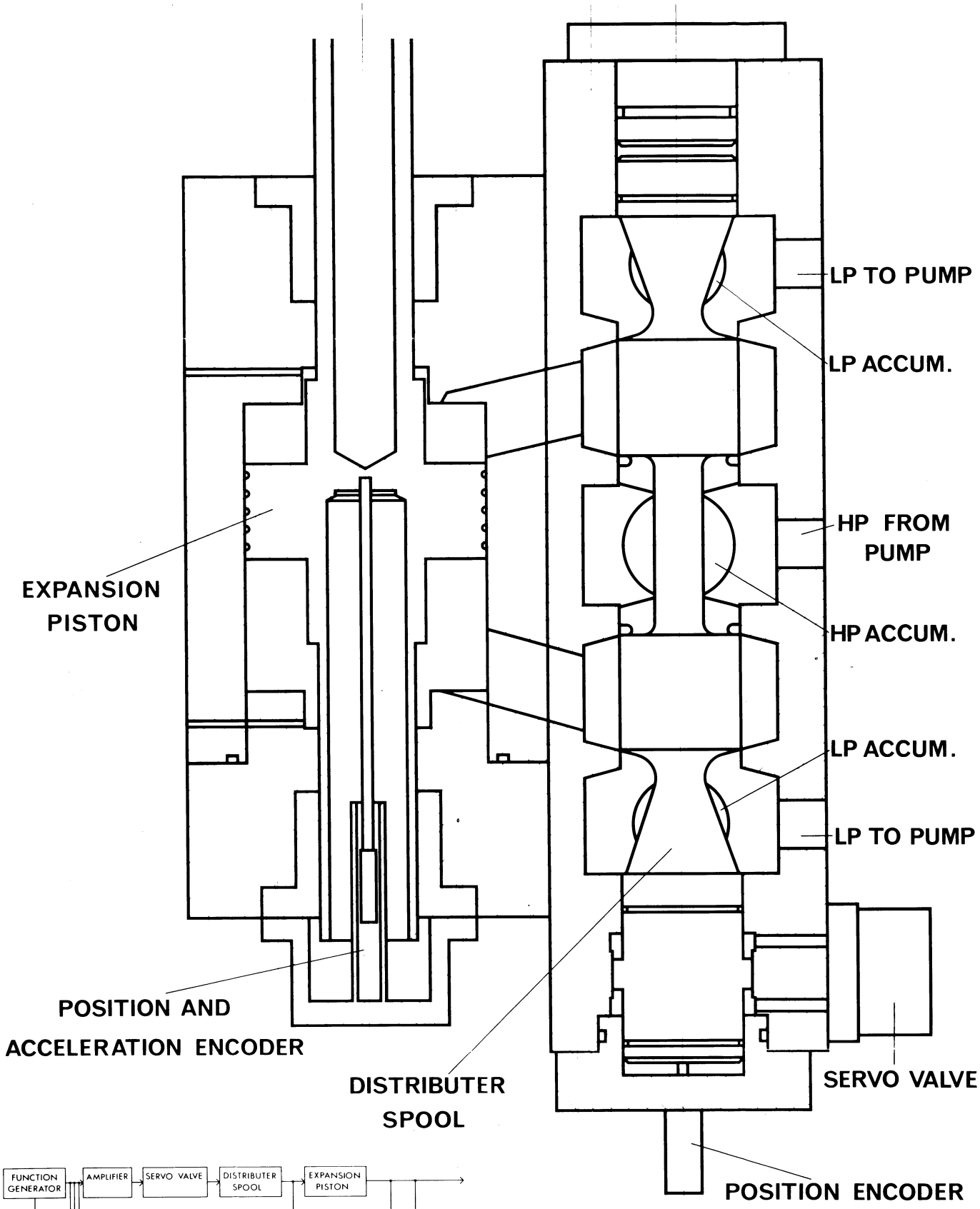

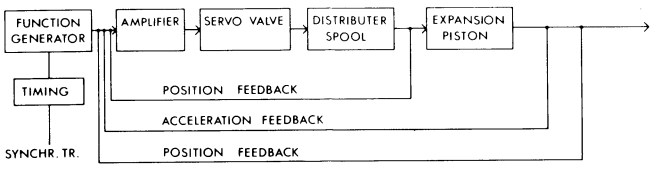

BLOCK DIAGRAM FOR SERVO SYSTEM

'SERVO CONTROLLED' EXP. SYSTEM

Fig. 2

6.3 A FLAT MEMBRANE INFLATABLE GASKET FOR A LARGE LIQUID HYDROGEN BUBBLE CHAMBER

R.G. Stierlin
CERN

The gasket described here has been developed at CERN for the 2m. liquid Hydrogen Bubble Chamber. Fig. No. 1 shows a vertical cross section of the instrument and the situation of the four gaskets which have to ensure leak tightness between the volume formed by the chamber proper and its attached safety tanks, and that of the surrounding vacuum tank during cool-down and warming-up operations.

During such operations, the volume chamber-safety tanks is filled with 1 atmosphere of H_2 gas to ensure the heat transfer by conduction between the glassware (windows and condenser lenses) and the heat exchangers whilst the vacuum tank is evacuated to approximately 10^{-6} mm Hg. The five components to be sealed, e.g., the chamber body, the two intermediate safety tanks and the two safety tank covers are made from stainless steel (17% Cr., 14% Ni with a C. content $\leq$ 0.035%). The same alloy has been used to manufacture the gaskets in order to avoid differential contraction or dilatation between the elements involved and the subsequent shearing action on the sealing medium: in this case a 4 mm diameter pure indium wire.

The pressing and forming of the indium wire can therefore be done at the assembly of the components.

The pressurization of the gasket by means of Helium gas is then required merely to maintain a constant pressure on the indium seals. consequently the total deflection which is expected from the gasket is of the order of 0.1 mm and is only needed to compensate the distortion of the flanges of the components and the somewhat delayed contraction of the fastening bolts during cool-down. Such a small total deflection can be absorbed by flat membranes which are produced without special forming tooling. The four gaskets in use on CERN 2m chamber marry the shape of the chamber body and safety tanks.

They have an oblong shape with semicircular ends; the overall dimensions are 2303 mm for the length, 903 mm for the width and the thickness is 44.2 mm.

Fig. No. 2 shows a cross section of the gasket which is composed of 8 elements joined together by welding under argon without filler metal.

The two outer members have two semcircular grooves which receive the 4 mm diameter indium wire. A groove of rectangular section is machined between the two indium carrying grooves to provide a pump-out channel between the two seals.

The edges are machined out to leave a 1 mm thick lip where the membranes are welded to the outer members.

Another rectangular shaped groove is machined out of the inner face of the outer members to prevent interference with the inner welds of the membranes.

The intermediate members are also machined out to leave lips of a thickness identical to that of the four membranes to which they are welded.

The purpose of the intermediate members is to separate the membranes and facilitate the welding of the latter to the outer members. The depth of the weld is approximately 1.5 mm, thus leaving a 3.4 cm width of the outer members exposed to pressure.

A helium pressure of 35 to 40 atmosphere is necessary to ensure leak tightness of the seal which corresponds to a specific pressure of approximately 0.9 kg/mm^2 on the pre-formed indium.

The total thickness of the gasket is arranged in relation to the gasket housing depth so as to leave a protrusion of 0.4 mm of indium from the face of the gasket after forming.

Various welding tests have been carried out before the manufacture of the gaskets. A destructive test by hydraulic pressure at 490 atmosphere has also been carried out on a circular test gasket 300 mm in diameter with a total deflection limited to 0.4 mm, that is 4 times the estimated service deflection of the gasket. Fig. No.3 shows a cross section of this gasket at the point of rupture.

The four gaskets mounted on the 2m chamber have been in service for 8 months and have previously been submitted to a pneumatic pressure test at 100 atmosphere in liquid nitrogen with a total deflection limited to that of service.

Tests of small gaskets of similar construction which will be used to seal the camera and flash windows of the safety tanks are now being prepared.

The rapid development and production of the gaskets now in service has been possible thanks to the advice and cooperation of a number of people, particularly Mr. T. Ball, head of CERN 2m liquid Hydrogen Bubble Chamber group and of Mr. Dozio, head of the Track Chamber division workshop.

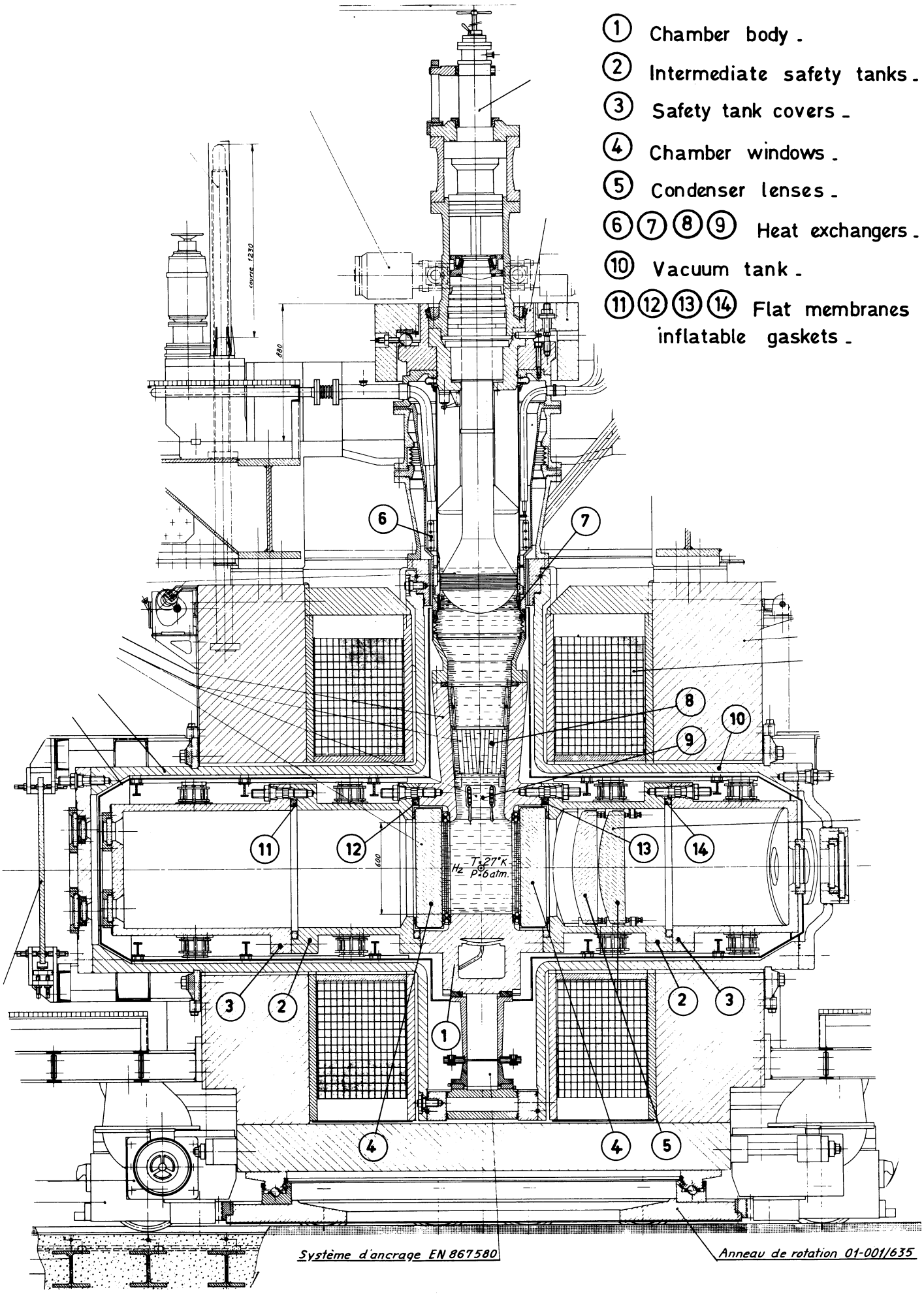

Fig. 1 - CERN 2 m. LIQUID HYDROGEN BUBBLE CHAMBER -
(Vertical cross section at right angle to beam) -

① Flat membranes (1 mm thick).
② Outer members.
③ Indium wires.
④ Pump out channels.
⑤ Intermediate members.

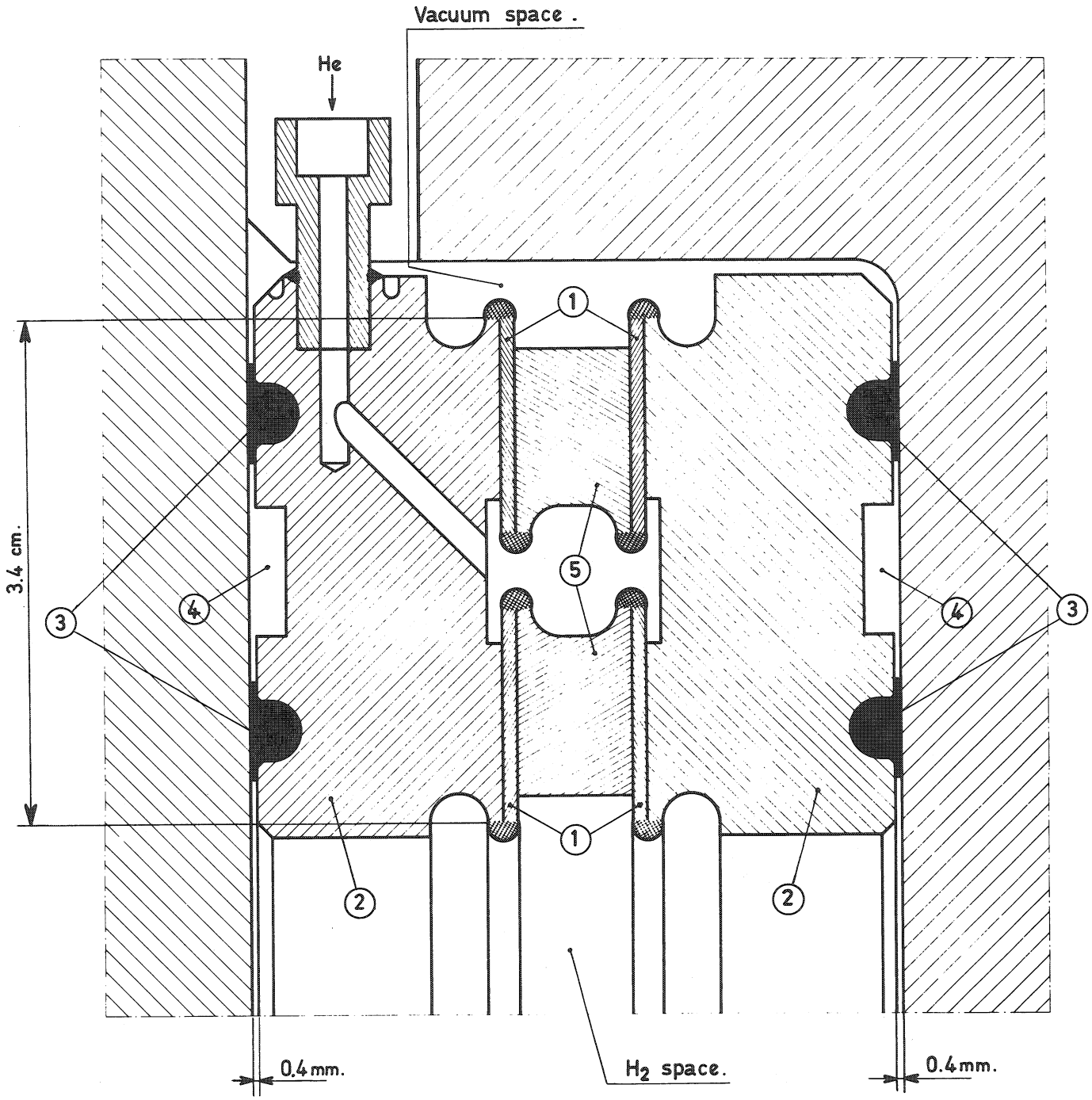

Fig. 2 - CROSS SECTION OF GASKET -

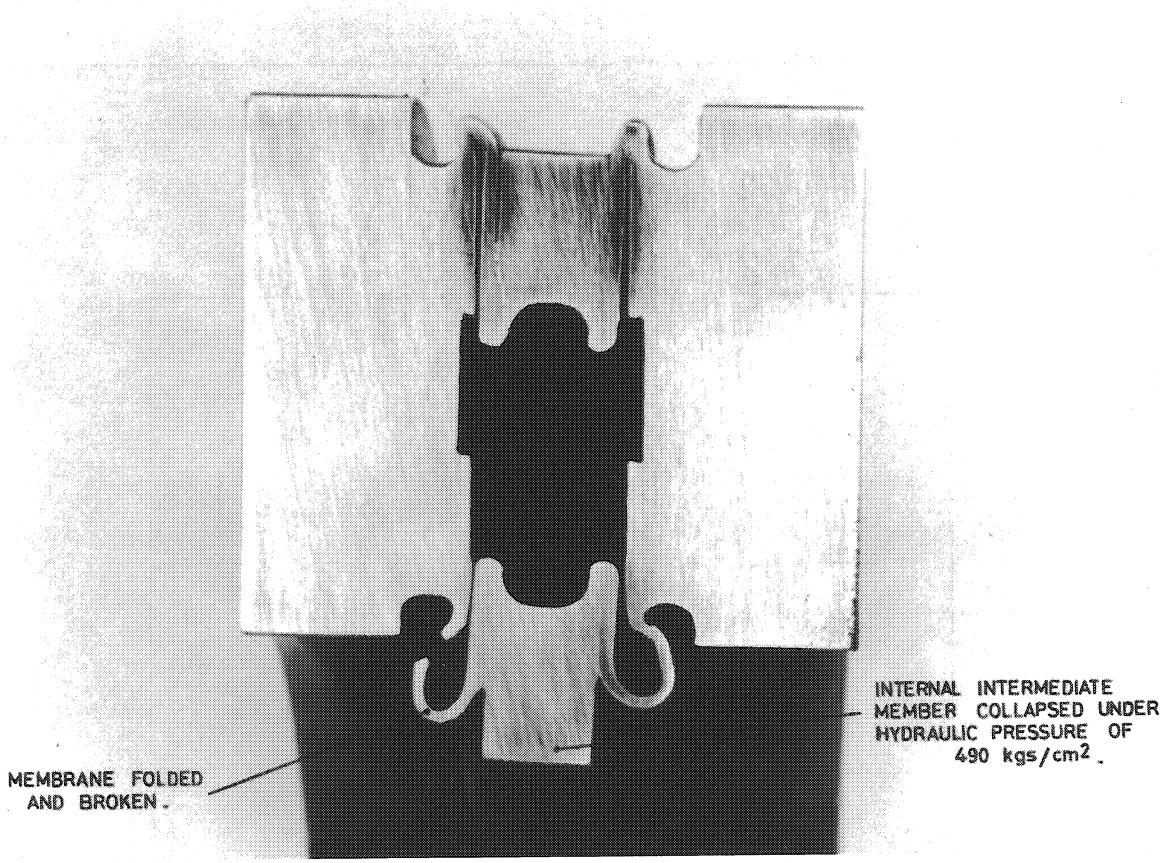

Fig. 3 - 300 mm. DIAMETER TEST GASKET.
(Cross section at the point of rupture.)

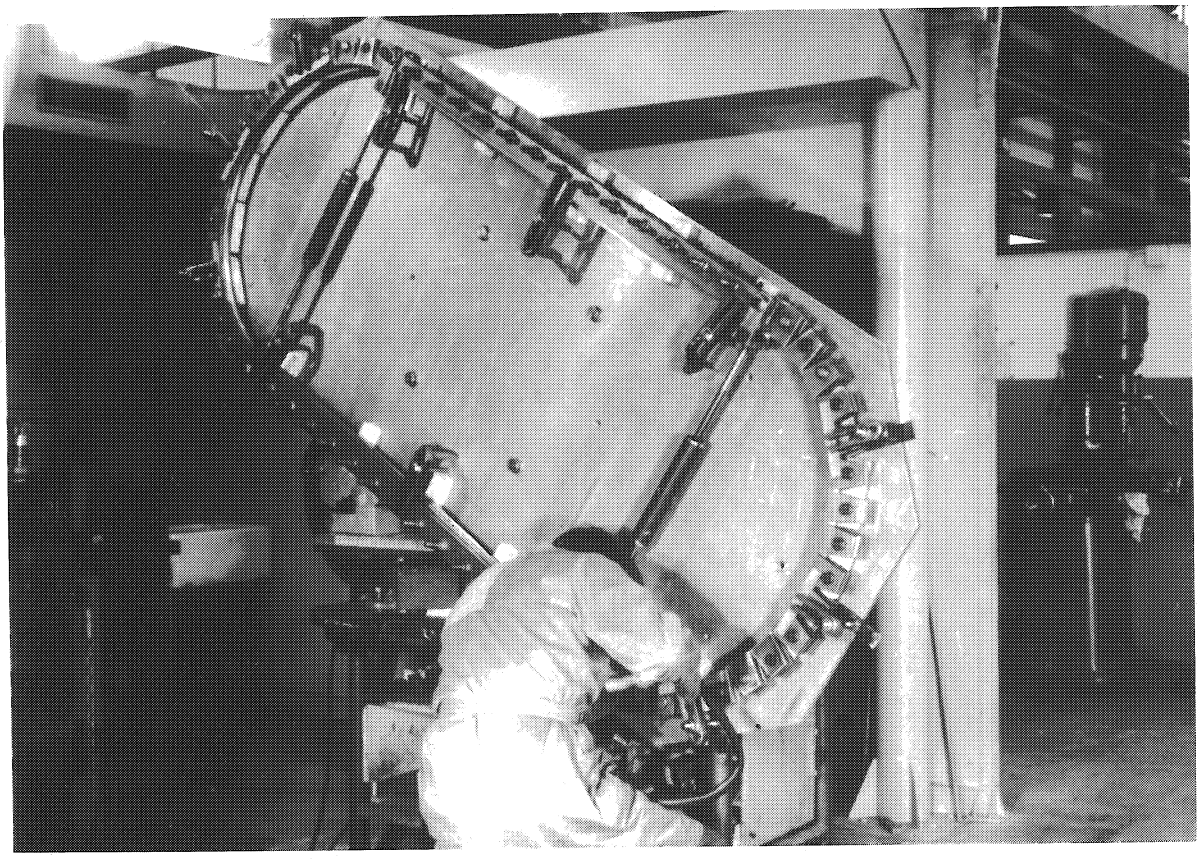

WELDING OPERATION OF AN INTERMEDIATE MEMBER TO TWO MEMBRANES.

6.4 OPTICS AND MAGNET OF THE HYDROGEN BUBBLE CHAMBER "MIRABELLE"

M. Gensollen

Centre d'Etudes Nucléaires, Saclay.

The magnetic field applied to the Bubble Chamber is horizontal with an intensity of 20 Kilogauss. It is generated by a classical C shape electromagnet (Fig 5). The power consomption is of 11 MW (660v 16 600 A). The iron core weighs 1150 T and its outer dimensions are 5.3 x 6.2 x 5 m.

The coils are made of aluminium. They weigh 30 tons each and are 4 meters high, 8 meters long and 0.85 meters thick. The spacing is 90 cm. They are placed in leak-proof containers in which nitrogen is continnously circulated under slight overpressure, in order to isolate the electrical circuits from the outside air.

Each coil contains 140 turns and is divided into 5 indentical double-pancakes, each of them being separately vacuum-impregnated with araldite.

The conductor is an aluminium tube of rectangular cross section 64 mm x 77mm with a circular hole of 33 mm in diameter for cooling water circulation. Aluminium was chosen mainly for reliability reasons; such a conductor can be supplied in continuous lengths of 250 m.which correspond to the length of one single pancake, and thus awoids the presence of joints inside the winding. Whilst with a copper conductor; there would have been about 50 joints inside each pancake.

In order to eliminate thermal stress on the conductor, the coils are left free to expand when heated. This is achieved by feeding the cold water on to the inside turn of the pancake and by placing mylar spacers between turns in the circular ends of the coils.

The only stresses experienced by the conductor are due to the electromagnetic forces and are limited to 3 kg/mm2, which are quite acceptable with aluminium.

The design of the magnet and the checking of the various characteristics are being carried out on a 1/25 scale model. This model has been equipped with superconducting coils in order to reach the desired current density. It is being tested at present time and it will be used for predetermining, the map of the magnetic field in the useful volume of the chamber and for optimising the shape of the hole pieces with respect to field homogeneity. The variations of the field are expected to be lower than 7% on the axis of the chamber and 5% in a transversal cross-section.

"MIRABELLE" Optics

I - OPTICS

Lens system consists of two parts (fig 1). A cold part of fish-eye type made up of a single spheric window and of a parabolic lens which reduces the field from 110° to 10°. A room temperature part rectifies the aberrations of the parabol and carries the image out of the magnet, the whole system is 2.5 m long.

Between these two parts a plane window made of quartz isolates the optics vacuum which is surronded by a stainless steel vessel.

Two floating screens made of stainless steel reduce radiance bewteen the cold and the room-temperature parts.

Scotchilte system is used for illumination. Flash tubes which are installed at the outer side of the vacuum tank illuminate the inner face of the parabolic lens through a separate optical system.

The use of the parabolic lens allows a demagnification of 15, which permits a good utilisation of scotchlite (average scattering angle bewteen flash and entrance pupil equal 1/3°).
Nevertheless this arrangement brings up ghost images, which are eliminated by a set of masks located where intermediate images are formed.

The utilisation of the parabolic lens for illumination leads to a field decreasing in terms of cosinus of incident angle, due to the pupil dilatation, whose surface increase in terms of 1/cos3.

II - PROTOTYPE

A prototype has been designed:

lenght	: 1 meter
field aperture	: 110°
focal	: - 18 m
aperture	: f/12
focal depth	: 1 meter
distorsion	: 1.5% at 50°

Caracteristic curves are shown in Fig 2,3,4. Flash power is 600 Joules under 10 KW distributed into six flashs. But optical system of the flash accepts only 1 per cent of the emitted flux.

Its cold face has been tested in liquid hydrogen (and under a pressure of 15 Kg/cm2), in a cryostat and this experiment has given satisfactory results relative to the mechanical way of fixing spherical window.

We have checked in laboratory the expected performance of this prototype in air, results on stigmatism, chromatism, distorsion are those waited by calculations.

Resolving power measured with a grating was 100 line/mm on the axis.

III - THE CAMERAS

The actually proposed number of objectives is eight, on two horizontal rows whose basis are 70 cm horizontally and 50 cm verticaly. Optical axis are parallel, giving an easy scanning.

Photographied volume is 6 m3 compared to the 8 m3 volume of the chamber body.

Dispersion of camera permits selecting the best cople of cameras in front of the tracks to be measured, and minimize the light path in hydrogen (maximum 2 meters).
Camera studed at present time will be two or four, by grouping pictures on the same film.

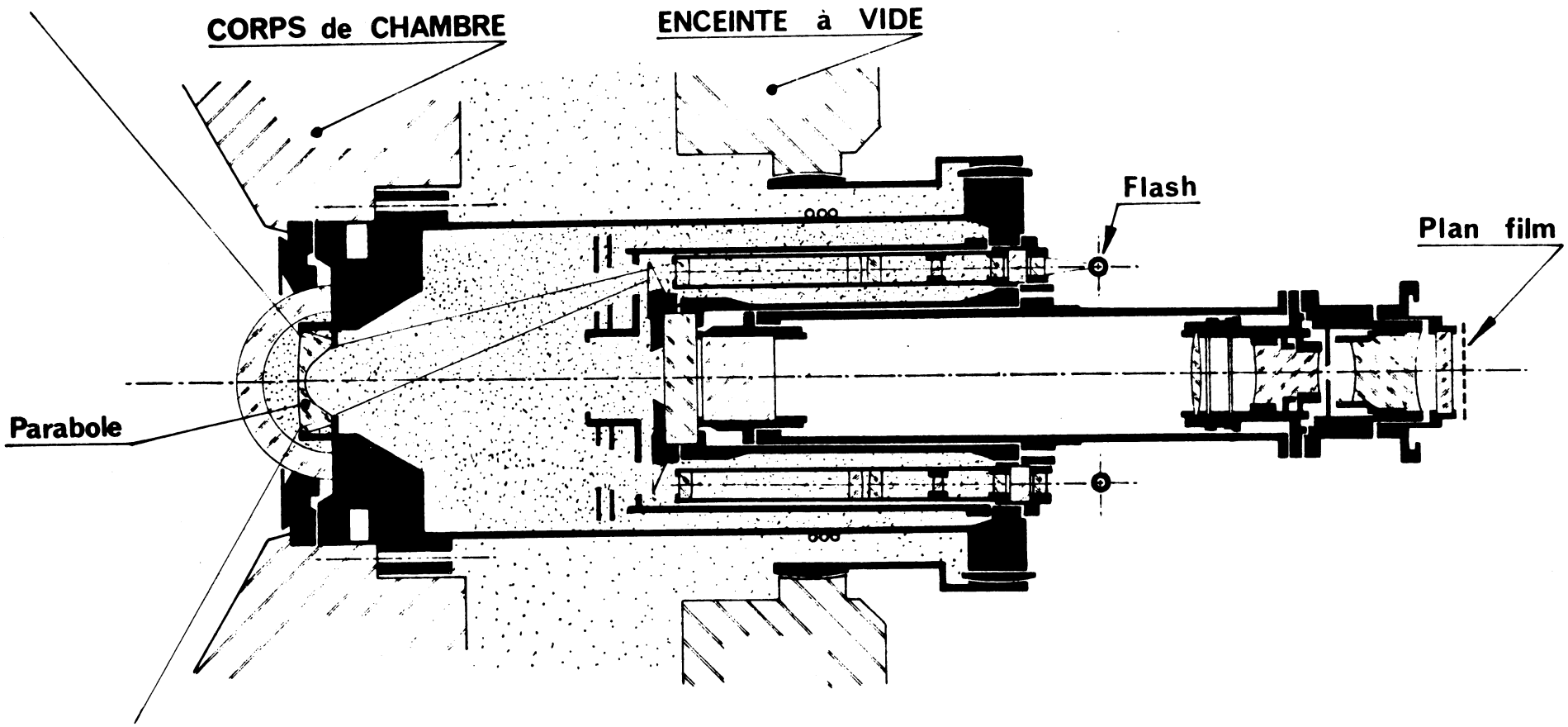

PROTOTYPE de L'OPTIQUE MIRABELLE

Fig. 1

Aberration sphérique de la pupille d'entrée

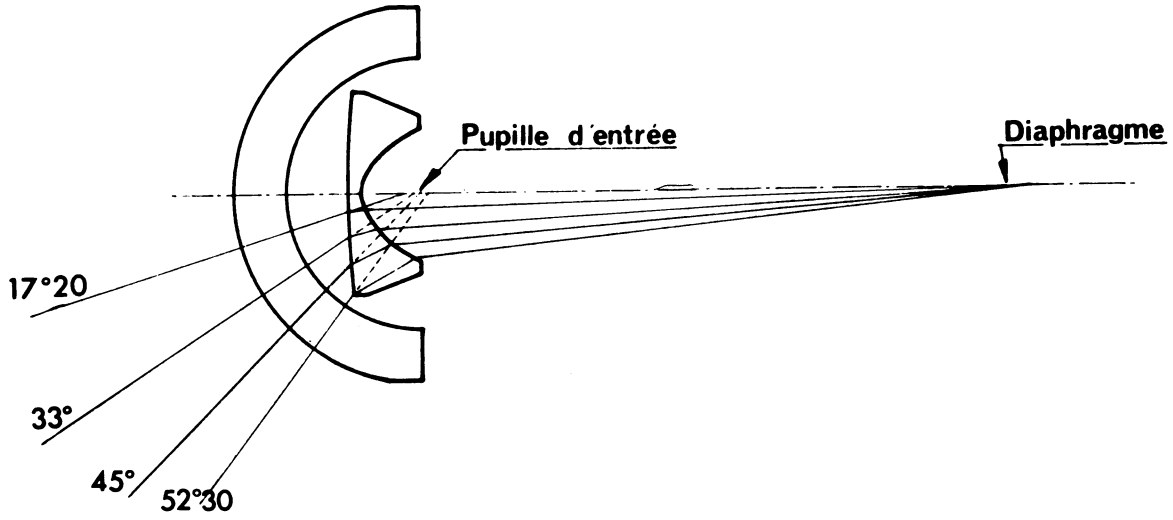

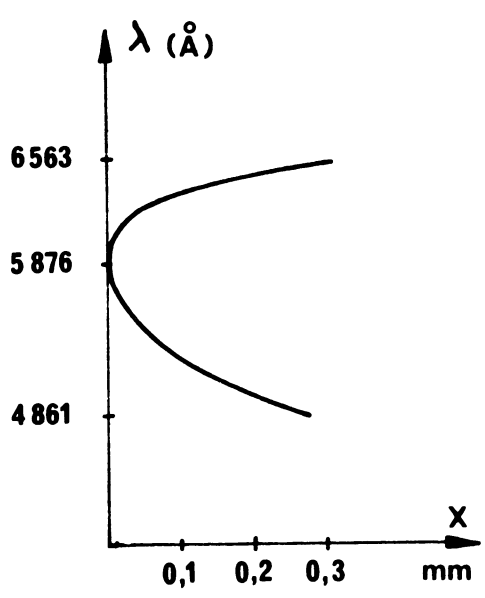

CHROMATISME LONGITUDINAL

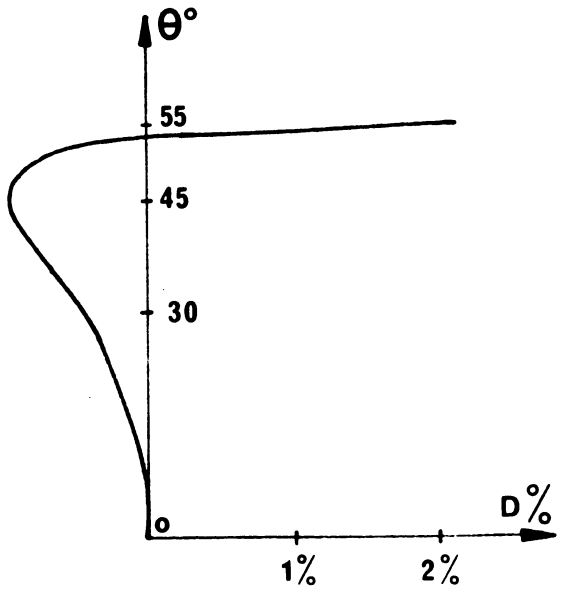

DISTORSION

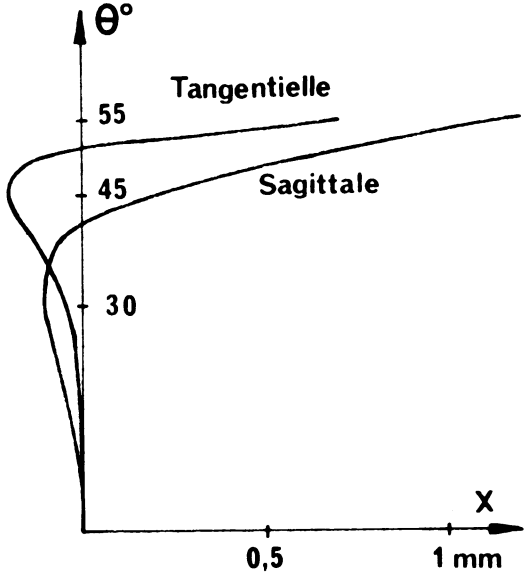

ASTIGMATISME

Fig. 2

SURFACES D' ONDE

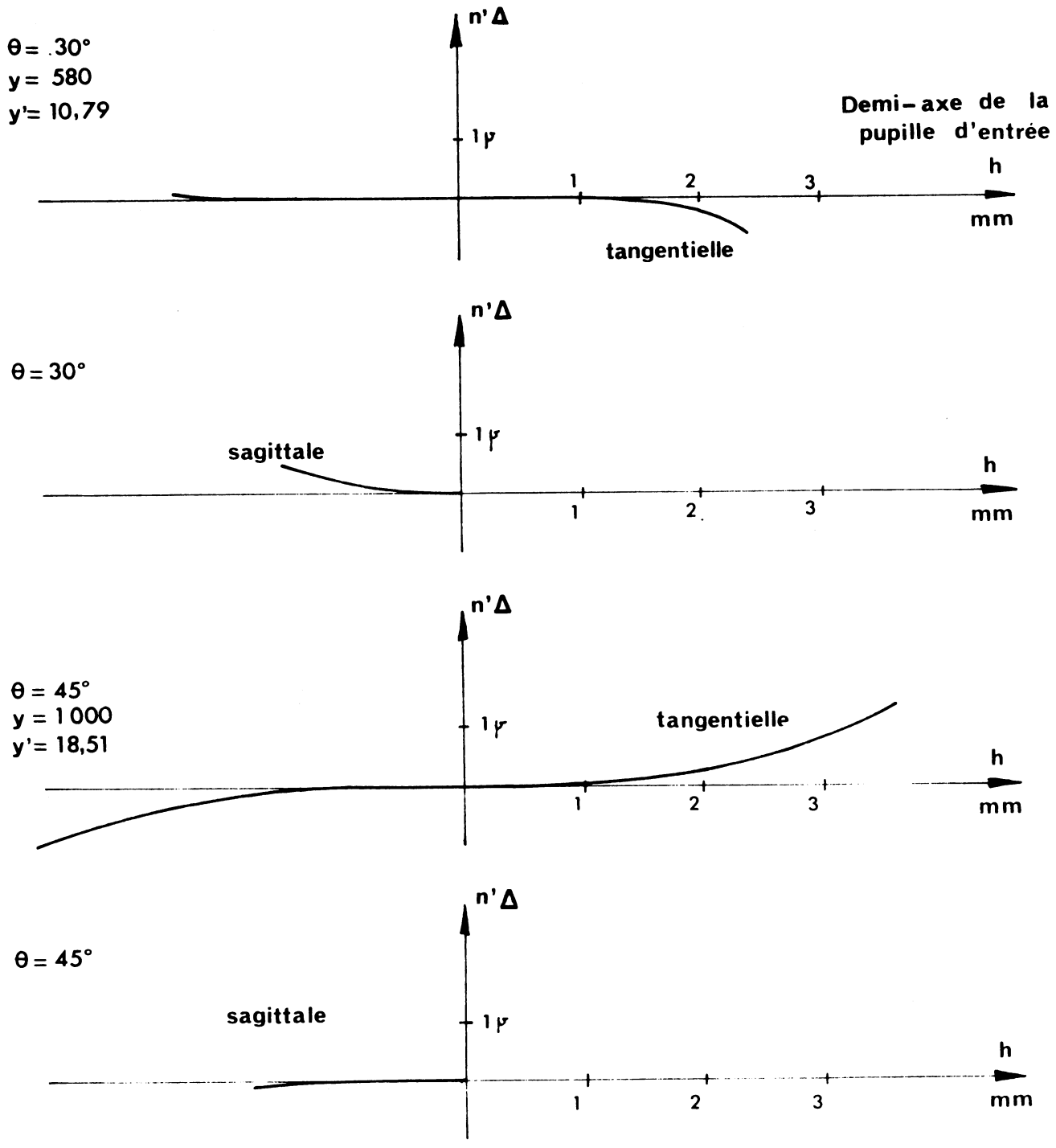

$I\lambda$

Fig. 3

RAYONS

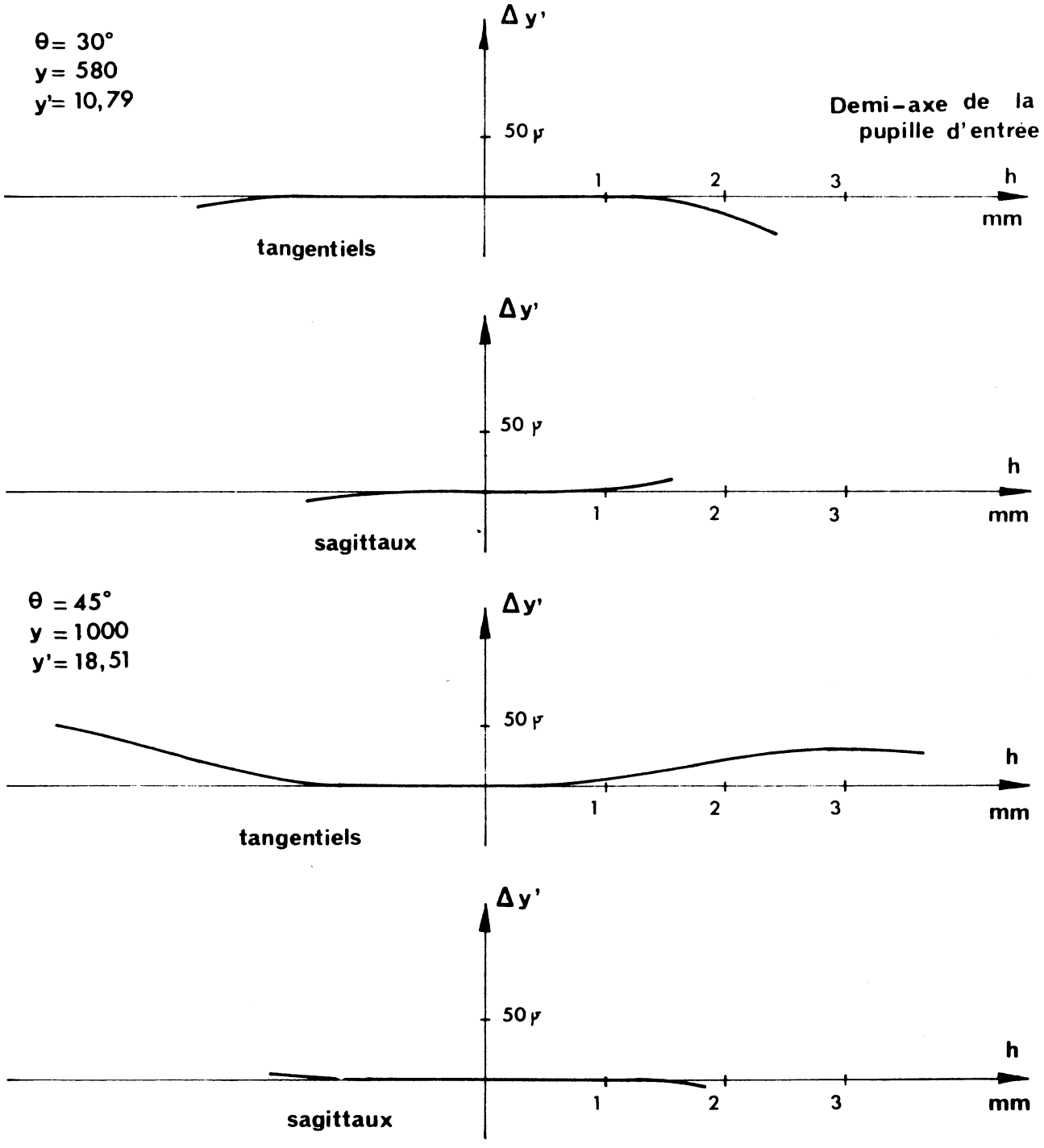
θ= 30°
y= 580
y'= 10,79
Δ y'
50 μ
Demi-axe de la pupille d'entrée
1
2
3
h
mm
tangentiels
Δ y'
50 μ
h
1
2
3
mm
sagittaux
θ = 45°
y = 1000
y'= 18,51
Δ y'
50 μ
h
1
2
3
mm
tangentiels
Δ y'
50 μ
h
1
2
3
mm
sagittaux

Fig. 4

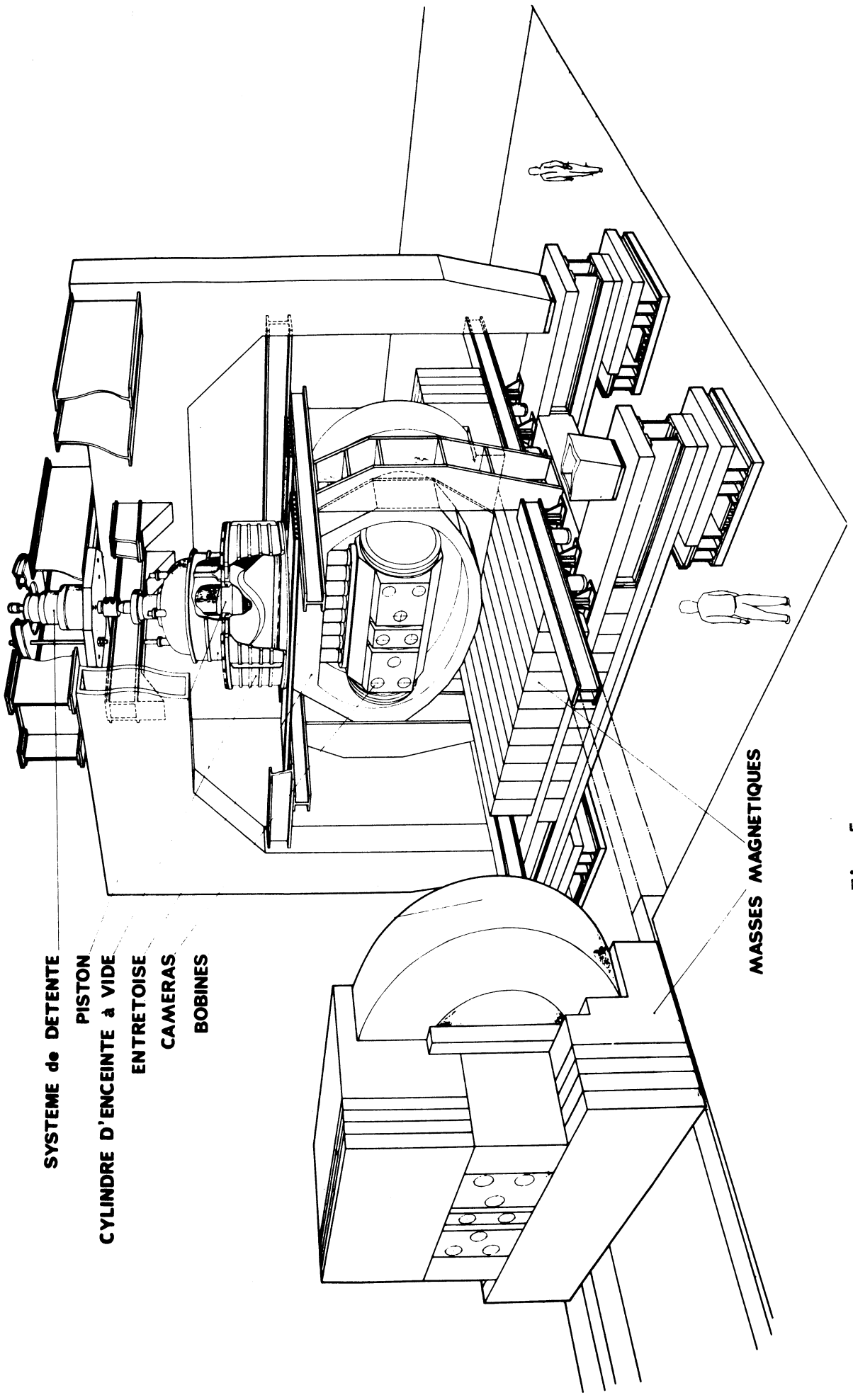
SYSTEME de DETENTE
PISTON
CYLINDRE D'ENCEINTE à VIDE
ENTRETOISE
CAMERAS
BOBINES
MASSES MAGNETIQUES

Fig. 5

6.5 ENGINEERING ASPECTS OF THE ANL 12-FT HYDROGEN BUBBLE CHAMBER*

A. Tamosaitis
Argonne National Laboratory.

The 12-ft hydrogen bubble chamber is one of the new large chambers under construction. The size of this chamber poses problems that require more thorough consideration than their counterparts in smaller chambers. The purpose of this presentation is to review some of these problems and to discuss the solutions or the proposed approach.

The chamber was conceived to be a physics instrument with the maximum economy of construction and operation. Consequently, an aspect ratio was chosen that provides good photographic utilization of the liquid inside a uniform magnetic field. These objectives immediately defined the direction for the design of various systems. The most unique problems due to the size of the chamber are in the following areas: operating considerations, photographic system, and the expansion system. The superconducting magnet is also a very important area, but it will not be discussed here.

Operating Considerations

The geometry of large chambers imposes two requirements: slow expansion rates for uniform sensitivity and thermal homogeneity for low optical distortion. An additional requirement, at least with bright field illumination, is fairly low bubble density and a large bubble diameter. This latter requirement necessitates operation at the low end of the temperature region and low expanded pressures. Since parasitic boiling sets the limit to the lowest expanded pressure as well as the rate of expansion, it becomes extremely important to determine the sources of it and to eliminate them.

An argument may be advanced that the parasitic boiling is inversely proportional to the characteristic dimension of the chamber; however, the maximum rate of expansion is also inversely proportional to the characteristic dimension. Thus, although the surface-to-volume ratio is lower, parasitic boiling has more time to develop. The net result may be that for equal surface

*Work performed under the auspices of the U. S. Atomic Energy Commission.

quality, the effect of chamber dimensions on reducing specific parasitic boiling is small. Although these arguments are only qualitative, it is clear that great care must be exercised to avoid cracks and gaps which are well proven empircally to produce boiling. It is even possible that once a clean chamber is achieved, its usefulness can be greatly increased because it may be feasible to use some of the classical heavy liquids such as Freon 13-B1 at low vapor pressures and low expanded pressure in the same chamber.

Tests have been made in our 2-ft model, shown in Fig. 1, in search of qualitative and quantitative answers. We found that it was not possible to expand below 18 psia independent of vapor pressure. We also found that at the same time we had about 0.5 J/liter of P-V work. We do not know the exact reasons for this, but believe that it was parasitic boiling and/or gas in the bellows. Steps have been undertaken to strip the chamber bare and to install a gas vent line in the bellows to determine which boiling is limiting the expansion. It is interesting that the P-V work increases quite suddenly with decreasing expanded pressure. It should be noted, however, that measurements of deviation from straight line in photographs of targets taken through 600-mm of hydrogen under the above conditions show no more than 30 μ rms deviation.

We have also done some additional thinking about modeling. Basically, there are the following unknowns that must be answered: thermal turbulence, kinetic losses, radiation, conduction, and the testing of some selected chamber components. It is evident from D. Thomas' work that a liquid hydrogen chamber of 1-ft dimension would be in a fully-developed turbulent regime and, therefore, a larger dimension gains only a longer single pass optical path. The kinetic losses scale as length to the fifth power and little can be measured until the dimensions are of the order of 10 ft. The radiation and conduction are, of course, calculable. Thus, the larger chamber size is useful only for checking some components; in our case we intend to check out the full-size optical cartridges. The penalties of a larger model than the minimum required are obvious.

We have found a small 6-in. Freon chamber extremely useful for quick qualitative check out of surface quality, cracks, valves, heat exchanger fins, and capillary tubes for boiling.

The 2-ft liquid hydrogen and the 6-in. Freon chambers have helped us to decide that the 12-ft chamber will have a heat exchanger at the top, that everything possible must be done to eliminate pluming due to crevices and cracks, and that a shroud may be useful in increasing the mixing length for heat prior to reentry into the fiducial volume.

Photographic System

It was decided in the early stages of the design to photograph the fiducial volume with wide-angle lenses rather than using either large windows or increasing the height of the chamber to reduce the lens and stereo angles. Initially, 110° lenses placed on approximately an 11-ft diameter circle were considered.

Scanning computer-simulated pictures with this camera arrangement was difficult. It was suggested to simulate photography with 140° lenses placed on a 7-ft diameter circle. These views were found to be much more scannable by bubble chamber physicists. Calculations also showed that good measuring accuracy in all three coordinates could be obtained with adequate volume coverage. Consequently, a feasibility study to design a 140° lens was conducted by Tropel, Inc. with excellent results.

The design is telecentric and, therefore, is relatively insensitive to film undulation. The lens is diffraction limited at f/8 over the entire field. The large symmetrical radial distortion in this lens was not found to be objectionable in the computer-simulated pictures. Tropel is currently finishing the optical and mechanical design, and expect to begin the construction of a prototype quite soon.

The illumination of the chamber volume has always been firmly anchored to 3M Scotchlite, although the bubble size imposed by the bright field illumination provides constant encouragement for ideas about dark field. Late in 1966 we began some tests with FE-582 bare-bead Scotchlite, which are discussed by M. Bougon in another session. With a 10° camera to light source angle, we have photographed electron tracks in hydrogen in dark field using FE-582. We have not done sufficient work to incorporate this feature into the 12-ft design; however, we are continuing (when time permits) with tests and calculations to see if dark field Scotchlite can be utilized with our geometry. Dark field photography allows more variation of the operating conditions of the chamber.

All lenses are placed behind three concentric hemispherical windows, shown in Fig. 2. These windows are strong mechanically for external pressure, eliminate the problem of chromatic aberrations due to dispersion of the chamber liquid, avoid distortion due to hydrogen-glass interface, and eliminate the reflections of the flashtubes. The convex side of the warm window is coated with a low emissivity gold film. The heat input into the chamber with this arrangement is about 0.45 mW/cm^2, which results in a stable thermal boundary layer with a small radial temperature gradient. The

radiation shield is a floating window and no large thermal stresses are encountered during cooldown. Our approach to the problem of the ever-present danger of cold window "fogging" will be either by a permanently sealed, evacuated glass-metal window assembly or by a similar arrangement plus ion or sorption pumping.

It has been determined experimentally that with 1042A Scotchlite, a gold-coated window, and a Wratten-22 filter, a maximum of 200 joules of capacitor energy per camera is needed to expose Microfile AHU film at f/16. Without gold the energy requirement is reduced to 100 joules per camera. The current design employs two concentric flashtubes for each lens. Tests with circular EG&G flashtubes of 15-cm total length and 100 joules capacitor discharge every second have shown that with current pulse shaping and 200 μs duration, the tubes will operate over one million cycles. The heat from the flashtubes, especially the infra-red, will be absorbed by the coolant and will not enter the chamber.

The energy requirements for the flashtubes may increase due to the possibility of installing a neutral density filter to equalize the exposure over the field. We are currently testing flashtubes with higher energy inputs in water-cooled containers.

The film is 70-mm perforated with a 60-mm diameter image, as shown in Fig. 3. The film advance is mechanical. The nominal film capacity is 1000-ft of 5-mil thick film. The random distortion due to change in R.H. is prevented by humidifying the camera wells to 50% R.H. The humidity also assists in preventing problems due to static electricity.

Expansion System

The expansion in this chamber occurs at the bottom. The main reason for this arrangement is to keep the glass windows at the top for safety and to separate the expansion system from the optics. The proximity of the expander to the optics may result in bad thermal turbulence as well as greater possibility of mechanical vibration. Furthermore, with the expander at the bottom, it is more convenient to provide localized cooling if it is required. The power required to drive a large expander by "brute" force is very large. It is, therefore, advantageous to make the expander a resonant system. In the ANL system, oil provides coupling between the bubble chamber piston and the accumulators. Energy makeup is pneumatic. A range of operating frequency can be obtained by filling the accumulators

with either liquid Freon or nitrogen gas. The details of the expansion system hydraulics are discussed by J. Simpson later in this session. I only wish to mention that with our uniform magnetic field, it is possible to use a metallic omega bellows. The cooling and condensation of the bubble in the bellows interior presents a challenging engineering problem, and no firm solution is yet reached; however, we do have several proposals under consideration.

LIST OF FIGURES

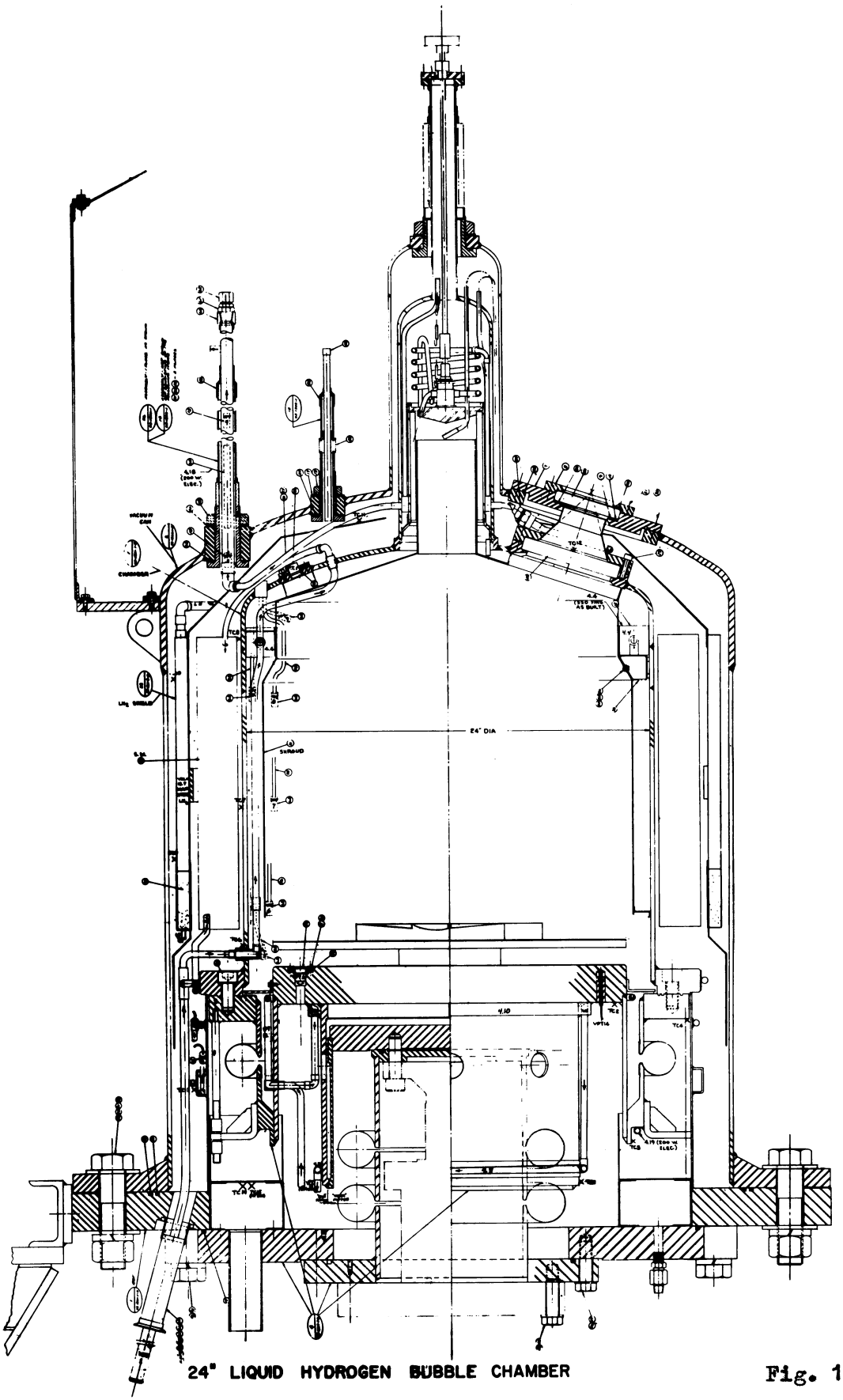

24" LIQUID HYDROGEN BUBBLE CHAMBER

Fig. 1

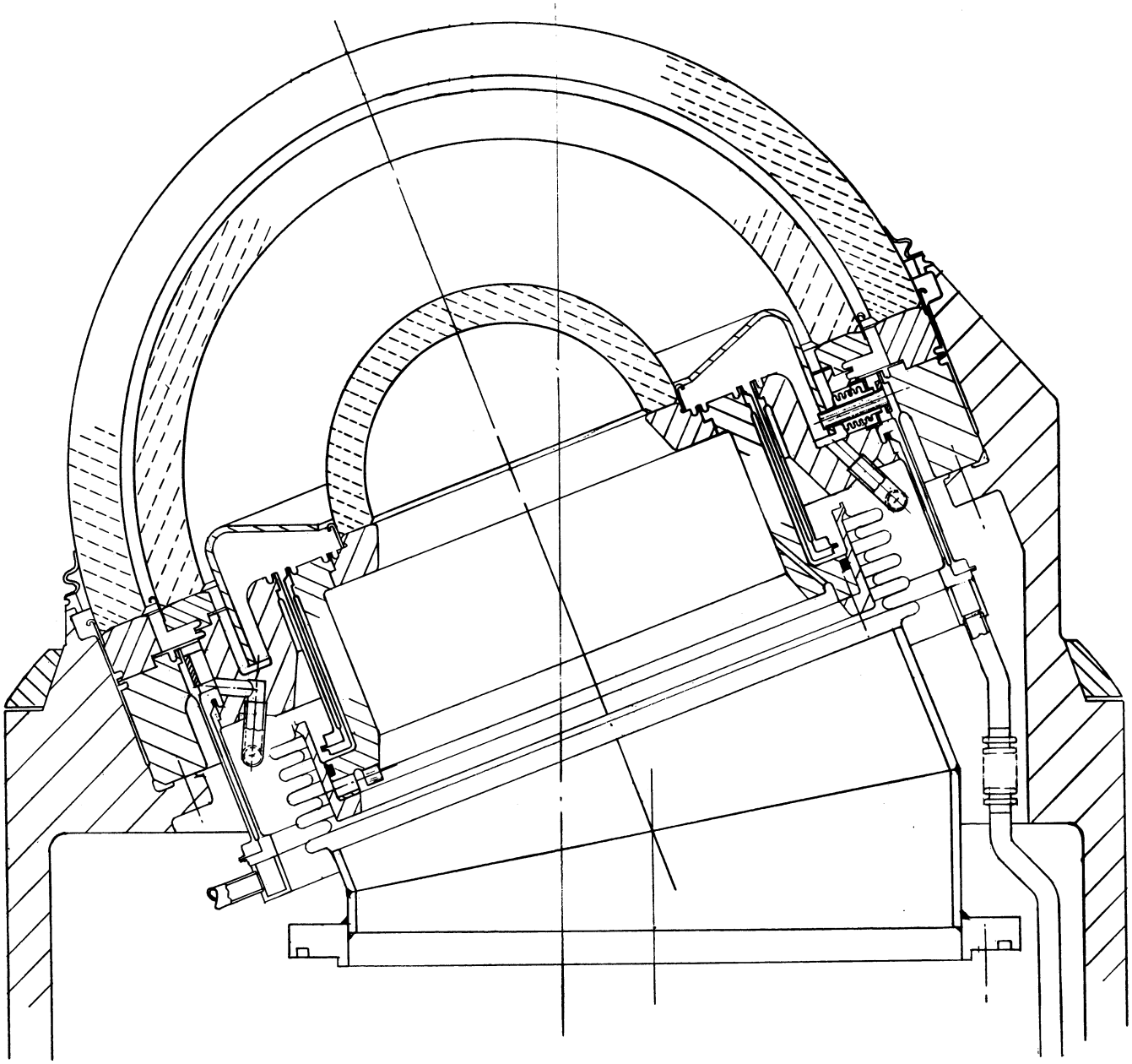

Fig. 2

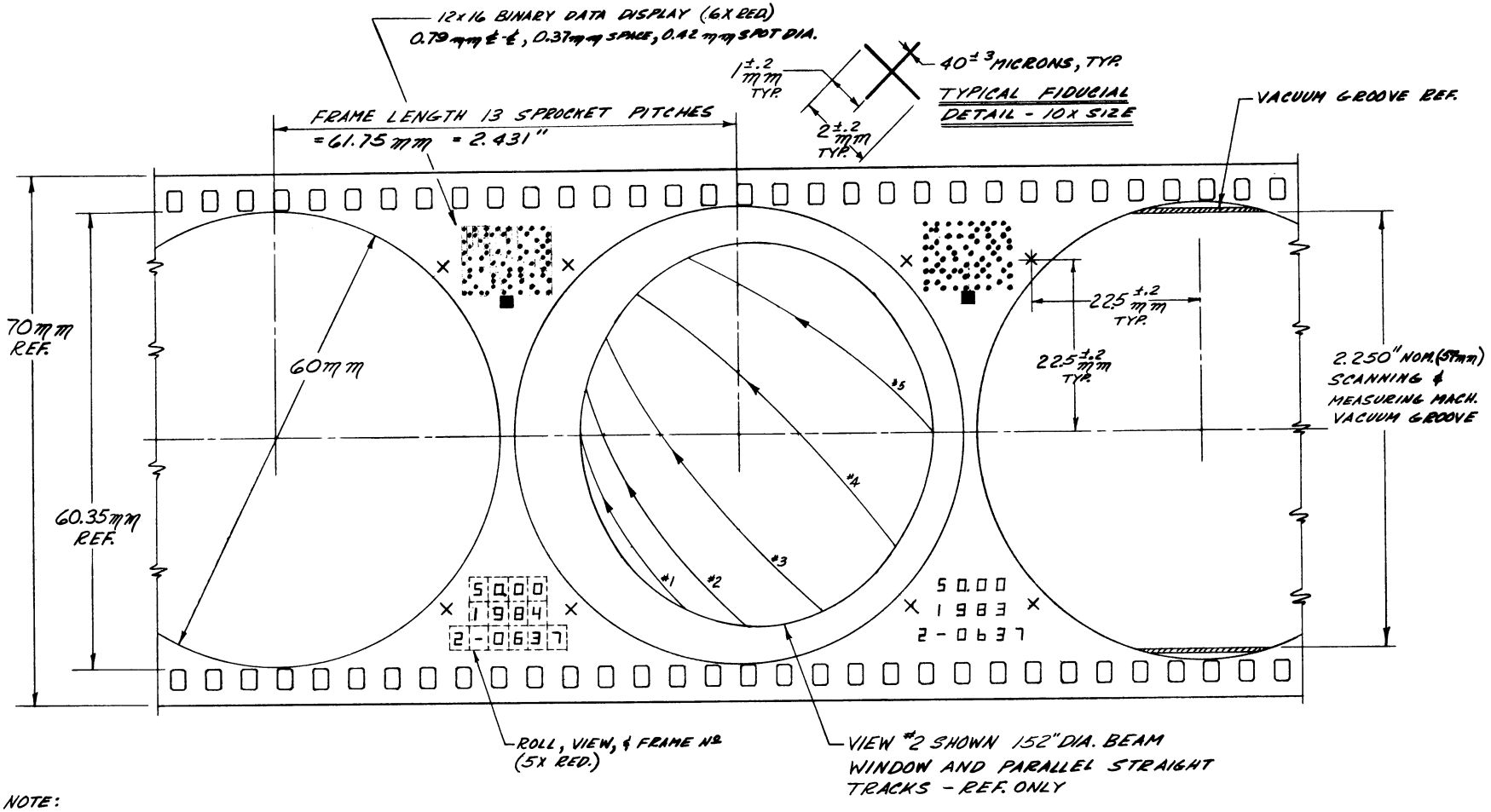

NOTE:

1) FILM CONFORMS TO A.S.A. STD. # PH1.20-1956 WITH TYPE II PERFORATIONS.

2) RELATIVE LONGITUDINAL LOCATION OF SPKT. HOLES AND IMAGE NOT FIXED. LOCATION TO REMAIN FIXED WITHIN ANY ROLL.

Fig. 3

6.6 INSTRUMENTATION FOR THE ANL 12-FT HYDROGEN BUBBLE CHAMBER*

J.D. Simpson

Argonne National Laboratory.

In most respects our approach to the instrumentation of the Argonne 12-ft bubble chamber is quite conventional. We have attempted to follow a straightforward approach wherever possible, carefully avoiding the temptations and pitfalls of doing something tricky or state-of-the-artish for the sake of our own self edification. However, we are using several techniques, which, although new in their application to bubble chambers, are in no way state-of-the-artish.

Figure 1 shows the general layout of the control room with respect to the bubble chamber area. The dimensions of the room are 30 x 40 ft, allowing adequate service space behind the racks and a small service area in one corner of the room. A network of cable troughts recessed into the concrete floor of the control room provides some flexibility in the placement of the racks and the console. This room is separated from the bubble chamber area by a blast wall designed to withstand an overpressure of 1-1/2 lbs/in^2. There are no direct access doors between the room and the chamber area. A 3-ft x 3-ft blast window will allow limited visual observation of the chamber area. Communication facilities in the control room include several closed circuit TV monitors viewing the chamber, expansion pit, and compressor room. Operation of the hydrogen and helium liquefiers is done from a separate area in the compressor building.

We intend to include a small computer in the control room to serve principally as an automatic data logging system. The machine will be in the DDP-416, PDP-8, or similar class. This system will be used mainly to provide a reliable, periodic log of significant parameters, and record alarms as indicated on the main alarm panels. It will also be used for analogue to digital conversion of the pressure pulse in the chamber and the chamber static pressure and VPT pressure for the data box presentation. No closed loop control is anticipated at this time, but, like most other groups, we do not exclude the possibility in the remote future. The system will incorporate a fast line printer to eliminate stacking problems should several alarms arrive in a short time interval. By operator request, the logger will record any subset of parameters. The purchase request has been filed for this equipment and we expect to place an order in the very near future.

---

*Work performed under the auspices of the U.S. Atomic Energy Commission.

Because of the logging equipment, we have endeavored to transmit signals to the control room electrically unless other considerations require otherwise. Thus, many indicators in the control room are electrical meters following transducers in local equipment. We have chosen to use potentiometric pressure transducers for static and quasi-static pressures after evaluating several types. Excitation of these transducers fulfills "intrinsically safe" requirements for added safety.

An important responsibility of bubble chamber instrumentation is to present pertinent data on the film in formats convenient to as many users of the film as possible. Figure 2 illustrates our planned film format, identical in each of the four views with exception of a view indicator. Decimal presentations consist of the magnet shunt voltage, frame number, view number, and roll number. Data such as chamber conditions, beam counts, date-time, plus the decimal data is presented in this 12 x 16 bit matrix of BCD coded integers. During multiple pulse operation, this data box information must expose the film within 30 milliseconds, the time during which film is stationary in the magazines. We considered several methods of illumination and decided to use pulsed incandescent lamps, both in the data box and segmented readouts. Segmented readouts lend themselves well to convenient handling by automatic readers. This feature provides a redundant check on these important parameters in the BCD matrix. We have pulsed some lamps for as long as 6 million pulses without bulb failure. The actual data box measures roughly 5 x 7 inches, requiring a rather high density of bulbs. Exposure of the microfile film to be used appears possible from either the emulsion side or the base side of the film.

The square area will serve as a locating base for the data box information and as a base from which to locate the lens-registered fiducial marks.

Timing for expansion and optics sequencing is obtained from preset scales driven by a 10 KC cryostal controlled source. Interface to the ZGS is such that in event of ZGS timing pulse failure, the chamber will continue to pulse at the established rate to maintain thermal equilibrium conditions in the chamber.

Other techniques employed include: piezoelectric dynamic pressure transducers in the chamber, an ultrasonic transducer at the chamber high point to detect any large bubble there, and Ga-As diodes to measure cool-down of the supermagnet cryostat. Instruments employed in the cryogenic process systems are of the conventional pneumatic type.

In the event of power failure, a steam turbine-driven generator will automatically assume the electrical load. However, the expander and optics systems will be disabled until a manual start commend is provided.

Whenever required, cables are being run in conduits purged with dry nitrogen. Conduits entering the control room from the bubble chamber area are fed through a sealed bulkhead.

LIST OF FIGURES

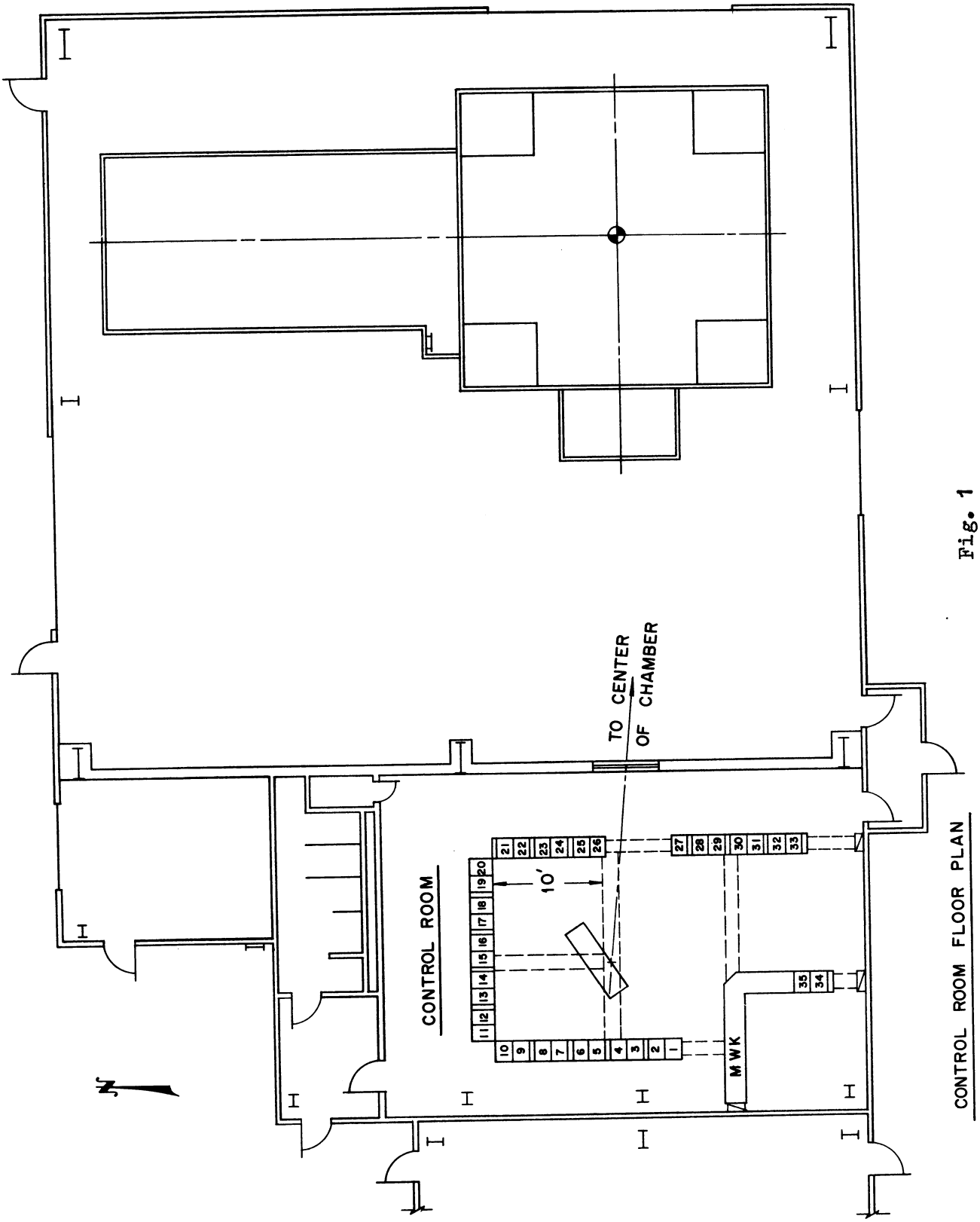

Fig. 1

CONTROL ROOM FLOOR PLAN

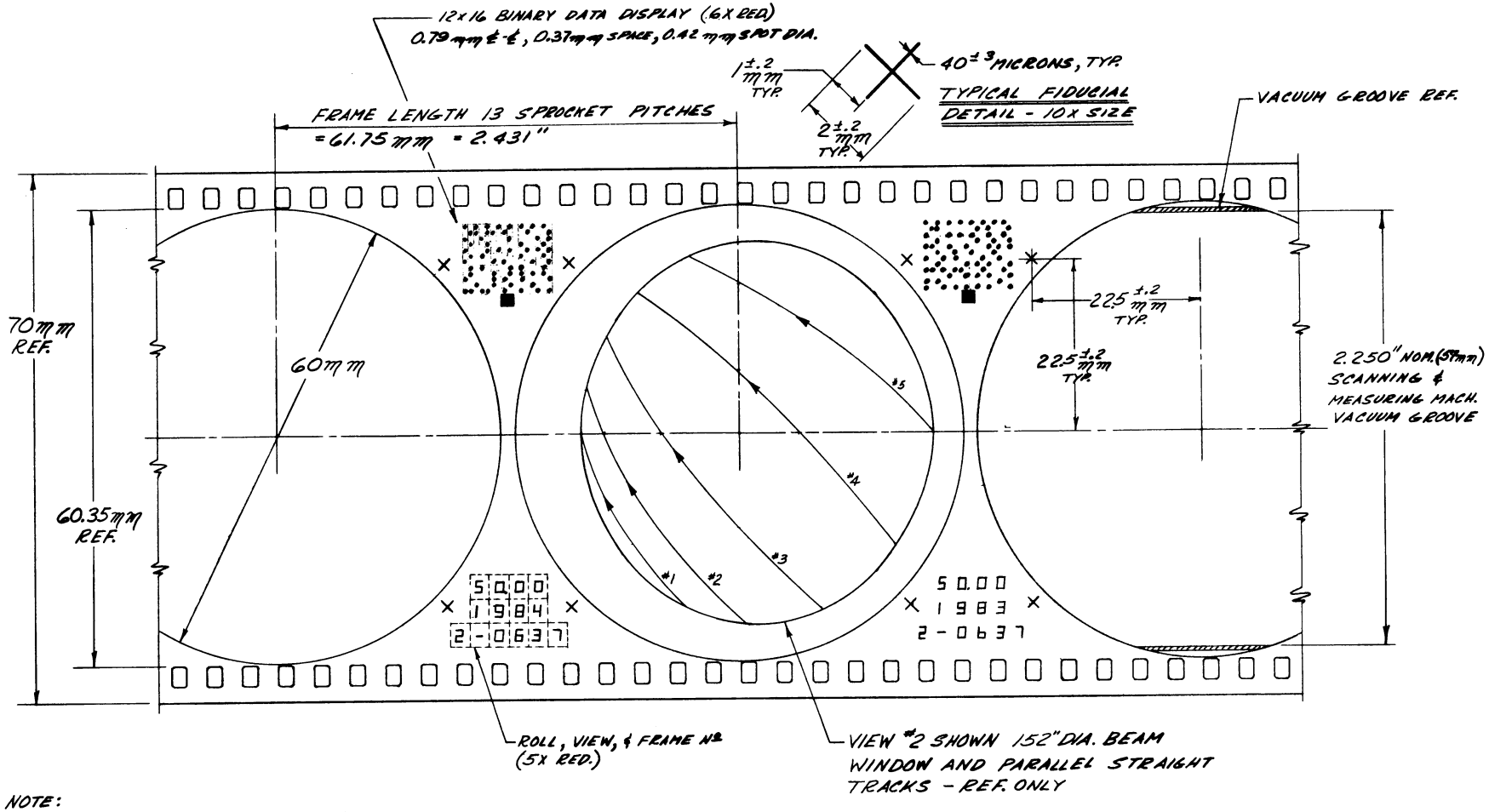

NOTE:

1) FILM CONFORMS TO A.S.A. STD. #PH1.20-1956 WITH TYPE II PERFORATIONS.

2) RELATIVE LONGITUDINAL LOCATION OF SPKT. HOLES AND IMAGE NOT FIXED. LOCATION TO REMAIN FIXED WITHIN ANY ROLL.

Fig. 2

6.7 EXPANSION SYSTEM FOR THE ANL 12-FT HYDROGEN BUBBLE CHAMBER*

J.D. Simpson
Argonne National Laboratory.

The purpose of this paper is to outline the design criteria, problems, and operating principle of the expander for the ANL 12-ft bubble chamber.

Until the advent of large chambers, the pulse period was usually as short as conveniently possible in order to avoid parasitic boiling problems which, not uncommonly, limited the minimum expanded pressure attainable. In large chambers, however, sizable pressure gradients are introduced within the chamber volume which increase as the expansion period decreases. Large pressure gradients not only produce variations in sensitivity through the chamber, but also produce thermal heating in the chamber fluid as they dissipate their energy. A reasonable compromise for the 12-ft chamber is a pulse duration of about 35 ms for hydrogen operation. This produces about 3 psi difference in the expanded pressure from top to bottom for 60 psi average drop.

The entire lower surface of the chamber is moved 1-1/8 in. to expand the chamber, providing about 1% volumetric change.

Figure 1 illustrates the important features of our design. In equivalent mechanical lumped constants, it consists of a mass (that of the real mass plus effective oil mass, totalling about 800 slugs), supported between two springs (that provided by the compressible chamber and that of accumulators). The large area of the main piston, together with a typical bulk modulus of 7000 psi for the hydrogen, provides an effective spring constant leading to a "natural" period of about 50 ms. Thus, to realize a 35 ms period, the accumulators need only to equal this spring rate. Air springs could provide this, but such springs have hyperbolic response. Consequently, higher accelerations result than if a linear system were used to obtain the same cycle period. To more nearly approach a sinusoidal piston motion, we plan to change the accumulators with liquid Freon-12†, which is quite compressible at moderate temperatures. An obvious method of "latching" such an oscillator would be to

---

*Work performed under the auspices of the U.S. Atomic Energy Commission.

†Trademark, DuPont Corporation.

control the oil flow in the spring accumulator lines, but as other bubble chamber expander designs have suggested, separation of the latching system from the spring system can reduce energy losses in the hydraulics.

The "latch" or "clamp" system consists of the 270-in.^{2} piston, the 5-in. valve, and the 2.5 gallon accumulators. The valve is a nearly balanced poppet check valve. To pulse the expander, the valve is unseated by applying oil pressure below the 4-in.^{2} actuating piston and held open for at least one half the cycle. During the second half, the oil pressure is removed, but the poppet remains held up by the forward flow of oil through the valve. As the flow diminishes, the valve closes by the force of a pressurized air cylinder. Figure 2 shows an assembly drawing of this valve. All moving parts are of titanium, with the main body being of steel. There are nine porting holes to relieve the balance piston area. We have designed the valve to open in about 10 ms and have calculated the closing behavior (shown in Fig. 3). The total effective moving mass (metal and oil) is about 1-1/2 slugs. The remaining kinetic energy of the poppet at closure will be about 100 ft-lbs.

Calculated energy losses in the system are about 6000 ft-lbs per cycle typically, with about 30,000 ft-lbs of initial energy in the system. This is then a relatively higher "Q" device. The dissipated energy is restored by controlling the air pressure in the clamp. During the downstroke of the piston, the air is maintained at lower pressure than during the return stroke. Air for this is furnished by two 60-hp air compressors.

The hydraulic fluid to be used is Skydroil because of its high bulk modulus and excellent lubricating properties. This requires ethylene-propylene to be used for all elastimer seals.

We feel that this system will provide a desirable range of operating conditions for the 12-ft chamber.

LIST OF FIGURES

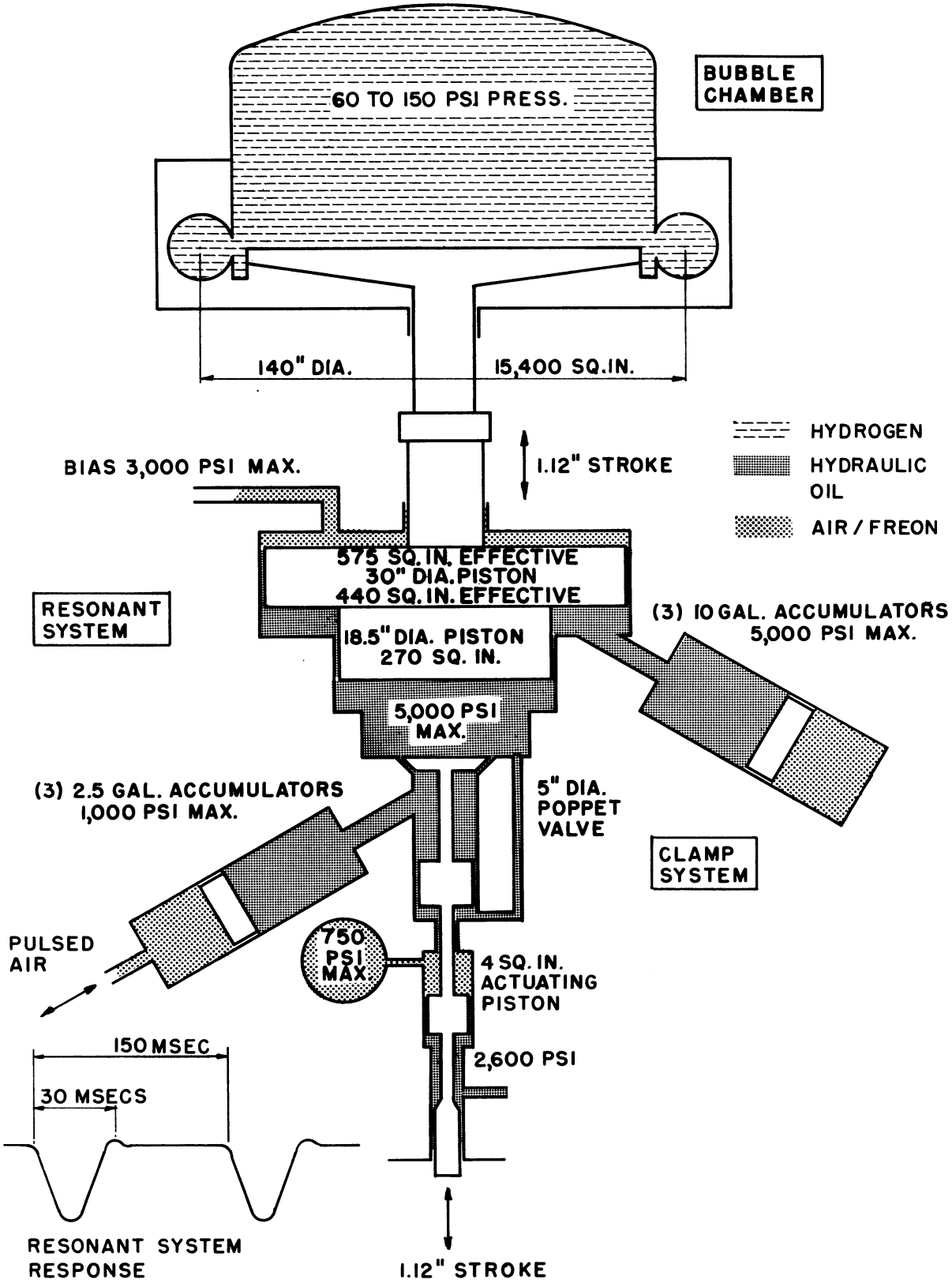

12 FT. BUBBLE CHAMBER-EXPANDER SYSTEM - SCHEMATIC

Fig. 1

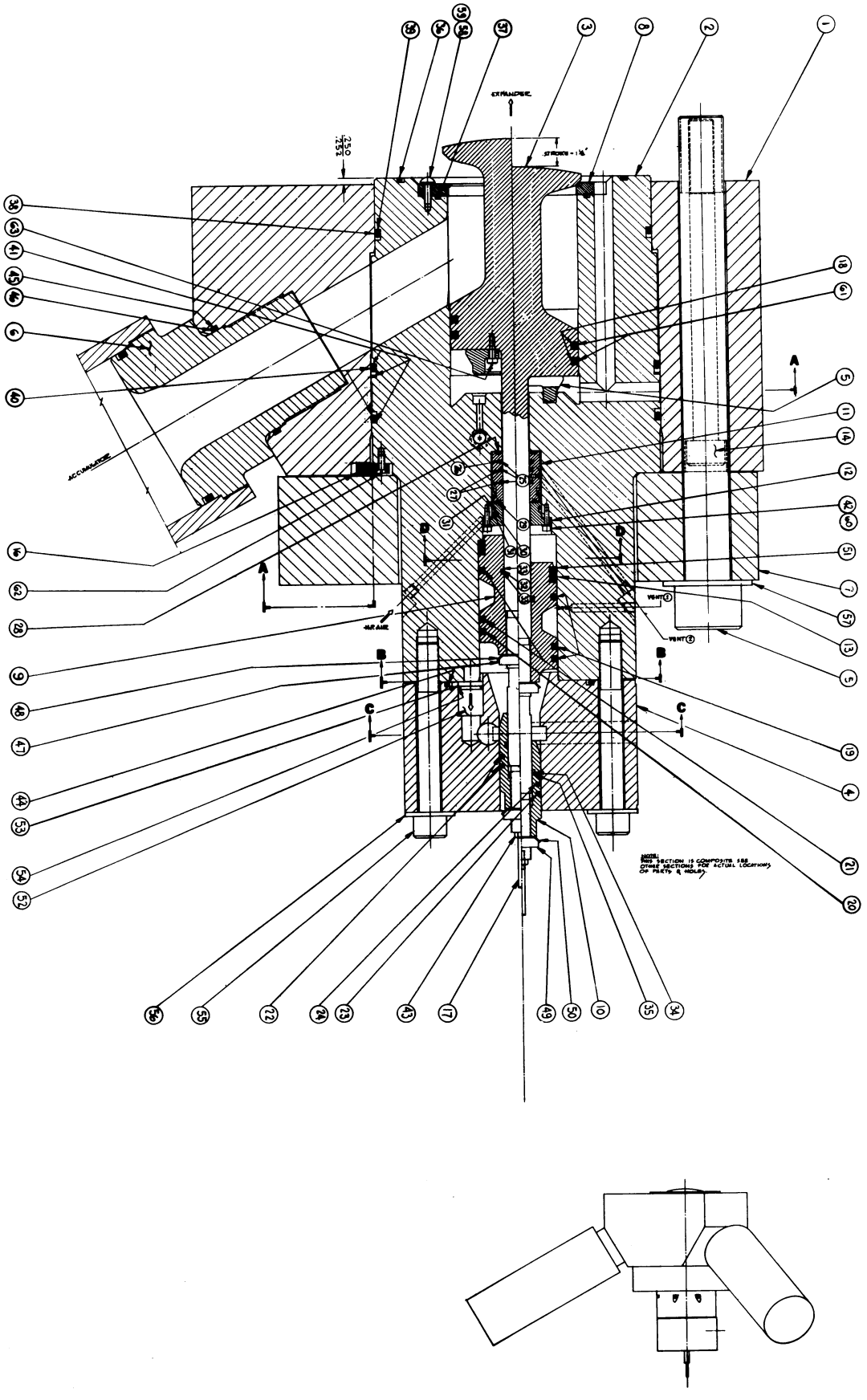
EXPANDED
STROKE - 1⅛"
ACCUMULATOR
AIR AIR
VENT
VENT
A
B
C
NOTE:
THIS SECTION IS COMPOSITE. SEE
OTHER SECTIONS FOR ACTUAL LOCATIONS
OF PARTS & HOLES.

Fig. 2

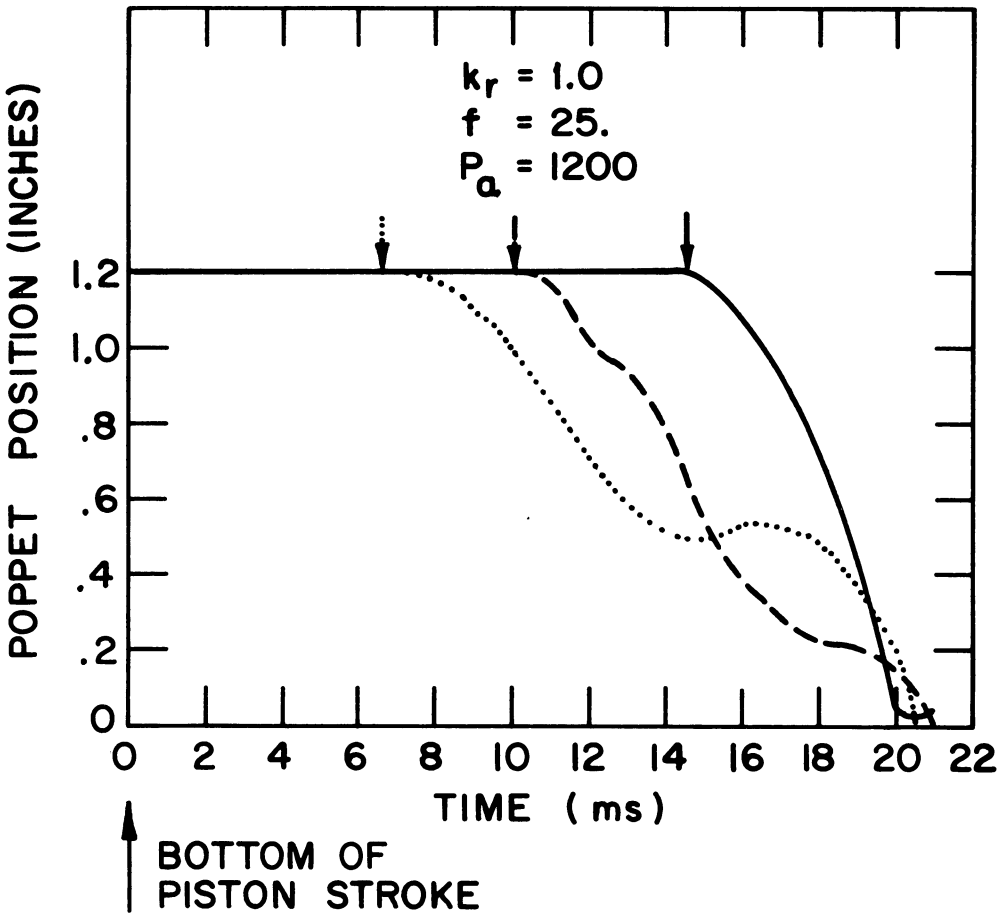

CALCULATED POPPET POSITION
— VS —
TIME AT CLOSURE

Fig. 3

6.8 DESCRIPTION OF THE MECHANICAL AND ELECTRICAL COMPONENTS, GENERAL OVER-ALL, OPERATION AND EXPANSION STUDIES OF THE MURA MODEL HEAVY LIQUID BUBBLE CHAMBER

C.A. Baumann, U. Camerini, W.F. Fry, M.C. Gams,
R.H. Hilden, J.F. Laufenberg, M.L. Palmer,
W.M. Powell, I.N. Sviatoslavsky and W.R. Winter
University of Wisconsin, Madison.
(Presented by I.N. Sviatoslavsky)

This report describes the mechanical and electrical components of the MURA model experimental heavy liquid bubble chamber and includes a discussion of the expansion studies performed on it. Another report which will be presented by Professor Wilson Powell describes the expansion dynamics and optical inhomogeneity studies performed on this model.

The intriguing question, "Can a tank car filled with propane be expanded and photographed through small ports?", leads to the basic concept of the 9 m^3 bubble chamber. After a few minutes of serious thought it became clear that many questions needed to be answered before a working chamber could be designed.

Some of these questions were: (1) What are the problems of keeping a large volume of liquid free from impurities so that good photographs could be taken through a long optical path; (2) how serious are the problems of optical inhomogeneity arising from temperature gradients in the liquid; (3) can such a large volume of liquid be expanded uniformly and what are the problems associated with that; (4) does wide angle photography offer serious problems; and, (5) can Scotchlite be successfully employed inside a liquid and used as a retrodirective device?

It was clear that optical inhomogeneities could be a serious problem in large heavy liquid chambers. The largest existing heavy liquid chamber at the time of the initiation of the program was the CERN heavy liquid chamber of Ramm. In this chamber, and even in smaller chambers such as the Berkeley and Paris chambers, optical inhomogeneities could easily be observed, suggesting that this could be a serious problem in a larger chamber.

Furthermore, experience with both the CERN and Paris chambers showed that boiling on the diaphragm occurred, suggesting that there could be serious problems associated with boiling on a diaphragm in expanding a still bigger chamber. Furthermore, it was not clear that the increased motion of the liquid near the walls, diaphragm, etc. might not cause specific problems.

With these questions in mind, it was decided to construct some sort of "model chamber" to study these problems before completing the ultimate design of the big chamber. Rather than build a scale model of the big chamber, it was decided to build a chamber which would permit a specific study of some of these problems. The shape of the model chamber was dictated by three factors: (1) the longest dimension should be at least as great as the path length to be photographed in the big chamber, (2) the column of liquid to be expanded should correspond to the same length as in the big chamber, and (3) the ratio of diaphragm area to liquid volume should be comparable to that of the big chamber.

Many other minor considerations enter into the detailed design of the model, but generally speaking the above criteria set the configuration of this model chamber. A photograph of the model during operation is shown in Fig. I.1

GENERAL DESCRIPTION OF THE MECHANICAL AND ELECTRICAL COMPONENTS

Chamber Body

The body of the chamber is a horizontal cylinder with flat ends. It is constructed of 24-in. schedule 40 carbon steel pipe with flanges welded on the ends. The inner diameter is 22.625 in., over-all length 72 in., and the cylinder wall thickness is 0.687 in. The ends are machined from 4-in. blind flanges and are attached to the body by 24 1.50-in. bolts. The expansion system occupies one entire end of the chamber.

Altogether there are seven windows in the chamber. One is in the center of the end flange, making it possible to look through six feet of liquid. The other six are equally spaced in the cylindrical portion, three on a side, separated by 90^{o} to permit stereo photography. Reinforcements for the windows consist of studding outlets welded into the body of the chamber. **(Figure I-2).**

The maximum design stress for the chamber body was 11,000 psi at a pressure of 600 psig. Special consideration was given regions which had large section transitions. Full penetration weldments were specified; these were die (dee) penetrant and radiographically tested for cracks.

Figure II-1 shows the double diaphragm and holey plate assembly. The inner diaphragm A had Freon on one side and Freon solvent with nearly the same density on the holey plate side. This meant that the inner diaphragm assumed a shape determined by the stretching of the diaphragm only, unaffected by gravity. The outer diaphragm B separated Freon solvent and the air manifold. In the compressed position this diaphragm pressed against the holey plate at the

top and bulged out at the bottom depending upon the volume of Freon solvent enclosed between the two diaphragms.

The holey plate C was machined from a 4-in. blind flange contoured on both sides. It was designed to be self-supporting and capable of sustaining 600 psig in the chamber. The front diaphragm is attached to the front of the holey plate by a contoured clamp ring. The diaphragm material is squeezed about 20% between the holey plate and the end flange. The cover plate D is another 4-in. blind flange which seals off the expansion end of the chamber. The whole assembly is then bolted to the end flange of the chamber by 24 1-1/2-in. bolts E. These bolts also provide the force needed to squeeze the diaphragms 20% which automatically takes place when all surfaces touch metal to metal. O-ring seals G are provided at the various interfaces, with double O-ring seals at the critical locations.

To fully exploit an experimental chamber such as this one, it was necessary to install numerous temperature and pressure sensors in it. There are four Kistler (Model 601A) quartz dynamic pressure transducers equally spaced along the bottom of the chamber. Temperature wells are installed on the bottom, one-third up, two-thirds up, and at the top of the chamber. There are more temperature probes along the length of the chamber to measure longitudinal gradients. TRI-R Type TP-7P thermister probes are used to measure the temperature. Three openings are provided on the bottom of the chamber for propeller shafts. One of these is presently used for an inlet valve. A vent valve is located in the end plate at the top where a relief valve and a gauge line are connected as well.

At the time when the body of the chamber was fabricated no attempt was made to polish up the interior surface. It was decided instead to paint the interior

with a paint compatible with Freon 13-B1 which would smooth out the surface well enough to reduce boiling. Rough spots and weldments were ground flush and sanded down. The whole interior was then painted with two coats of O'Brian's white polyurethane paint. The choice of paint was made after an intensive investigation of many brands tested in liquid Freon 13B-1 for weeks at a time. It was discovered that although most of the polyurethane paint gave the desired smooth finish, some had poor adhesion properties and were more easily penetrated.

Precautions were taken to reduce boiling from various objects in the chamber. Openings were rounded off, sharp edges smoothed down and the "O" ring grooves in the end plate undercut to provide free access of the liquid to the seal. This prevented a squirt of high velocity liquid and consequently reduced boiling.

The temperature of the chamber is controlled by means of coils attached to the outside of the body. These coils consist of 1/4-in. copper tubes cemented to the wall with Devcon-F aluminum-loaded epoxy. Although the thermal conductivity of the epoxy is low, it was decided that with adequate insulation on the outside, a sufficiently stable condition of thermal equilibrium could be reached. Altogether there are 20 individual coils. Two temperature-controlled water baths are used to supply water to any of the coils. In this way desirable temperature gradients can be established in the chamber. Temperature sensors (TRI-R thermistor probes) monitor the incoming and outgoing water temperatures at the manifolds. Flow checks can be performed by diverting the water into a calibrated container. This system has allowed us to do reasonably accurate heat load studies.

In order to be able to photograph tracks through the end window, it was necessary to provide a retrodirective surface in front of the diaphragm. To make

this possible a Ramm plate was installed. The first Ramm plate was made of 1/8-in. aluminum plate, had a clearance of 1-3/4 in. all around, and was located 8 in. in front of the diaphragm. It was suspended by springs attached to its front which allowed it to move backwards freely but restricted its forward motion. This plate did not perform as a true Ramm plate because of the large clearance and has subsequently been replaced by another 1/8-in. aluminum plate which has only 3/8-in. clearance. It has fiducial lines alternately 1 mm and 0.5 mm in width forming a grid of one inch squares. There has been a noticeable improvement in the operation of the chamber since the new plate was installed.

Soon after the chamber was pulsed for the first time, it became obvious that some means of agitation will be needed to eliminate thermal turbulence. The first attempt was to install a small propeller on the end flange. Since this propeller was coaxial with the cylindrical portion of the chamber, it tended to produce a rotation in the liquid. Intermittent operation of the propeller between pulses was tried with a certain amount of success.

The second attempt was to install three propellers equally spaced along the bottom of the chamber. They were driven by electric motors with individual controls capable of rotating in either direction at any speed. Conventional carbon seals were used at the shafts and performed quite well. Outboard motor propeller were tried and a study was made to determine the best shaped propeller. One of the propellers had a skirt on the bottom to capture the bubbles from the seal. We felt that enough is known now to minimize and contain the boiling from propeller seals.

Although propellers give adequate mixing and do eliminate temperature gradients, they also produce excessive liquid motion which is detrimental to the

operation of a bubble chamber. In order to minimize liquid movement, it was decided that a rake consisting of round rods be tried out. After conducting some experiments in a water tank, we finally settled on a rake made up of 1/4-in. stainless steel tubing, 14-in. long spaced on 3/4-in. centers covering the entire length of the chamber (see Fig. II-1 H) These tines were heli-arc welded into holes drilled in a 3/4-in. stainless steel tube; their tips were crimped shut, welded and polished after which the whole assembly was leak checked.

The rake is driven by a shaft which goes through a seal in the end flange and is attached to the rake inside the chamber. A pneumatic cylinder which is bolted to the outside of the end flange is used to power the rake, driving it through 85° of circular motion. In its rest position the rake (Fig. II-3 A) is against the side of the chamber covering the windows through which pictures are not being taken. With the present setup the total travel time for a round trip is three seconds. The rake actually traverses the chamber in one second and takes one second to decelerate and start in the opposite direction. It has been clearly demonstrated that a rake does eliminate thermal turbulence and produces very little liquid motion. This will be discussed in more detail elsewhere in the report

Windows

There are seven windows altogether in the chamber, six in the cylindrical portion and one in the end flange. One of these is shown in Fig. II-2. At first we used flat rounds of tempered glass (Herculite) 6 in. in diameter and 1-1/4 in. thick. Later on we obtained two hemispherical annealed glass windows. By positioning the camera lens at the center of curvature distortions due to the light passing through various glass thicknesses are eliminated and also

reflections from the ring light don't get into the lens.

Conventional "O" rings are used to seal the windows. A teflon spacer confines the "O" ring on the outside periphery. No stop was provided for the "O" ring on the inside periphery. Experience has shown that a teflon spacer there, no matter how well designed, will always boil and obscure photography. Precautions are taken to evacuate behind the "O" rings when the chamber is evacuated to prevent the seals from being sucked in. This pumpout is built into a metal spacer which also acts as a stop for the clamp ring giving a predetermined squeeze on the seal. Pumping is continued during chamber operation providing an excellent means for immediately identifying a leak in the window seal.

The windows were designed for a maximum stress concentration of 700 psi giving a safety factor of about 10. The stresses in the hemispherical windows are considerably smaller.

The window assembly is attached to the body by a clamp ring with six 1/4-in. bolts. Metal-to-metal contact between the clamp ring, the spacer and the chamber give the predetermined amount of squeeze on the "O" ring seal.

During operation of the chamber all the windows which are not being used are covered with a 1-in. round steel plate with an "O" ring seal. When the chamber is left full overnight, all the windows are thus sealed. For visual observation a 1/4-in. plastic shield is used to cover the window for protection.

Photography and Illumination

A modified Beattie model CS-48 film transport was used to advance the film and the camera was made at MURA except for the lens which was changed depending on the nature of the experiment.

About three-quarters of the cylindrical portion of the chamber is covered by 3 M (SPR-704) Scotchlite retrodirective sheeting*). This Scotchlite has a very narrow angle of retrodirection and the beads are quite uniform in size and very well distributed. In order to protect the Scotchlite from the Freon it was necessary to encapsulate it in mylar film. An intensive program was initiated to determine the best method of encapsulation. The method which was finally used and which proved to be very successful was to glue the Scotchlite on a mylar sheet (0.003 in.) using its own adhesive (care must be taken to prevent capturing air bubbles), then covering the Scotchlite with epoxy (General Mills Versamid Genepoxy combination) and finally placing another sheet of mylar (0.005 in.) on top of that. It is necessary to roll the top sheet on in order to squeeze out the excess epoxy and also the captured air bubbles. The sandwich resulting from this process is about 0.012-in. thick. It is then necessary to flame seal the edges, by placing the sandwich between two flat metal bars with the sheet protruding about 1/32 in. and passing over it with a cool torch. This fuses the mylar together permanently.

The Scotchlite mylar sandwich was then epoxied to the wall of the chamber with Armstrong C-1 epoxy. While the epoxy was curing, the Scotchlite was held in place by means of an inflated polyethylene bag. The chamber was held stationary while the epoxy was curing and this caused some of it to run down to the middle leaving some voids on the sides. These small airpockets were a continuous nuisance to us since they expanded when the chamber was evacuated and tended to pull the Scotchlite off the wall. It would have been desirable to rotate the chamber slowly while the epoxy was curing. This would prevent the epoxy from running out.

Scotchlite was also applied to the front side of the Ramm plate.

---

*) (Figure I-5)

Expansion Recompression

The expansion recompression system is connected to the bubble chamber by means of a slip-on flange such that the straight-through section is coaxial with the chamber. The 10-in. expansion Grove valve is attached to one end of the straight section and the 8-in. recompression valve to the trunk section. Since all of this plumbing provided a large dead space, we inserted volume occupiers in this plenum providing only slightly more space for the flow of air than there is in the Grove valve orifice itself. The Grove valves are then connected to the expansion and recompression tanks by means of an 8-in. steel pipe*).

Four 3/4-in. Barksdale (N.O. 2-110-23) solenoid valves are externally manifolded on the expansion Grove valve. These Barksdales are connected by ball valves such that any one or more could be completely isolated from the system. This allowed us to expand the chamber with different numbers of solenoid valves. The recompression Grove valve has two Barksdale valves externally manifolded on it, also through ball valves. We have found that only one of them was needed for adequate recompression. Faster recompressions, using both Barksdale valves excited the natural frequency of the chamber and lead to undesirably high surges in pressure.

Figure II-4 shows a schematic of the air system. A 50-horsepower 10 x 4-1/2 x 9 Worthington compressor located in a shack outside the laboratory building pumped air into a main reservoir. The top pressure in this reservoir was 570 psig. Grove diaphragm regulator valves then supplied air to the recompression tank at 300 psig and the Grove valve recompression tank at 320. A back pressure regulator maintained the expansion tank at a predetermined pressure.

---

*) (Figure I-7)

Another pressure regulator connected the expansion tank to the compressor intake. This was set at the design intake pressure.

There is a separate tank for the expansion pressure of the Grove valve. This tank is connected to the suction unloader on the compressor and as a result is maintained at atmospheric pressure.

Pilot pressure for the Barksdale valves was supplied from a dry N_2 bottle and was usually set at about 350 psig.

Temperature Controls

The temperature of the bubble chamber was controlled by two independent water systems. One system controlled the top one-third of the chamber and the other system controlled the bottom two-thirds. Each system consisted of a water tank in which a controller maintained the temperature at a preselected level. Two types of controller were used, a YSI Model 71 thermistemp temperature controller and a YSI Model 72 thermistemp temperature control. The former is a full load on and off controller while the latter is a proportional controller. Both of them operated heaters in the tanks when heat was needed and solenoid valves which dumped cold water into the tank when the water got too hot.

Separate pumps then pumped the water through the bubble chamber coils, through a bypass, and returned it to the tank. A single overflow maintained the level in the tanks. The bypass flow was adjusted so as to produce a lot of turbulence in the tanks and thus keep the temperature uniform throughout. Both systems worked extremely well, maintaining stable water temperatures to within $\pm$ 0.05^{o}C and were very versatile and troublefree.

BUBBLE CHAMBER ELECTRONICS

I will now very briefly describe the function of the electronic equipment used in the operation of the model bubble chamber. Figure II-5 is a typical block diagram of the chamber control equipment. Control and monitoring are the two main functions of the electronic gear.

All events that occur during the chamber cycle are triggered by a master trigger generator and its associated time delays. It is a MURA-built transistorized unit designed for general laboratory use and modified for chamber operation. The trigger generator, synchronized with the line frequency or self-exciting, supplies a 10-microsecond positive 12 volt pulse which triggers the time delays or other circuits. Presently the generator is set up to pulse the chamber at a repetition rate of three times per minute; however, this rate is variable and can be set to meet the requirements of the experiment.

When a radioactive source is used to produce tracks in Freon, the chamber cycle must be synchronized with the source. A solid steel rotating cylinder with a slot perpendicular to its axis placed between the chamber and the source acts as a shield except for a short period of time. This period of time is dependent on the speed of the drum (100 rpm), and the number of particles is dependent on the size of the slot and the strength of the source. Particles were allowed to enter the chamber every 50 ms in a pulse 2 ms wide.

A photo-voltaic diode is used to pick up a light source corresponding to the radiation pulse every 50 ms. The diode pulse fed to a signal conditioner

and then to a pulse counter enables the operator to pick off a trigger pulse every 20 seconds. This method merely replaces the master trigger generator so that the chamber cycle can be synchronized with the radiation pulse.

Rake Control

During operation with the rake, the first function of the master trigger generator is to start the rake cycle. The rake is operated by a pneumatic valve which is controlled by a solenoid. A variable monostable multivibrator, triggered by the master trigger generator, controls a relay that applied 110 VAC to the solenoid. The rake cycle time, determined by air pressure, takes approximately 3 seconds. Because this cycle must finish just before the chamber is expanded, a second pulse 3 seconds later must start the expansion cycle. This 3-second delay is supplied by the master time delay.

Barksdale Valve Control

The Barksdale valves, of which four are expansion and two recompression, control the Grove valves. The Barksdale control circuits consist of:

1. Valve timing circuit.
2. Valve driver circuit and associated power supplies.

The valve timing circuit consists of six identical channels which are independent of each other. This is a versatile unit and can be operated in several modes which are:

1. Automatic Mode

   An external trigger starts six variable gate circuits with a range of 10 to 200 milliseconds. These energized the valves. This mode was used most of the time.

2. External Turn-Off Mode

An external start and stop trigger determined the open time of the valves.

3. Single Pulse Mode

A push button excites the trigger initiating the gates.

4. Continuous Mode

A valve can be opened and closed by means of a push button. This push button bypasses the variable gate.

These pulses go to the Barksdale driver units of which there are eight. A pulse from any of the six variable gates can energize any of the eight driver units.

The Barksdale driver units are fed from two power supplies, the booster power supply, and the sustainer power supply. A short pulse of a few milliseconds is given by the booster supply followed by one from the sustainer which stays on for the full length of the gate. The booster supplies - 70 volts from a 400 f condenser. The sustainer delivers 2 amperes per coil at - 15 volts.

A Barksdale disabler circuit opens the lines to these two supplies, turns them off, and discharges all capacitors.

Barksdale Valve Monitoring

It is important to know if the Barksdale valves are operating, therefore a monitoring system was devised to detect valve-stem movement. A steel slug attached to the stem moves inside a stainless steel tube when the valve is operated. A transformer with 5-kc fed primary is wound on the stainless tube. The slug movement through the transformer changes the

inductance and therefore changes the induced signal at the secondary. This signal is rectified, filtered, and sent to the alarm circuit and scope for monitoring. This signal is not a linear function of the distance the valve stem travels but it will tell the operator it is moving and how fast.

Xenon Flash Lamp Control

When photographing cosmic rays in the chamber, it was required that a picture be taken only when a cosmic ray went through the chamber during its sensitive time. In addition, the Xenon flash lamps must flash at a known time after the passage of the cosmic ray. The chamber was pulsed at 20-second intervals and no pictures were taken if no cosmic ray appeared in the right interval.

The 20-50 ms T. D. time delay in Fig. II-5 opened the gate timing circuit. The gate timing circuit removes the inhibit signal which prevents a cosmic ray pulse from initiating a flash. If a cosmic ray appears during this gate, it generates a pulse in the AND GATE.

The pulse from the AND GATE initiates the flashes through the Flash T. D. time delay and the double pulse flash delay. A 2-kV power supply and a capacitor bank, variable from 4 f to 24 f, supply the energy to the flash lamp.

The double flash system requirements are a little more sophisticated because in addition to the basic single flash system of a power supply and capacitor bank the following functions must be performed by these double flash circuits:

1. Two charged capacitor banks must be isolated by an electronic switch.
2. The Xenon flash lamps must be triggered twice within a 10 to 25 ms period.
3. Xenon flash lamp must be capable of operating in single flash or double flash mode.

Film Transport

The film transport is a modified Beattie model CS-48 that attaches to the flash lamp unit with four mounting bolts. The lens, also mounted in the flash lamp unit, will not be described in this section.

A 110 VAC motor drives a gear train which advances the film. The pulse that triggers this circuit also triggers a binary counter which records the frame number on the film and at a readout panel. The bulbs used for film readout are miniature penlite bulbs with focusing lenses.

Pressure Monitoring

Dynamic pressures are monitored by seven Kistler quartz pressure transducers, of which four are mounted in the chamber body, one in the tee, and one in each of two Grove valves. The signals from the seven pressure transducers are carried to a patch panel via shielded cable and here the operator can program any three of these signals to the three charge amplifiers.

Oscilloscope and Camera

A Tektronix-type RM564 storage oscilloscope with a four-trace plug-in plays a very vital role in the operation of the chamber. It allows the

operator to set up the timing sequence of the different components very accurately which is very important in chamber operation. Its storage mode allows the operator to study or compare waveforms for one or more cycles of the chamber plus the fact that a photograph can be taken of the stored image at any time. A Tektronix-type C-27 camera is used for this purpose.

GENERAL OVER-ALL OPERATION

The purpose of a model is fulfilled when mistakes in design are discovered rapidly and the resulting corrected designs are tested and found satisfactory.

A partial list of the many things discovered will give an idea of the usefulness of the model.

1. Mounting of windows.
2. Reduction in bubbling around window gaskets, probes and rotating seals.
3. Tests of paints used to cover rough walls.
4. Mounting of gaskets and diaphragms.
5. Tests of rotating gas-tight seals.
6. Experience in assembly.
7. Proper methods for transferring large amounts of Freon or propane.
8. Proper throttling and time controls on expansion and recompression valves.
9. Study of unexpectedly large pressure rises at the end of the chamber as the result of rapid recompression.
10. Advantages of expanding a chamber at the top of the liquid.
11. Study of strains in the walls of the chamber.
12. Dynamic effects of the gas in expansion and recompression.
13. Optical properties of Freon at nonuniform temperature.

14. Heat loads and requirements for proper thermal controls.

15. Experience in protecting Scotchlite from Freon and propane.

16. Bubble growth study with cosmic rays.

17. Dynamics study of Barksdale and Grove valves.

18. Study of methods for reducing thermal turbulence.

The model has been most successful from all points of view both in its original conception and in the details of its operation.

Initially the diaphragms of the chamber were made of a rubber belt material which had unfortunate characteristics and was easy to rupture. The oscilloscope traces did not repeat and showed erratic behavior. After installation of quarter-inch thick diaphragms made of 83 D durometer polyurethane, there was no further trouble with the diaphragms. The new clamping scheme shown in Fig. II-1 F was very successful.

The double diaphragm described in Section II was restricted in motion by the space available for the motion of the outer diaphragm. This allowed a maximum expansion of about 2.5%.

The chamber was evacuated before filling to about 50 microns of pressure. A liquid Freon pump was used in filling the chamber, and the final topping off was done with a hydraulically controlled piston in a cylinder. The chamber was filled until the rate of rise of pressure increased sharply indicating that all gas bubbles had collapsed. Then a measured amount of Freon was removed with the piston.

Initially the dirt left in the system sank to the bottom of the chamber and caused excess bubbling. Pieces of dirt floating in the liquid were

observed to bubble. Introduction of a one-half micron filter reduced this markedly. The liquid Freon pump was used to recirculate Freon through the filter for several hours.

Early analysis of the dynamics of the expansion of the chamber indicated the necessity for a sinusoidal expansion wave with a period three times that of the fundamental period of the pressure wave in the chamber. It was found possible to control this by varying the pressures and timing of the Barksdale valves used in controlling the expansion and recompression Grove valves.

The capacity of the compressor was just sufficient to permit an expansion to be made every 20 seconds. Leaks in the air system necessitated stopping expansions so as to build up the supply. The chamber would run for 40 minutes or 120 expansions before this was required. Figure II-4 shows a schematic of the air system. More detailed discussion of speeds and modifications to Grove valves and Barksdales are given in Section IV.

It was possible to expand the chamber five times in succession at two-second intervals. The expanded pressure rose each time, so that all expansions were not to the same depth. However, it was possible to see tracks in all five expansions.

A very marked improvement in operation resulted from the use of propellers to stir the Freon. When a large bubble at the top of the chamber was recompressed, the heat of condensation increased the temperature of the Freon. The bubble collapsed very slowly, and the liquid at the top remained hot. When the propellers were turned on, this problem was removed, the bubble collapsed quickly, and uniform temperature was reached quickly.

A great convenience in operating the chamber was the persistent pattern oscilloscope Type RM 546 Tektronix storage oscilloscope. The pattern remains indefinitely and can be photographed subsequently. A second trace on top of the previous one makes it very easy to see small changes from pulse to pulse.

Presented on the four-channel scope were:

1. Pressures at five different points in the chamber and the TEE.
2. Boot pressures in the Grove valves.
3. Opening times of the Barksdales.
4. Arrival time of cosmic rays.
5. Two light timing pips for double flash photographs.
6. Opening and closing of gate for acceptance of a cosmic ray.

Four traces could be made simultaneously. A typical setup would be: (1) pressure wave in chamber, (2) arrival time of cosmic ray, (3) double light flash pips, (4) opening and closing of gate for acceptance of a cosmic ray.

Two cameras were used, one at the far end of the chamber and one at the side. Both cameras looked through fisheye windows of glass with inner and outer radii of 5 and 6 inches. The camera lenses were located at the center of curvature of the windows.

High speed movies were made at 1600 frames per second, and movies at 50 and 70 frames per second from the end window. These exposures will be described below.

Gaseous Freon was recovered from the chamber when emptying after a run. This was done by attaching a helix of 3/4-in. copper pipe to the chamber and to the Freon storage tank. The helix was submerged in a dry ice alcohol mixture while open to the chamber. It was then submerged in hot water and connected to the storage tank. This was repeated until the pressure inside the chamber was reduced to 1 or 2 atmospheres.

Operating Conditions

Cosmic ray tracks could be obtained over a wide range of conditions. Typical temperatures of Freon 13B1 went from 27.5°C to 31.7°C. The recompression pressure was set 25 psi above the vapor pressure which varied from 248 psia to 275 psia. The expanded pressure ran at about 150 psig and down as low as 110 psig on some occasions.

The amount of liquid removed to permit expansion never exceeded 2.4% of the volume. This was an unwelcome limitation of the geometry of the double diaphragm. Because of this restriction, it was not possible to lower the expanded pressure to increase the rate of growth of the bubbles.

EXPANSION STUDIES

(1) A program was initiated to try to speed up Barksdale solenoid valves operating under bubble chamber conditions. A new coil was wound which could take a larger current than the one supplied. A stiffer upper spring was wound and the pilot stem modified. All of these steps were taken in a trial and error method until optimum conditions were obtained. It was possible to reduce valve opening time by 25%, valve closing time by 15%, and stem dwell time by 50%, reducing the total valve cycle from 50 msec to 32 msec for a 10 msec electric pulse.

The Grove valves were modified such that they had more than one Barksdale valve externally manifolded. The poorly designed gas exhaust port in the original Grove valve was improved by the addition of flow channels and a holey plate over the exhaust port to prevent damage to the boot.

(2) The polyurethane diaphragm has shown no deterioration except for a small amount of stretching. There was no marked effect of heating from hysteresis in the diaphragm.

(3) Parasitic bubbling was greater at higher temperatures. Limitation in expansion ratio to 2.5% prevented study of bubble growth at low temperatures and expansion to lower pressures.

(4) Attempts to expand and recompress the chamber more rapidly resulted in marked stimulation of the fundamental period of the chamber with consequent large overshoots in pressure.

(5) Heat load studies before and after installation of the Ramm plate showed that the heat load was reduced from 14.9 x joules/liter to 11.2 y joules/liter.

(6) The Ramm plate tilted in the direction of expansion at the top so that the top moved 3/8 inch more than the bottom. The Ramm plate was 8 inches from the inner diaphragm. The diaphragm moved more at the top than at the bottom and was the cause of this tilt in the Ramm plate. This motion came from the fact that there were two diaphragms. The outer diaphragm, bowed out at the bottom during compression due to the greater hydrostatic pressure there from the Freon solvent between the two diaphragms. The inner diaphragm was under tension and assumed a symmetric form. On expansion the bulge at the bottom of the outer diaphragm first moved out until it was restrained by the boundary of the air space behind it. Then the top moved out further because there was more room for it to move.

There was an oscillation which persisted until the chamber was re-compressed. This had a period of 57 milliseconds and probably corresponded to a transverse oscillation of the liquid around the Ramm plate and in the solvent-filled space between the two diaphragms.

Heat Load

The heat load caused by pulsing the chamber was determined by measuring the flow and temperature change of the heating water. To maintain the chamber without pulsing at 30°C against room temperature required about 37 BTU/min. Pulsing at a rate of 3 pulses per minute required 19 BTU/min. This means that each pulse developed 6 BTU of heat. This corresponds to the formation of bubbles amounting to .90% of the volume if all the irreversible work went into formation and collapse of bubbles. This amounts to 11.2 joules/liter.

Cosmic rays entering at one per sq. cm. per minute produce bubbles. If we assume a senstive time of 33.3 milliseconds, ten bubbles per cm on each track, and that the bubbles grow to a diameter of 3 mm each at maximum size, this corresponds to 0.008% of the chamber volume and results in irreversible work of 53 joules for the whole chamber or 0.11 joules per liter. An equivalent amount of work would be produced by 1.5 tracks going the full length of the chamber.

The change in pressure on expansion was 170 psi. This expansion could be as great as 2.5% which leaves a difference of 1.35% for bubbles at their maximum size. This agrees with the heat load as measured. It should be pointed out that our measurements did not determine that the inner diaphragm moved the full 2.5%. However, a slightly longer delay between expansion and recompression gave audible evidence that the diaphragm was hitting the holey plate. The Freon removed corresponded to 2.5%. It was removed at the vapor pressure of 260.8 psia. The liquid was recompressed to 311.4 psia which reduced its volume further so that it occupied a volume about 0.36% smaller. The maximum possible motion of the diaphragm was therefore 2.86%.

The reasonable conclusion appears to be that the heat load came from formation of bubbles which reached maximum size of about 1.4% of the chamber volume.

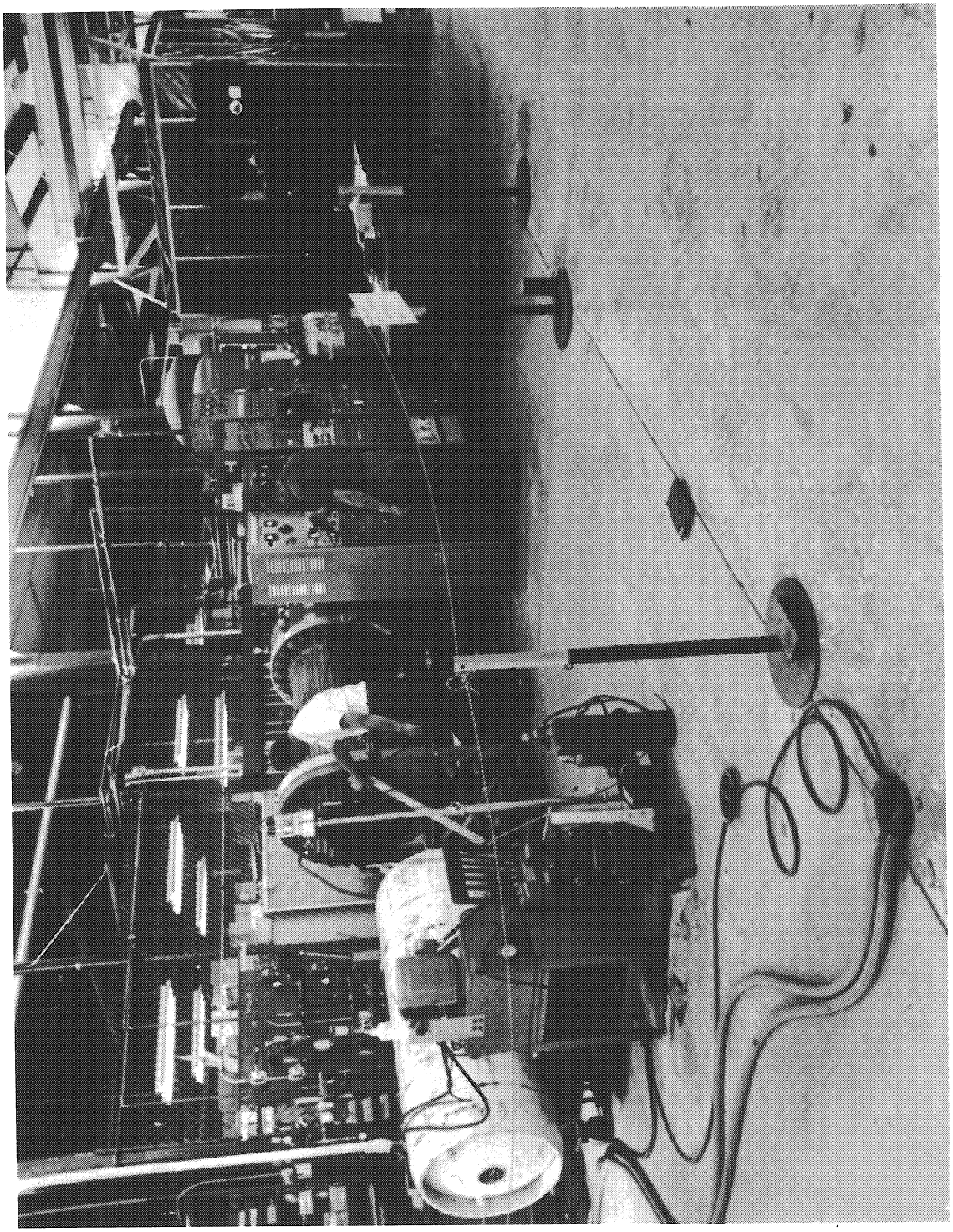

Fig. I-1. The Model Chamber

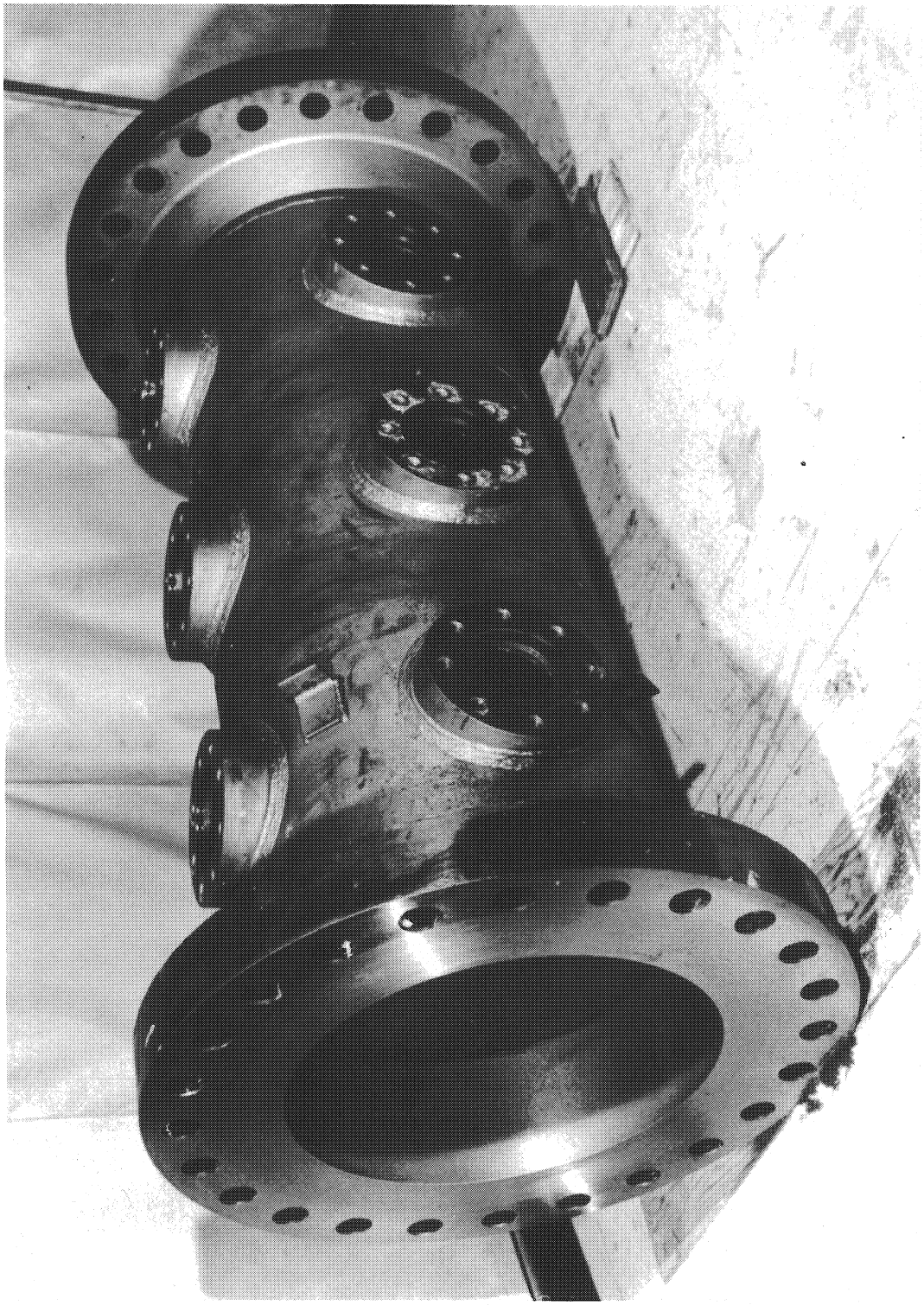

Fig. I-2. The Chamber Body After Welding

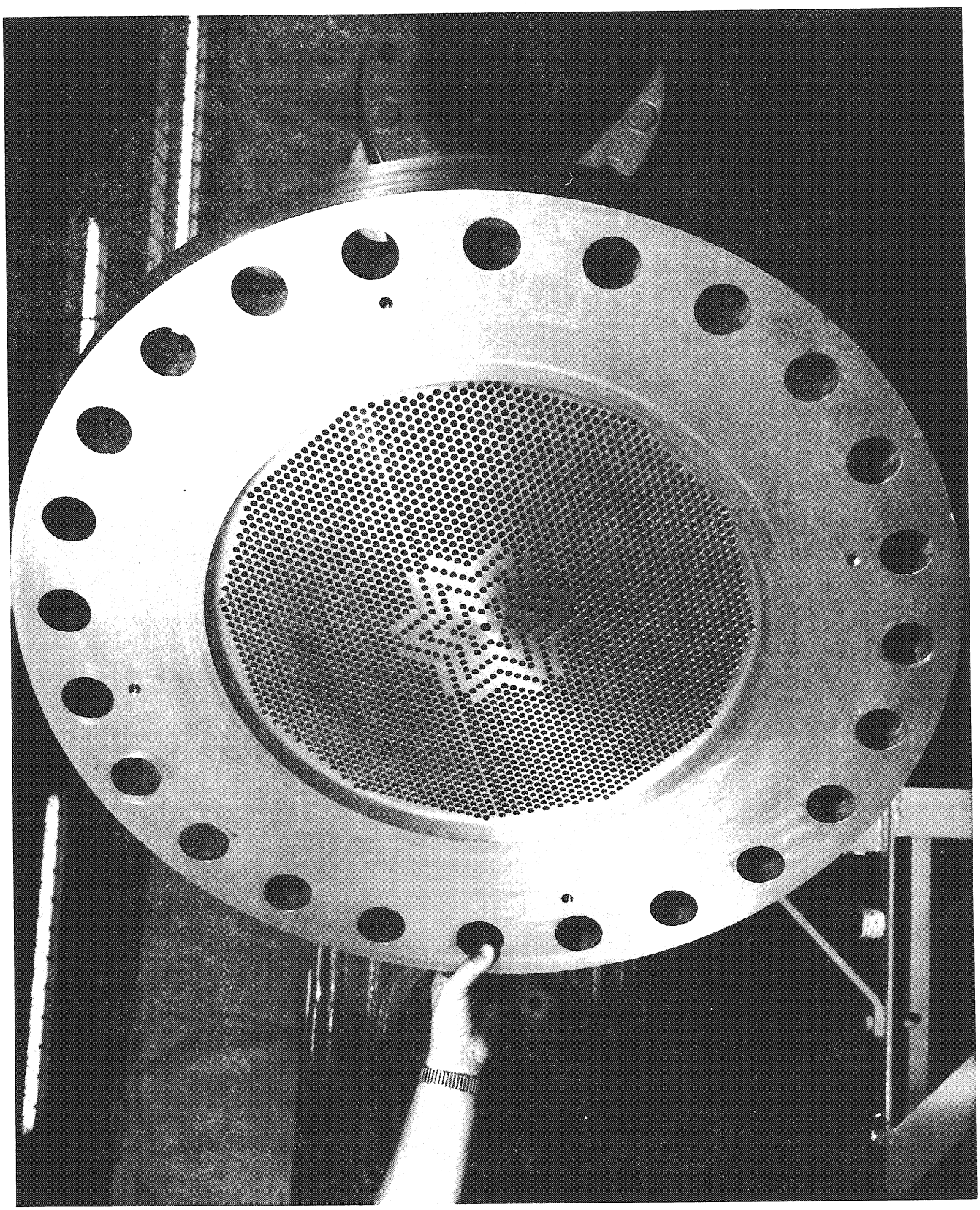

Fig. I-3. The Convex Side of the Holey Plate.

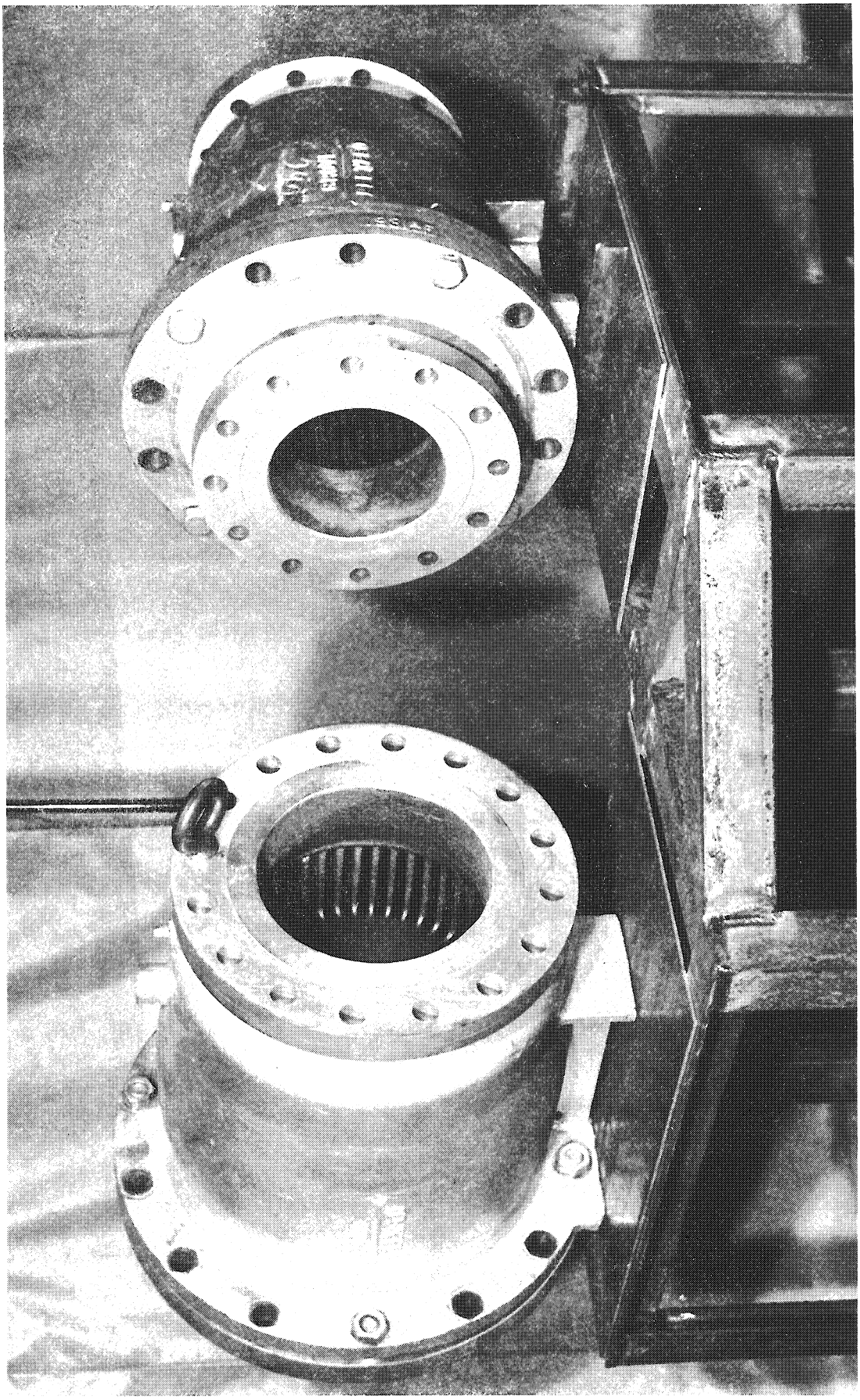

Fig. I-4. The 10-in. and 8-in. Grove Valves

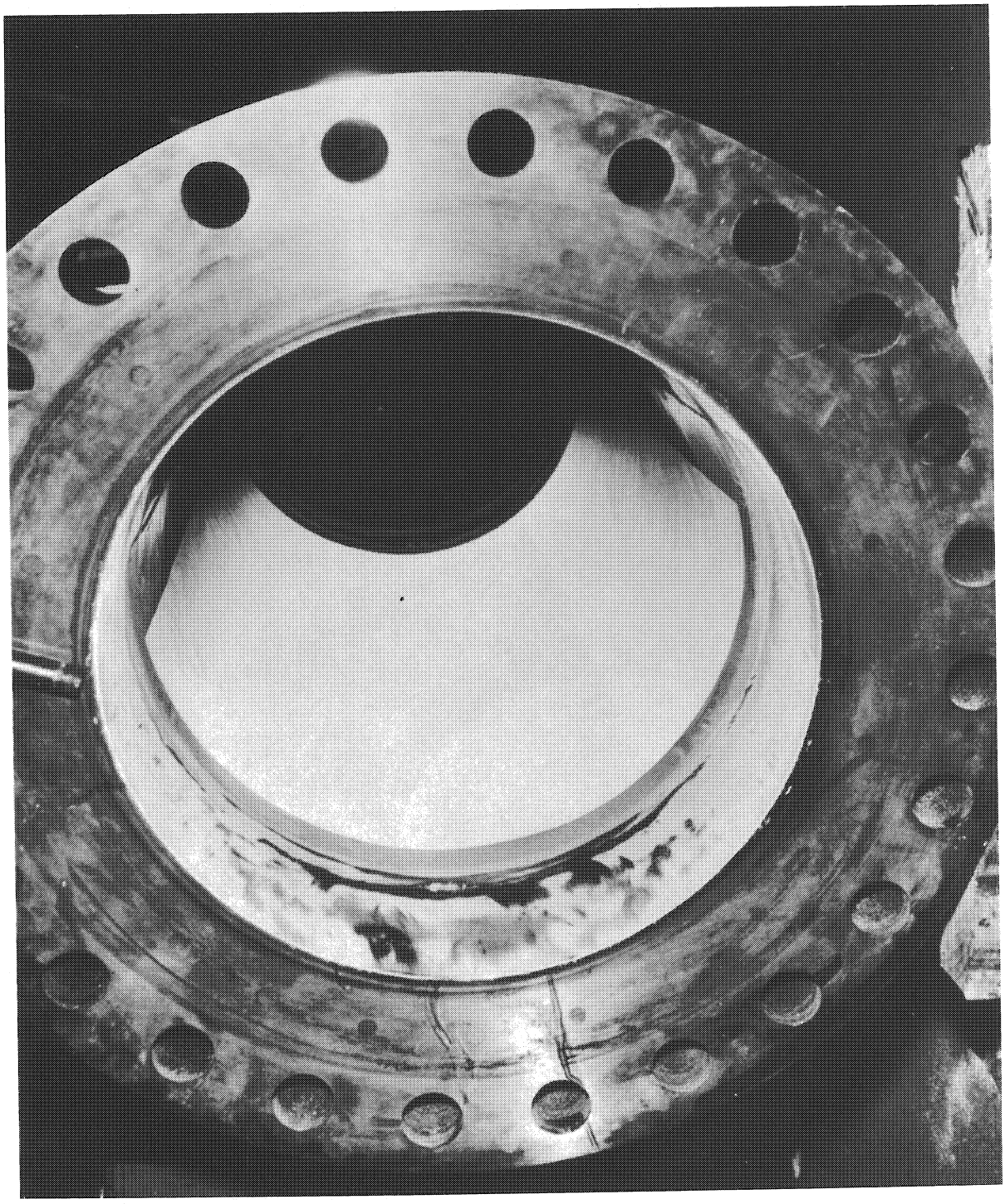

Fig. I-5. The Scotchlite on the Inner Wall of the Chamber

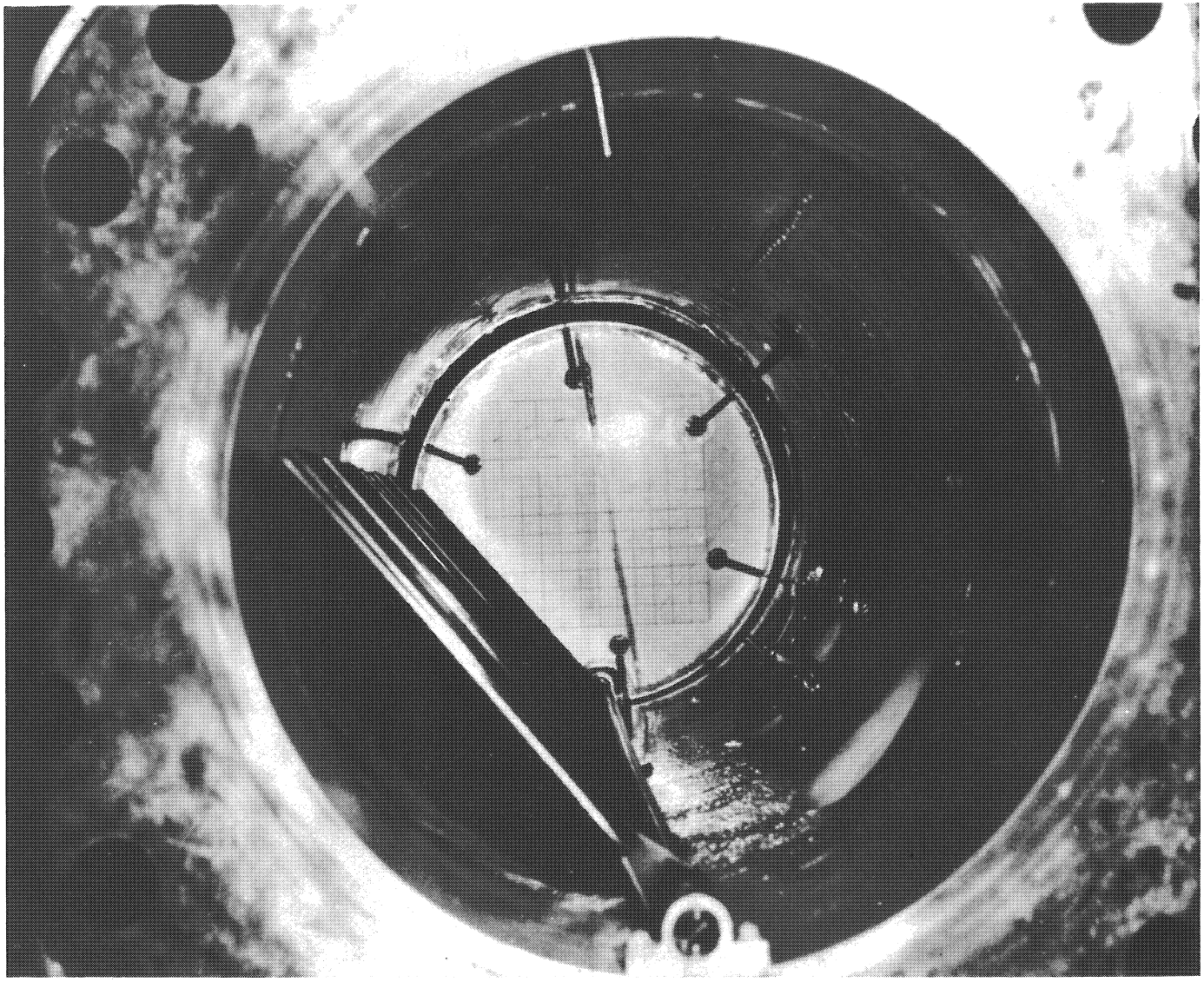

Fig. I-6. A View From the Closed End of the Chamber Showing the Rake and the Ramm Plate

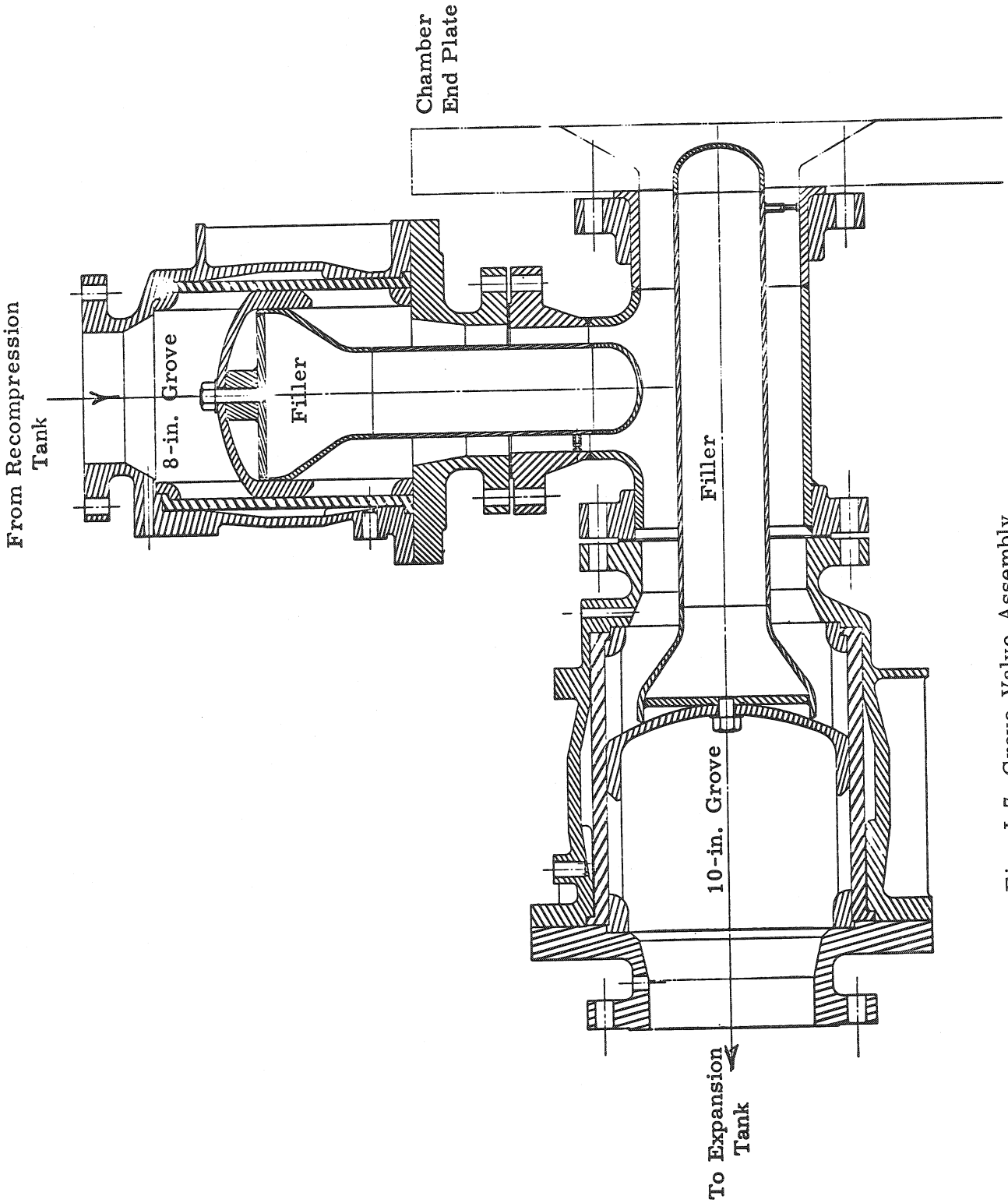

Fig. I-7. Grove Valve Assembly

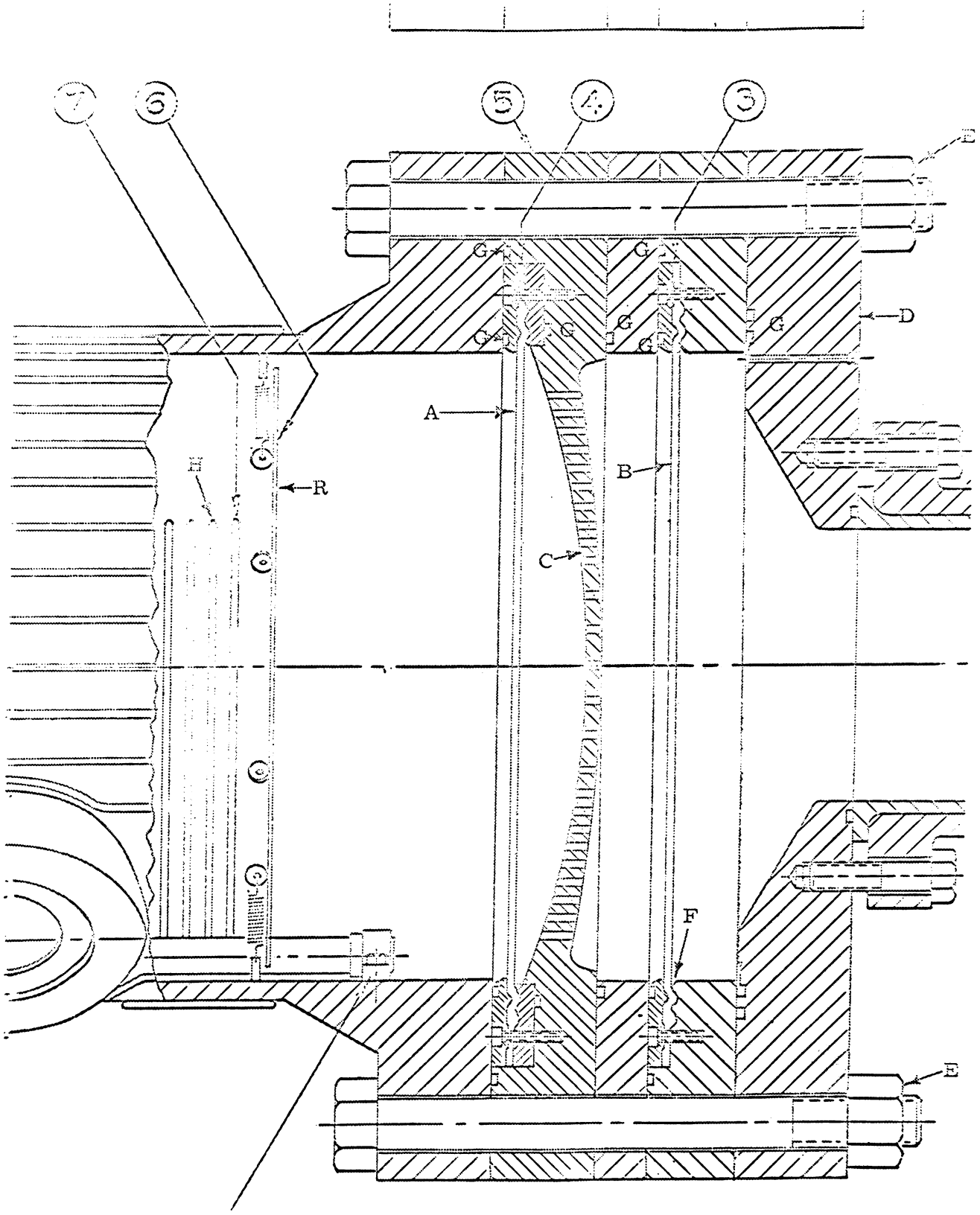

Fig. II-1. Expansion End of Chamber

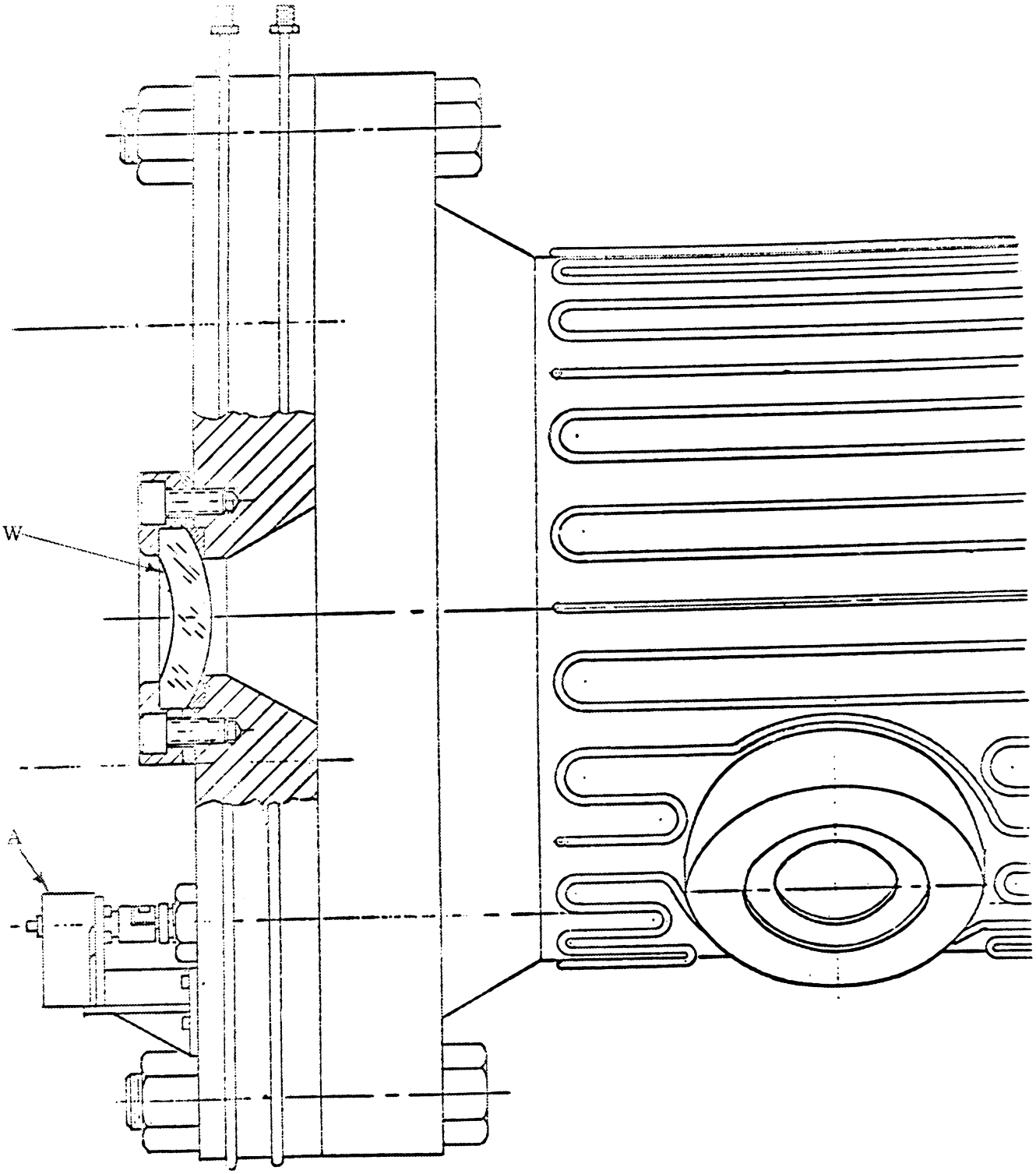

Fig. II-2. Closed End of Chamber

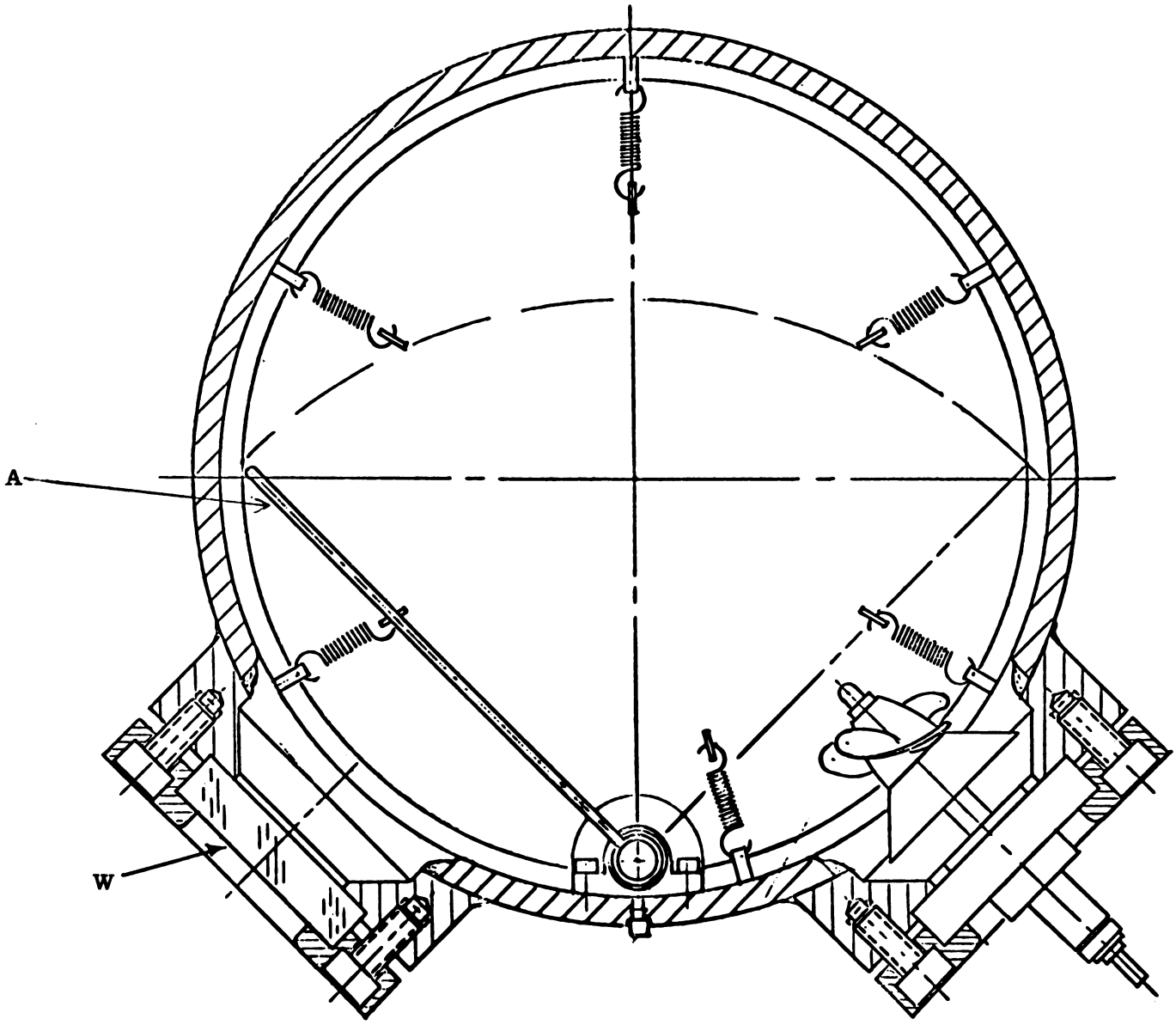

Fig. II-3. Ramm Plate, Propellor and Rake
Viewed from Closed End of Chamber

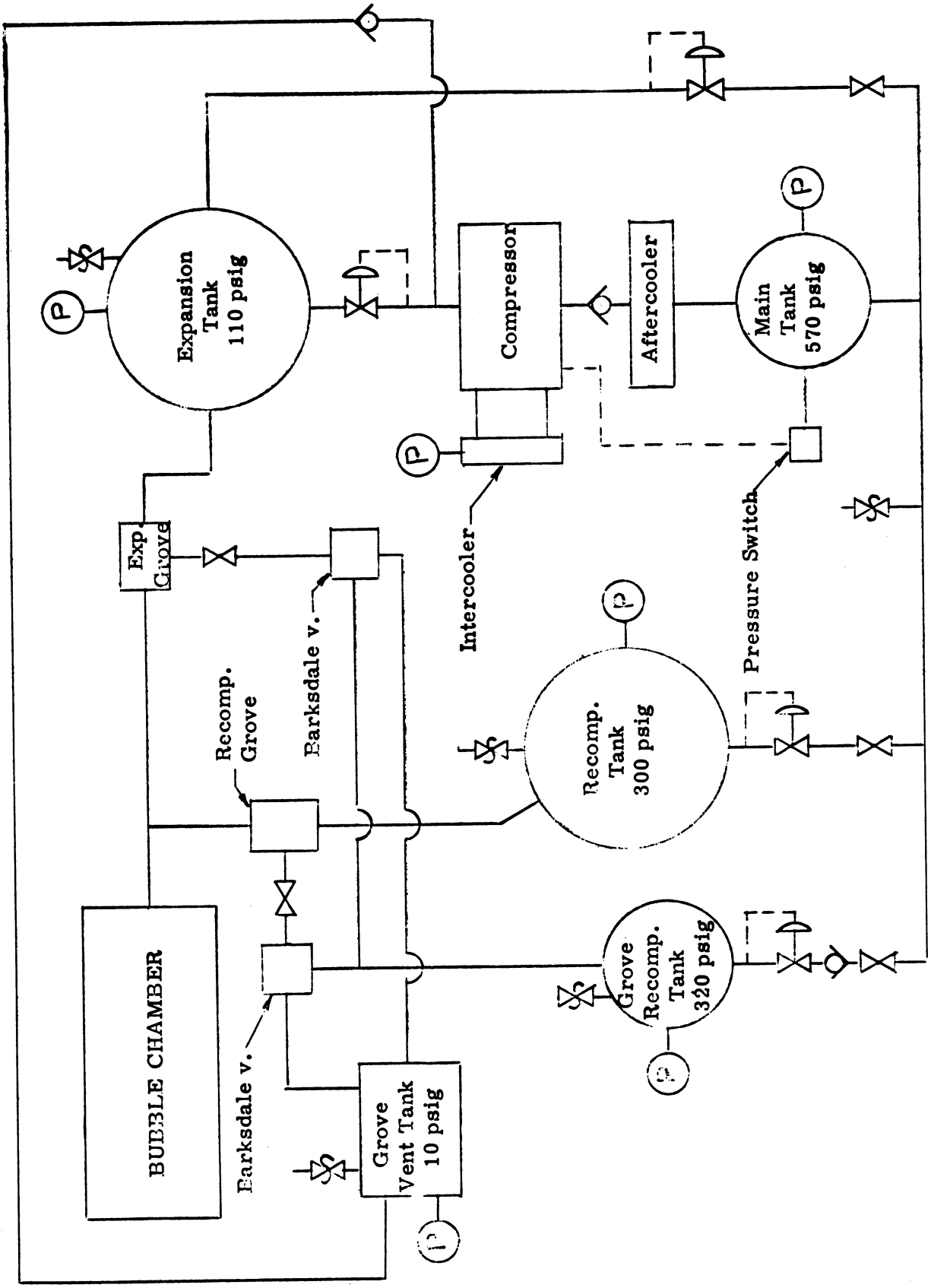

Fig. II-4. Schematic of the Air System

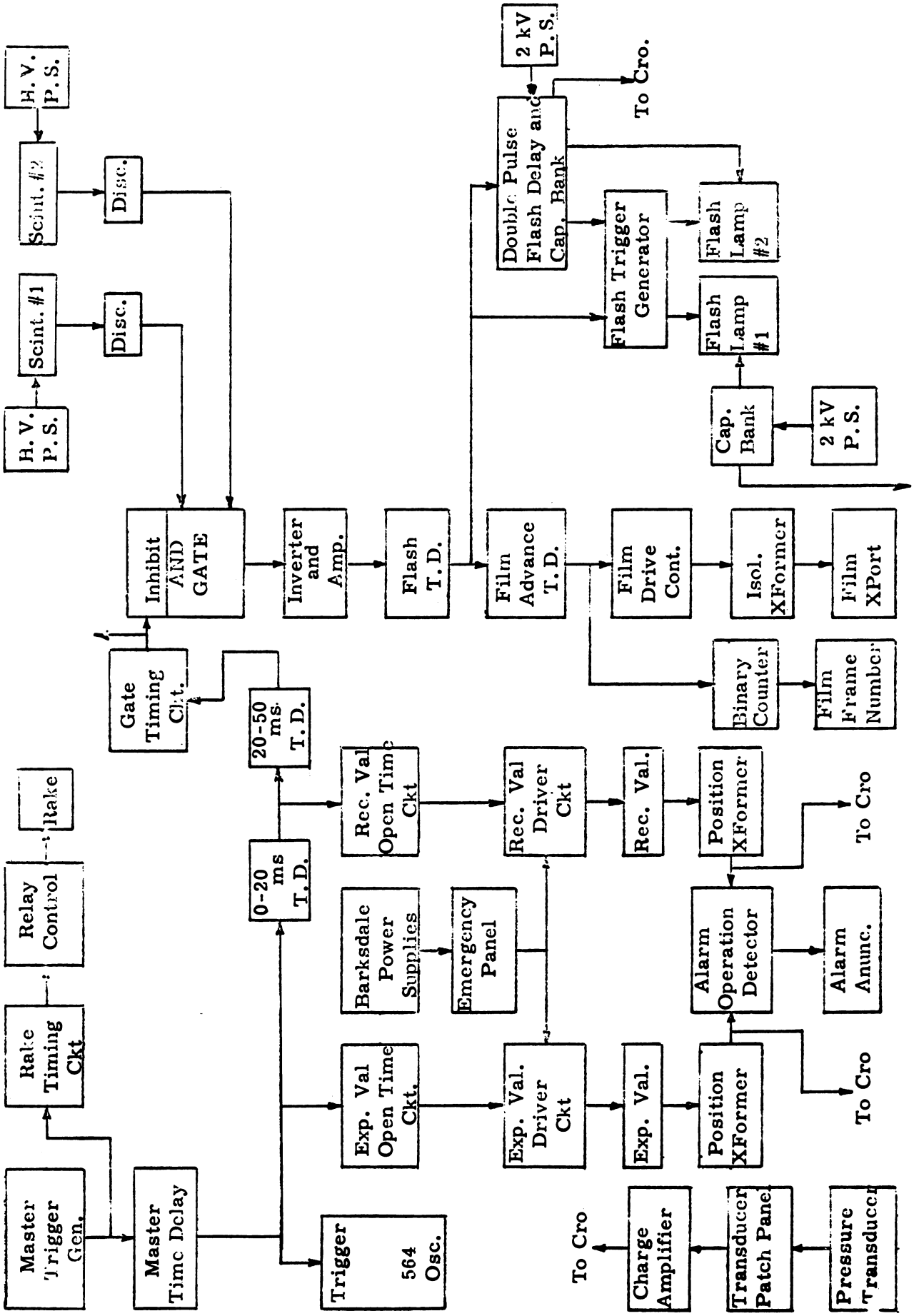

Fig. II-5. Block Diagram of Chamber Electronics

Index of Authors

P. Musset	1.4	73
P. Negri	3.7	313
M.L. Palmer	3.5/6.8	263/513
P. Pétiau	3.6	295
E.G. Pewitt	2.1/5.1	97/427
W.M. Powell	3.5/6.8	263/513
C.A. Ramm	6.1	467
H.P. Reinhard	3.9	341
M. Scheer	4.5	405
Ch. Scherer	6.1	467
J. Schmid	2.7	181
I.N. Sviatoslavsky	3.5/6.8	263/513
J.D. Simpson	6.6/6.7	501/507
R.G. Stierlin	6.3	479
A. Tamosaitis	6.5	493
D.B. Thomas	2.5/2.8/3.2	147/191/215
W.T. Welford	3.1/3.8	201/329
W.R. Winter	3.5/6.8	263/513
F. Wittgenstein	5.3	457
S. Wolff	4.4	389